

Université de Montréal

**Exploring the Role of Fibronectin
in Spondylometaphyseal Dysplasia**

par

Nissan Vida Baratang

Département de biochimie et médecine moléculaire

Faculté de Médecine

Mémoire présenté à la Faculté des études supérieures en vue de l'obtention du
grade de maîtrise en Sciences en biochimie, option Générale

Octobre 2018

© Nissan Vida Baratang, 2018

RÉSUMÉ

La fibronectine (FN), une glycoprotéine largement exprimée, a été associée à de nombreux processus biologiques fondamentaux, mais n'a jamais été impliquée dans des maladies osseuses. L'identification de mutations dans le gène qui code pour cette protéine chez des patients présentant un sous-type rare de dysplasie spondylométaphysaire (SMD) a révélé un aspect inexploré de cette protéine. Des études récentes ont montré que ces mutations empêchent la sécrétion de la FN dans les cellules HEK293, mais comment ce défaut contribue mécaniquement à la pathogenèse de la SMD est encore inconnu. Pour étudier les effets des mutations *in vitro*, un protocole de différenciation des chondrocytes a été optimisé et testé sur des cellules ATDC5. En outre, pour déterminer si les phénotypes des patients étaient dus à une réduction globale de la FN, des souris simples knock-out (KO) et double KO dépourvues de FN dans le foie et/ou le cartilage ont été générées. Les résultats révèlent que la suppression de la FN dans ces tissus ne nuit ni à la croissance ni à la viabilité. Aucune modification n'a été détectée dans le poids ni dans la longueur du corps des KO par rapport aux souris témoins, et aucune anomalie du squelette n'a été observée sur les radiographies. Ces résultats montrent que la suppression de FN dans ces deux tissus ne conduit pas aux phénotypes observés dans les SMD. De plus, le séquençage du gène *FNI* chez des individus soupçonnés d'être atteints de SMD a permis l'identification d'une mutation *de novo* chez un patient. Cette découverte élargit les caractéristiques cliniques de cette maladie induit par *FNI*.

Mots-clés: FN1, fibronectine, dysplasie osseuse, SMD, fractures en coin, chondrocyte, matrice extracellulaire, cartilage, knock-out

ABSTRACT

A widely expressed glycoprotein, fibronectin (FN), has been associated with many basic biological processes, but has never been implicated with skeletal disorders. Identification of mutations in the gene that encodes this protein in patients with a rare subtype of spondylometaphyseal dysplasia (SMD) reveals an unexplored aspect in the field. Recent studies have shown that these mutations impair FN secretion in HEK293 cells, but it is still not known how this defect mechanistically contributes to SMD pathogenesis. To investigate the effects of the mutations *in vitro*, a chondrocyte differentiation protocol was optimized and tested on ATDC5 cells. Furthermore, to determine if the patients' phenotypes were caused by a global reduction of FN, single and double knockout (KO) mice that lack FN in the liver and/or the cartilage were generated. Results reveal that deletion of FN in these tissues does not impair growth or viability. No changes were detected in the body weight nor length in the KO compared to control mice, and no skeletal abnormalities were observed in radiographs. These results show that the deletion of FN in these two tissues does not lead to the phenotypes observed in SMD. Additionally, sequencing of the *FNI* gene in individuals with suspected SMD identified a *de novo* mutation in one patient. This finding expands the clinical features of *FNI*-induced SMD.

Keywords: FN1, fibronectin, skeletal dysplasia, SMD, corner fractures, chondrocyte, extracellular matrix, cartilage, knockout

TABLE OF CONTENTS

RÉSUMÉ	II
ABSTRACT	III
TABLE OF CONTENTS	IV
LIST OF TABLES	VII
LIST OF FIGURES	VII
LIST OF ABBREVIATIONS	VIII
ACKNOWLEDGEMENTS	X
Chapter 1: INTRODUCTION	1
1.1 SKELETAL DEVELOPMENT	2
1.1.1 Endochondral Bone Formation	3
1.1.2 Mesenchymal Stem Cell Condensation	5
1.1.3 Chondrocyte differentiation and proliferation	7
1.1.4 Chondrocyte terminal differentiation and hypertrophy	8
1.1.5 Vascular invasion and Ossification	10
1.2 SPONDYLOMETAPHYSEAL DYSPLASIAS	12
1.2.1 Sutcliffe-type SMD	13
1.2.1.1 Clinical characteristics	13
1.2.1.2 Challenges in Diagnosis	16
1.2.1.3 Treatment	17
1.2.1.4 Pathogenesis	17
1.3 FIBRONECTIN	18
1.3.1 Structure	18
1.3.1.1 Basic structure	18
1.3.1.2 Functional domains	20
1.3.2 Heterogeneity of FN1	23
1.3.2.1 Alternative splicing	23
1.3.2.2 Post-translational modifications	24
1.3.3 Forms of Fibronectin	25
1.3.3.1 Plasma Fibronectin	25
1.3.3.2 Cellular Fibronectin	26
1.3.4 Fibronectin and the ECM	26
1.3.4.1 Steps of FN-Matrix Assembly	27
1.3.4.2 Regulation of FN-matrix assembly	30
1.3.5 Fibronectin in skeletal formation	31
1.3.5.1 Endochondral bone formation	32
1.3.5.2 Intramembranous ossification	33

1.3.6 FN-associated Disorders	33
1.4 RESEARCH PROJECT	36
Chapter 2: MATERIALS AND METHODS	37
2.1 POLYMERASE CHAIN REACTION	38
2.2 SANGER SEQUENCING	38
2.3 MICE GENERATION AND BREEDING	40
2.3.1 Knock-out mice	40
2.3.2 Knock-in mice	40
2.4 MICE GENOTYPING	41
2.4.1 DNA isolation	41
2.4.2 Genotyping	41
2.5 GROWTH MEASUREMENTS	42
2.6 RADIOGRAPHY	42
2.7 CELL CULTURE	43
2.7.1 ATDC5 Cells	43
2.7.2 Chondrogenic Differentiation	43
2.8 RNA EXTRACTION AND CDNA SYNTHESIS	43
2.9 REAL-TIME PCR	44
2.9.1 Data analysis	45
2.10 HISTOCHEMICAL STAINING	45
2.10.1 Alizarin Red	45
2.10.2 Alcian Blue	46
Chapter 3: RESULTS	47
3.1 CHONDROGENESIS OF ATDC5 CELLS	48
3.1.1 ATDC5 Cell Morphology	49
3.1.2 Gene Expression of Chondrogenic Markers	51
3.1.3 ECM formation and mineralization	54
3.2 GENETICALLY MODIFIED MICE	56
3.2.1 Generation of knock-out mice	56
3.2.2 Characterization of knock-out mice	57
3.2.2.1 Single KO mice	57
3.2.2.2 Double KO mice	59
3.2.3 Generation of CRISPR knock-in mice	60
3.3 CASE STUDY OF A PATIENT WITH SUTCLIFFE-TYPE SMD	65
3.3.1 Clinical Features	65
3.3.2 Sequencing of patient DNA	66

Chapter 4: DISCUSSION	68
Chapter 5: CONCLUSION	80
BIBLIOGRAPHY	83
ANNEXE I: Mutations in Fibronectin Cause a Subtype of Spondylometaphyseal Dysplasia with “Corner Fractures”	i
ANNEXE II: Characterization of genes involved in the biosynthesis of GPI-anchored proteins	xi

LIST OF TABLES

Table I:	Types of Spondylometaphyseal Dysplasias	13
Table II:	Sequencing primers for the human <i>FNI</i> gene	39
Table III:	Primers used for mouse genotyping	42
Table IV:	Primers used for real-time PCR	45

LIST OF FIGURES

Chapter 1: INTRODUCTION

Figure 1:	Sequence of events during chondrogenesis	4
Figure 2:	Zones of cartilage proliferation in the growth plate	5
Figure 3:	Clinical features of patients with SMD with corner fractures	15
Figure 4:	Structure of Fibronectin	19
Figure 5:	Steps of fibronectin (FN) matrix assembly	29
Figure 6:	Immunofluorescence analysis of HEK293 cells	35

Chapter 3: RESULTS

Figure 7:	Chondrogenic differentiation of ATDC5 cells	50
Figure 8:	Expression of ECM genes during chondrogenesis of ATDC5 cells	53
Figure 9:	Calcium deposition in differentiated ATDC5 cells	54
Figure 10:	Glycosaminoglycan (GAG) accumulation in differentiated ATDC5 cells	55
Figure 11:	Generation of FN double knockout (dKO) mice in liver and cartilage	58
Figure 12:	Weight and length of FN knockout mice	59
Figure 13:	Bone analysis of FN knockout mice	61
Figure 14:	CRISPR knock-in strategy	62
Figure 15:	Genotyping CRISPR knock-in mice	64
Figure 16:	Radiographs of patient with Sutcliffe-type SMD	65
Figure 17:	Sanger sequencing of the <i>FNI</i> gene	67

LIST OF ABBREVIATIONS

Acan	Aggrecan
ALP	Alkaline phosphatase
AMEM	Minimum Essential Medium, alpha modification
BMD	Bone mineral density
BMP	Bone morphogenic protein
cFN	cellular fibronectin
Col10a1	Collagen Type X Alpha 1
Col1a1	Collagen type I, alpha 1
Dex	Dexamethasone
dKO	double knock-out
DTSDT	Diastrophic dysplasia sulfate transporter
ECM	Extracellular matrix
EDA/EIIIA	Extra-domain repeat A
EDA/EIIIB	Extra-domain repeat B
ER	Endoplasmic reticulum
FAK	focal adhesion kinase
FBS	Fetal bovine serum
FGF	Fibroblast growth factor
FN	Fibronectin protein
<i>FNI</i>	Fibronectin gene
GAG	Glycosaminoglycan
GFND	Glomerulopathy with FN deposits
HA	Hyaluronan
HDAC	Histone deacetylase
HDR	Homology directed repair
IHH	Indian hedgehog
IS	idiopathic scoliosis
ITS	insulin-transferrin-selenium

KI	knock-in
LTBP	latent transforming growth factor-beta-binding proteins
MAPK	Mitogen activated protein kinase
MMP	Matrix metalloproteinase
MPa	Megapascal
MSCs	Mesenchymal stem cells
N-CAM	Neural cell adhesion molecule
PAM	Protospacer adjacent motif
PCR	Polymerase chain reaction
pFN	plasma fibronectin
PTH	Parathyroid hormone
PTHrP	Parathyroid hormone-related peptide
Runx2	Runt-related transcription factor 2
SEMD	Spondyloepimetaphyseal dysplasia
sgRNA	single guide RNA
SHH	Sonic hedgehog
SMD	Spondylometaphyseal dysplasia
SMD-CF	Spondylometaphyseal dysplasia with corner fractures
Sox9	SRY-Box 9
ssODN	single-stranded donor oligonucleotide
β -GP	β -glycerophosphate
TGF- β	Transforming growth factor- β
TIMP	Tissue inhibitor of metalloproteinases
UPR	unfolded protein response
VEGF	Vascular endothelial factor
WT	Wild-type

ACKNOWLEDGEMENTS

First and foremost, I would like to thank Dr. Philippe Campeau for giving me an opportunity to pursue a Master's degree. Thank you for believing in my potential, and for the never-ending patience, support and understanding. No one knows how you manage to juggle all your responsibilities, but you magically do, and it is what inspired me to stay motivated when life became overwhelming. Thank you for opening up your home for our lab BBQs and for making sure that everyone in the lab feels valued. I will never forget the Jenga song you taught us and your amazing bowling skills. A million times, thank you.

To Justine, I don't know how the lab can manage without you. Thank you for making sure that we do not run out of material, and for taking initiative when tasks needed to get done. I am grateful for all the times you spent with me when I felt lost in my experiments, and for always being available when I needed help. I truly learned a lot from you, and I promise to "go on vacation" like you tell me to.

To Sophie, these past two years would not have been the same without you. Thank you for sharing my stress, listening to my random stories, encouraging me to participate in social events, participating in my vlogs, and for the most life-changing: introducing me to coffee. I just want you to know that I support your new healthy lifestyle and thank you for teaching me that "new year, new me" can be said any day and every day of the year.

To the "West blot crew" Sophie, Joshua and Levi: thank you for an unforgettable summer. Long live western blots! To Jean-Philippe, Alex, and Li Xin, thank you for the many memories in just a short amount of time. I especially appreciate you guys keeping me company in the cell culture room. If I can attach memes of you on here, I would. Daniel, gracias for letting me practice my Spanish contigo and for the entertaining debates you manage to get yourself into with Sophie. To Yassine and Ashley, thank you for your hard work and your patience with me. I hope you learned something useful during your time in the lab. Wishing you all success in your future endeavors and I hope we can all stay in touch.

I would also like to thank Mai and He for training me when I first started. To the other members of the lab, past and present, who I got the chance to meet: Doy, Norbert, Vito, Bettina, Thomas; to Joy (thank you for the hugs), and to all the amazing people I've encountered in the research center, I am blessed to have met you all on this journey.

To Brian, you came at the right time. Thank you for the fries at the end of a long day and for constantly reminding me why I'm doing this. You kept me sane and I cannot express how truly grateful I am for you.

Finally, I would like to thank my parents and my sister for the unlimited support and tough love since day one. I would not have been able to get this far without you. Thank you for preparing me for the real world. I hope I make you proud.

CHAPTER 1: INTRODUCTION

1.1 SKELETAL DEVELOPMENT

The mammalian skeleton is composed mainly of bone and cartilage. The early development of the skeletal system starts in the third week of embryonic life with the formation of the notochord. The cranial neural crest cells give rise to the craniofacial bones, and the somites to vertebrae and ribs. The limb skeleton comes from the lateral plate mesoderm and begins to appear by the fourth week, and around the seventh week, all bones of the human body are formed [1]. However, they consist mostly of hyaline cartilage and fibrous membranes and are therefore not yet “bony”. Bone development, termed “ossification” or “osteogenesis” begins by the seventh week of embryonic life, completes in early adulthood, but continually undergoes remodeling during the adult life [1]. There are two pathways in which bone forms: intramembranous ossification and endochondral ossification. Both processes start with mesenchymal stem cells (MSCs) which are undifferentiated cells that have the capacity to differentiate into multiple lineages [2].

Intramembranous ossification forms most of the cranial bones, the flat bones of the face and collarbones [3]. In this process, MSCs condense and differentiate directly into bone precursor cells known as osteoblasts within sheets of connective tissues. Osteoblasts secrete a collagen-proteoglycan matrix which hardens within a few days as it binds calcium salts. The osteoblasts then either get separated from this calcified layer or get trapped within the matrix. They eventually become osteocytes which form mature bone [3, 4].

The bones at the base of the skull and long bones such as the femur, tibia, humerus, and radius are formed via endochondral ossification [3]. This pathway can be summarized in two parts: chondrogenesis, a process in which MSCs aggregate and differentiate into chondrocytes to form cartilage tissue, and ossification, where this cartilage is replaced by bone. Note that cartilage does not become bone, but is rather used as a template on which bone is formed [5]. This review will focus on endochondral bone formation, discussing the signaling pathways and transcription factors involved in this complex process.

1.1.1 Endochondral Bone Formation

Endochondral bone formation is a sequential process that can be divided into five main stages after the commitment of MSCs to become cartilage cells (Figure 1) [4]. The first phase involves the condensation of committed MSCs. Condensed MSCs then differentiate into chondrocytes which proliferate to form a hyaline cartilage model and begin to produce a cartilage-specific extracellular matrix (ECM). In the third stage, they reach terminal differentiation, stop dividing and become hypertrophic chondrocytes [4, 6]. Hypertrophic chondrocytes die by apoptosis at the fourth stage, followed by the invasion of blood vessels, osteoblasts, and the mineralization of the ECM [7]. The last phase involves the formation of mature bone by osteoblasts. The first areas of osteogenesis appear in primary ossification centers, located in the central part of the developing bone. In long bones, it is in the shaft termed the diaphysis. By the 4th month of prenatal development, most primary ossification centers have appeared in the diaphysis of long bones, and from birth to approximately 5 years of age, secondary ossification centers appear in each end (epiphyses) of long bones [1, 8]. These secondary centers emerge as a result of the apoptosis of epiphyseal cartilage cells, and they undergo a similar ossification process as the primary ossification center [3].

Between the two ossification centers is a layer of hyaline cartilage called the “epiphyseal plate”, also known as the growth plate [9]. It is located in the metaphysis, an area between the diaphysis and the epiphyses. This plate continues to form new cartilage which is later replaced by bone, resulting in bone elongation. Ossification continues between 5 years of age to early adulthood. When growth is complete at around 20 years old, the epiphyses and diaphysis fuse together. This leads to growth plate closure, and no further growth occurs [1, 3, 8].

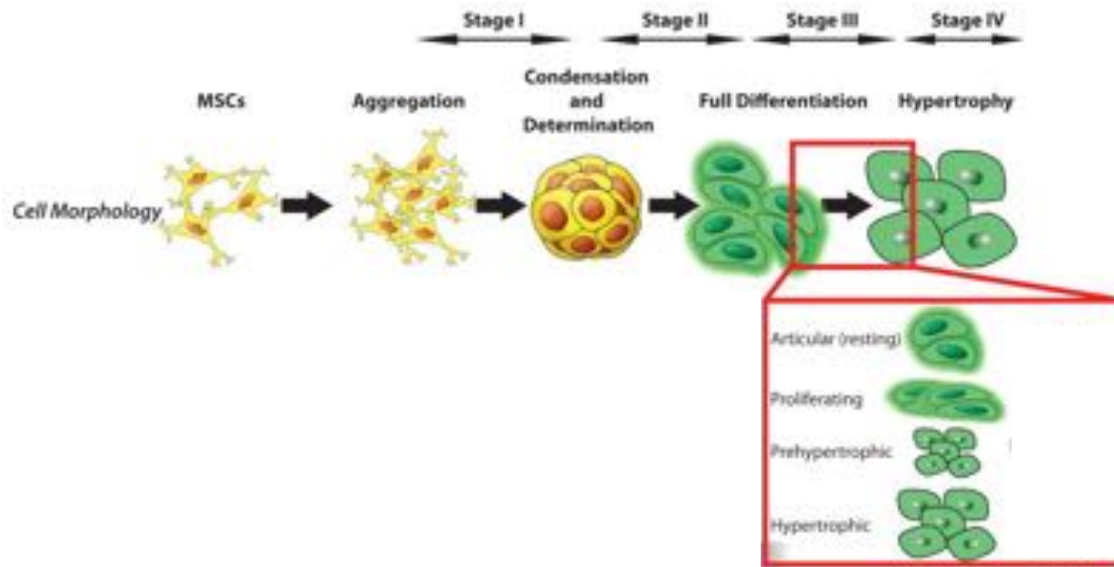


Figure 1: Sequence of events during chondrogenesis. Committed mesenchymal stem cells (MSCs) condense and differentiate into chondrocytes at the site of the future bone to form a hyaline cartilage model. Proliferating chondrocytes secrete a cartilage-specific extracellular matrix, reach full differentiation and become hypertrophic chondrocytes. Adapted from Gadjanski *et al.*, 2012 [6].

Cells that are destined for chondrocytic differentiation are organized in morphologically defined zones in the growth plate which reflect changes in their functional state [10] (Figure 2). The cells start in their undifferentiated form in the distal epiphyseal end of the growth plate, known as the resting zone [10, 11]. As they undergo chondrogenic differentiation, they move towards the proliferating zone where they flatten as they are packed into multicellular clusters [6, 10]. Differentiated chondrocytes initiate active secretion of cartilaginous matrix and progressively enlarge as they hypertrophy and mature towards the hypertrophic zone. Hypertrophic chondrocytes increase their volume dramatically while simultaneously secreting cartilage-specific ECM [12]. Eventually, the enlarged cells undergo apoptosis, and as they do so, the cartilage matrix surrounding them is degraded. This deterioration allows the entry of blood vessels and cells surrounding the cartilage model in the ossification zone [13]. Some MSCs differentiate into osteoblasts and begin the formation of bone matrix on the cartilage [12, 14].

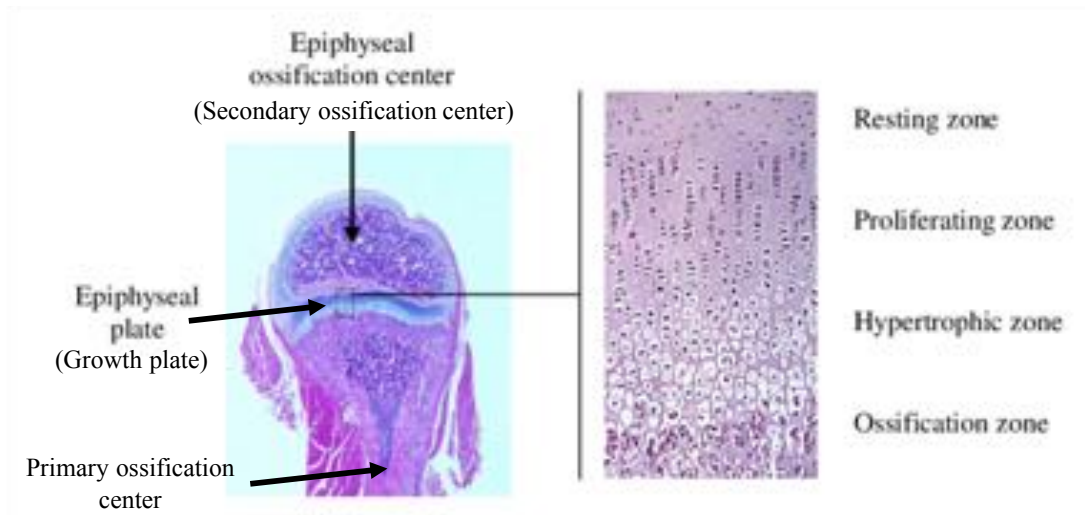


Figure 2: Zones of cartilage proliferation in the growth plate. Undifferentiated cells start in the resting zone in the distal epiphyseal end of the growth plate. They then move towards the proliferating zone as they differentiate into chondrocytes and begin secreting cartilaginous matrix. Differentiated chondrocytes progressively enlarge and become more rounded as they move towards the hypertrophic zone. Hypertrophic chondrocytes undergo apoptosis, leaving cavities in the cartilage matrix, and allowing the entry of blood vessels and osteogenic cells in the ossification zone. Adapted from Bleumink *et al.*, 2004 [15].

These events undergo multiple transcriptional, epigenetic, and hormonal regulation which can influence the fate of the cells, their proliferation, morphology and organization. In fact, depending on how they are regulated, various signaling pathways can either promote or delay chondrogenesis and osteogenesis.

1.1.2 Mesenchymal Stem Cell Condensation

Condensation of MSCs is required for successful chondrogenic differentiation [16]. It involves the movement of cells and the formation of aggregates. In the first steps, MSCs are found in a matrix rich in fibronectin (FN), collagen type I, hyaluronan (HA) and the proteoglycan versican [17, 18]. Studies have indicated that transforming growth factor- β (TGF- β) and Wnt/ β -catenin signaling govern this process [19, 20].

The clustering of cells requires cell-cell interactions facilitated by cell adhesion molecules. The most upregulated cell-cell adhesion proteins found in condensing cells are N-cadherin and neural cell adhesion molecule (N-CAM) [17]. It has been suggested that N-cadherin initiates the condensation, and N-CAM maintains it [21]. Preventing these molecules from having homotypic interactions reduces condensation [17, 22]. Cadherins are anchored to the actin cytoskeleton through complexes involving β -catenin, a molecule downstream of the Wnt signaling pathway. The high expression of β -catenin and N-cadherin during condensation suggests the importance of Wnt signaling in this process [23]. In fact, the absence of Wnt signaling in this stage results in craniofacial deformities in vertebrates [19]. Bone morphogenic proteins (BMPs) have also been shown to be involved in all phases of chondrogenesis, but they especially play a key role in the aggregation of chondroprogenitor cells into a single distinct cluster [24].

The formation of tight aggregates is associated with an increase in hyaluronidase activity. The degradation of HA in the surrounding matrix decreases cell movement and allows for close cell-cell interactions [6]. FN in the ECM is also necessary for the stabilization of mesenchymal-endothelial junctions [25]. Prior to cell condensation, FN is assembled into a fibrillary matrix, providing a scaffold in which cells can associate with collagens and other ECM proteins [26, 27]. The knockdown of FN or the inhibition of FN matrix assembly blocks cell condensation. Studies have suggested that TGF- β stimulates FN synthesis during this stage [20, 28].

SRY-Box 9 (Sox9), a prochondrogenic factor, is stated to be the most important regulator of chondrogenesis and is thought to be the earliest marker of chondrogenesis. Sox9 expression levels begin increasing in condensing MSCs, both *in vitro* and *in vivo*, and reaches high levels during chondrogenesis [29, 30]. Knocking out the *Sox9* gene in mice resulted in the inability of their MSCs to condense [31, 32]. In humans, mutations in the gene cause campomelic dysplasia, a skeletal disorder where most affected patients die in infancy from respiratory failure caused by inadequate cartilage formation in the trachea and ribs [33].

1.1.3 Chondrocyte differentiation and proliferation

Once condensed, MSC aggregates begin differentiating and initiate the production of cartilaginous ECM.

Sonic hedgehog (SHH) signaling works with the BMP pathway in determining cell fate in early chondrogenesis. SHH expression regulates the synthesis of certain members of the BMP family including BMP2, BMP4, and BMP7 [34]. Together, SHH and BMP enhance Sox9 expression by establishing a positive regulatory loop with Sox9 and the transcription factor Nkx3.2. As a result, Sox9 is able to potentiate BMP2's prochondrogenic properties [35, 36]. Sox5 and Sox6 also enhance Sox9's function. Sox5/6/9 form the Sox trio. This trio controls early chondrogenic differentiation through the interaction with other prochondrogenic factors, and maintains the chondrocyte phenotype at later stages [37]. They directly regulate expression of many genes and ECM molecules by activating elements in the promoters of type II, type IX, type X and type XI collagens, as well as proteoglycans such as aggrecan [30].

SHH and BMP signaling also significantly enhance chondrogenesis in the presence of fibroblast growth factors (FGFs), a family of cell signaling proteins [36]. Both FGF2 and FGF9 upregulate Sox9 expression levels [38]. FGF9 also increases expression of Indian hedgehog (IHH), another mammalian hedgehog family of proteins, and type II collagen, resulting in early chondrogenic differentiation and an increase of ECM production. At later stages, FGF9 regulates chondrocyte hypertrophy [39, 40]. FGF2 is mostly involved in the early stages of chondrogenesis by preparing MSCs for chondrocyte differentiation [39]. It also enhances cell proliferation speed by amplifying TGF- β expression [41].

There is an important switch that occurs from Wnt-mediated signaling during condensation to TGF- β signaling during differentiation [36, 42]. Sox9 targets Wnt/ β -catenin promoters for degradation via the ubiquitination/proteasome system [43]. Meanwhile, TGF- β activates mitogen activated protein kinase (MAPK) proteins p38, ERK and JNK in MSCs which also inhibits Wnt signaling. This leads to the downregulation of N-cadherin expression, allowing cells to progress from condensation to differentiation and proliferation [36, 42, 44].

The matrix deposited by differentiated chondrocytes is rich in Sox9, collagens type II and IX, and aggrecan (Acan), a non-collagenous matrix protein [45]. This matrix provides the optimal stiffness for chondrocyte differentiation. Allen *et al.* suggested that the stiffness of the ECM primes TGF- β to efficiently activate Smad-dependent signaling pathways in cells, including Smad2/3 and Smad1/5/8, which have a stimulatory effect on chondrogenic differentiation [46, 47]. This has been shown through *in vitro* experiments in which Smad3 phosphorylation and transcriptional activity are specifically increased in cells grown on 0.5-megapascal (MPa) substrates, the stiffness of the secreted ECM [46]. In contrast, the continued TGF- β -mediated SMAD1/5/8 signaling that leads to cartilage hypertrophy is counterbalanced by epigenetic signaling. Histone deacetylases (HDACs) such as HDAC4 modulates TGF- β 1 activity and inhibits progression to osteogenesis [36, 48].

Once the cells reach differentiation, they can either continue to proliferate and maintain a cartilaginous structure and function, or undergo chondrocyte hypertrophy.

1.1.4 Chondrocyte terminal differentiation and hypertrophy

The largest proliferating cells eventually lose their ability to divide and terminally differentiate into hypertrophic chondrocytes [13]. Since differentiated chondrocytes can follow two fates, opposing signaling pathways come into play to favor either chondrogenesis or osteogenesis.

IHH, synthesized by pre-hypertrophic chondrocytes, regulates both chondrogenesis and ossification by coupling the two processes through signaling pathways involving chondrocytes and pre-osteoblasts [49]. Disruption of IHH signaling has been shown to result in reduced longitudinal bone growth, and mutations in the *IHH* gene leads to a condition involving the shortening or absence of phalanges known as brachydactyly type A-1 [50].

To follow the chondrogenic fate, IHH stimulates and maintains parathyroid hormone (PTH) and parathyroid hormone-related peptide (PTHrP) [51]. These peptide hormones

maintain chondrocytes in a proliferative state and prevents them from transitioning to a hypertrophic state [52-54]. They are expressed by early proliferating chondrocytes and diffuse to act on G-coupled PTH/PTHrP receptors on cells. These receptors are expressed at low levels by proliferating chondrocytes, but at higher levels in non-proliferating cells [53]. PTH/PTHrP thus negatively regulates its own expression and controls the rate of chondrocyte differentiation. The cells farther from the site of PTH/PTHrP production will be able to escape and undergo early stages of hypertrophy [51]. Absent or defective PTH/PTHrP receptors can lead to Bloomstrand chondrodysplasia, a skeletal condition characterized by short limbs due to premature ossification [51]. In contrast, constitutive activation of the receptor is found in Jansen-type metaphyseal dysplasia, also characterized by short limbs, but is associated with delayed chondrocyte hypertrophy [55]. PTHrP activates Sox9 and inhibits Runt-related transcription factor 2 (Runx2), a transcription factor known to stimulate osteogenesis. Sox9 also depresses the expression of other hypertrophic factors including osterix, collagen type I alpha 1 (Col1a1), and collagen type X alpha 1 (Col10a1) [56-58]. These actions help mediate the effect of PTHrP to delay chondrocyte hypertrophy [59]. Pre-hypertrophic chondrocytes that manage to escape from PTH/PTHrP signaling synthesize IHH which feeds back and maintains PTH/PTHrP production [51]. The level of IHH and PTHrP signaling regulates and determines the zones of proliferation and hypertrophy during bone formation [51, 60, 61].

To follow the osteogenesis pathway, IHH crosstalks with other signaling mechanisms such as Wnt, FGF, SHH and BMP [62, 63]. Wnt is among the earliest signals required, occurring upstream of IHH in the late proliferative zone [64, 65]. The effect of Wnt expression is highly sensitive and localized, and can vary based on the proliferating cell type. For example, activation of β -catenin in immature chondrocytes suppresses hypertrophy, but its expression in mature chondrocytes promotes it. During terminal differentiation, Wnt9a induces IHH expression through the direct interaction with the IHH promoter by its effector β -catenin/Lef1 complex [65, 66]. Wnt induces the production of FGFs as well, which also acts upstream of IHH signaling. FGF signaling accelerates terminal differentiation by activation of the FGF3 receptor expressed in proliferating and early hypertrophic chondrocytes [60]. Mutations in FGF3 receptor that leads to constitutive activation of the receptor results in dwarfism in humans due to premature closure of the growth plates [67].

The effects of IHH and FGF activation are opposed by BMP signaling [60, 63]. BMP signaling increases the rate of proliferation by inducing the expression of IHH in cells that escape from the range of PTHrP signaling [68, 69]. Further, Minina et al. found that blocking BMP signals results in a phenotype similar to that of FGF2 treatment [70]. The balance between these signaling pathways adjusts the speed and pace of differentiation.

Many changes occur in the cells, including their morphology and the matrix proteins they secrete. At this phase, hypertrophic cells begin to secrete a matrix rich in non-fibrillar Col10a1 and alkaline phosphatase (ALP), in contrast to proliferating chondrocytes which produce mostly type II collagen (Col2a1) [12, 71]. They also secrete vesicles into the ECM containing enzymes that contribute to the generation of calcium and phosphate ions. These components initiate the mineralization process of the cartilaginous matrix surrounding late hypertrophic chondrocytes [14, 72].

Hypertrophic cells also express terminal differentiation genes which influence mineralization, including the endopeptidase matrix metalloproteinase-13 (MMP13), Runx2 and Runx3 [73, 74]. Studies have shown that the degradation of Col2a1 exposes a cryptic peptide which induces hypertrophy and the expression of MMP13 [74]. Additionally, Runx2 expression, aided by Runx3, promotes the full progression into terminal hypertrophic differentiation through the direct regulation of Col10a1, and the stimulation of IHH expression [49, 73]. Pro-chondrogenic factor Sox9 is downregulated by Runx2 at this stage, but Acan continues to be expressed during hypertrophy [30, 75].

1.1.5 Vascular invasion and Ossification

Enlarged hypertrophic chondrocytes eventually undergo apoptosis. This cell death leaves cavities in the cartilaginous matrix which becomes the bone marrow [76]. Blood vessels penetrate the resulting spaces, an event termed vascular invasion. This invasion also allows the entry of osteogenic cells which become osteoblasts and form the primary ossification center. This stage initiates the replacement of cartilage with bone [4].

Hypertrophic chondrocytes and osteoblastic cells produce several angiogenesis activators such as vascular endothelial factor (VEGF) and FGF [77, 78]. In contrast, cells in the resting and proliferating zones express inhibitors of angiogenesis [79]. This angiogenic switch therefore seems to rely on a balance between the levels of activators and inhibitors at the vascularization front. Runx2's increased expression in hypertrophic chondrocytes enhances VEGF and FGF18 expression which promotes osteogenesis by inhibiting chondrocyte hypertrophy. FGF9 expression also encourages the vascularization of the growth plate prior to osteogenesis [80-82].

Moreover, proteolysis of the ECM releases factors that initiate angiogenesis. One of these are MMPs such as MMP13 which further degrade a range of ECM proteins including fibrillary collagens, FN, Acan, and proteoglycans [83]. Its expression is regulated through transcriptional control and by tissue inhibitors of metalloproteinases (TIMPs) [79, 84]. The balance between MMP and TIMP concentrations is in fact a major initiating factor for angiogenesis. TIMP expression is highest in the resting and proliferating zones, whereas MMP expression is highest in hypertrophic cartilage [85]. Absence of MMP13 results in a growth defect known as Missouri type spondyloepimetaphyseal dysplasia [86].

The differentiating osteoblasts use the remainders of the cartilage matrix as a scaffold for the deposition of bone matrix [14]. Most of the cartilage in the primary ossification center is replaced with bone by the time the fetal skeleton is fully formed. After birth, a similar process occurs in the secondary ossification centers in the epiphyseal regions [1]. In the growth plate, as the chondrocytes proliferate before undergoing hypertrophy, they push the ossification zone farther outward, allowing the remaining cartilage cells to proliferate. This results in the elongation of bone [14]. As long as the growth plates are able to produce chondrocytes, the bone continues to grow.

At puberty, the ossification front meets the growth plate, resulting in the fusion of the bone formed from the two ossification centers. The only remaining cartilage at this stage is the permanent articular cartilage at the joint surface [14]. Bone remodeling occurs throughout adult life.

1.2 SPONDYLOMETAPHYSEAL DYSPLASIAS

The development of the mammalian skeleton is a highly-regulated process in which perturbations in any of the signaling pathways or dysregulation of ECM proteins can lead to abnormal bone development. A few skeletal diseases were mentioned in the overview of endochondral bone formation, but many more have been observed, including rare bone diseases that start during infancy. One such disease is spondylometaphyseal dysplasias (SMDs).

SMDs are a heterogeneous group of rare skeletal disorders with an estimated prevalence of 1/1,000,000 [87]. It was first defined by Kozlowski in 1967 with primary involvement of the spine and metaphyseal centers [88]. ‘Dysplasia’ refers to abnormal growth, ‘spondylo’ refers to spine and ‘metaphyseal’ refers to the metaphysis [89]. The general characteristics observed in patients with this disease are short stature, short trunk, vertebral anomalies such as scoliosis or platyspondyly (flattened vertebrae), as well as striking metaphyseal alterations of the tubular bones [90].

According to the last Nosology and classification of genetic skeletal disorders from 2015, which provides a list of all reported genetic skeletal disorders, SMDs include eight disorders [91] (Table I). The identification of the different subtypes of SMDs first takes into consideration the properties of the bones involved, the pattern of inheritance, and the clinical features [92]. They are then further classified according to the localization and severity of the affected metaphyses, and other associated symptoms of the disease. For example, in patients with Kozlowski type, the most common form of SMD, patients were reported to suffer from severe kyphoscoliosis, a deformity of the spine in which there is excessive forward rounding of the back and abnormal curvature of the spine to the side, as well as a large delay in the ossification of bones [88], while patients with SMD Sedaghatian type presents with lace-like appearance of the iliac crests during the neonatal period. [93] Further, individuals affected with SMD with retinal degeneration, axial type, report early and progressive vision loss, in contrast with SMD with cone-rod dystrophy in which patients also have ophthalmological anomalies such as retinal cone-rod dystrophy, but manifests less severely than axial-type [93, 94].

Table I. Types of Spondylometaphyseal Dysplasias (SMDs).

Disorders that are part of the SMD group of skeletal dysplasias according to the Nosology and classification of genetic skeletal disorders from 2015 [91].

Spondylometaphyseal Dysplasia	OMIM #	Gene
Kozlowski	184252	<i>TRPV4</i>
Sedaghatian	250220	<i>GPX4</i>
Severe SMD (Sedaghatian-like)	None	<i>SBDS</i>
Odontochondrodysplasia (ODCD)	184260	None
SMD with cone-rod dystrophy	608940	<i>PCYT1A</i>
SMD with retinal degeneration, axial type	602271	None
Spondyloenchondrodysplasia (SPENCD)	271550	<i>ACP5</i>
Sutcliffe-type	184255	None

My project will focus on Sutcliffe-type SMD. For a long time, this rare form of SMD escaped molecular diagnosis, but recently, advances in sequencing technologies allowed the identification of mutations in patients affected with this disease.

1.2.1 Sutcliffe-type SMD

Sutcliffe-type SMD is a rare autosomal dominant skeletal disorder [95]. It is also known as “SMD with corner fractures” (SMD-CF) due to the observation of small triangular bone fragments that look like fractures at the edge of the metaphyses of long bones [96]. The prevalence of this disease is < 1:1,000,000 [95]. The first cases were reported in 1965 by Dr. John Sutcliffe in Africa [97], and thereafter, only a handful of cases were published by various groups, leading to a total of less than 30 affected patients reported so far in the literature [96-107].

1.2.1.1 Clinical characteristics

The main clinical phenotypes seen in patients affected by this type of SMD is short stature and a waddling gait, as well as several radiographic features (Figure 3) [105].

One of the observed imaging features in the spine are oval vertebral bodies. In early infancy, cervical vertebral bodies have an oval shape, and in physiological cases, these bodies take on a rectangular appearance as the child grows [108]. In Sutcliffe-type SMD, however, the oval shape is conserved in the first few years of life and creates an appearance of anterior wedging [97, 109] (Figure 3B). There is also an observed underdevelopment or absence of ossification of the odontoid process, a growth that projects from the second cervical vertebra and serves to support the rotation of the head [101]. Most individuals with odontoid hypoplasia are asymptomatic. These spinal anomalies therefore require careful examination as they tend to be overlooked [110].

The most prominent feature is developmental bilateral coxa vara, a deformity of the hip resulting in shortened legs and a waddling gait [111] (Figure 3C). The radiographic appearance of this condition is usually detected only following the observance of a waddling gait as it is not noticeable until the child starts walking, between two and six years old [96]. In normal cases, the angle between the head and the shaft of the femur is between 135-145 degrees in children [111]. In patients with coxa vara, this angle is reduced to less than 110 degrees, or in more severe cases, less than 90 degrees [96].

Another radiographic characteristic are metaphyseal plate irregularities at the end of long bones with corner fractures [100]. The corner fractures are not real fractures as the name might imply. Instead, they simulate fractures, presenting as small triangular fragments at the edges of the metaphyses next to the growth plates (Figure 3D). It is usually already apparent when coxa vara is identified. These fracture-like lesions are commonly only observed in early development, as they tend to disappear as the bone matures [101]. Although the name of the disease is “SMD with corner fractures”, it is important to note that corner fractures are not a diagnostic feature of Sutcliffe-type SMDs as it also occurs in other bone disorders. Rather, metaphyseal abnormalities implicating progressive bilateral coxa vara constitute the most important radiological sign for the diagnosis of Sutcliffe-type SMD [112]. In contrast to the other SMDs, there is usually absence of flattened vertebral bodies and kyphoscoliosis, a spinal abnormality in which the spine curves on both the coronal and saggital plane, in Sutcliffe-type SMD [109].

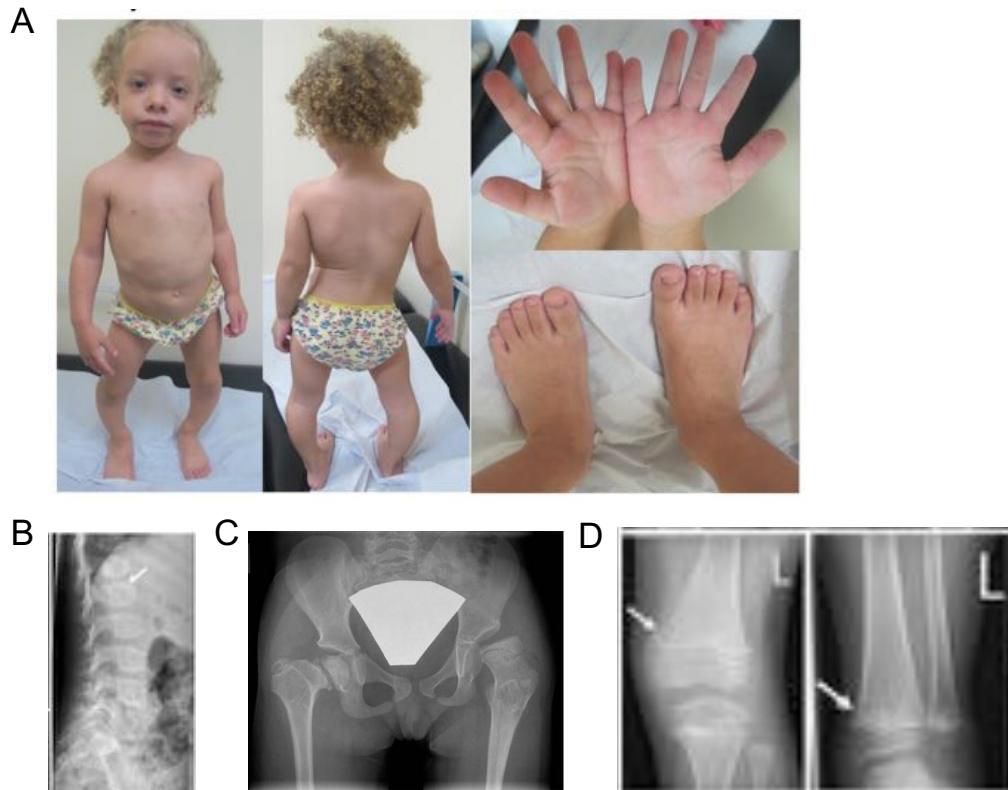


Figure 3: Clinical features of patients with SMD with corner fractures. (A) Affected child with scoliosis and genu varum. Normal hands and feet. (B) Image of the spine showing oval vertebral bodies. (C) Radiograph of pelvis and hips showing coxa vara. (D) Arrows indicate corner fractures. Images from Lee et al., 2017 [106].

1.2.1.2 Challenges in Diagnosis

Some of the clinical features mentioned can be detected in other conditions which results in many differential diagnosis for Sutcliffe-type SMD. For example, corner fractures are also reported in other bone disorders such as metaphyseal chondrodysplasia and Strudwick type spondyloepimetaphyseal dysplasia (SEMD) [101, 103], and in non-skeletal diseases including abused child syndrome, scurvy, Menkes kinky hair syndrome, Blount's disease, rickets and congenital contractures [113]. Similarly, coxa vara has been observed in developmental diseases such as cleidocranial dysostosis [114], and as a symptom of other bone diseases as seen in osteogenesis imperfecta and Paget's disease [115, 116].

Another source of challenge for the diagnosis of SMD is that the overall symptoms can change depending on the patient's age. Indeed, upon reaching skeletal maturity, corner fractures disappear in radiographs of affected patients [88]. There is also a large clinical overlap between Sutcliffe-type and the other types of SMDs. To give an example, Kozłowski type SMD frequently manifests with coxa vara, but no corner fractures [117]. Rather, there is presence of kyphoscoliosis and marked flattened vertebrae in affected patients [118]. This highlights the importance of considering all phenotypic manifestations of the disease during diagnosis as each characteristic have their own distinct clinical history and their own set of radiological findings.

Furthermore, variations in the symptoms between patients with Sutcliffe-type SMD can occur. One of Machol et al.'s patients with Sutcliffe-type, for example, did not present with apparent femoral neck irregularity [104], and one of Langer et al.'s patients had unilateral coxa vara instead of bilateral [96]. It may therefore be possible that the clinical spectrum for this disorder is wider than initially thought. Another explanation would be that these researchers encountered a different form of SMD. Sutton et al. identified patients with all of the phenotypes associated with SMD-corner fracture type, but with the absence of coxa vara and the presence of congenital scoliosis which is not usually seen in this subtype [102]. The phenotypic variability and the rarity of these disorders make it challenging to correctly diagnose this specific disease.

1.2.1.3 Treatment

The general outlook for individuals affected by SMDs depend on the extent of the bone deformities. Severe abnormalities usually result in considerable disability especially since metaphyseal irregularities and coxa vara are progressive [97]. There is currently no cure for SMDs, only surgical correction of the bone deformities. When diagnosed early, surgery can improve the outlook for patients with hip deformities [119], and the use of braces can help by relieving the vertebrae from persistent forces [120]. Other symptoms associated with SMDs such as ophthalmological anomalies or breathing difficulties are managed individually by different specialists.

1.2.1.4 Pathogenesis

The pathogenesis of SMD-CF was until recently largely unknown. Most of the affected individuals were published as case reports with no clear evidence on the cause of the disease. Pedigrees of affected patients and their families showed that the disease can be inherited or appear de novo. Mutations in the *COL2A1* gene have been identified in three patients affected with SMD-CF [103, 104]. Mutations in these genes were initially discovered in SEMD Strudwick type, a type II collagenopathy disorder which shares many similar phenotypes to SMD-CF including corner fractures and metaphyseal abnormalities [121]. The clinical overlap is significant enough that these *COL2A1* patients could be considered a part of the SEMD group [103, 104].

In 2017, novel mutations in the *FNI* gene of affected individuals have been identified by our group [106]. No skeletal disorder had been associated with this gene prior to the identification of mutations in patients with SMD-CF.

1.3 FIBRONECTIN

Fibronectin (FN) is a large dimeric glycoprotein that is widely distributed in the body. It is encoded by the *FNI* gene, a large gene of around 75kb located at the chromosomal position 2q35 [122]. It is well proven in the literature that FN plays many key roles throughout development such as heart formation and wound healing, and that it is involved in the ECM as well as in many basic biological functions including cell migration, adhesion, growth and differentiation [122-127]. All of these functions hint at its crucial role in vertebrate development. To support this, experiments have shown that genetically modified mice lacking fibronectin died at embryonic day 9 [126].

1.3.1 Structure

1.3.1.1 Basic structure

FN structure is widely represented as a beads-on-a-string model. It mainly exists as a ~500 kDa dimeric glycoprotein with each monomer measuring approximately 240 kDa subunits, and consists of three different repeating modules: twelve type I, two type II and 15-17 type III repeats [128] (Figure 4A). The number of type III repeats vary due to the presence of extra-domain repeats EIIIA (EDA) and EIIIB (EDB) which are alternatively spliced [124, 129]. These three modules account for 90% of the sequence while the other 10% is composed of flexible connector sequences between repeats known as type III connector segments (IIICS) and a variable (V) region [122, 130]. Due to the observation that the three modules have also been found in other molecules, it has been suggested that *FNI* evolved through exon shuffling, a process through which exons from different genes are brought together to form a new gene [131]. At the C-terminal of each FN subunit, there are two disulfide bonds which maintains the FN as a dimer when it is secreted [132]. This covalent bond is required for FN matrix assembly as studies have found that monomeric FN cannot form fibrils, nor interact with other FN molecules [133].

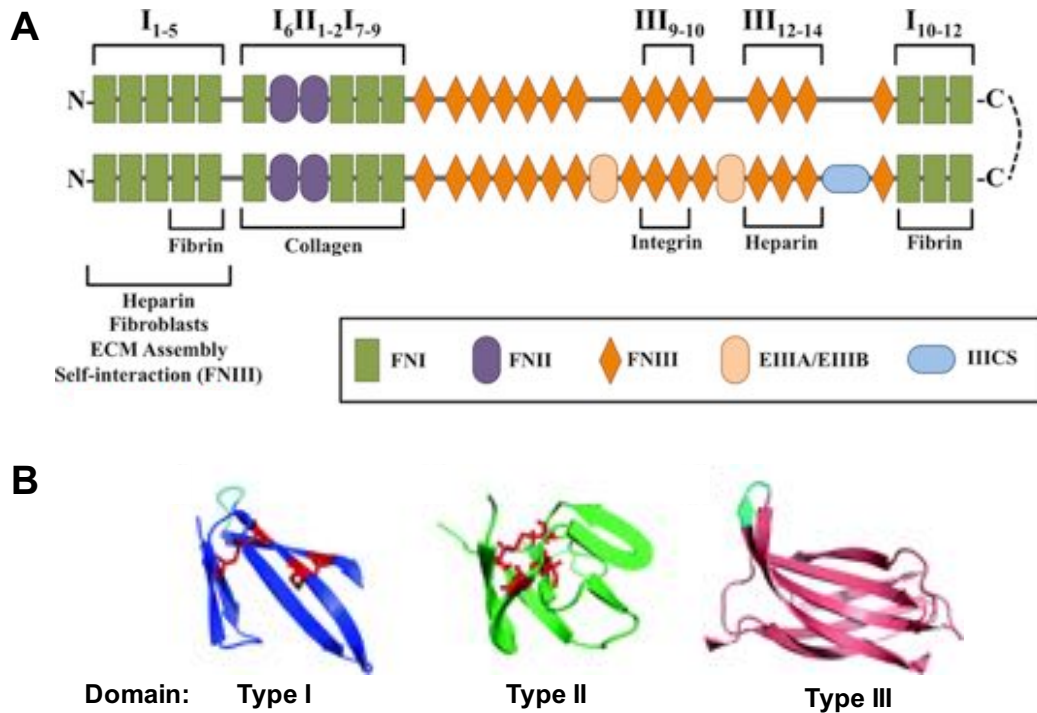


Figure 4: Structure of Fibronectin. (A) Schematic diagram of a fibronectin heterodimer protein connected by disulphide bonds at the C-terminus. Each monomer consists of 12 type I repeats (FNI), 2 type II repeats (FNII), and 15-17 type III repeats (FNIII). The bottom branch of the dimer includes the extra-domain repeat A and/or B (EIIIA/EIIIB), as well as the connecting segment (IIICS). The variable region is not shown in this diagram. The repeats are numbered on top of the diagram and functional domains are described on the bottom. Adapted from Hymes et al., 2016 [134]. (B) Ribbon diagrams of the three fibronectin modules. FN type I and type II domains show the cysteine residues and disulfide bonds in red. FN type III shows the Arg-Gly-Asp (RGD) binding motif in green. Image from Xu et al., 2011 [135].

Each type I module is about 45 amino acid residues long and contains stacked β -sheets linked by two intrachain disulfide bonds [129]. The β -sheets surround a hydrophobic core that contains highly conserved aromatic amino acid residues [129] (Figure 4B). Similarly, type II modules which are around 60 residues in length, also contain two intrachain disulfide bonds in each repeat, several highly conserved aromatic residues, and two double-stranded anti-parallel β -sheets perpendicular to each other [136]. Type III modules, on the other hand, are 90 residues long and lack disulfide bonds. Instead, they contain two anti-parallel β -sheets formed by seven β -strands which are connected by flexible loops [129, 137].

1.3.1.2 Functional domains

To perform its many roles, FN contains several functional domains that allow it to bind to other cells, and to interact with proteins such as collagen, heparin sulfate, fibrin, as well as to itself [129]. These functional domains are composed of the different modules (Figure 4A).

Fibrin-binding domains

Fibrin is an ECM component that plays a role in wound healing through its interaction with fibroblasts. Fibroblast adhesion to fibrin requires FN [138]. There are three fibrin-binding domains in FN. Two sites are in the type I module: one is at the N-terminal which is the major site, and another is close to the C-terminus [139, 140]. The third site is adjacent to the collagen-binding domain which is only revealed after the breakdown of FN by chymotrypsin, a digestive enzyme [136]. Studies have found that the removal of any of the type I modules in the N-terminal end is enough to reduce FN binding, incorporation in the ECM, and fibrillogenesis [107, 141]. At physiological temperatures, FN-fibrin interaction is very weak. Factor XIII transglutaminase, an enzyme that circulates in the plasma, stabilizes this interaction and helps incorporate FN into the fibrin clot [136, 142].

Collagen-binding domains

Within the 70 kDa fragment of the N-terminal domain, there is a 40 kDa collagen/gelatin binding domain located in the type I (repeats I₆₋₉) and II (repeats II₁₋₂) modules [26]. Collagen's interaction with FN is crucial in the proper assembly and organization of type I and type III collagen fibrils [130, 143, 144]. Two types of interactions between FN and collagen are thought to take place in *in vivo* collagen fibrillogenesis: the first is the binding of collagen molecules to a polymerized FN fibril, and the second is the association of FN molecules with sites displayed on hydroxylated and polymerized collagen fibrils [130]. FN binds to denatured collagen, also known as gelatin, more strongly than native collagen [145]. This property allowed the development of methods such as gelatin affinity chromatography using gelatin sepharose beads as a simple way to purify FN [146].

Integrin-binding domains

Integrins are heterodimeric cell-surface receptors with α and β subunits that interact with ECM glycoproteins [147]. FN-integrin interactions is critical for ECM assembly as it promotes many processes such as the unfolding of FN and cytoskeleton reorganization [148]. The importance of these processes will become evident when we discuss the steps of ECM assembly. The major binding domain that allows FN to interact with integrins is the Arg-Gly-Asp (RGD) sequence, contained in the type III module. Many integrins, including $\alpha 3\beta 1$, $\alpha 5\beta 1$, $\alpha 8\beta 1$, $\alpha v\beta 1$, $\alpha IIb\beta 3$, $\alpha v\beta 3$, $\alpha v\beta 5$, and $\alpha v\beta 6$ also bind to this motif [149, 150]. This RGD sequence was shown to be essential for normal development as the cell can lose up to 95% of its cell adhesion function when mutating parts of this sequence [127, 136, 151]. Animal models of mice in which the aspartic acid residue (D) was replaced with a glutamate (E) to generate a non-functional RGE motif showed that these genetically modified mice died at embryonic day 10 with multiple organ abnormalities. Surprisingly however, these mice had a normal FN matrix assembly suggesting that the RGD sequence was not absolutely necessary for fibril assembly. This was shown to be likely possible due to additional integrin-binding sites on FN [152].

Other motifs include the Gly-Asn-Gly-Arg-Gly (GNRGRG) motif in the type I FN_{I1-5} module, the Ile-Gly-Asp (IGD) sequence in FN_{I9}, Leu-Asp-Val (LDV) and REDV sequence located within the V region, the IDAPS and KLDAPT sequences in the type III module, and the EDGIHEL sequence in the EDA module [122, 124, 153-155]. These different cell recognition sequences can bind to different integrins.

Heparin-binding domains

FN interacts with high affinity to heparin sulfate proteoglycans (HSPGs). HSPGs are glycoproteins found at the cell surface and in the ECM. They play a role in cell migration and in cell-ECM attachment [156]. FN contains at least two heparin-binding domains with the strongest site located the C-terminus of the type III module, and the weaker site in the N-terminus of type I module [139, 157]. Additional sites have also been identified in the V region [158]. Mutations in heparin-binding domains can lead to lower binding to heparin which can affect cell spreading and the reorganization of the cytoskeleton [159]. These alterations were found in diseases such as glomulopathy with fibronectin deposits, a kidney disease in which FN accumulates in the glomeruli [159, 160].

Self-interaction domain

In ECM assembly, individual FN dimers come together to form fibrils. This occurs through self-association sites on the FN molecule [161]. Exposed sites that are available for binding are on the N-terminal portion of the molecule in the type I module FN_{I1-5}. One self-interaction site can have more than one FN bound to it [128]. Through this property, many different alignments of dimers can occur within the fibrils, generating a three-dimensional matrix appropriate for the function of the tissue [162]. Cryptic self-interaction domains are located along the protein (FN_{III1-2}, FN_{III4-5}, and FN_{III12-14}), and only become accessible after conformational changes such as the stretching of the FN molecule during self-assembly [122]. These cryptic binding sequences are highly effective in regulating and forming FN-FN

interactions. The peptide sequence FNIII₁ can stimulate the formation of a “superfibronectin”, a high molecular weight structure that crosslinks aggregates of FN [124].

1.3.2 Heterogeneity of *FN1*

1.3.2.1 Alternative splicing

Alternative splicing is a process that allows a gene to produce multiple isoforms of a protein by including or excluding certain exons [163]. Three regions are prone to alternative pre-mRNA splicing of FN: the V, EDA, and EDB regions [164]. Compared to the EDA and EDB regions which are either wholly included or excluded from the mRNA by exon skipping, the splicing pattern of the V region can be fully or only partially included [164, 165]. In humans, alternative splicing results in five different V region variants ranging between 0-120 amino acids: V0, V64, V89, V95, and V120 [129]. In total, 20 different versions of the protein can be generated exclusively from the random assortment of the EDA, EDB and V regions [124], but many additional isoforms can be produced from different versions of homodimers and heterodimers [130, 163, 166, 167].

Alternative splicing is regulated by cell type, age, and stage of development [136]. Two forms of FN exist: plasma FN and cellular FN. Plasma FN derived from hepatocytes almost always lacks the EDA and EDB sequences but contains the subunit V0. Cellular FN, on the other hand, is composed of variable proportions of EDA, EDB and V region isoforms [164]. It was also observed that during embryonic development, many alternatively spliced regions are included in FN, but this number gradually decreases with aging [168]. However, specific events in adulthood can re-establish this embryonic splicing pattern such as wound healing. During tissue repair, some isoforms of FN, especially those containing the EDA and EDB modules are upregulated in cells at the base of the wound site [169].

The expression of all the different isoforms is not required for normal functioning. The V region was shown to be important for FN secretion and integrin-binding, making it critical

for survival, but absence of the EDA and EDB modules does not affect viability nor fertility [123, 128]. However, the EDA module plays an important role for a normal life span and wound healing as it enhances the interaction between the RGD motif and the $\alpha 5\beta 1$ integrin [170]. To support this, an experiment by Muro et al. has shown that genetically modified mice lacking the EDA region developed normally, but with abnormal skin healing and a shorter life span [170]. EDB-knockout mice also developed normally, but with reduced cell growth and FN matrix assembly [171]. With these findings, it was suggested that exons EDA and EDB are not critical for matrix assembly, but can affect matrix levels [128].

In cartilage, another type of splicing exists in which the entire V region along with the FNI₁₀ and FNIII₁₅ repeats are absent. This isoform can exist both as a homodimer and as a monomer [122]. In addition, FN isoforms are expressed in a characteristic manner during chondrocyte maturation. During condensation, the presence of the EDA region is required, but during chondrocyte commitment and maturation, FN isoforms that include the EDB but exclude the EDA domain are favored [172, 173]. In osteoblasts, the inclusion of both EDA and EDB are preferred [174]. These two extra binding domains play a role in osteoblast differentiation in which the EDA-containing isoform activates the $\alpha 4\beta 1$ integrin, and the EDB-containing isoform enhances the binding of FN to $\beta 3$ -containing integrin through the RGD sequence. These associations result in increased mineralization [175].

1.3.2.2 Post-translational modifications

FN can be glycosylated, phosphorylated, and sulfated, resulting in the differences seen between plasma FN and cellular FN within and between species. FN is processed and terminally glycosylated in the Golgi apparatus [176]. Differences in molecular weight of 10-20 kDa between FN from different human tissues have been attributed to increased addition of sugars [177]. It was suggested that this modification stabilizes FN against hydrolysis and regulates its binding affinity to other proteins [136]. Glycosylation can also occur in disease states. Oncofetal FN (onfFN) is a form of FN synthesized by fetal tissue such as placenta or by tumours. Researchers have therefore suggested that the presence of onfFN in adults can act as a disease

marker. This form is defined by the presence of an O-glycosylation site in the V region, and is associated with a decrease in the number of osteoblasts and bone formation *in vivo*, as well as a decrease in osteoblast mineralization *in vitro* [174].

FN has a highly conserved protein structure. This is not surprising as it is involved in most of the basic cellular functions such as cell adhesion and migration. This conservation is reflected by modifications on the protein such as phosphorylation which only occurs on a limited number of serine sites, and sulfation which is mostly observed on tyrosine residues [129, 178]. It has also been shown that FN that is secreted by actively growing cells exhibits a significantly higher level of phosphorylation than FN secreted by quiescent cells, demonstrating a specific pattern of expression [179].

1.3.3 Forms of Fibronectin

1.3.3.1 Plasma Fibronectin

As briefly mentioned, two forms of FN exist: plasma FN (pFN) and cellular FN (cFN) [128]. An experiment on the fractionation of plasma in 1948 led to the discovery of pFN. It was initially thought to be a contaminant of plasma fibrinogen, but is now known to play an important role in cell attachment. Plasma FN is synthesized by hepatocytes in the liver and is released as a compact, soluble, dimeric protein in the bloodstream at a concentration of around 300-400 ug/ml in humans and 600 ug/ml in mice [180]. This concentration can increase in vascular tissue damage, after inflammation, and in diseases such as atherosclerosis and stroke [124]. Studies have suggested that maintenance of pFN in an inactive compact conformation is necessary to prevent aberrant interactions between FN and other molecules. Dysregulation could lead to spontaneous FN assembly in tissues and contribute to thrombus formation in the circulation [130].

1.3.3.2 Cellular Fibronectin

Cellular FN is synthesized by many cell types such as fibroblasts, myocytes, and chondrocytes [124]. The cFN secreted by the different cell types can vary in structure resulting in the different isoforms of FN. This variety helps to modulate the properties of the ECM and different cellular processes by being differentially expressed at different times, in specific tissues or cells, and in different physiological or pathological conditions [124, 167].

Cellular FN is incorporated in the ECM as insoluble fibrils [124]. In contrast with pFN, cFN can exist in a dimeric or multimeric form. Further, while pFN can be found in high amounts in tissues, cFN only exists in plasma at very low levels (1.3-1.4 $\mu\text{g/ml}$) [124]. However, elevated plasma levels of cFN have been reported in patients with conditions such as rheumatoid vasculitis, collagen vascular disorders, and diabetes. Increased plasma levels of circulating cFN can therefore increase in certain pathological conditions and can be a marker for vessel wall damage [181]. These two forms of FN can play very distinct roles as observed in certain events such as tissue repair, or they can both contribute equally in processes like cartilage and bone development [124].

1.3.4 Fibronectin and the ECM

One of the major roles of FN is its involvement in the ECM. The ECM is an organized meshwork of polysaccharides and proteins including collagen, laminin, elastin, and FN [182]. It was initially thought to only be an inactive scaffold that stabilizes the physical structure of tissues, but studies have discovered that it is a dynamic structure that actively influences cell adhesion, proliferation, differentiation, shape and survival [183].

The ECM is mostly found in connective tissues. It exists in varying degrees and in different forms depending on the organ. For example, it is highly abundant in the skeletal structure, but exists at a lesser amount in the brain [184, 185]. It can also form hard structures in organs such as bone or generate a transparent structure like that found on the cornea [186].

Most of the ECM molecules are secreted by fibroblasts which has a specific name in specialized types of connective tissue; for instance, chondroblasts in cartilage and osteoblasts in bone [182]. ECM assembly is important for normal development. Loss of assembly leads to embryonic lethality in mice, and improper or delayed assembly can promote undesired conditions including scarring, fibrotic disease, birth defects, and skeletal malformation [123, 128].

1.3.4.1 Steps of FN-Matrix Assembly

FN fibrillogenesis is the process in which soluble FN dimers are assembled into fibrils [187]. FN in solution alone will not polymerize and will not form a 3D matrix in the absence of cells [124]. It is a step-wise process that requires the presence of cells that are able to interact with cell-surface receptors as well as with other FN proteins [188]. The steps of FN assembly are the same for both pFN and cFN (Figure 5). FN fibrillogenesis is one of the earliest steps in ECM formation. In this event, pFN is taken up by tissues and deposited in ECM fibrils alongside locally synthesized cFN.

Soluble FN dimers are secreted in an inactive compact conformation maintained by intramolecular interactions between the FN_I₁₋₅, FN_{III}₁₋₂, FN_{III}₂₋₃ and FN_{III}₁₂₋₁₄ domains [127]. The first step of FN fibril assembly is the binding of a single compact FN dimer to active cell-surface integrin receptors, primarily the $\alpha 5\beta 1$ integrin, to its RGD integrin-binding domain on FN-III₁₀ [127, 189]. The $\alpha 5\beta 1$ integrin is also able to bind to a short peptide on FN-III₉, known as the synergy site. This additional binding allows $\alpha 5\beta 1$ to achieve the sufficient bond strength for assembly by increasing the activation of focal adhesion kinase (FAK). The combination of both these activities result in the enhancement of the FN-integrin interaction [128, 147]. Integrins can also bind to FN isoforms lacking the synergy site but it would require the help of other molecules such as Mn²⁺ or antibodies to successfully assemble FN into fibrils [124].

The interaction between integrins and FN causes a positive feedback loop in which integrins aggregate at focal adhesions which leads them to bind to FN with a higher affinity [190]. In addition, more integrin-binding sites are revealed allowing the large accumulation of integrin

receptors with a bound FN [26]. The integrin-FN binding elicits the recruitment of intracellular proteins including FAK and Src kinase to the integrin cytoplasmic domains and activate intracellular signaling [26, 128]. These domains associate with the actin cytoskeleton network inside the cell, reorganizes it and induces the formation of cytoskeletal connections. These connections lead to an increase in cell contractility which pulls on the FN and stretches it, inducing a conformational change that converts inactive compact FN into an active extended dimer [148, 190]. Since the structure of type III modules are not stabilized by disulfide bonds, the β -sheets has some conformational flexibility [128]. As a result of this stretching, FN's self-assembly domains along the length of the molecule become exposed, allowing FN-FN interactions. Integrin clustering and exposed FN-binding sites lead to the formation of fibrils [26]. Initially, only thin fibrils of 5nm in diameter are formed, but as more FN modules unfold and more FN-FN bindings sites are exposed, longer and thicker fibrils of 6-22 nm in diameter are generated [128, 191]. These fibrils can form complex networks by binding to each other in different configurations [124].

Two types of interactions therefore occur in this process: first is the binding of integrin with FN which ultimately leads to a conformational change in FN and exposure of binding sites, and the second are hemophilic interactions that allow other FN molecules in solution to join the existing fibrils without first needing to bind to integrin [128]. These events promote the formation of a stable insoluble fibrillary matrix [192]. However, the ECM is not static. It undergoes continuous polymerization and remodeling to adapt to the tissue's needs [124]. In fact, when there is absence of FN or inhibition of polymerization, the existing matrix is lost [188]. Proteolysis of FN can also expose self-assembly sites during remodeling which promotes assembly [193].

Note that many more proteins other than the ones described here also take part in FN fibrillogenesis, such as interactions with glycosaminoglycans (GAGs) and proteoglycans [194-196].

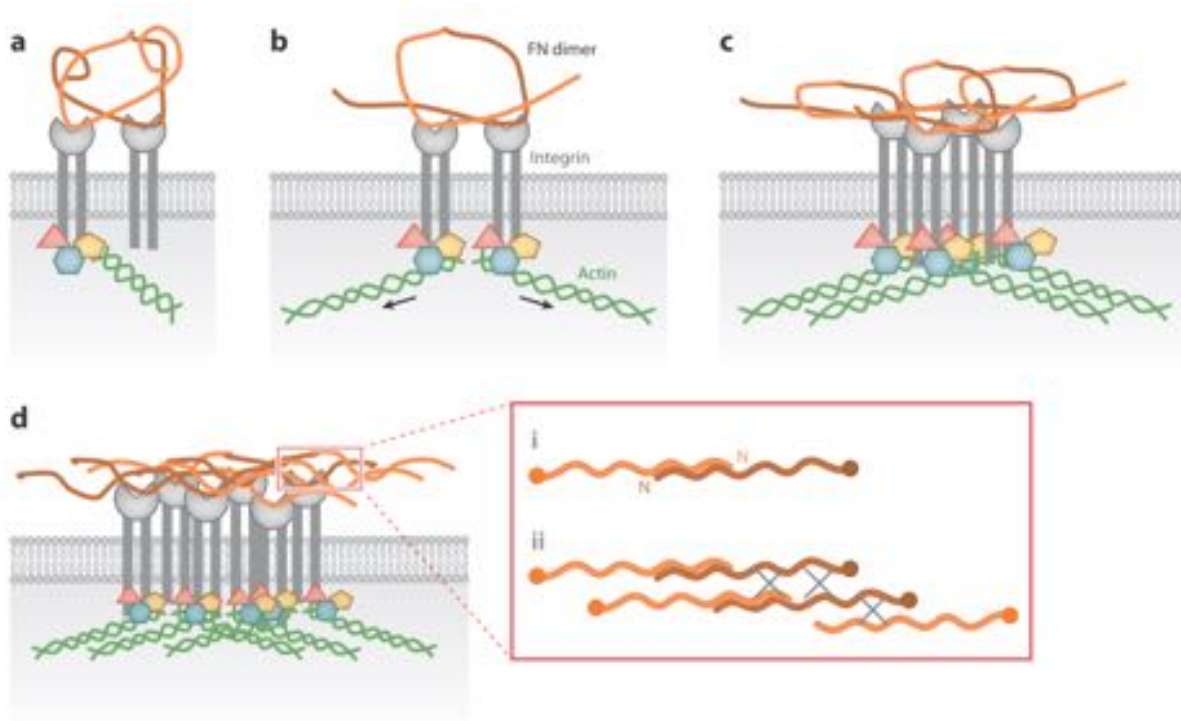


Figure 5: Steps of fibronectin (FN) matrix assembly. (A) A soluble compact FN dimer (each monomer is in a different shade of orange) binds to active cell-surface integrin receptors (gray). This integrin-FN binding elicits the recruitment of intracellular proteins (blue, red, orange) to the integrin cytoplasmic domain connected to the actin cytoskeleton (green). (B) Cytoskeletal connections increase cell contractility (arrows). This pull stretches the FN protein inducing a conformational change that converts inactive compact FN into an active extended dimer. As result of this stretching, FN's self-assembly domains along the length of the molecule become exposed. (C) Exposed FN-binding sites and integrin clustering allows interactions with other FN proteins and the formation of fibrils. (D) As more FN molecules unfold and more FN-binding sites are exposed, thicker fibrils are generated and a stable fibrillary matrix is formed. The red box shows how two subunits of FN can bind to each other. Figure from Singh et al., 2010 [128].

1.3.4.2 Regulation of FN-matrix assembly

Since the FN matrix is a highly dynamic structure, it constantly undergoes changes in expression to be able to assemble and remodel in an appropriate manner. This expression is tightly regulated, and is stimulated or halted by a multitude of molecules and signaling pathways [124]. Most of the regulation influence integrin binding since it is one of the earlier steps in the process.

The upregulation of FN expression in development is often preceded by an increase in connective tissue growth factors and TGF- β 1 expression [197]. TGF- β is involved in a crosstalk with integrins and modulates its activation [198]. In turn, FN recruits latent transforming growth factor-beta-binding proteins (LTBPs) into the matrix to store TGF- β 1 in the ECM. This regulation is necessary to prevent overexpression of TGF- β 1 which can result in an overly stiff matrix [199, 200].

One of the components important for the assembly of FN into a matrix is the Diastrophic dysplasia sulfate transporter (DTSST) [195]. The functional role of this protein has mostly been elucidated in the context of bone formation; it is important for the proper synthesis of glycosaminoglycans which are integral parts of the ECM. Knockdown of this transporter early in chondrogenesis blocked cell condensation *in vitro* and caused a significant reduction in FN matrix [201-203]. Similarly, Forlino et al. showed that a DTDST knock-in mutant mouse model that disrupts DTDST function leads to defects in chondrocyte size, proliferation and terminal differentiation [203].

Among ECM components, different levels of vitronectin (VN) has varying effects depending on its concentration. Low levels have been shown to enhance FN-matrix assembly, while high concentrations are inhibitory. This variation is due to the ability of the HepII domain of VN to interact with α v β 3 and α v β 5 integrins. High levels of VN leads to less available integrins that can bind to FN, resulting in a decrease in FN-matrix assembly [204, 205]. In the level of the actin cytoskeleton, inhibiting actin polymerization with drugs such as cytochalasin causes FN fibrils to detach from the cell surface [206]. The same result can occur with the

inhibition of the Rho GTPase signaling pathway, essential for cell contractility, or deletion of the β -integrin cytoplasmic domain [190, 207].

Focal adhesion proteins such as FAKs are also involved in the assembly, as well as in the maintenance of the matrix through its role in mediating the intracellular signaling events that accompany integrin-FN binding. FAKs work with the Src kinase family to efficiently phosphorylate substrates that stimulate assembly [208]. Although the absence of Src kinase was not found to inhibit the process, it was found to delay it [17]. Other players implicated in the process of focal adhesion formation, FAK activation and cell contractility are syndecan transmembrane proteoglycans, especially syndecan-2 and syndecan-4 [209]. They bind to the hepII domain of FN which is located next to the $\alpha 5 \beta 1$ integrin-binding domain. The spatial localization of the binding sites allows them to contribute to cell-FN interactions [210].

During the remodeling and repair phase of the FN-matrix, FN gets endocytosed, targeted to the lysosomes and either degraded intracellularly by proteases such as MMP9 and MMP13, or recycled [211]. Endocytosis of soluble FN is much faster than the endocytosis of FN from assembled matrices. Furthermore, integrin clustering can induce expression of MMPs in specific locations to cause localized ECM degradation. When this occurs, the resulting FN fragments can inhibit FN-matrix assembly by competing with full-length FN for the FN-FN interaction sites [212]. This acts as a feedback system to regulate the levels of FN on the cell surface.

1.3.5 Fibronectin in skeletal formation

FN has connective properties that allow it to participate in cell migration, adhesion, differentiation or ECM assembly. These roles lead to its involvement in the formation of many organs including the heart and blood vessels [123], and interestingly, in the skeletal development.

1.3.5.1 Endochondral bone formation

As described in the process of endochondral ossification, cartilage originates from mesenchymal cells that reside within the ECM of the limb bud. In the mesenchyme, FN is one of the most abundant among the matrix proteins. It is assembled into an insoluble and highly organized FN matrix prior to and during condensation, and continues to accumulate during the post-condensation differentiation process [17, 27].

FN plays an important role particularly in the condensation phase [27]. Plasma FN stimulates and enhances the migration and proliferation of mesenchymal progenitor cells by creating more contact sites between FN and the mesenchymal cells [213, 214]. Further, it facilitates aggregation through the assembly of a FN matrix [126]. It was thought that the FN matrix helps in maintaining the cells close together to maintain its rounded shape. Gao *et al.* have shown that preventing cells from spreading out encouraged its differentiation towards chondrocytes [215].

Moreover, the presence of a FN matrix is crucial for collagen deposition and assembly. Many groups have demonstrated that the absence of the matrix prevents the accumulation of collagen fibrils [128, 188]. In fact, *in vivo*, FN is found in developing tissues prior to the deposition of collagen. The temporal and spatial connections between FN and collagen suggest that the FN matrix helps in the parallel alignment of collagen fibrils [128]. During chondrocyte differentiation, the FN matrix acts as a platform for type II collagen assembly, and later in the process, for type I collagen [17]. It might also contribute to the differentiation program by enhancing Sox9 expression. Blocking the incorporation of cFN into the ECM reduces Sox9 mRNA levels by 25% [27]. As differentiation proceeds, the “old” ECM is replaced with a matrix in which FN is only expressed at low levels [17, 27]. This level can increase in situations such as tissue injury, suggesting FN’s involvement in tissue repair. Similar to the process of wound healing in which EDA and EDB containing FN is upregulated to induce cell proliferation and migration to the injured site, in early stages of cartilage tissue injury, expression of certain isoforms of FN promotes cell recruitment around the top layer of the cartilage known as the superficial layer [216]. Studies in chondrocyte cell cultures have shown a decrease in the

synthesis of collagen type II and proteoglycan when exogenous FN was added, suggesting that increased FN expression may induce the chondrocytes to revert back to a pre-chondrocytic state in order to facilitate tissue repair [216]. TGF- β helps in this process by increasing FN synthesis and by controlling the process of alternative splicing to generate FN isoforms that are appropriate for healing [217].

1.3.5.2 Intramembranous ossification

In intramembranous ossification, FN has a critical role in osteoblast adhesion, in osteogenic differentiation of MSCs, and proliferation [218]. FN derived from osteoblasts participates in FN assembly. However, in contrast with the previously outlined FN matrix assembly, matrix assembly with osteoblast-derived FN is not mediated by integrins that bind to the RGD motif [174].

FN derived from osteoblasts solely affects osteoblast function and differentiation without causing any changes in bone matrix properties. Circulating FN derived from the liver, on the other hand, does not affect osteoblast or osteoclast function, but affects bone matrix properties [174]. In fact, Bentmann *et al.* showed that FN derived from osteoblasts does not greatly contribute to the FN that is deposited in the bone matrix, but rather pFN which permeates into tissues and deposits in bone [174]. The accumulation of pFN in the osteoblast ECM was shown to facilitate type I collagen deposition and assembly which plays a role in osteoblast mineralization [219]. In mice experiments, conditional deletion of FN in the liver caused a decreased FN content in the bone matrix, decreased hydroxyapatite, and decreased bone mineral density (BMD), but no effect on osteoblasts or osteoclasts [174]. It is thus concluded that FN derived from osteoblasts plays a role in the initial FN assembly, then liver-derived FN provides a continuous source of FN into the ECM which is critical for the integrity of the matrix [188].

1.3.6 FN-associated Disorders

Surprisingly, only a few diseases caused by FN have been identified despite its widespread involvement in many biological processes. Some of the identified diseases are due

to unregulated levels of FN. For example, defective or excessive FN matrix assembly during a wound healing event can lead to fibrosis [220]. In cancer, it was found to be involved in the tumor's ability to metastasize due to the fact that transformed cells produced less FN than normal cells, leading to poor cell adhesion [221, 222]. This defect allows cancer cells to break away from the primary tumor and move to other organs [223]. Furthermore, in osteoarthritis, a disease of the joints in which there is a breakdown of joint cartilage and altered bone properties, affected individuals were reported to have a twofold increase of FN in their joint fluid [224-226]. This is a feature that was found to be due to an excessive production of FN by chondrocytes causing it to accumulate in the ECM [216, 227].

Diseases can also occur as a consequence of mutations in the *FNI* gene. One known disease is glomerulopathy with FN deposits (GFND), a kidney disease characterized by FN aggregates [159]. Affected patients were reported to have mutations in the FN-binding domains (FNIII₄) and heparin-binding domains (FNIII₁₃) [159]. The etiology of this disease continues to be explored as more recently, in 2016, Ohtsubo *et al.* identified a mutation in the integrin-binding domain in one affected patient [160].

Our group has shown that another disease caused by mutations in the *FNI* gene is SMD-CF [106]. These mutations are located in the N-terminal domain, in contrast to GDNF mutations which are mostly located in the C-terminal half of the protein. Interestingly, patients with SMD-CF do not have any renal abnormalities, and patients with GDNF do not have any skeletal abnormalities. To date, only 10/28 patients with Sutcliffe-type SMD are known to have mutations in the *FNI* gene [101, 106, 107]. The distinguishable difference between SMD-CF patients harboring *FNI* mutations compared to the 18 other affected individuals is that most of the patients with *FNI*-mediated SMD-CF presented with scoliosis [106]. Through *in vitro* experiments in HEK293 cells, it was found that cells stably transfected with mutant FN showed a strong accumulation of the mutant protein within the cells, demonstrating a defect in FN secretion (Figure 6) [106]. Cadoff *et al.*, who reported a 10th patient, supported these findings (their experiments are discussed after the results section of this thesis) [107].

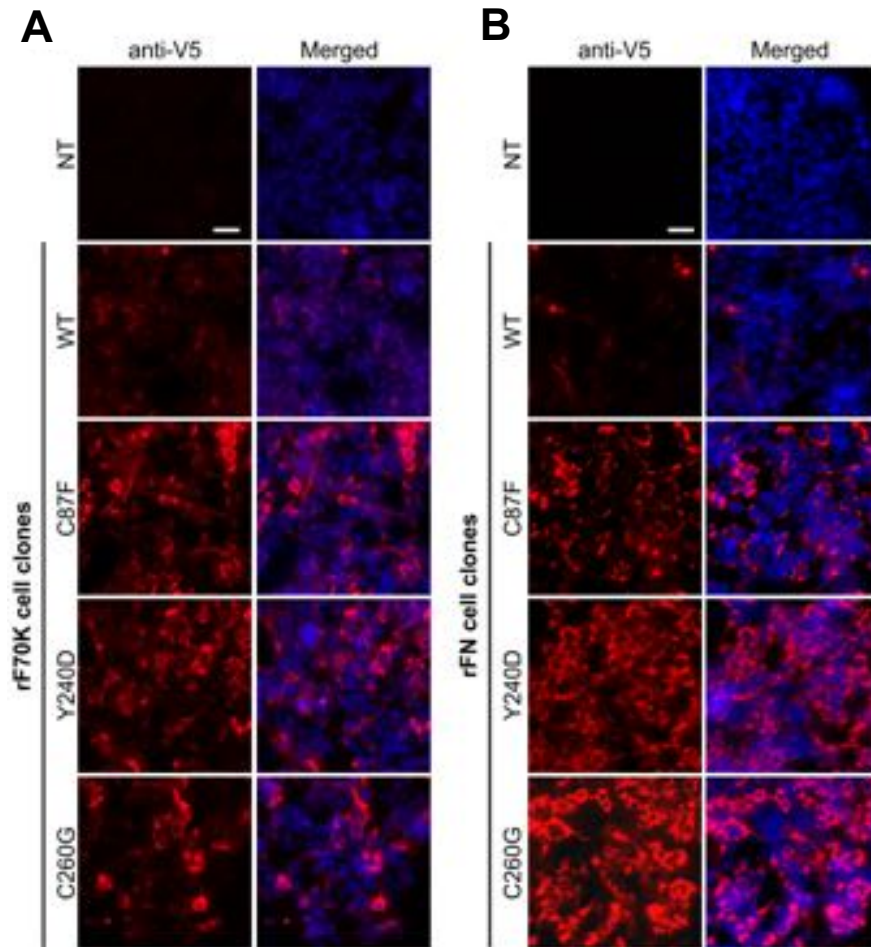


Figure 6: Immunofluorescence analysis of HEK293 cells. HEK293 cells were transfected with the 70 kDa N-terminal fragment of fibronectin (A) and the full-length fibronectin (B). These constructs were either wild-type (WT), or harbored the identified mutations found in patients with SMD-CF (C87F, Y240D, C260G; the letters indicate the amino acids and the number refers to the position of the amino acid where the change occurred). NT refers to non-transfected controls. Fibronectin is shown in red, and the nuclei of cells are shown in blue. Compared to NT controls and the WT protein, there is a larger presence of mutant fibronectin in the cells. This demonstrates intracellular retention, suggesting a defect in the secretion of mutant fibronectin. rF70K: 70 kDa N-terminal fragment of fibronectin; rFN: full length fibronectin. Adapted image from Lee *et al.*, 2017 [106].

1.4 RESEARCH PROJECT

Given the involvement of growth plates in patients with SMD-CF, it was presumed that the proliferating or hypertrophic cartilage is the main tissue affected by the disease. FN mutations leading to skeletal disorders is a novel and unexplored aspect in the field. This study is a collaboration with Dr. Dieter Reinhardt (McGill University, Montreal, QC) who is an expert on ECM biology. Our teams have reported novel *FNI* mutations in 9 of the patients with SMD-CF (see paper by Lee *et al.*, 2017 in Annexe I), and have shown that these mutations impair FN secretion in HEK293 cells. However, it is still not known how this defect in secretion mechanistically contributes to SMD pathogenesis. It is hypothesized that the intracellular retention of FN leads to less FN in the ECM which can disrupt chondrocyte survival, differentiation or function, impair FN and ECM assembly, and affect growth factor regulation and/or the binding of other FN-interacting proteins. All this can lead to improper skeletal growth as seen in patients with Sutcliffe-type SMD.

The main objective of this work is to understand how specific FN mutations affect chondrocyte function and ECM organization in SMD. For this purpose, the functional consequences of FN mutations on cell and tissue function will be assessed through *in vitro* and *in vivo* methods.

Specific Objectives:

1. Optimize a chondrogenesis protocol to differentiate ATDC5 cells expressing mutant FN constructs into chondrocytes. This will be used to determine how FN mutations affect the chondrogenic process.
2. Generate mice lacking FN in the liver and cartilage (double knock-out) to assess if the phenotypes observed in SMD-CF are indeed due to the retention of FN in the cells, or if it is due to the overall reduced expression of the protein.
3. Sequence the DNA of new patients with suspected SMD-CF to check for the presence of mutations in the *FNI* gene. This will increase the cohort of patients, allowing a more accurate investigation of the pathophysiology of the disease.

CHAPTER 2: MATERIALS AND METHODS

2.1 POLYMERASE CHAIN REACTION

Polymerase chain reaction (PCR) was done using the T100™ Thermal Cycler (Bio-Rad). Each reaction contained 10x PCR buffer (Bio Basic Canada), Taq DNA polymerase (5u/ul, Bio Basic Canada), dNTP (Wisent), primers (10 uM), nucleic acids (DNA or cDNA) and dH₂O. Products were loaded on agarose gels (1.5-3%), separated by gel electrophoresis, and viewed using UV transillumination.

2.2 SANGER SEQUENCING

PCR was done on the patient and parents' genomic DNA to amplify the exon of interest. Primers used to sequence the exons of the *FNI* gene were selected using the ExonPrimer software through the UCSC Genome Browser (<https://ihg.helmholtz-muenchen.de/ihg/ExonPrimer.html>) using the human genome reference GRCh37/hg19. All primer sizes are between 20-25 bp in length with an annealing temperature of around 60°C. They were designed to amplify a maximal exon size of 500bp. Exons longer than this length were separated and amplified with different pairs of primers. Primers are listed in Table II. The PCR products were separated by gel electrophoresis on 1.5% agarose gels. The bands corresponding to exons 5 and 6 were purified using the Monarch® DNA gel extraction kit (New England BioLabs) according to manufacturer's protocols. PCR products were then sent to the McGill University and Genome Quebec Innovation Centre for sanger sequencing. The reads were mapped to the human *FNI* genomic sequence (NG_012196.1 RefSeqGene) which was downloaded from the NCBI database, and analyzed using the Geneious computer software version R8.

Table II: Sequencing primers for the human *FN1* gene.

Primer name	Sequence (5' → 3')	Product length (bp)
FN1_seq_Exon1_F	GAAGGGAAGCAAACCTTGGTG	279
FN1_seq_Exon1_R	CAACTTTGGTCGGCTTTAGG	
FN1_seq_Exon2_F	TCCATAATTTTGGGAAAAGGAG	255
FN1_seq_Exon2_R	TGCAAAGTTTAAACAATTACCACTTC	
FN1_seq_Exon3_F	TGGGTTTTCTTTAGAGGGG	321
FN1_seq_Exon3_R	TTCGGAATATCCAGTCATGG	
FN1_seq_Exon4_F	CCTACCATGGGTGGAATATG	274
FN1_seq_Exon4_R	CTGGTCCAACCCACATTAG	
FN1_seq_Exon5_F	ACAGGGAGCTTGCACAATTC	438
FN1_seq_Exon5_R	ATGTCAGTGGCAGTGAGCTG	
FN1_seq_Exon6_F	TTGAATTGACCACTTGCGAC	295
FN1_seq_Exon6_R	AAAGGAAAGATGGATTTGCG	
FN1_seq_Exon7_F	CCAGGCCAGTAGCGACATAG	434
FN1_seq_Exon7_R	CAGGGTGGTAAGATTACAGGC	
FN1_seq_Exon13_F	TGACTGTCCATGTACACAGTTTTAAG	259
FN1_seq_Exon13_R	CCATCAGAATTGATAAGATTAGGAG	
FN1_seq_Exon14_F	AACATCATCTTCAAATGTTTCATCC	318
FN1_seq_Exon14_R	GCCTCAGGAGAGCCTAGC	
FN1_seq_Exon15_F	GATGTTGGCGACGAGGAC	306
FN1_seq_Exon15_R	AAGGAGAGTTTTCCAGCAGC	
FN1_seq_Exon16-17_F	CATTACCTTCTAGTCGCTTTTCC	537
FN1_seq_Exon16-17_R	AAAGTGATATGCAGGTCCGC	
FN1_seq_Exon18_F	AAAGGGAGGATTTATGGTGTTTC	333
FN1_seq_Exon18_R	CCCTCCTTCAGGAACAATCC	

2.3 MICE GENERATION AND BREEDING

2.3.1 Knock-out mice

Mice with lox sites flanking the *Fn1* gene (*Fn1*(fl/fl)) as well as *Fn1*(fl/fl); *AlbCre*/+ mice were obtained from Dr. Dieter Reinhardt (McGill University, Montreal, Quebec). *Fn1*(fl/fl) mice were crossed with mice expressing constitutive Cre recombinase specifically in chondrocytes (B6;SJL-Tg(Col2a1-cre)1Bhr/J mice obtained from Dr. René St-Arnault (Shriner's Hospital for Children, Montreal, QC) to generate *Fn1*(fl/fl); *Col2Cre*/+. *Fn1*(fl/fl); *AlbCre*/+ were then crossed with *Fn1*(fl/fl); *Col2Cre*/+ to generate double knock-out (dKO) mice in which the *Fn1* gene is conditionally deleted in both plasma and cartilage. Mice were produced after several breeding rounds. See mouse breeding plan. Breeding was done in the animal facility of the CHU Sainte-Justine Research Center according to a protocol approved by the Animal Ethics Board.

2.3.2 Knock-in mice

Knock-in mice harboring the p.Cys260Gly *FNI* mutation were generated using the CRISPR-Cas9 method. Guide-RNA with the sequence 5'- CAGTGTGTCTGCACAGGCAA-3', was co-injected in mouse embryos with Cas9 mRNA and the ssODN repair template 5'- GGCGTGGAGCTGTCCCCGGTCCCAGCGCCTCACCGGCTGAAGCACTTTGTAGAGCATGTCGCTCACACTTCCACTCCCCTCTGCCATTGCCCGTGCCGGACGCACTGCAGCAGGTTTCCTCGGTTGTCCTTCTTGCTCCACGTGTCTC-3' at the McGill University (Montreal, QC) mouse transgenesis facility. Positive CRISPR knock-in mice were bred with C57BL/6 mice in the animal facility of the CHU Sainte-Justine Research Center.

2.4 MICE GENOTYPING

2.4.1 DNA isolation

Mouse tails (~2mm) were cut off at 3 weeks by technicians at the animal facility. DNA was then extracted from mouse tails using the “DNA Isolation from Tails” protocol from Jackson labs with a few modifications. Briefly, each tail sample was incubated in tail lysis buffer containing 0.4 mg/ml of proteinase K in a water bath overnight. 330ul of 5M NaCl was then added to each tube, then incubated on ice for 10min and centrifuged at 4C for another 10 min. The supernatant was then transferred into a clean Eppendorf tube and purified with isopropanol. DNA was recovered by centrifugation at 13000 rpm for 10min at room temperature, then resuspended in 200ul sterile water.

2.4.2 Genotyping

Genotypes were determined by PCR on DNA isolated from mouse tails. PCR amplification products were loaded on 2-3% agarose gels, and separated using gel electrophoresis. To genotype knock-out mice, primer sequences were obtained from Jackson labs (Table III). The presence of the floxed allele in the gene-targeted mice was confirmed using the primers for FN1-flox. The expression of Cre recombinase in chondrocytes was detected using primers for Col2a1Cre obtained from Jackson labs, and primers for AlbCre were used to detect Cre recombinase in the liver.

To genotype CRISPR knock-in mice, primers were designed using the Geneious computer software version R8 (Table III). Specific primers were designed to bind to the wild-type sequence of *FN1* and run in the forward direction (WT_F) and another forward primer was designed to bind to the mutant sequence (mutant_c.778T>G_F). The specific forward primers are paired with a common reverse primer to amplify the DNA using PCR. The mutant specific primer is expected to bind if the DNA strand harbors the mutation. To confirm the presence or absence of the mutation, DNA was amplified by PCR using common forward and reverse primers. The common primers bind to regions at either side of the region where the mutation is located to avoid any sequence bias. PCR products were then sent for Sanger sequencing.

Table III: Primers used for mouse genotyping

Primer	Sequence (5' → 3')
Knock-out mice	
FN flox	F: GTACTGTCCCATATAAGCCTCTG
FN flox	R: CTGAGCATCTTGAGTGGATGGGA
AlbCre Wild-type	F: TGCAAACATCACATGCACAC
AlbCre Common	R: TTGGCCCCTTACCATAACTG
AlbCre Mutant	F: GAAGCAGAAGCTTAGGAAGATGG
Cre transgene	F: GCGGTCTGGCAGTAAAACTATC
Cre transgene	R: GTGAAACAGCATTGCTGTCACTT
Col2a1 Internal Positive Control	F: CTAGGCCACAGAATTGAAAGATCT
Col2a1 Internal Positive Control	R: GTAGGTGGAAATTCTAGCATCATCC
CRISPR Knock-in mice	
WT-specific	F: CTGCTTCAGTGTGTCTGCACA
Mutant-specific (c.778T>G)	F: CTGCAGTGCCTCGGCACG
Common1	F: GGTAAACCACGTGGGTGACT
Common1	R: CTTCCAAAGTAGTGTAAGCTGG
Common2	F: CAGACAGATGCAACGATCAGG
Common2	R: TGAGTCTCATGCTCATAAGCC

2.5 GROWTH MEASUREMENTS

Weight. Each mouse was weighed at the indicated times using an electronic balance. A plastic container was placed on the weighing scale. The scale was then tared to 0, the mouse was placed in the container and the weight was recorded.

Length. Nasal-to-anal distance of each mouse was measured to determine body length. The mouse was held using the one-handed mouse restraint technique. A ruler was then held up against the body to measure the length with an accuracy within 0.2cm. Measurements of long bones were determined from radiographs.

2.6 RADIOGRAPHY

Mice were anesthetized with isoflurane (2.5 L/min O₂, 4% isoflurane) using the Moduflex Labvet machine (Dispomed) before being euthanized in a CO₂ chamber (9 L/min). X-ray images were taken with the Kubtec Xpert 80 Digital Cabinet X-ray System at the specified magnifications at the McGill Center for Bone and Periodontal Research (Montreal, QC).

2.7 CELL CULTURE

2.7.1 ATDC5 Cells

The pre-chondrogenic mouse ATDC5 cell line was obtained from Dr. Monzur Murshed (Shriner's Hospital for Children, Montreal, QC). The cells were grown in Minimum Essential Medium, alpha modification (AMEM, Wisent), containing 5% fetal bovine serum (FBS, Wisent), and 1% antibiotic-antimycotic solution (Life Technologies). The ATDC5 cultures were maintained at 37°C and 5% CO₂ in a humidified incubator. The cells were passaged at 70-80% confluency and the medium was replaced every 2-3 days.

2.7.2 Chondrogenic Differentiation

To induce chondrogenic differentiation in ATDC5 cells, cells were plated at 30% confluency in 6-well cell culture plates (6000 cells/cm²) in AMEM. The media was then changed to differentiation media containing AMEM with 5% FBS and 1% AA, 1% Glutamax (ThermoFisher), 1% insulin-transferrin-selenium (ITS, ThermoFisher), 0.5% of 50mg/mL gentamicin (ThermoFisher) and 10 ng/mL human transforming growth factor (TGF-β1, Abcam). On the 6th day, TGF-β1 was removed. When the cells reached 70% confluency, 50 µg/ml L-ascorbate-2-phosphate (ascorbic acid, Sigma) and 10 mM β-glycerophosphate (β-GP, Sigma) were added to the differentiation medium. Cell media was refreshed every 3 days.

2.8 RNA EXTRACTION AND cDNA SYNTHESIS

Cell layers were washed with Dulbecco's phosphate buffered-saline (DPBS, ThermoFisher) to remove any residual medium. Total RNA was then isolated from ATDC5 cells at the indicated time points, using the RNeasy® Mini Kit (Qiagen) according to the manufacturer's protocol. Total RNA content for each the sample was determined by measuring absorbance at 260 nm and purity by A260/A280 ratios with the Epoch Microplate Spectrophotometer (BioTek). The reverse transcriptase reaction was performed using the 5x all-in-one RT Mastermix Kit (ABM)

according to the manufacturer's protocol. For each reaction, 500ng of RNA was mixed with 4ul of the mastermix, and completed with RNase-free H₂O to 20ul. Samples were then incubated at 25°C for 10min, 42°C for 50min, and 85°C for 5min in a PCR machine. The cDNA samples were stored at -20°C.

2.9 REAL-TIME PCR

Sequences for primers that were used for real-time PCR were either taken from the literature, from primer databases or were designed using the Primer-BLAST program from NCBI (<https://www.ncbi.nlm.nih.gov/tools/primer-blast/>). To design primers, the longest transcript variant (NM number) of each gene was chosen as the reference sequence. Primers were designed to span exon-exon boundaries to prevent amplification of genomic DNA, and generate a product size between 70-150 bp. See primer sequences in Table IV.

Quantitative real-time PCR was performed using the RT-PCR Lightcycler 96 system (Roche Diagnostics). Template cDNA was mixed with 5 µL of PowerUp™ SYBR® Green Mastermix (ThermoFisher), 0.6 µL each of forward and reverse primer (5 µM), and 1.8 µL dH₂O for a total reaction volume of 10 µL. Reactions were run in triplicate. The qPCR plate was centrifuged for 1 min at a speed of 1000g to ensure proper mixture of the reagents, and then underwent an initial activation of 50°C for 2min and 95°C for 2min, followed by 40 amplification cycles (15 sec at 95°C for denaturation and 1 min at 60°C for annealing/extension). A threshold cycle (Ct) value for each gene was calculated using the Lightcycler® 96 version 1.1 software (Roche Diagnostics). Relative mRNA expression from ATDC5 cells was calculated using the comparative $\Delta\Delta\text{Ct}$ method. β -actin was used as a housekeeping gene to normalize the data between samples. First, the ΔCt value was calculated by subtracting the Ct value of β -actin from the Ct value of each gene of interest (GOI) ($\Delta\text{Ct} = \text{Ct}_{\text{GOI}} - \text{Ct}_{\beta\text{-actin}}$). The $\Delta\Delta\text{Ct}$ was then calculated by subtracting the average ΔCt for the experimental control from the ΔCt of each sample ($\Delta\Delta\text{Ct} = \Delta\text{Ct}_{\text{control}} - \Delta\text{Ct}_{\text{sample}}$). The average Ct value of untreated cells was used as the control. The fold change of each gene in comparison to the control was calculated using $2^{-\Delta\Delta\text{Ct}}$. The standard deviation between the triplicates for each sample was calculated and shown on the graph.

Table IV: Primers used for real-time PCR.

Gene target	Primer Sequences (5' → 3')	Reference
Col2a1	F: CGGTCCTACGGTGTTCAGG	Han <i>et al.</i> [228]
	R: GCAGAGGACATTCCCAGTGT	
Sox9	F: CACAAGAAAGACCACCCCGA	Fitter <i>et al.</i> [229]
	R: GGACCCTGAGATTGCCCAGA	
Aggrecan	F: CGCCACTTTCATGACCGAGA	Imaizumi <i>et al.</i> [230]
	R: TCATTCAGACCGATCCACTGGTAG	
Col10a1	F: CATAAAGGGCCCACTTGCTA	Han <i>et al.</i> [228]
	R: CAGGAATGCCTTGTTCTCCT	
MMP13	F: AAGATGTGGAGTGCCTGATG	Tsukamoto <i>et al.</i> [231]
	R: TGGGACATATCAGGAGTATAG	
Runx2	F: GTTCAACGATCTGAGATTTGTG	Tsukamoto <i>et al.</i> [231]
	R: GGATTTGTGAAGACTGTTATGG	
Colla1	F: CGATGGATTCCCGTTCGAGT	Designed
	R: GAGGCCTCGGTGGACATTAG	
FN EDB exon	F: CATGCTGATCAGAGTTCCTG	Han <i>et al.</i> [228]
	R: GGTGAGTAGCGCACCAAGAG	
β-actin	F: GTGCTATGTTGCCCTGGATT	Designed
	R: TGCTAGGGCTGTGATCTCCT	

2.9.1 Data analysis

All data were expressed as means±standard deviations. Differences between groups were examined for statistical significance using the Student's t-test. Results were considered statistically significant when the value of probability of error (p) was less than 0.05.

2.10 HISTOCHEMICAL STAINING

2.10.1 Alizarin Red

Staining was done on cells plated in 6-well plates. Alizarin red staining was done using the Alizarin Red Staining Quantification Assay kit (ARed-Q, ScienCell Research Laboratories) to evaluate calcium deposition in ATDC5 cells. Staining was done according to the manufacturer's protocol. Briefly, the cells were washed with DPBS (ThermoFisher), then fixed in 10% formalin

(4% v/v formaldehyde) for 15 min. The fixative was then removed with dH₂O, and replaced with 1 mL of 40 mM Alizarin Red stain per well of a 6-well plate. After a 20-30 min incubation at room temperature, the cells were washed with dH₂O and were observed with a Leica DMI8 inverted microscope. Images were captured under bright light using the Leica LAS-X software. To quantify Alizarin Red staining, 10% acetic acid was added to the cells for 30 min. The cells were then collected using a cell scraper and transferred to 1.5 mL microcentrifuge tubes. After steps of heating, cooling and centrifugation as described in the protocol, 10% ammonium hydroxide was added to the samples to neutralize the acid. Samples were then pipetted onto a 96-well plate in triplicates and absorbance was determined by spectrophotometry using an Epoch Microplate Spectrophotometer (BioTek) at 405 nm.

2.10.2 Alcian Blue

Alcian Blue was used to detect proteoglycan synthesis in ATDC5 cells, an indicator for cartilage formation. A staining protocol by Biological Industries was followed. Briefly, 1% Alcian Blue solution was first prepared by dissolving 0.2g of Alcian Blue 8GX (ThermoFisher) in 20 mL of 0.1 N HCl, and filtering it through a 0.45 micron syringe filter. The cells were washed with DPBS then fixed with 10% formalin (4% v/v formaldehyde, 1 mL/well of a 6-well plate) for 30-60min. The fixed cells were washed with dH₂O and 1 mL of 1% Alcian Blue solution was added to each well for overnight incubation at room temperature. The samples were protected from light at all times. The staining solution was removed the next day and the cells were washed with 0.1N HCL. dH₂O was added before visual inspection under the Leica DMI8 inverted microscope. Digital images were captured under bright light using the Leica LAS-X software. The Alcian blue dye was extracted overnight at 4°C using 8M guanidine-HCH, and the samples were aliquoted the next day on 96-well plates for quantification. The optical density of the dye was determined at 600nm by spectrophotometry (Epoch Microplate Spectrophotometer, BioTek). Each sample was measured in triplicate and guanidine-HCH served as blank.

CHAPTER 3: RESULTS

3.1 CHONDROGENESIS OF ATDC5 CELLS

To assess the effects of *FNI* mutations in chondrogenesis, ATDC5 cells were chosen as an *in vitro* model. ATDC5 is a mouse chondrogenic cell line derived from teratocarcinoma cells. It can efficiently undergo the steps of proliferation, chondrocyte differentiation and chondrocyte hypertrophy under the right conditions [232]. While HEK293 cells represent an efficient system for generating ECM proteins, ATDC5 cells provide a more accurate view to evaluate mechanisms involved in chondrogenesis. In fact, it has been used in over 200 studies to study skeletal development [232]. To date, two popular methods exist to induce chondrogenesis in cells: the cell pellet method and the monolayer culture method.

The cell pellet method is a 3D culture method that closely mimics the *in vivo* condensation of MSCs prior to the onset of chondrogenesis and the production of ECM by the chondrocytes. This method involves the culturing of cell aggregates in differentiation media consisting of a cocktail of growth factors [233, 234]. While this approach is closer to what occurs *in vivo*, it was found that a high level of apoptosis or necrosis can occur at the center of the pellet when cultured for long periods of time, and that cells can spontaneously undergo chondrogenic differentiation without any external stimulating factors [235, 236].

For simplicity and reproducibility, the monolayer culture method was chosen. Cells can undergo chondrogenic differentiation in a monolayer due to their ability to form their own 3D environment [237]. In this work, several chondrogenesis protocols in the literature were studied, and a standard method was modified to increase the efficiency and reproducibility of chondrocyte differentiation in ATDC5 cells.

3.1.1 ATDC5 Cell Morphology

Brightfield images of ATDC5 cells in control conditions (untreated cells) and in differentiated medium (treated cells) were taken on days 3, 14 and 28 for visual inspection of the chondrogenic process and the efficiency of our differentiation media.

Cells were plated at day 0 at 30% confluency. At day 1, the maintenance medium consisting of Minimum Essential Medium, alpha modification (AMEM), 5% fetal bovine serum (FBS) and 1% antibiotic-antimycotic solution was changed to differentiation medium (maintenance medium with insulin, transferrin and selenium (ITS)) in cells undergoing treatment. Gentamicin was also added to avoid bacterial contamination [238]. Control cells remained in maintenance medium throughout the experiment. At day 3, both untreated and treated ATDC5 cells exhibited a fibroblastic morphology, with treated cells appearing more confluent than untreated cells (Figure 7A-D). 10 ng/mL TGF- β 1, 50 μ g/ml ascorbic acid, and 10 mM β -glycerophosphate (β GP) were then added to the differentiation medium to facilitate cell differentiation and the secretion of a cartilaginous ECM. 3 days later, TGF- β 1 was removed from the media. After 14 days in culture, untreated ATDC5 cells started to condense and began aggregating into cartilage-like nodules with the formation of ECM at the early stages (Figure 7E, asterix). Cells still appeared fibroblast-like, but were beginning to take on a more rounded morphology compared to day 1 (Figure 7F). In contrast, treated cells were overconfluent in the well. They possessed multiple cartilaginous condensations with prominent nodules at discrete locations (Figure 7G, white arrow). ECM production was advanced and ECM mineralization was starting as indicated by opaque regions (Figure 7G, blue arrows). The cells displayed a round phenotype, characteristic of chondrocytes (Figure 7H). At day 28, untreated cells displayed more obvious nodule formation and ECM production, but never reached the level of nodule formation seen in treated cells (Figure 7I-J). Meanwhile, at the same time point, there was increased cellular hypertrophy in treated cells. Cartilaginous nodules conjoined over the ECM (Figure 7K) and mineralization was observed as shown by the black deposits observed within the nodules (Figure 7L). This indicated terminally differentiated hypertrophic chondrocytes [239].

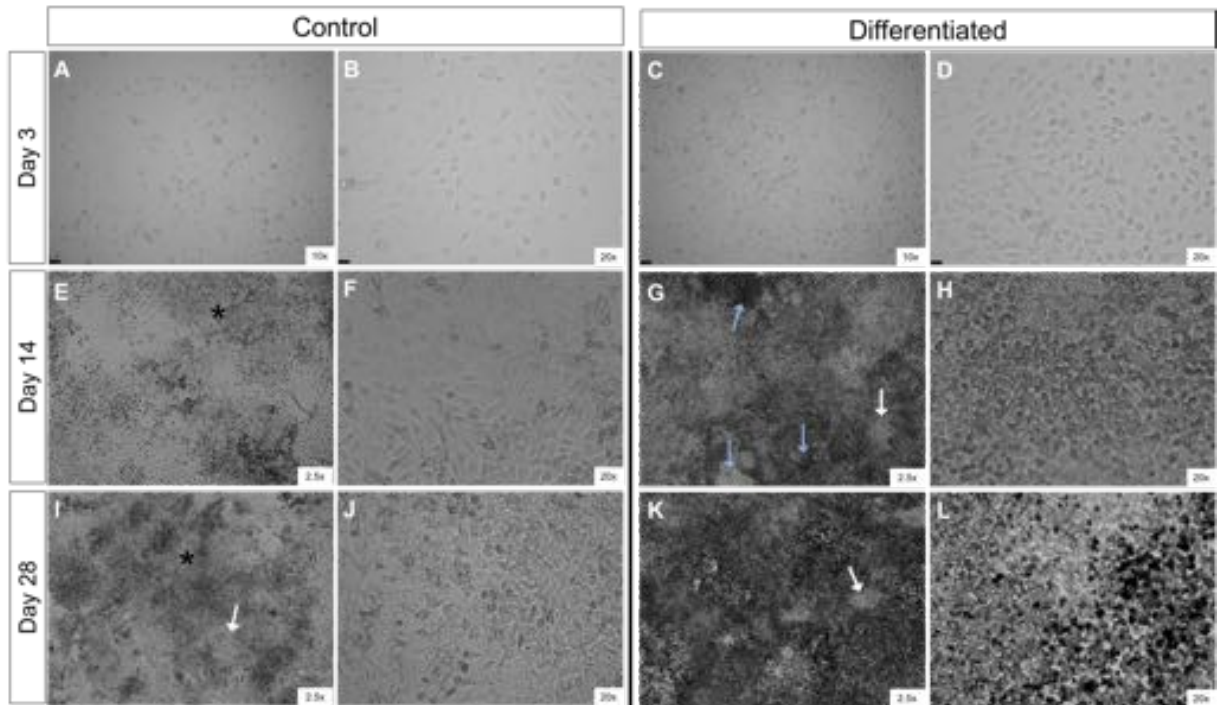


Figure 7. Chondrogenic differentiation of ATDC5 cells. ATDC5 cells were grown over a period of 28 days under either maintenance medium (AMEM with 5% FBS and 1% antibiotic-antimycotic solution) for the control cells or differentiation medium (as described in the materials and methods section) for the differentiated cells. Brightfield images were captured on days 3, 14, and 28. Magnification is indicated on the bottom right of each image. Both control and differentiated cells displayed a fibroblast-like morphology on day 3 of culture with control cells (A-B) appearing less confluent than treated cells (C-D). On day 14, translucent extracellular matrix began to form (asterisk) in the untreated control (E), and the fibroblast-like were starting to condense (F). Treated cells, on the other hand, showed an onset of mineralization on the same day (G), indicated by opaque regions on the well (blue arrows). Many cartilaginous nodules were also apparent in the extracellular matrix (white arrow). (H) A magnified view illustrates the round morphology of the cells, indicating differentiation into chondrocytes. On day 28, (I) nodules started to appear in untreated cells (white arrow) and they start to become more rounded (J). In differentiated cells, the increased formation of cartilaginous nodules conjoin over the extracellular matrix (K) and there is mineralization shown by the black deposits (L). Data shown is representative of biological triplicates.

3.1.2 Gene Expression of Chondrogenic Markers

To examine the changes in gene expression that occur as a consequence of chondrogenic differentiation in monolayer culture, gene transcription of a number of well-known chondrogenic markers was analyzed by qRT-PCR and were compared to the mean expression of control cells at day 1.

The collagen profile of Col2a1 and Col10a1 showed a sustained increase in expression in both treated and untreated cells compared to day 1. Col2a1 is known as the main chondrogenic marker in which immature chondrocytes progressing from the prechondrogenic to the proliferative stage express Col2a1 [240, 241]. Its expression increased significantly between day 3 to 14 in differentiated cells by 22-fold, and continued to increase until day 28, although less abundantly (Figure 8A). In control cells, this large increase arrived later between days 14 and 28, and at day 28, Col2a1 levels in both conditions were not significantly different. It is well documented that Col2a1 expression is regulated by the Sox trio (Sox9/5/6) [242]. Sox9, expressed in immature chondrocytes [240, 241], directs cell condensation and allows cell survival in the condensation stage [30]. Our results show that its expression gradually increased from day 1 to day 14, consistent with the increase of Col2a1 expression, indicating that the cells were undergoing chondrogenesis [243]. Sox9 levels slightly decreased by day 28 in differentiated cells illustrating the progression towards terminal differentiation (Figure 8B). Markers of chondrogenesis can be seen decreasing or slowing down to indicate the end of differentiation, a clear example of the defined temporal regulation of factors in chondrogenesis [30, 243, 244]. Aggrecan (Acan) maintained low constitutive levels in differentiated medium from day 1 to day 14. This protein accounts for 90% of the proteoglycan content in the ECM of articular cartilage [6, 245]. Acan levels significantly peaked at day 28 with a 13.5-fold upregulation compared to day 1 (Figure 8C). These results are similar with studies done in chick limb-bud chondrogenesis where the dramatic increase in the accumulation of Acan was preceded by the expression of Col2a1, and continues to increase during hypertrophy [6, 246].

To assess chondrocyte hypertrophy, Col10a1, MMP13, and Runx2 expression were measured, as well as the expression of a marker of osteogenesis, Col1a1. Mature chondrocytes

from the proliferative/prehypertrophic to the hypertrophic stage express Col10a1 [240, 241]. Transcription of this gene is known to be active only in hypertrophic chondrocytes [247]. Col10a1 gene expression increased significantly in differentiated cells at day 28, over a 1,000-fold range compared to day 14 (Figure 8D, $*p<0.05$). Transcription was also higher in the control cells, although not as great as the treated cells, with only a 500-fold increase. The delayed onset of Col10a1 can be explained by events that first need to occur before the cells can become hypertrophic: a deposition of glycosaminoglycans (GAGs), and an increase in Runx2 expression [237].

MMP13 peaked at day 28 in both control and differentiated cells, but the levels in control cells is significantly lower than differentiated cells (mean levels of 27.41 and 57.19 respectively) (Figure 8E). Levels of hypertrophic marker Runx2, which is also considered as a regulator of osteogenesis, was highest at day 14, then decreased to lower levels compared to control cells at day 28. Runx2 expression between days 14-28 in control cells remained relatively stable (Figure 8F). Runx2 plays a role in prehypertrophic cells before mineralization by promoting prehypertrophic cells to enter hypertrophy. One of the ways it does this is through the stimulation of Col10a1 expression [240, 241, 247]. Thus, as the cells underwent hypertrophic differentiation, Runx2 mRNA reached high levels. The downregulation of its expression at day 28 may be explained by active Sox9 expression which seems to antagonize its expression and prevents the progression to osteogenesis [36]. It would be interesting to analyze the gene expression at later time points to see if Sox9 expression remains higher than Runx2. Col1a1 showed the same pattern of expression as Runx2, but it first decreased at day 3 before upregulating at day 14 (Figure 8G).

FN expression was also analyzed during the chondrogenic process. Primers that amplified the EDB region were used in real-time PCR. Results show that EDB expression increased significantly by day 14 and subsequently decreased (Figure 8H). This pattern of expression indicates chondrocyte maturation after two weeks of treatment, and the progression to hypertrophy thereafter [228]. From these results, pre-hypertrophic cells were present at day 14, and hypertrophic cells at day 28. The progression from pre-hypertrophic to hypertrophic

stage can also be seen by the change in cell morphology as cells undergoing hypertrophy increase in size.

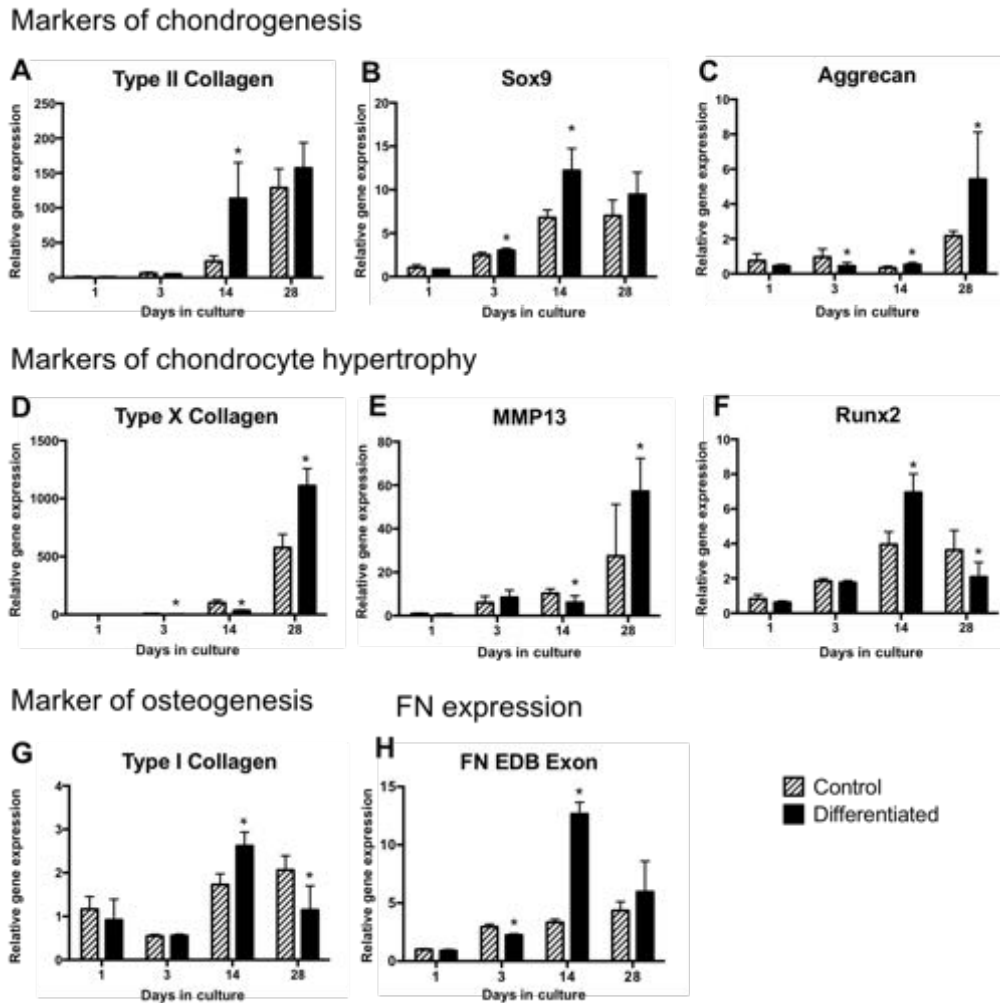


Figure 8. Expression of ECM genes during chondrogenesis of ATDC5 cells. ATDC5 cells were cultured either in maintenance media (Control) or differentiation media (Differentiated) for 28 days. Samples were collected on days 1, 3, 14 and 28. Total RNA was extracted at the indicated times, reverse transcribed, and the cDNA was used to determine the expression of different extracellular matrix (ECM) genes with real-time PCR. Markers of chondrogenesis (Type II Collagen (Col2a1), SOX9 (SRY-Box 9), Aggrecan) (A-C), markers of chondrocyte hypertrophy (Type X Collagen (Col10a1), MMP13 (matrix metalloproteinase), Runx2 (Runt-related transcription factor 2)) (D-F) and a marker of osteogenesis (Type I Collagen (Col1a1)) (G) were analyzed. (H) FN was also analyzed by measuring the expression of the EDB exon. Ct values were normalized to β -actin. The expression of each gene is presented as a fold change relative to the expression of control cells on day 1. The graph shows the mean values \pm standard deviation of three biological replicates, each measured in triplicate. The asterisk represents statistically significant differences between the gene expression of differentiated cells and the corresponding same-day control cells (* $p < 0.05$, calculated using the t-test method).

3.1.3 ECM formation and mineralization

To further evaluate ECM formation and mineralization, GAG accumulation in the ECM and calcium deposition were monitored in differentiating ATDC5 cells. The cells underwent the same chondrogenesis protocol as previously described, and were monitored over a 21-day time course.

Calcium deposition was evaluated by Alizarin red staining. Captured images show fibroblast-like cells at confluency by day 7 and rounded cells at day 14 (Figure 9A). Mineralization of the ECM was apparent by day 21 of chondrogenesis. Quantification of this staining showed a small increase in the early stages of chondrogenesis, then a large deposition occurred from day 14 to 21 (Figure 9B). Studies in the literature indicate that this initial delay is due to the cells undergoing early differentiation during this stage of chondrogenesis [237].

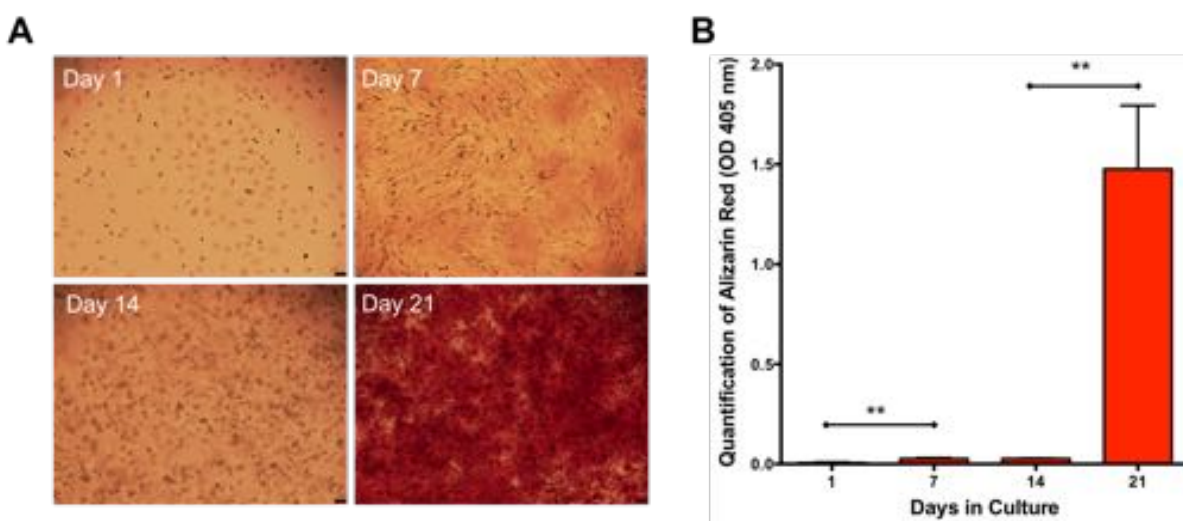


Figure 9. Calcium deposition in differentiated ATDC5 cells. (A) Calcium deposition was evaluated by Alizarin red staining of differentiated cell cultures fixed at days 1, 7, 14 and 21. Brightfield images show increased mineralization. (B) Quantification of Alizarin red staining was done on the time points indicated on the graph using the Epoch microplate spectrophotometer at 405 nm. Data is presented as the mean values of the absorbance readings \pm standard deviation of three biological replicates, each measured in triplicate. Differences were identified using the t-test method, $**p < 0.01$.

The accumulation of GAGs, a marker for chondrogenesis [245] was detected with Alcian blue. Images show an increase in GAG deposition as chondrogenesis occurs (Figure 10A). By day 14, a large proportion of the cells were Alcian-blue positive, indicating that the cells were successfully undergoing chondrogenesis. At day 21, an increase in Alcian blue staining demonstrated a GAG-rich ECM. This was confirmed by quantification of the staining in which there was an upregulation over the 21-day time course (Figure 10B). The predominant proteoglycan present in the cartilage is Acan. The onset of Alcian blue staining of cartilaginous nodules correlated with the increased mRNA expression of Acan in differentiating ATDC5 cells between days 14 and 28.

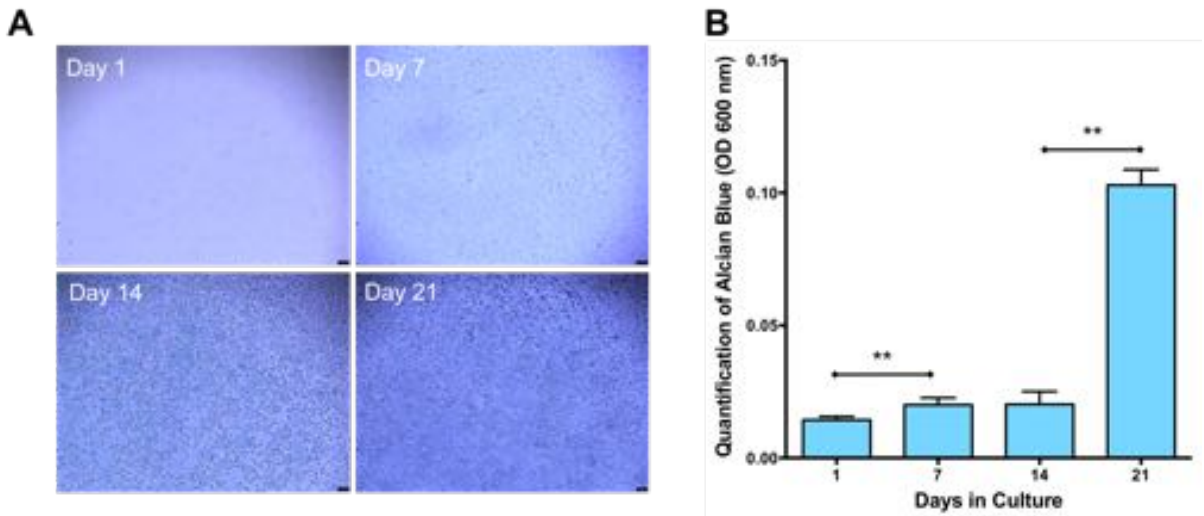


Figure 10. Glycosaminoglycan (GAG) accumulation in differentiated ATDC5 cells. Extracellular matrix (ECM) production was examined using Alcian blue staining of differentiated ATDC5 cells fixed at days 1, 7, 14 and 21. **(A)** Brightfield images show GAG accumulation in the ECM. **(B)** Quantification of the staining was determined at an optical density (OD) of 600 nm by spectrophotometry. The graph shows an increase in GAG deposition by day 28 compared to day 1. Data is presented as the mean values of the absorbance readings \pm standard deviation of three biological replicates, each measured in triplicate. Significant differences were identified using the t-test method, $**p < 0.01$.

Alizarin and Alcian staining thus showed different patterns of staining indicative of the cells undergoing chondrogenesis. This differentiation protocol will facilitate the analysis of ATDC5 cells harboring specific FN mutations as they undergo the chondrogenic process. The overall results demonstrated successful induction of chondrogenesis with ATDC5 cells.

3.2 GENETICALLY MODIFIED MICE

Recent discoveries of mutations in the *FNI* gene in patients with Sutcliffe-type SMD suggest an important role for FN in bone formation. However, the importance of the presence of FN in cartilage formation and skeletal growth has not been fully addressed *in vivo*. Thus, we address it in this work with a focus on skeletal phenotypes that reflect the features observed in affected patients.

3.2.1 Generation of knock-out mice

Mouse embryos that completely lack FN are not viable [125]. Therefore, to assess the importance of the presence of FN in endochondral bone formation, the Cre-lox system was employed to conditionally delete the *Fnl* gene both in plasma and in cartilage to create double knock-outs (dKO). The liver is the site of pFN synthesis. Thus, to knock out the *Fnl* gene in the liver, mice with lox sites flanking the *Fnl* gene (*Fnl*(fl/fl)) were crossed with transgenic mice expressing the Cre recombinase under the control of the albumin promoter (Alb-Cre) which is active in hepatocytes. Many researchers have successfully obtained liver-specific KO mice with the Alb-Cre/+ strain [174, 248]. Mice with lox sites flanking the *Fnl* gene (*Fnl*(fl/fl)) as well as *Fnl*(fl/fl);AlbCre/+ mice were obtained from Dr. Dieter Reinhardt. Their *Fnl*(fl/fl); AlbCre/+ mice delete pFN synthesized by liver cells by day P3. To knock out *Fnl* in the cartilage, (*Fnl*(fl/fl)) mice were crossed with Tg(Col2a1-cre)1Bhr/J mice obtained from Dr. René St-Arnault (Shriners' Hospital for Children, Montreal, QC). These mice express constitutive Cre recombinase under the control of a Col2 promoter which is expressed by chondrocytes [249]. *Fnl*(fl/fl); Col2Cre/+ mice were produced by breeding Col2Cre/+ mice with *Fnl*(fl/fl) mice.

Fnl(fl/fl); AlbCre/+ mice were crossed with *Fnl*(fl/fl); Col2Cre/+ mice and dKOs were generated after several rounds of breeding (Figure 11A). The presence of Cre recombinase in the specific tissues leads to the recombination of the *Fnl* gene at the two loxP sites which are located within the 5' UTR and within the first intron. This recombination event removes the region between the two sites to generate the null allele [250].

PCR analysis was used to genotype the mice to ensure that the KO is homozygous for the floxed allele (fl/fl) and positive for Cre (cre+). The presence of the floxed allele in the gene-targeted mice was confirmed using primer pairs where the sense primer targets a site upstream of the first loxP site and the antisense primer targets a site within the *Fnl* gene. The expression of Cre recombinase in chondrocytes and liver was detected using primers obtained from Jackson labs (Figure 11B).

3.2.2 Characterization of knock-out mice

3.2.2.1 Single KO mice

Mice lacking *Fnl* in cartilage (*Fnl*(fl/fl); Col2Cre/+) proved to be viable and fertile with no apparent phenotypic differences. *Fnl*(fl/fl); Col2Cre/+ crosses with homozygous *Fnl*(fl/fl) resulted in offspring of the expected Mendelian ratio of 1:1 for control (*Fnl*(fl/fl)) and transgenic (*Fnl*(fl/fl); Col2Cre/+) mice. These results can be explained by studies which have shown that pFN is able to permeate into tissues and incorporate into the ECM alongside the cFN. In fact, Moretti *et al.* have shown that up to 60% of the FN present in the ECM of tissues is derived from plasma [251]. Plasma FN therefore seems to be compensating for the lack of FN synthesized in the cartilage. In another litter, *Fnl*(fl/fl) and *Fnl*(fl/fl);AlbCre/+ did not show any abnormal phenotypes as well.

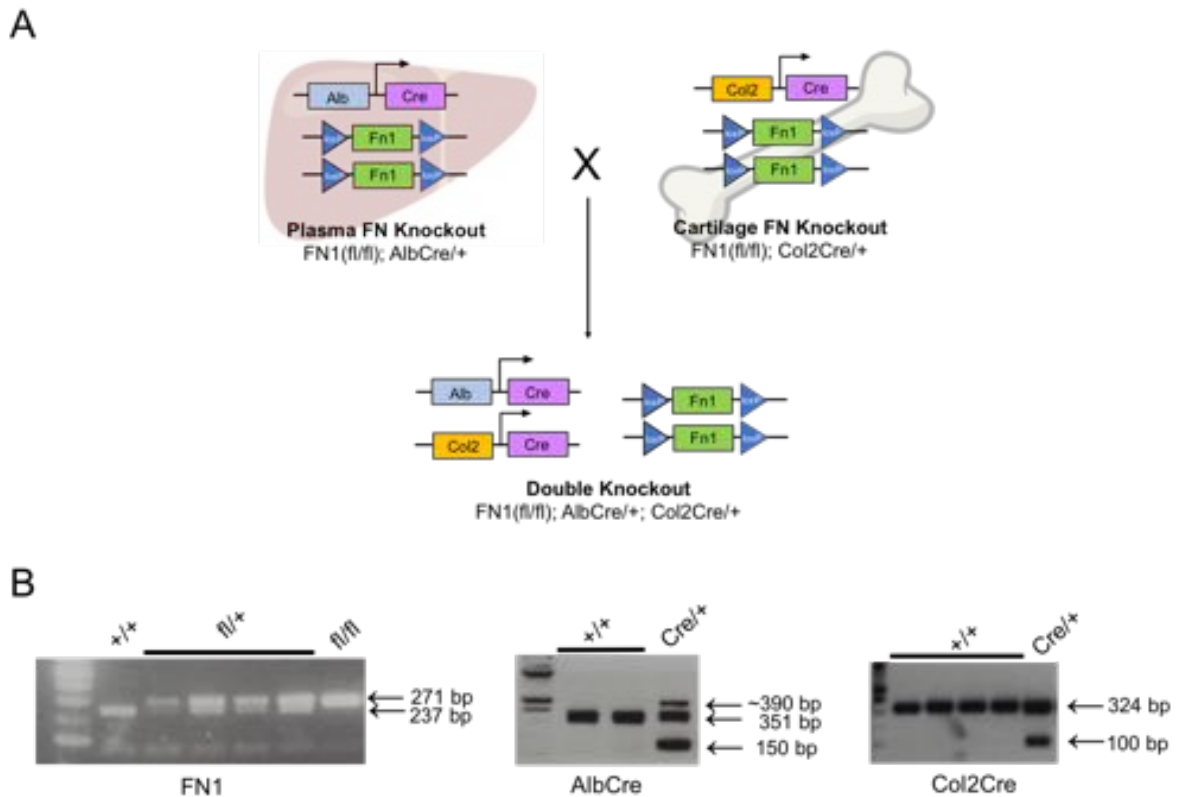


Figure 11. Generation of FN double knockout (dKO) mice in liver and cartilage.

(A) Plasma FN knockout (pFN KO) mice were generated by breeding mice with loxP sites (blue triangles) flanking the *Fn1* gene (FN1(fl/fl)) with transgenic mice expressing the Cre recombinase under the control of the albumin promoter (AlbCre/+) in the hepatocytes. Similarly, cartilage FN knockout (cFN KO) mice were generated by breeding FN(fl/fl) with Col2Cre/+ mice expressing the Cre recombinase in chondrocytes. The pFN KO and the cFN KO mice were then bred together to generate dKO mice (FN1(fl/fl); AlbCre/+; Col2Cre/+). Determination of the genotype and identification of edited animals was done by PCR amplification using primer sequences from The Jackson Labs. (B) Images of gels show examples of possible genotyping results. On the left, integration of the loxP sites in the *Fn1* gene and zygosity (wild type (+/+), heterozygous (fl/+), homozygous (fl/fl)) are shown by bands amplified at either 271 or 237 bp. Mouse DNA in which the Cre recombinase gene is present in the liver show a band at 390bp (AlbCre/+). The lower band at 150bp is an artifact that usually appears from the mutant allele. AlbCre-negative mice only show a band at 351 bp (+/+). The expression of Cre recombinase in chondrocytes was confirmed by an amplification at 100bp (Col2Cre/+). The band at 324bp is an internal positive control, and mice with only this amplification is Col2Cre-negative (+/+). *Fn1*: mouse fibronectin gene; FN: fibronectin protein; Alb: Albumin promoter; Col2: Col2a1 promoter; Cre: Cre recombinase enzyme; fl: flox.

3.2.2.2 Double KO mice

The KO mice that were generated were viable and did not show any gross anatomical abnormalities. From the same litter, FN1(fl/fl) (n=3), chondrocyte single KO (n=1) and dKO mice (n=3) were obtained. Fn1(fl/fl) mice lacking Cre were considered as WT mice and are used as controls in these experiments. Since males and females differ in bone size and bone mass despite having a similar body size, only males were analyzed as they present with better skeletal integrity [252]. From 2 to 8 weeks of age, the mice were weighed (Figure 12A), and due to the observation that patients with Sutcliffe-type SMD have a shortened trunk, their body length from nose to anus was measured (Figure 12B). No difference in either weight or length was observed between the three groups.

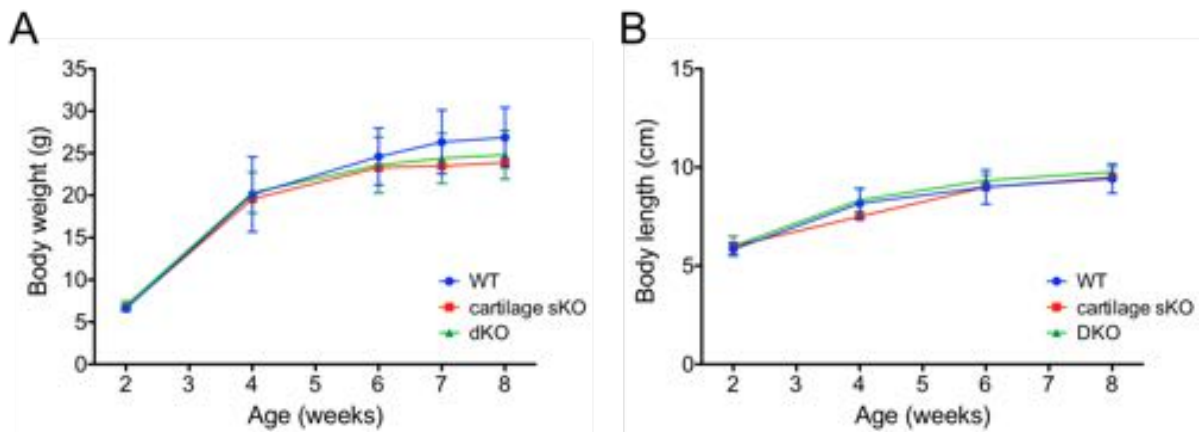


Figure 12. Weight and length of FN knockout mice. Male mice from the same litter were phenotypically characterized. Wild-type (WT) mice represent the control animals with the genotype FN1(fl/fl) (n=3). Mice in which FN was knocked out only in the cartilage is represented by cartilage FN single KO (cartilage sKO) (FN1(fl/fl);Col2Cre/+) (n=1), and mice in which FN production is ablated in the liver and the cartilage are the double knockout mice (FN1(fl/fl); AlbCre/+; Col2Cre/+) (n=3). Body weight (**A**) and length from nose to anus (**B**) of each mice were measured at the indicated time points in the graph between 2 and 8 weeks. Data are presented as the mean \pm standard deviation of all the animals in the corresponding group.

At 2 months, X-ray images were taken to further assess any skeletal abnormalities in the long bones (Figure 13A). Two months in mice age is approximately equivalent to 6 years in humans [253]. This is the age at which radiological features such as corner fractures can be observed in patients. In these mice, no evidence of scoliosis was found, no difference in the vertebral bodies between control and KO mice, no “corner fractures”, and no manifestation of coxa vara. The femur, tibia, humerus and radius were similar in morphology, and measurements of these long bones did not reveal any significant differences in size (Figure 13B-E). These findings point to what seems to be normal ossification in the KO mice.

When the dKOs were subjected to breeding, they proved to be fertile, giving birth to litters with a size and gender ratio similar to those of WT litters. These negative results thus make it seem less probable that the phenotypes seen in patients with SMD-CF are caused by a global reduction of FN in the body.

3.2.3 Generation of CRISPR knock-in mice

To assess if the dysregulation in cartilage formation is caused by specific *FNI* mutations, mice with a knock-in (KI) mutation (NM_212482.1:c.778T>G, p.(Cys260Gly)) were generated using the CRISPR-Cas9 approach. The p.Cys260Gly mutation was chosen out of the other published mutations because it showed very strong cellular retention in *in vitro* experiments done in HEK293 cells [106]. A 20-nucleotide single-guide RNA (sgRNA) harboring the desired edit was chosen based on the analysis of on-target score, off-target score, and its location next to a protospacer adjacent motif (PAM) site TGG (See Figure 14). A single-stranded donor oligonucleotide (ssODN) homology directed repair (HDR) template was designed complementary to the “no PAM” strand with homology arms of 40nt on the PAM distal side and 91 bp on the PAM proximal side. Asymmetric ssODN templates have been shown to enhance the efficiency to targeted mutations [254]. The ssODN contains the desired edit (blue

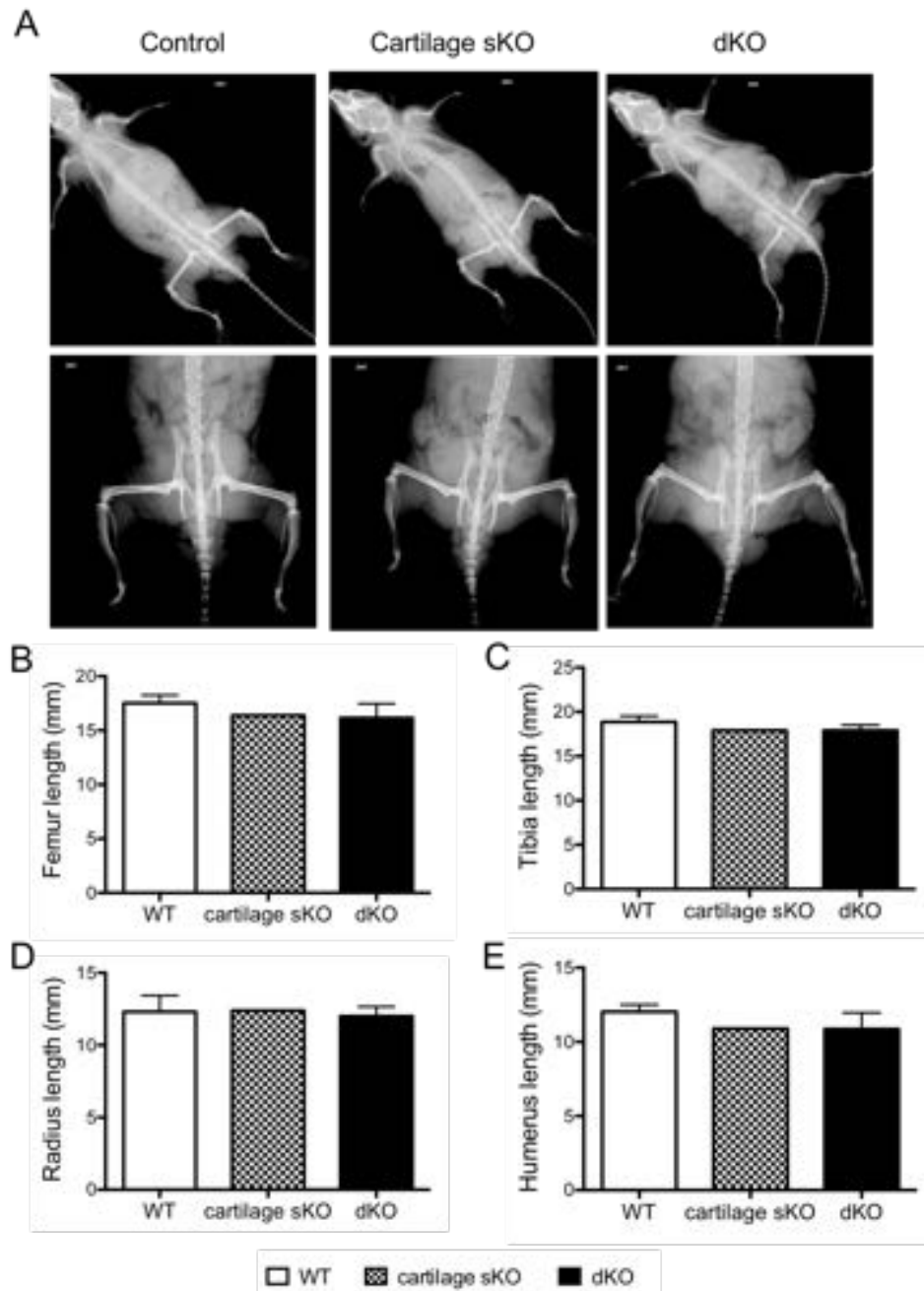


Figure 13: Bone analysis of FN knockout mice. (A) Radiographs of 8 week old wild-type (WT, n=3), cartilage FN single KO (cartilage sKO, n=1) and double knock-out (dKO, n=3) mice were taken. Lengths were measured for the (B) femur, (C), tibia, (D) radius, and (E) humerus. Measurements are represented as mean \pm standard deviation. No difference was seen in the measurements nor in the radiographs.

box) as well as three silent mutations (highlighted in blue and yellow) proximal to PAM to prevent unwanted cleavage after the desired edit was completed. A Pst1 restriction site was simultaneously introduced in one of the silent mutations (CTT → CTG). This restriction enzyme site will help to easily identify modified mice by PCR restriction digest analysis [255]. Injection of mouse embryos with guide RNAs, Cas9 mRNAs and repair templates were done at the McGill University mouse transgenesis facility.

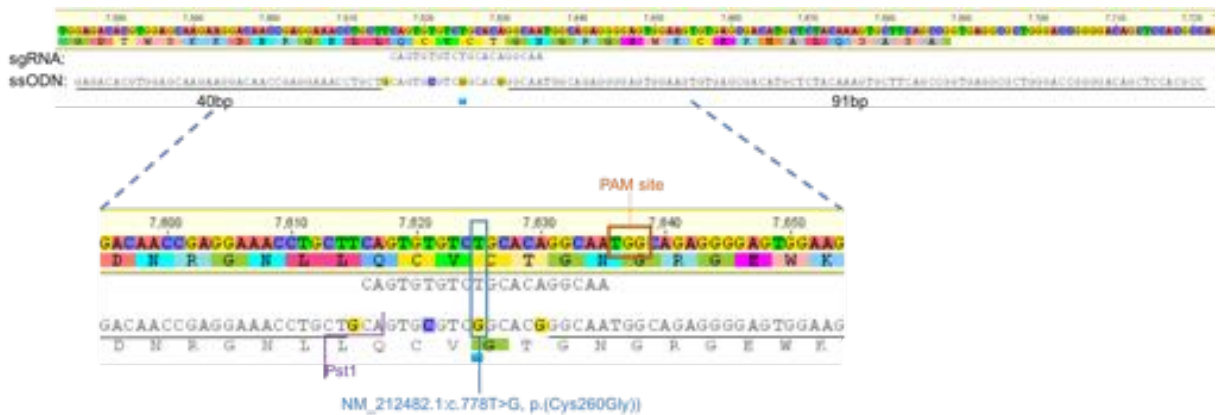


Figure 14. CRISPR knock-in strategy. Schematic illustration of the CRISPR-Cas9 approach to generate mice with a p.(Cys260Gly) mutation. A partial region of the exon 6 of *FNI* gene is shown with the sgRNA and the asymmetric ssODN repair template. The sgRNA is located next to a PAM site (brown box). The repair template contains the desired edit (blue box) along with three silent mutations (highlighted in blue and yellow on the ssODN strand, excluding the desired edit). The first silent change shown on the illustration introduces a Pst1 restriction enzyme site (purple line). sgRNA: single-guide RNA; ssODN: single-stranded donor oligonucleotide; HDR: homology directed repair.

To genotype the animals, PCR analysis was done with mouse tails using a combination of different primers (Figure 15A). WT-specific primers were designed to bind to the WT sequence, while mutant-specific primers were designed to bind only to the edited sequence. Gel electrophoresis of the PCR products showed that the WT-specific primers amplified the genomic DNA of all mice, whereas only mouse #4 produced a band at the right height with mutant-specific primers (Figure 15B). This indicated that this mouse is heterozygous for the mutation. To confirm the presence or absence of the mutation, PCR products were sent for Sanger sequencing. The PCR products were first amplified using primer pairs that bind to regions on either side of the mutation to avoid any sequence bias in the region being amplified. Sanger sequencing confirmed the presence of the mutation in mouse #4, as well as the heterozygous change of two of the silent mutations (Figure 15C).

A female mouse carrying the knocked-in mutation was therefore successfully generated (Fn1^{emhC260G}). This mouse is bred with a WT C57bl/6N male to generate more mice harboring the mutation. Whether these mice will present any of the phenotypes seen in the patients remains to be determined. The p.Cys260Gly mutation is predicted to break disulfide bonds between two residues at the *FN1* type I domain in the N-terminal half of the protein [106]. This region is known to be important to initiate FN assembly on the cell surface. The ECM may therefore be compromised by this specific mutation, consequently affecting the viability of chondrocytes, and the quality and function of the cartilage and bone *in vivo*. Characterization of these knock-in mice will need to be done to determine if such is the case and if the mutation affects FN secretion as seen *in vitro*.

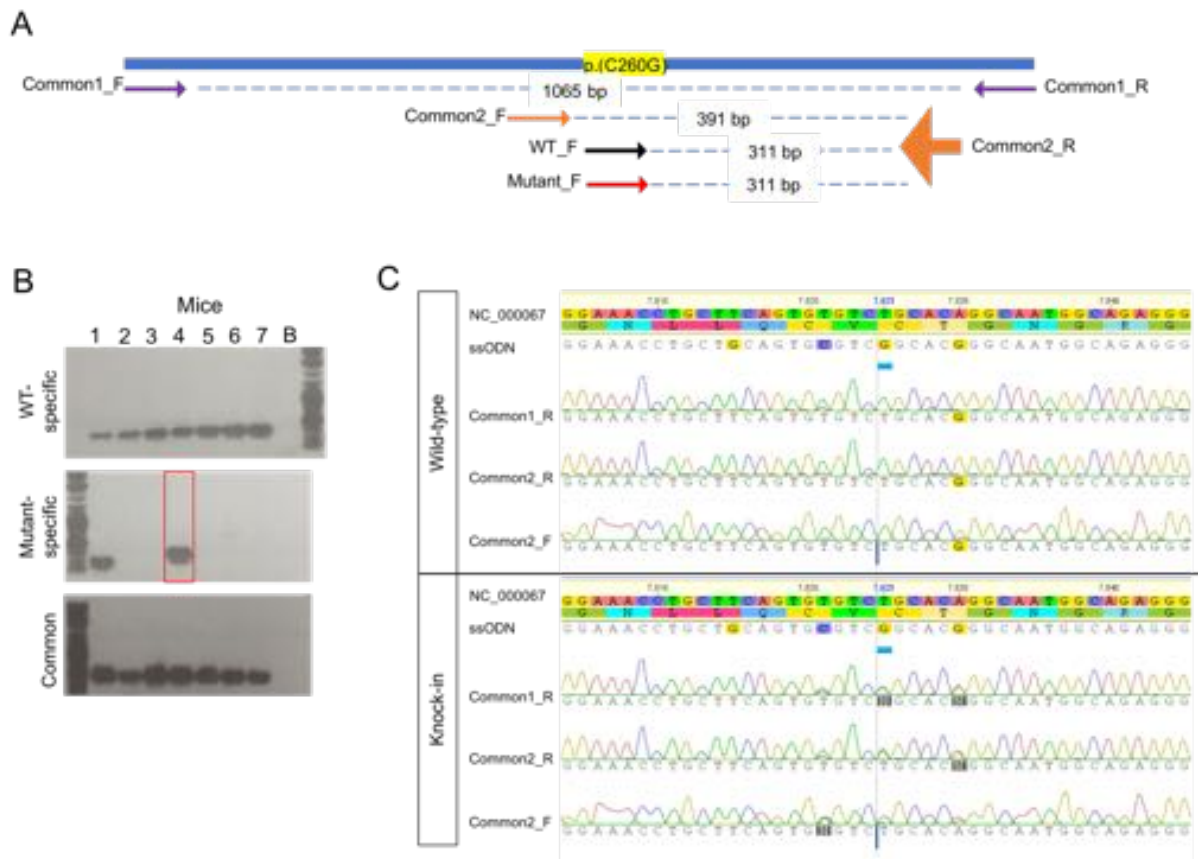


Figure 15. Genotyping CRISPR knock-in mice. (A) To genotype the mice, primer pairs were designed to bind to different regions of the *FNI* gene surrounding the location of the desired mutation. Common forward and reverse primers (Common1 and Common2) bind to sequences outside of the mutation, whereas wild-type specific (WT_F) and mutant specific (Mutant_F) primers bind to the region of the mutation. Product sizes are indicated for each primer pair. Mutant_F will only bind if the DNA strand contains the desired edit. (B) Mouse DNA was amplified by PCR and run on gel. All mice had a WT DNA strand as seen on the top gel (amplified with WT_F and Common2_R primers). The middle gel shows one positive knock-in. Mouse #4 had the desired edit indicated by a red box (amplified with Mutant_F and Common2_R primers), suggesting that this mouse is heterozygous for the mutation. Mouse #1 also showed amplification but did not migrate at the right height. DNA was also amplified with the Common2 primer pair (bottom gel) and were sent for Sanger sequencing to confirm the presence or absence of the mutation. (C) Chromatograms of the mice shows successful integration of a heterozygous mutation in mouse #4 (bottom chromatogram). The DNA of the other mice did not contain the desired edit (top chromatogram).

3.3 CASE STUDY OF A PATIENT WITH SUTCLIFFE-TYPE SMD

In a study published in 2017 by our lab in collaboration with Dr. Reinhardt's team, mutations in the *FNI* gene were identified in patients using sequencing technologies [106] (See Annexe I). Throughout the duration of this work, patients with suspected SMD-CF were brought to our attention from different sources, including various registries and collaborations. One individual who fit the phenotypic profile of the disease was a boy from New Zealand.

3.3.1 Clinical Features

Collaborators from New Zealand notified Dr. Campeau of a patient with suspected SMD-CF. This patient had genu varum and walked with a waddling gait. He presented with a short stature with short long bones and was overall disproportionate. Facial features included a flat profile (Figure 16D). Radiographic findings showed widespread irregular metaphyses, abnormal vertebral bodies, as well as corner fractures in long bones (Figure 16A-C, E). It was these radiographic findings that raised the suspicion of SMD-CF at 6 years of age. This patient did not present with coxa vara, scoliosis, chest anomalies or renal abnormalities.

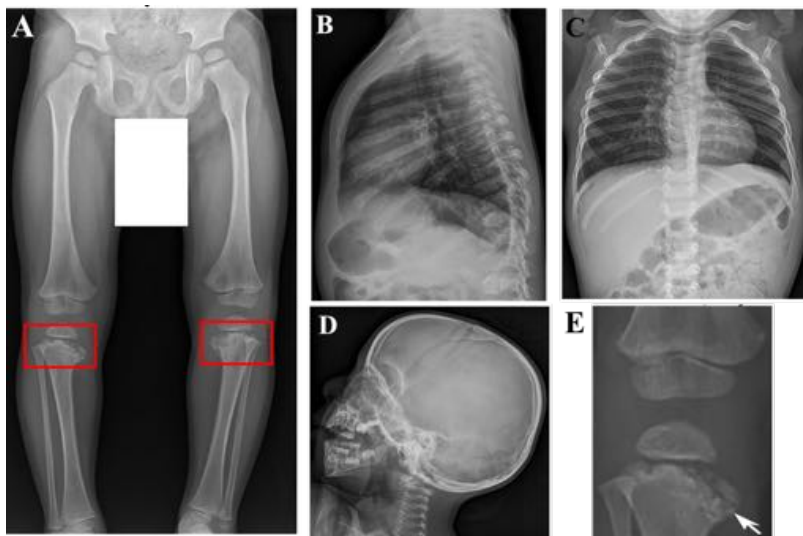


Figure 16. Radiographs of patient with Sutcliffe-type SMD. X-rays were taken of an affected patient at 2.8 years old. (A) Metaphyseal abnormalities and corner fractures are shown in red boxes. (B-C) Flattened vertebral bodies. (D) Flat facial profile. (E) Arrow points to corner fractures.

3.3.2 Sequencing of patient DNA

Genomic DNA from this patient was shipped to our laboratory after a written informed consent was obtained from the patient's legal guardian. Primers were designed to sequence *FNI* exons 1-7 and 13-18, which are the known mutational hotspots of *FNI* mutations in SMD-CF based on what has been published so far [106]. PCR was done using the exon-specific primer pairs (Figure 17A) and the amplified regions were sent for Sanger sequencing.

By mapping the sequencing results to the human *FNI* genomic sequence (NG_012196.1 RefSeqGene), a mutation on exon 3 was identified: NM_212482.2:c.368G>A, p.Cys123Tyr. Sequencing of the parents' genomic DNA for the same exon demonstrated the *de novo* nature of the mutation (Figure 17B, red box). This novel heterozygous missense variant is not present in the GnomAD database. It is found to be located in the *FNI* type-I domain and is predicted to destroy disulphide bridges between cysteine residues at the protein level.

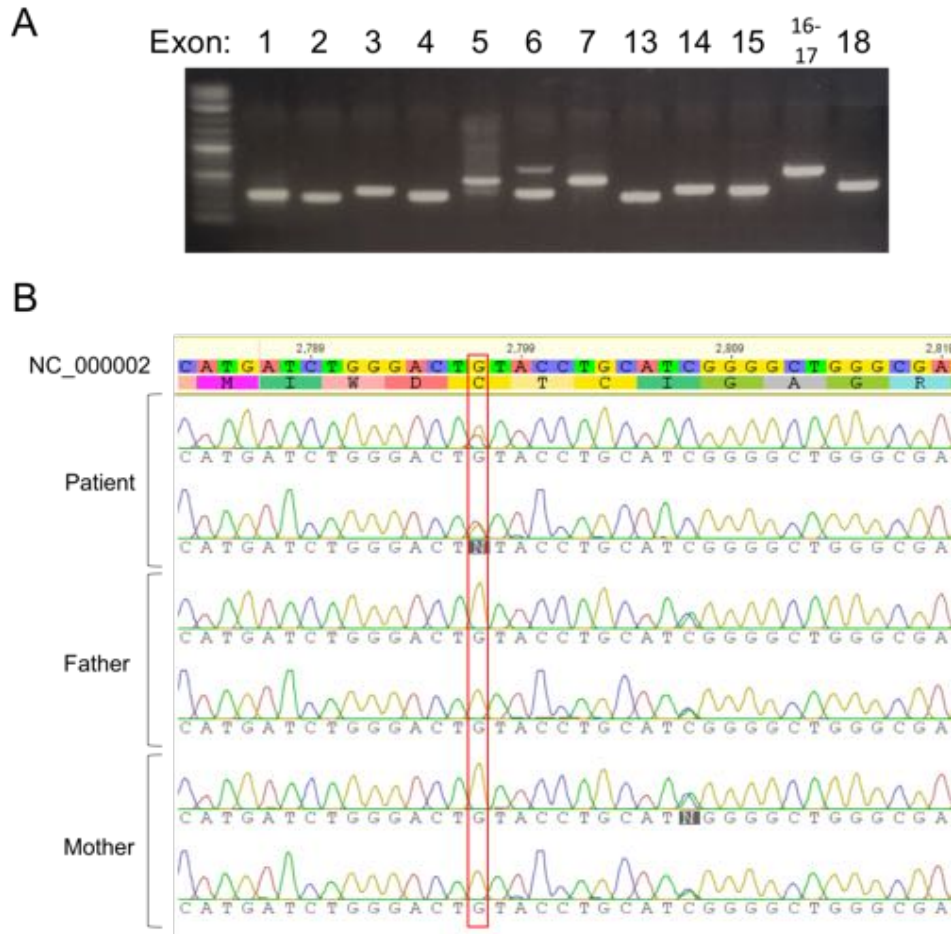


Figure 17. Sanger sequencing of the *FNI* gene. A PCR reaction was done on the DNA of a patient with SMD with corner fractures (SMD-CF) using primer pairs that amplify exons 1-7 and 13-18. These exons are the known mutational hotspots of *FNI* mutations in SMD-CF. (A) PCR products were run on gel and sent for Sanger sequencing. Sanger sequencing results showed a heterozygous mutation on the patient's 3rd exon when mapped to the human *FNI* genomic sequence (NG_012196.1 RefSeqGene) downloaded from the NCBI database. Father and mother's DNA were subsequently sequenced to determine if it was a de novo mutation. (B) Each individual was sequenced with forward and reverse primers (first and second sequence respectively) for exon 3. The red box shows the position in which the patient shows a de novo G>A mutation. Sequences were analyzed using the Geneious computer software version R8.

CHAPTER 4: DISCUSSION

FN's presence in the formation and maintenance of cartilage and bone suggests its importance in skeletal tissue. However, little is currently known about its functional role in the development and homeostasis of cartilage. The identification of mutations in the gene that encodes FN in patients with SMD-CF offers the opportunity to determine its function.

An optimization of the standard chondrocytic differentiation protocol on ATDC5 cells as an *in vitro* model was performed to allow us to better examine the consequences of *FNI* mutations in the chondrogenic process. Although the ATDC5 cell line is widely used as a model system, different studies use different formulations of differentiation media. Previous studies have demonstrated that the ATDC5 cells favored the medium with a supplementation of ITS, TGF- β 1, ascorbic acid and dexamethasone (Dex) for chondrocytic differentiation [228, 237, 256].

Additions that were shown to be essential for cell survival are ITS and ascorbic acid [257]. ITS was included in all consulted protocols throughout the whole chondrogenic program as it assists the metabolic activities in chondrocytes for it to undergo differentiation [257]. In its absence, the cells remain at the condensation phase, and if removed during the hypertrophic stage, the cells are not able to maintain their morphology and convert back into fibroblast-like cells [228]. Most protocols added ITS at confluence, but it was added to subconfluent cells in this protocol to promptly start the differentiation process [258]. This seemed to be beneficial because at day 14, treated ATDC5 cells were at a higher cell confluence than untreated cells, and had formed many cartilage-like nodules. This is consistent with the literature which has shown that ATDC5 condense into nodules when stimulated with ITS [27]. Formation of cartilage nodules is important for mineralization of chondrocytes [259].

The induction of Col2a1 and Col10a1 expression was aided by the addition of L-ascorbic acid. Ascorbic acid is essential for the energy metabolism of cells, as well as for collagen fibril formation and assembly in the ECM which is necessary for successful ATDC5 differentiation [130, 257]. The ECM produced by the ATDC5 cells exposed to ascorbic acid reduces the proliferative phase and promotes hypertrophic differentiation [258]. It also helps in the

upregulation of Col10a1 expression which encourages mineralization, as demonstrated by the onset of mineralization in our cultures of differentiated ATDC5 cells.

Contrary to most protocols that use the DMEM/F-12 media for chondrocytic differentiation, AMEM media was used here as it was shown to contain higher amounts of calcium and non-essential amino acids [228, 258, 260]. AMEM's standard formulation by itself already contains ascorbic acid. ATDC5 cells can therefore undergo the whole chondrogenesis program, from undifferentiated to mineralization just with AMEM containing 5% FBS, 1% antibiotic-antimycotic and ITS [260]. However, findings in this work show that the process occurred much more rapidly in media with added supplements. Cells cultured in only the maintenance medium of DMEM/F-12 do not undergo chondrogenesis [258]. Differentiating cells in DMEM/F-12 thus requires more growth factors at higher concentrations.

TGF- β 1 and Dex are added in published protocols to facilitate the differentiation of pre-chondrogenic ATDC5 cells into chondrocytes. TGF- β 1 helps in speeding up the proliferation phase and increasing ECM production [36]. Han *et al.* also found that TGF- β 1 efficiently regulates FN isoform expression, which induces the early stages of chondrogenic maturation [228]. TGF- β 1 was removed after 4 days because while it is known to enhance proliferation speed and enhance maturation at the early phase, it was shown to inhibit chondrocyte hypertrophy at later stages [228].

Dex, a glucocorticoid known to play a role in cell growth and differentiation [261], was omitted in this protocol. There is conflicting evidence with its use during chondrogenesis in which some studies showed that it induced differentiation, whereas others demonstrated that it inhibited the process [262-264]. The current consensus seems to be that it inhibits chondrogenesis when applied at the stage of cellular condensation, but had beneficial effects on hypertrophic or mineralizing chondrocytes at late stages [261]. Since the exact time point at which the cells entered hypertrophy was not yet known, this supplement was not included in the differentiation media. While it did not seem to delay differentiation in our findings, adding it in further experiments might be beneficial for enhanced mineralization.

Instead of Dex, the differentiation medium was supplied with the phosphatase inhibitor β GP to induce mineralization. In matrix mineralization studies, it acts as a phosphate group donor, promoting calcification of the bone matrix [265]. It was added to confluent cells because it can induce mineral deposition only once an appropriate ECM has been laid down. Certain protocols do not include β GP. Instead, to facilitate mineralization, CO₂ concentration would be shifted from 5% to 3% as studies have shown that chondrogenic differentiation is favored in anaerobic conditions [260]. The effect of β GP in the treated cells can be seen by the onset of mineralization at day 14 and advanced mineralization at day 28. Once cells have reached hypertrophy, β GP is cleaved by phosphohydrolases such as ALP produced by hypertrophic chondrocytes [237]. The release of inorganic phosphate which helps form the physiological mineral mimics the availability of phosphate *in vivo* [237]. Together, ascorbic acid, TGF- β 1, and β -GP reduced the proliferation phase and promoted differentiation.

The challenge in studying chondrogenesis *in vitro* is that differentiated chondrocytes have the tendency to de-differentiate back into fibroblast-like cells when cultured for long periods of time. De-differentiation was not witnessed in the treated cultures as the cells did not appear to lose their round phenotype throughout the process, and the expression profile of cells was consistent with the gene expression observed in previous chondrogenesis studies [232, 237, 266].

While one of the goals was to generate a protocol that induced differentiation at a shorter time period than what is already published, the overall results still demonstrated successful induction of chondrogenesis in ATDC5 cells, as shown by the increase in chondrogenesis factors until terminal differentiation. Differentiation of ATDC5 cells into chondrocytes was thus achieved in which an extensive ECM production was produced 14 days after seeding, and hypertrophic cells were present by day 28. Analysis at later time points is necessary to determine if Sox9 expression is maintained, if the cells remain at the hypertrophic stage, and if the downregulation of osteoblastic markers Runx2 and Col1a1 is caused by signaling pathways that act to prevent excessive mineralization.

As future experiments, the laboratory of Dr. Dieter Reinhardt will stably transfect ATDC5 cells with FN constructs harboring the p.Cys87Phe, p.Cys260Gly, and p.Tyr240Asp mutations similar to what has been done with HEK293 cells [106]. These mutations have been shown to destabilize FN type I domains, consequently affecting the FN's ability to assemble at the cell surface as well as to bind to fibroblasts [106]. The transfected cells will then be induced to undergo the chondrogenic process using our differentiation media and assess how mutations in the *FNI* gene affect chondrocyte differentiation and function. Knocking in the FN mutations using the CRISPR/Cas9 method described in the generation of the mouse knock-in can also be done to introduce the mutations in the cells. Since ATDC5 cells produce their own FN, CRISPR knock-ins can eliminate the expression of endogenous FN that often appears as a background in functional experiments. Apart from ATDC5 cells, another cell model that can be used is induced pluripotent stem cells (iPSCs). iPSCs derived from fibroblasts and/or peripheral blood mononuclear cells (PBMCs) of affected patients can be differentiated into a number of various cell types, including chondrocytes, using commercial or home-made differentiation protocols and kits [267]. Since these iPSCs are derived from affected individuals, no genetic manipulation is required to obtain cells harboring the desired mutation. Differentiation of the cells into chondrocytes will thus allow us to investigate the consequences of *FNI* mutations on chondrocyte function as accurately as possible to what occurs in the patients. In the long-term, generating patient-specific iPSCs can also provide us with a large resource of *FNI*-mutant cells that could later be used to develop treatments for the disease [268].

For the two cell models, in addition to assessing the rate and efficiency of chondrocyte differentiation by gene expression analysis and staining, structural integrity will also be evaluated. Further histology will be done to determine the shape and alignment of the cells by haematoxylin and eosin staining, and the distribution of FN inside and outside of the chondrocytes (immunohistochemistry) will be examined.

Recently, a paper was published by Cadoff *et al.*, supporting the findings that mutant FN was retained in the cells. Briefly, they performed mass spectroscopy to determine the abundance of mutant FN relative to wild type (WT) in an affected individual bearing a FN mutation. Their findings indicated that mutant FN was present at much lower amounts than WT FN in the

patient's plasma, as well as in the cell culture media of their primary dermal fibroblasts [107]. Based on these observations, western blot and indirect immunofluorescence can be done to examine if the mutant FN induces a deficient secretion of FN in differentiated ATDC5 and iPSC cells harboring *FNI* mutations. Whether the mutant protein is retained or not, the formation and function of the FN network is expected to be affected. Moreover, since FN acts as a master organizer of different ECM networks and is involved in cross-talks with many regulatory and signaling pathways including BMP and TGF- β , the mutations are expected to affect ECM networks and dysregulate the activity of many growth factors stimulated by these pathways.

In vivo studies were conducted in this work to determine how FN mutations mechanistically contribute to SMD pathogenesis. Since the affected patients had heterozygous *FNI* mutations, it was hypothesized that the phenotypes observed in patients were due to haploinsufficiency in which there is only one functional copy of the gene instead of two. A loss of half of the gene function can lead to a global reduction in the level of FN, resulting in the disease. To determine if this was indeed the case, dKO mice were generated. The strategy involved knocking out *Fnl* in the liver and cartilage to halt production of FN in those tissues (Fn1(fl/fl); AlbCre/+; Col2Cre/+). The mice were then characterized phenotypically during the first two months.

The mice were expected to have some of the features of SMD, such as metaphyseal irregularities, shorter limbs and abnormality in the vertebral bodies. From the human disease, given the metaphyseal abnormalities but normal bone mass, the mice were not predicted to have impaired osteoblast or osteoclast function, but chondrocyte dysfunction and/or altered cartilage matrix was expected. Our results show that mice lacking *Fnl* in the cartilage (Fn1(fl/fl); Col2Cre/+) did not portray any abnormal features, and that the phenotype of dKO mice were indistinguishable from that of our control mice from the same litter. Length and weight measurements revealed no differences during development between dKO mice, cartilage-FN single KO mice, and their littermate controls. The mutants were viable and fertile. Further, skeletal malformations were not detected on radiographs, and the dKO mice did not seem to have any abnormal behaviour typical of the human patients. It might therefore be the case that the phenotypes observed in *FNI*-induced SMD-CF are not due to the global reduction of FN in

the body, but rather by an accumulation of mutant FN in the cells. Further comparisons would require a litter that also contains mice with FN KO only in the liver (Fn1(fl/fl);AlbCre/+) in addition to dKO, cartilage-FN KO and mice only expressing floxed FN for a better phenotypic evaluation. Previous studies which knocked out pFN *in vivo* by conditional deletion of FN in the liver have shown decreased FN content in the bone matrix associated with a decreased mineral-to-matrix ratio, but no effects on osteoblasts or osteoclasts [174]. Thus, bone density can be affected without any impact on bone formation in the mice. Analysis of the bone matrix by micro-computed tomography (micro-CT) will be able to better show such subtle changes. It would also be interesting to have mice that only expresses Cre without any floxed alleles to account for any possible Cre toxicity [269].

It is known that FN is produced and secreted by a multitude of cells including hepatocytes, chondrocytes, fibroblasts, endothelial cells and macrophages [124]. Due to its widespread expression in different tissues, it is possible that FN originating from sources other than the liver and cartilage might be contributing to the development of the skeletal system. The observation that *FNI* mutations linked to SMD are not embryonic lethal suggests that any affected process is only delayed or altered, but not entirely halted. Cadoff *et al.* have shown that 50% of normal FN production is enough for proper assembly and function of the FN matrix [107]. In fact, only when completely absent (homozygous FN-null) does it cause embryonic lethality [251, 270]. FN produced by other cells might therefore be “rescuing” tissues lacking FN.

Since FN has a crucial role particularly in the earlier stages of cartilage formation, there may have been an initial dysregulation, followed by a delay in which the system tries to compensate for the defect. In humans, clinical features such as spinal abnormalities may have appeared as a symptom of this early shortcoming seeing that the spine is one of the earliest structures to form, but through the compensation, patients later develop normal hands and feet. This mechanism has been shown by other *in vivo* experiments in which tissue-specific deletion of FN in mice resulted in healthy and viable mice. However, the mice still presented with subtle defects. Heterozygous FN-null mice, for example, appeared to be healthy and fertile even with only half of the normal level of FN. Yet, when examined more extensively, they showed delayed

tissue repair in injured arterioles [271, 272]. This possibility raises a clear limitation of our work: the experiments presented here only looked at basic phenotypes and not functions that might occur under special conditions (e.g. changes in bone density, effects on tissue repair, bone strength). Further experiments therefore need to be done to examine these features, evaluate if any signaling pathway is disrupted, as well as measure the level of gene expression of ECM markers by extracting the RNA from growth plates. Histology of the bone and the cartilage can also be done to assess the structure of these tissues and look at the level of GAG and calcium deposition.

Moreover, the *FNI* gene is well conserved throughout evolution, suggesting that many mechanisms act to protect its integrity, as well as ensure that its functions are not disrupted. This phenomenon points to genetic robustness. One of the mechanisms that lead to this is gene redundancy in which two genes share all or some functions. FN may therefore be functionally compensated for by similar matrix proteins with the same ability [273]. This mechanism was found to occur when N-cadherin is absent [274]. In experiments done to examine limb development ex vivo, N-cadherin-null limb bud explants were generated in which expression of N-cadherin was ablated. Surprisingly, condensation was not affected and resulted in the formation of normal skeletal structures. Further analysis revealed that bone formation proceeded through compensation by cadherin-11, another cell adhesion molecule, which upregulated in the absence of N-cadherin [274]. A similar compensation event may therefore be occurring in our dKO mice, although these speculated proteins remain to be identified. In mice, it has been estimated that around 50% of its genes have a related member in the genome with identical functions, and some of these genes may not even be present in humans [275, 276]. Interestingly, if it is, in fact, a case of functional redundancy in which a compensatory mechanism prevents a massive reduction in FN in tissues, it may reveal a potential therapeutic avenue for patients. Upregulating the expression of genes which encode a protein with functions similar to FN early during development may help patients who cannot produce or secrete the optimal levels of FN that is required for proper bone development. Thus, the importance of finding the cellular and molecular mechanisms of *FNI* mutations that lead to skeletal disease.

In a different point of view, the clinical manifestations reported in patients with SMD-CF may not actually be due to a reduction in global FN, but rather arise from the accumulation of mutant FN in the cells. This could be assessed by knocking-in a mutation (p.(Cys260Gly)) in the mouse. This mutation is located in the N-terminal domain of FN which is known to play an important role in matrix assembly, but now may also play a role in proper FN secretion from the cell.

The general secretory pathway dictates that shortly after synthesis, FN monomers are disulfide-bonded into dimers in the lumen of the endoplasmic reticulum (ER), the main site where proteins are synthesized and folded. Dimers are then transported through the Golgi apparatus and onto the cell surface [277]. Although this may hold true, much of the molecular details concerning the secretory pathway and assembly of FN are still unknown [130, 278]. Ishikawa *et al.* attempted to use the model of collagen secretion, but did not succeed in showing that the same mechanism applies to FN [278]. Studies have shown that a protein called periostin promotes secretion of FN from the ER [279, 280], and others have proposed that FAK, Rho-GTPases, and MAPK pathways are some of the regulatory mechanisms that play a role in this system. Looking into the mechanism of how FN mutants are retained in the cells can help fill in these blanks.

Recently, mutant FN harboring a mutation in the N-terminal domain was shown to accumulate within the ER of the cells, and thus not efficiently transported through the secretory pathway [107]. The same problem occurred with the cartilage oligomeric matrix protein (COMP), another cartilage protein which leads to the skeletal disorders pseudoachondroplasia (PSACH) and multiple epiphyseal dysplasia (MED). This protein was found to accumulate in the rough ER in chondrocytes when mutated. This resulted in the decreased secretion in the culture medium, similar to what was observed with mutant FN [280].

Improper folding can impede secretion from the ER. When there is accumulation of misfolded proteins in the ER, an unfolded protein response (UPR) is activated to prevent any global disruption in the pathway. This can lead to apoptosis in prolonged stress [281]. However, it was shown that the accumulation of mutant FN did not induce the UPR or apoptosis in the

cells [106]. Most of the *FNI* mutations found in patients with SMD-CF disrupt disulphide bonds between cysteine residues, which leads to the disruption of the tertiary structure [106]. While the absence of stress responses suggests that they were properly folded, it may be more likely that the mutant proteins simply managed to avoid being detected by these mechanisms.

The ER recognizes misfolding through the decreased amount of N-linked glycosylation on the protein. ER enzymes and heat shock proteins then attempt to fix the misfolded proteins and prevents them from continuing the pathway [282]. The process of how FN is assembled into a compact protein is still not well-known. However, it is known that the FN structure has many cryptic sites that are only revealed in certain situations. Mutations may lead to these sites being exposed due to improper folding. This can result in the binding of proteins such as chaperones that can inhibit the activation of the ER stress response, and even allow some mutated proteins to “leak out” of the cell as shown by FN proteins harboring a p.Y240D mutation [106].

Assuming that mutant FN are indeed misfolded and therefore not in an entirely inactive compact conformation, these mutated proteins may bind to other cartilage proteins in the ER which can prevent their transit towards the Golgi apparatus. The accumulation of ECM components in the ER can seriously impair the activity of chondrocytes and lead to their death as well as result in a defect in ECM production [280, 283, 284]. The mutational hotspots on the *FNI* gene in SMD-CF are in the type I domain of *FNI*. This domain plays an important role in ECM assembly, and contains sites important for binding to fibrin, heparin, and to other FN molecules [124, 141]. Schwarzbauer *et al.* has shown that FN lacking all or part of the first five type I repeats (FN_{I-5}) is unable to form fibrils [133]. Based on what is known in the literature, the p.C260G mutation is expected to disrupt fibrillogenesis and ECM formation. Indeed, Cadoff *et al.* found that the mutant FN causes reduced FN and collagen matrices, ultimately affecting ECM assembly [107].

In addition, mutant proteins that manage to get secreted out of the cells may also contribute to a defective matrix. Wang *et al.* have shown that substituting a lysine amino acid for glutamine in the FN IIICS region resulted in a loss of FN matrix formation which had important implications in tumor metastasis [285]. A similar consequence was demonstrated in

other ECM proteins such as collagen. The replacement of glycine amino acids with serine in the FN-binding domain of collagen led to decreased binding between collagen and FN. This resulted in the degradation of collagen and an inadequate matrix formation [143]. Given the role of the FN domains in which the identified *FNI* mutations are located, similar outcomes are expected.

Many reasons have been elucidated as to the patho-mechanism of SMD-CF caused by *FNI* mutations. Perhaps the combination of both the retention of mutant FN in cells and the reduced FN levels in the tissues contribute to the overall development of the disease. Many proteins may work to compensate for the deficit in FN, but the disruption in the system will lead to a phenotype, whether it be minor or severe.

Patients with *de novo FNI* mutations published in our previous paper [106] were identified from different sources such as collaborations, registries, the International Skeletal Dysplasia Society emailing list, Shriners Canada Skeletal Dysplasia Clinic and GeneMatcher. Throughout this work, more individuals with phenotypes corresponding to SMD-CF were brought to our attention, and with targeted Sanger sequencing, a patient with a *de novo* mutation in the *FNI* gene was identified. This patient presented with irregular metaphyses, abnormal vertebral bodies and corner fractures in long bones which are features that are characteristic of patients with SMD-CF. The absence of coxa vara and scoliosis in this patient demonstrates a phenotypic variability in this disease, expanding the clinical features of *FNI*-induced SMD-CF.

This variability may be explained by differences in the location of the mutations. Other mutations on FN have been found that caused GFND, but they clustered on the C-terminal half of the protein in contrast to the N-terminal half where most SMD-CF mutations are located. Our patient did not have any renal abnormalities, and neither did the other patients diagnosed with SMD-CF. Similarly, patients with GFND do not have any skeletal abnormalities, suggesting that the location of the mutation within the FN protein is crucial for the manifestation of either one of the disease. The alteration of a specific residue can also contribute to the variability of the phenotype as no two affected individuals have the exact same phenotypes [106]. No pattern can be seen just yet between the location of the mutation and the severity of the phenotype, but

the identification of more patients may allow us to eventually make this type of correlation. From a molecular point of view, variations in the clinical characteristics presented by patients can also be due to the differences in the amount of mutant FN retained or secreted by the cells or the degree at which FN from other sources can rescue the defect [107]. The advent of sequencing technologies has therefore allowed the identification of additional patients with *FNI* mutations. In fact, in an article we have written with our collaborators, four other patients with SMD-CF with slightly different clinical features were also found to have mutations in the N-terminal portion of the *FNI* gene (Costantini *et al.*, manuscript under review). These patients expand the phenotypic and genetic spectrum of SMD-CF.

With FN's involvement in bone formation and homeostasis in SMD-CF, it is not unlikely that mutations in the *FNI* gene are found in other bone diseases. Indeed, *FNI* mutations are now being identified in another skeletal disease, namely idiopathic scoliosis (IS). IS is a more frequent condition compared to SMD-CF affecting up to 3% of the population [286]. It is defined by a 3D deformity of the spine characterized by lateral curvature of the spine and rotation of the vertebral bodies [287]. The etiology of IS is currently not well understood, but several studies suggest a genetic contribution [288]. An analysis of rare coding variants performed by the laboratory of Dr. Campeau and his collaborators found *FNI* variants in some of these families with IS (preliminary data, unpublished). Thus, in a broader context, certain *FNI* variants may predispose individuals to scoliosis as this is a common clinical feature between IS and *FNI*-related SMD-CF. Determining the contribution of FN in IS is an area of future work that may help to better understand the role of FN in skeletal development and maintenance.

CHAPTER 5: CONCLUSION

FN is known to be involved in many basic molecular functions and is widely expressed in different tissues. Its importance in embryonic development mainly stems from its ability to assemble into a fibrillar matrix and its participation in the regulation of growth factor pathways. However, despite its involvement in many processes, its functional role in bone formation has not been fully explored. The discovery of mutations in the *FNI* gene in patients affected with Sutcliffe-type SMD, a rare skeletal disorder, brings to light this gap in the current knowledge.

The involvement of growth plates in affected patients led to the speculation that the cartilage is the main tissue affected in the disease. This observation, combined with the identification of *FNI* mutations, generated the hypothesis that mutations in the N-terminal domain of the protein can affect protein secretion, impair ECM assembly, cause chondrocyte dysregulation, and affect the function of growth factors. All this can lead to improper skeletal growth. The conservation of the *FNI* sequence is therefore more crucial than previously expected.

ATDC5 cells as an *in vitro* chondrogenic model will allow for the better understanding of the effect of the mutations in chondrocyte and ECM function. An optimized protocol to induce chondrogenesis in these cells has been successfully tested and evaluated in wild-type cells, and is ready to be applied on ATDC5 cells harboring a number of *FNI* mutations. These experiments may also help reveal details on how FN is secreted from cells in physiological conditions as such information is currently lacking in the literature.

The generation of mice in which *FNI* was ablated in the liver and the cartilage did not replicate the clinical features observed in the patients based in the analyses performed thus far, indicating that the gross phenotypes of SMD-CF may not be due to the global reduction of FN. However, more tests are required to determine if the knockout of the gene disrupted other pathways that could result in more subtle phenotypes such as changes in the bone matrix, bone strength and stiffness, or affected processes that can only be observed in special circumstances such as tissue repair during injury. Biomechanical testing and micro-CT are some tests that can be performed to further analyze the bone phenotype of these mice. Nevertheless, the absence of

expected skeletal malformations in the mice may have revealed a phenomenon of compensation that has not previously been shown with FN.

Experiments and analyses done in this work are only the first steps towards the discovery of a whole unexplored area in the field of skeletal formation. Once the transfected ATDC5 cell lines and knock-in mice are generated, there is no doubt that it will uncover many unknown details. Not only will it explain how mutations in *FN1* can lead to Sutcliffe-type SMD and reveal its functional role in bone development, but it can also reveal details about its secretory pathway in cells which can be relevant for other diseases that involve a deficiency in protein secretion. Furthermore, understanding the effect of the mutations can also improve the counseling of the patients and families affected by skeletal disorders. In fact, the continued identification of *FN1* mutations in patients affected with Sutcliffe-type SMD, and more recently, in patients with IS, raises questions on how important FN is in skeletal growth. A larger cohort of patients will further validate current results and allow for the development of targeted treatments. It can also enable the creation of diagnostic tests to determine the presence of this disease in a newborn or to estimate the probability for an individual to develop the disease. Preventive measures can therefore be taken by the patient or early intervention can be provided to limit disease progression.

Bibliography

1. Hill, M.A. *Musculoskeletal System - Bone Development Timeline*. Embryology [cited 2018 September 20]; Available from: https://embryology.med.unsw.edu.au/embryology/index.php/Musculoskeletal_System_-_Bone_Development_Timeline.
2. Knight, M.N. and K.D. Hankenson, *Mesenchymal Stem Cells in Bone Regeneration*. Adv Wound Care (New Rochelle), 2013. **2**(6): p. 306-316.
3. Olsen, B.R., A.M. Reginato, and W. Wang, *Bone development*. Annu Rev Cell Dev Biol, 2000. **16**: p. 191-220.
4. SF, G., *Osteogenesis: The Development of Bones.*, in *Developmental biology*, S. Associates, Editor. 2000, Sunderland (MA).
5. Stanton, L.A., T.M. Underhill, and F. Beier, *MAP kinases in chondrocyte differentiation*. Dev Biol, 2003. **263**(2): p. 165-75.
6. Gadjanski, I., K. Spiller, and G. Vunjak-Novakovic, *Time-dependent processes in stem cell-based tissue engineering of articular cartilage*. Stem Cell Rev, 2012. **8**(3): p. 863-81.
7. Martinez Sanchez, A.H., et al., *Chondrogenic differentiation of ATDC5-cells under the influence of Mg and Mg alloy degradation*. Mater Sci Eng C Mater Biol Appl, 2017. **72**: p. 378-388.
8. Kovacs, C.S., *Bone development in the fetus and neonate: role of the calciotropic hormones*. Curr Osteoporos Rep, 2011. **9**(4): p. 274-83.
9. Boskey, A.L. and R. Coleman, *Aging and bone*. J Dent Res, 2010. **89**(12): p. 1333-48.
10. Egawa, S., et al., *Growth and differentiation of a long bone in limb development, repair and regeneration*. Dev Growth Differ, 2014. **56**(5): p. 410-24.
11. Abad, V., et al., *The role of the resting zone in growth plate chondrogenesis*. Endocrinology, 2002. **143**(5): p. 1851-7.
12. Melrose, J., et al., *The cartilage extracellular matrix as a transient developmental scaffold for growth plate maturation*. Matrix Biol, 2016. **52-54**: p. 363-383.
13. Hatori, M., et al., *End labeling studies of fragmented DNA in the avian growth plate: evidence of apoptosis in terminally differentiated chondrocytes*. J Bone Miner Res, 1995. **10**(12): p. 1960-8.
14. Mackie, E.J., et al., *Endochondral ossification: how cartilage is converted into bone in the developing skeleton*. Int J Biochem Cell Biol, 2008. **40**(1): p. 46-62.
15. Bleumink, G.S., et al., *Insulin-like growth factor-I gene polymorphism and risk of heart failure (the Rotterdam Study)*. Am J Cardiol, 2004. **94**(3): p. 384-6.
16. Ghosh, S., et al., *In vitro model of mesenchymal condensation during chondrogenic development*. Biomaterials, 2009. **30**(33): p. 6530-40.
17. Singh, P. and J.E. Schwarzbauer, *Fibronectin and stem cell differentiation - lessons from chondrogenesis*. J Cell Sci, 2012. **125**(Pt 16): p. 3703-12.
18. Hall, B.K. and T. Miyake, *Divide, accumulate, differentiate: cell condensation in skeletal development revisited*. Int J Dev Biol, 1995. **39**(6): p. 881-93.
19. Regard, J.B., et al., *Wnt signaling in bone development and disease: making stronger bone with Wnts*. Cold Spring Harb Perspect Biol, 2012. **4**(12).

20. Chimal-Monroy, J. and L. Diaz de Leon, *Expression of N-cadherin, N-CAM, fibronectin and tenascin is stimulated by TGF-beta1, beta2, beta3 and beta5 during the formation of precartilaginous condensations*. Int J Dev Biol, 1999. **43**(1): p. 59-67.
21. Tavella, S., et al., *N-CAM and N-cadherin expression during in vitro chondrogenesis*. Exp Cell Res, 1994. **215**(2): p. 354-62.
22. Aomatsu, E., et al., *Cell-cell adhesion through N-cadherin enhances VCAM-1 expression via PDGFRbeta in a ligand-independent manner in mesenchymal stem cells*. Int J Mol Med, 2014. **33**(3): p. 565-72.
23. Ryu, J.H., et al., *Regulation of the chondrocyte phenotype by beta-catenin*. Development, 2002. **129**(23): p. 5541-50.
24. Pizette, S. and L. Niswander, *BMPs are required at two steps of limb chondrogenesis: formation of prechondrogenic condensations and their differentiation into chondrocytes*. Dev Biol, 2000. **219**(2): p. 237-49.
25. Burdan, F., et al., *Morphology and physiology of the epiphyseal growth plate*. Folia Histochem Cytobiol, 2009. **47**(1): p. 5-16.
26. Wierzbicka-Patynowski, I. and J.E. Schwarzbauer, *The ins and outs of fibronectin matrix assembly*. J Cell Sci, 2003. **116**(Pt 16): p. 3269-76.
27. Singh, P. and J.E. Schwarzbauer, *Fibronectin matrix assembly is essential for cell condensation during chondrogenesis*. J Cell Sci, 2014. **127**(Pt 20): p. 4420-8.
28. Ignatz, R.A. and J. Massague, *Transforming growth factor-beta stimulates the expression of fibronectin and collagen and their incorporation into the extracellular matrix*. J Biol Chem, 1986. **261**(9): p. 4337-45.
29. Hino, K., et al., *Master regulator for chondrogenesis, Sox9, regulates transcriptional activation of the endoplasmic reticulum stress transducer BFF2H7/CREB3L2 in chondrocytes*. J Biol Chem, 2014. **289**(20): p. 13810-20.
30. Akiyama, H., et al., *The transcription factor Sox9 has essential roles in successive steps of the chondrocyte differentiation pathway and is required for expression of Sox5 and Sox6*. Genes Dev, 2002. **16**(21): p. 2813-28.
31. Bi, W., et al., *Sox9 is required for cartilage formation*. Nat Genet, 1999. **22**(1): p. 85-9.
32. Wright, E., et al., *The Sry-related gene Sox9 is expressed during chondrogenesis in mouse embryos*. Nat Genet, 1995. **9**(1): p. 15-20.
33. Wagner, T., et al., *Autosomal sex reversal and campomelic dysplasia are caused by mutations in and around the SRY-related gene SOX9*. Cell, 1994. **79**(6): p. 1111-20.
34. Rahman, M.S., et al., *TGF-beta/BMP signaling and other molecular events: regulation of osteoblastogenesis and bone formation*. Bone Res, 2015. **3**: p. 15005.
35. Zeng, L., et al., *Shh establishes an Nkx3.2/Sox9 autoregulatory loop that is maintained by BMP signals to induce somitic chondrogenesis*. Genes Dev, 2002. **16**(15): p. 1990-2005.
36. Green, J.D., et al., *Multifaceted signaling regulators of chondrogenesis: Implications in cartilage regeneration and tissue engineering*. Genes Dis, 2015. **2**(4): p. 307-327.
37. Liu, C.F. and V. Lefebvre, *The transcription factors SOX9 and SOX5/SOX6 cooperate genome-wide through super-enhancers to drive chondrogenesis*. Nucleic Acids Res, 2015. **43**(17): p. 8183-203.
38. Murakami, S., et al., *Up-regulation of the chondrogenic Sox9 gene by fibroblast growth factors is mediated by the mitogen-activated protein kinase pathway*. Proc Natl Acad Sci U S A, 2000. **97**(3): p. 1113-8.

39. Correa, D., et al., *Sequential exposure to fibroblast growth factors (FGF) 2, 9 and 18 enhances hMSC chondrogenic differentiation*. Osteoarthritis Cartilage, 2015. **23**(3): p. 443-53.
40. Hung, I.H., et al., *FGF9 regulates early hypertrophic chondrocyte differentiation and skeletal vascularization in the developing stylopod*. Dev Biol, 2007. **307**(2): p. 300-13.
41. Zhou, X., et al., *Roles of FGF-2 and TGF-beta/FGF-2 on differentiation of human mesenchymal stem cells towards nucleus pulposus-like phenotype*. Growth Factors, 2015. **33**(1): p. 23-30.
42. Delise, A.M. and R.S. Tuan, *Analysis of N-cadherin function in limb mesenchymal chondrogenesis in vitro*. Dev Dyn, 2002. **225**(2): p. 195-204.
43. Akiyama, H., et al., *Interactions between Sox9 and beta-catenin control chondrocyte differentiation*. Genes Dev, 2004. **18**(9): p. 1072-87.
44. Zhang, Y., T. Pizzute, and M. Pei, *A review of crosstalk between MAPK and Wnt signals and its impact on cartilage regeneration*. Cell Tissue Res, 2014. **358**(3): p. 633-49.
45. Kronenberg, H.M., *Developmental regulation of the growth plate*. Nature, 2003. **423**(6937): p. 332-6.
46. Allen, J.L., M.E. Cooke, and T. Alliston, *ECM stiffness primes the TGFbeta pathway to promote chondrocyte differentiation*. Mol Biol Cell, 2012. **23**(18): p. 3731-42.
47. Wang, W., D. Rigueur, and K.M. Lyons, *TGFbeta signaling in cartilage development and maintenance*. Birth Defects Res C Embryo Today, 2014. **102**(1): p. 37-51.
48. Vega, R.B., et al., *Histone deacetylase 4 controls chondrocyte hypertrophy during skeletogenesis*. Cell, 2004. **119**(4): p. 555-66.
49. Ohba, S., *Hedgehog Signaling in Endochondral Ossification*. J Dev Biol, 2016. **4**(2).
50. Gao, B., et al., *Mutations in IHH, encoding Indian hedgehog, cause brachydactyly type A-1*. Nat Genet, 2001. **28**(4): p. 386-8.
51. Kronenberg, H.M., *PTHrP and skeletal development*. Ann N Y Acad Sci, 2006. **1068**: p. 1-13.
52. Kim, Y.J., H.J. Kim, and G.I. Im, *PTHrP promotes chondrogenesis and suppresses hypertrophy from both bone marrow-derived and adipose tissue-derived MSCs*. Biochem Biophys Res Commun, 2008. **373**(1): p. 104-8.
53. Fischer, J., et al., *Intermittent PTHrP(1-34) exposure augments chondrogenesis and reduces hypertrophy of mesenchymal stromal cells*. Stem Cells Dev, 2014. **23**(20): p. 2513-23.
54. Zhang, W., et al., *Inhibitory function of parathyroid hormone-related protein on chondrocyte hypertrophy: the implication for articular cartilage repair*. Arthritis Res Ther, 2012. **14**(4): p. 221.
55. Schipani, E., K. Kruse, and H. Juppner, *A constitutively active mutant PTH-PTHrP receptor in Jansen-type metaphyseal chondrodysplasia*. Science, 1995. **268**(5207): p. 98-100.
56. Zhou, G., et al., *Dominance of SOX9 function over RUNX2 during skeletogenesis*. Proc Natl Acad Sci U S A, 2006. **103**(50): p. 19004-9.
57. Zhang, H., et al., *An immunohistochemistry study of Sox9, Runx2, and Osterix expression in the mandibular cartilages of newborn mouse*. Biomed Res Int, 2013. **2013**: p. 265380.

58. Dy, P., et al., *Sox9 directs hypertrophic maturation and blocks osteoblast differentiation of growth plate chondrocytes*. Dev Cell, 2012. **22**(3): p. 597-609.
59. Guo, J., et al., *PTH/PTHrP receptor delays chondrocyte hypertrophy via both Runx2-dependent and -independent pathways*. Dev Biol, 2006. **292**(1): p. 116-28.
60. Minina, E., et al., *Interaction of FGF, Ihh/Pthlh, and BMP signaling integrates chondrocyte proliferation and hypertrophic differentiation*. Dev Cell, 2002. **3**(3): p. 439-49.
61. Lai, L.P., K.A. DaSilva, and J. Mitchell, *Regulation of Indian hedgehog mRNA levels in chondrocytic cells by ERK1/2 and p38 mitogen-activated protein kinases*. J Cell Physiol, 2005. **203**(1): p. 177-85.
62. Mak, K.K., et al., *Indian hedgehog signals independently of PTHrP to promote chondrocyte hypertrophy*. Development, 2008. **135**(11): p. 1947-56.
63. Wu, M., G. Chen, and Y.P. Li, *TGF-beta and BMP signaling in osteoblast, skeletal development, and bone formation, homeostasis and disease*. Bone Res, 2016. **4**: p. 16009.
64. Mak, K.K., et al., *Wnt/beta-catenin signaling interacts differentially with Ihh signaling in controlling endochondral bone and synovial joint formation*. Development, 2006. **133**(18): p. 3695-707.
65. Guo, X., et al., *The Wnt/beta-catenin pathway interacts differentially with PTHrP signaling to control chondrocyte hypertrophy and final maturation*. PLoS One, 2009. **4**(6): p. e6067.
66. Tamamura, Y., et al., *Developmental regulation of Wnt/beta-catenin signals is required for growth plate assembly, cartilage integrity, and endochondral ossification*. J Biol Chem, 2005. **280**(19): p. 19185-95.
67. Ornitz, D.M., *FGF signaling in the developing endochondral skeleton*. Cytokine Growth Factor Rev, 2005. **16**(2): p. 205-13.
68. Grimsrud, C.D., et al., *BMP signaling stimulates chondrocyte maturation and the expression of Indian hedgehog*. J Orthop Res, 2001. **19**(1): p. 18-25.
69. Yoon, B.S., et al., *Bmpr1a and Bmpr1b have overlapping functions and are essential for chondrogenesis in vivo*. Proc Natl Acad Sci U S A, 2005. **102**(14): p. 5062-7.
70. Minina, E., et al., *BMP and Ihh/PTHrP signaling interact to coordinate chondrocyte proliferation and differentiation*. Development, 2001. **128**(22): p. 4523-34.
71. Leitinger, B. and A.P. Kwan, *The discoidin domain receptor DDR2 is a receptor for type X collagen*. Matrix Biol, 2006. **25**(6): p. 355-64.
72. Wu, L.N., et al., *Physicochemical characterization of the nucleational core of matrix vesicles*. J Biol Chem, 1997. **272**(7): p. 4404-11.
73. Yoshida, C.A., et al., *Runx2 and Runx3 are essential for chondrocyte maturation, and Runx2 regulates limb growth through induction of Indian hedgehog*. Genes Dev, 2004. **18**(8): p. 952-63.
74. Tchetina, E.V., et al., *Chondrocyte hypertrophy can be induced by a cryptic sequence of type II collagen and is accompanied by the induction of MMP-13 and collagenase activity: implications for development and arthritis*. Matrix Biol, 2007. **26**(4): p. 247-58.
75. Li, I.M.H., et al., *Differential tissue specific, temporal and spatial expression patterns of the Aggrecan gene is modulated by independent enhancer elements*. Sci Rep, 2018. **8**(1): p. 950.

76. Stevens, D.A. and G.R. Williams, *Hormone regulation of chondrocyte differentiation and endochondral bone formation*. Mol Cell Endocrinol, 1999. **151**(1-2): p. 195-204.
77. Zelzer, E., et al., *VEGFA is necessary for chondrocyte survival during bone development*. Development, 2004. **131**(9): p. 2161-71.
78. Yang, Y.Q., et al., *The role of vascular endothelial growth factor in ossification*. Int J Oral Sci, 2012. **4**(2): p. 64-8.
79. Hall, A.P., F.R. Westwood, and P.F. Wadsworth, *Review of the effects of anti-angiogenic compounds on the epiphyseal growth plate*. Toxicol Pathol, 2006. **34**(2): p. 131-47.
80. Zelzer, E., et al., *Tissue specific regulation of VEGF expression during bone development requires Cbfa1/Runx2*. Mech Dev, 2001. **106**(1-2): p. 97-106.
81. Hinoi, E., et al., *Runx2 inhibits chondrocyte proliferation and hypertrophy through its expression in the perichondrium*. Genes Dev, 2006. **20**(21): p. 2937-42.
82. Behr, B., et al., *Fgf-9 is required for angiogenesis and osteogenesis in long bone repair*. Proc Natl Acad Sci U S A, 2010. **107**(26): p. 11853-8.
83. Sivaraj, K.K. and R.H. Adams, *Blood vessel formation and function in bone*. Development, 2016. **143**(15): p. 2706-15.
84. Werb, Z., C.M. Alexander, and R.R. Adler, *Expression and function of matrix metalloproteinases in development*. Matrix Suppl, 1992. **1**: p. 337-43.
85. Ortega, N., D.J. Behonick, and Z. Werb, *Matrix remodeling during endochondral ossification*. Trends Cell Biol, 2004. **14**(2): p. 86-93.
86. Kennedy, A.M., et al., *MMP13 mutation causes spondyloepimetaphyseal dysplasia, Missouri type (SEMD(MO))*. J Clin Invest, 2005. **115**(10): p. 2832-42.
87. Orphanet. *Spondylometaphyseal dysplasia*. 2008 [cited 2018 June 23]; Available from: https://www.orpha.net/consor/cgi-bin/OC_Exp.php?Lng=GB&Expert=254.
88. Nural, M.S., et al., *Kozlowski type spondylometaphyseal dysplasia: a case report with literature review*. Diagn Interv Radiol, 2006. **12**(2): p. 70-3.
89. NIH. *Spondylometaphyseal dysplasia, Kozlowski type*. Genetic and Rare Diseases Information Center [cited 2017 Nov. 7]; Available from: <https://rarediseases.info.nih.gov/diseases/3047/spondylometaphyseal-dysplasia-kozlowski-type>.
90. Duarte, M.L., et al., *Spondylometaphyseal dysplasia: an uncommon disease*. Radiol Bras, 2017. **50**(1): p. 63.
91. Bonafe, L., et al., *Nosology and classification of genetic skeletal disorders: 2015 revision*. Am J Med Genet A, 2015. **167A**(12): p. 2869-92.
92. Krakow, D. and D.L. Rimoin, *The skeletal dysplasias*. Genet Med, 2010. **12**(6): p. 327-41.
93. Suzuki, S., et al., *Axial spondylometaphyseal dysplasia: additional reports*. Am J Med Genet A, 2011. **155A**(10): p. 2521-8.
94. Kitoh, H., et al., *Spondylometaphyseal dysplasia with cone-rod dystrophy*. Am J Med Genet A, 2011. **155A**(4): p. 845-9.
95. OMIM. *SPONDYLOMETAPHYSEAL DYSPLASIA, CORNER FRACTURE TYPE (OMIM #184255)*. [cited 2017 Nov. 2]; Available from: <https://www.omim.org/entry/184255?search=SPONDYLOMETAPHYSEAL%20DYSPLASIA&highlight=spondylometaphyseal%20dysplasia%20dysplastic>.

96. Langer, L.O., Jr., et al., *Spondylometaphyseal dysplasia, corner fracture type: a heritable condition associated with coxa vara*. Radiology, 1990. **175**(3): p. 761-6.
97. Beighton P., K.K., *Spondylometaphyseal dysplasia sutcliffe type (case report)*. Nowa Pediatria, 2003: p. 121-122.
98. Felman, A.H., J.L. Frias, and O.M. Rennert, *Spondylometaphyseal dysplasia: a variant form*. Radiology, 1974. **113**(2): p. 409-15.
99. Kozlowski, K. and M.C. Bellemore, *Spondylo-metaphyseal dysplasia of Sutcliffe type*. Br J Radiol, 1989. **62**(741): p. 862-4.
100. Kozlowski, K., M. Napiontek, and E.R. Beim, *Spondylometaphyseal dysplasia, Sutcliffe type: a rediscovered entity*. Can Assoc Radiol J, 1992. **43**(5): p. 364-8.
101. Currarino, G., J.G. Birch, and J.A. Herring, *Developmental coxa vara associated with spondylometaphyseal dysplasia (DCV/SMD): "SMD-corner fracture type" (DCV/SMD-CF) demonstrated in most reported cases*. Pediatr Radiol, 2000. **30**(1): p. 14-24.
102. Sutton, V.R., et al., *A dominantly inherited spondylometaphyseal dysplasia with "corner fractures" and congenital scoliosis*. Am J Med Genet A, 2005. **133A**(2): p. 209-12.
103. Walter, K., et al., *COL2A1-related skeletal dysplasias with predominant metaphyseal involvement*. Am J Med Genet A, 2007. **143A**(2): p. 161-7.
104. Machol, K., et al., *Corner fracture type spondylometaphyseal dysplasia: Overlap with type II collagenopathies*. Am J Med Genet A, 2017. **173**(3): p. 733-739.
105. Nair, N., et al., *Spondylometaphyseal Dysplasia Corner Fracture (Sutcliffe) Type*. Indian J Pediatr, 2016. **83**(10): p. 1191-4.
106. Lee, C.S., et al., *Mutations in Fibronectin Cause a Subtype of Spondylometaphyseal Dysplasia with "Corner Fractures"*. Am J Hum Genet, 2017. **101**(5): p. 815-823.
107. Cadoff, E.B., et al., *Mechanistic insights into the cellular effects of a novel FNI variant associated with a spondylometaphyseal dysplasia*. Clin Genet, 2018.
108. Lustrin, E.S., et al., *Pediatric cervical spine: normal anatomy, variants, and trauma*. Radiographics, 2003. **23**(3): p. 539-60.
109. Campeau, P. and A.E. Schlesinger, *Skeletal Dysplasias*, in *Endotext*, L.J. De Groot, et al., Editors. 2000: South Dartmouth (MA).
110. Stevens, C.A., R.G. Pearce, and E.M. Burton, *Familial odontoid hypoplasia*. Am J Med Genet A, 2009. **149A**(6): p. 1290-2.
111. Lam, F., S. Hussain, and J. Sinha, *An unusual cause of a limp in a child: developmental coxa vara*. Emerg Med J, 2001. **18**(4): p. 314.
112. Arun Kumar Gupta, V.C., Niranjana Khandelwal, Ashu Seith Bhalla, *Skeletal Dysplasias*, in *Diagnostic Radiology Paediatric Imaging*. 2011, Jaypee Brothers Medical. p. 314-315.
113. Alessandro Castriota-Scanderbeg, B.D., *Metaphyseal Abnormalities*, in *Abnormal Skeletal Phenotypes: From Simple Signs to Complex Diagnoses*. 2006, Springer. p. 351.
114. Richie, M.F. and C.E. Johnston, 2nd, *Management of developmental coxa vara in cleidocranial dysostosis*. Orthopedics, 1989. **12**(7): p. 1001-4.
115. Parvizi, J., G.R. Klein, and F.H. Sim, *Surgical management of Paget's disease of bone*. J Bone Miner Res, 2006. **21 Suppl 2**: p. P75-82.
116. Aarabi, M., et al., *High prevalence of coxa vara in patients with severe osteogenesis imperfecta*. J Pediatr Orthop, 2006. **26**(1): p. 24-8.

117. NIH. *Spondylometaphyseal dysplasia, Kozlowski type*. [cited 2017 Nov. 2]; Available from: <https://rarediseases.info.nih.gov/diseases/3047/spondylometaphyseal-dysplasia-kozlowski-type>.
118. Schindler, A., C. Sumner, and J.E. Hoover-Fong, *TRPV4-Associated Disorders*, in *GeneReviews(R)*, M.P. Adam, et al., Editors. 1993: Seattle (WA).
119. Chotigavanichaya, C., et al., *Results of surgical treatment of coxa vara in children: valgus osteotomy with angle blade plate fixation*. J Med Assoc Thai, 2014. **97 Suppl 9**: p. S78-82.
120. Ibrahim, S., H. Labelle, and J.M. Mac-Thiong, *Brace treatment of thoracolumbar kyphosis in spondylometaphyseal dysplasia with restoration of vertebral morphology and sagittal profile: a case report*. Spine J, 2015. **15(6)**: p. e29-34.
121. Tiller, G.E., et al., *Dominant mutations in the type II collagen gene, COL2A1, produce spondyloepimetaphyseal dysplasia, Strudwick type*. Nat Genet, 1995. **11(1)**: p. 87-9.
122. Pankov, R. and K.M. Yamada, *Fibronectin at a glance*. J Cell Sci, 2002. **115(Pt 20)**: p. 3861-3.
123. Astrof, S. and R.O. Hynes, *Fibronectins in vascular morphogenesis*. Angiogenesis, 2009. **12(2)**: p. 165-75.
124. To, W.S. and K.S. Midwood, *Plasma and cellular fibronectin: distinct and independent functions during tissue repair*. Fibrogenesis Tissue Repair, 2011. **4**: p. 21.
125. George, E.L., H.S. Baldwin, and R.O. Hynes, *Fibronectins are essential for heart and blood vessel morphogenesis but are dispensable for initial specification of precursor cells*. Blood, 1997. **90(8)**: p. 3073-81.
126. George, E.L., et al., *Defects in mesoderm, neural tube and vascular development in mouse embryos lacking fibronectin*. Development, 1993. **119(4)**: p. 1079-91.
127. Hynes, R.O., *Fibronectins*. 1990, New York: Springer-Verlag.
128. Singh, P., C. Carraher, and J.E. Schwarzbauer, *Assembly of fibronectin extracellular matrix*. Annu Rev Cell Dev Biol, 2010. **26**: p. 397-419.
129. Xu, J. and D. Mosher, *Fibronectin and Other Adhesive Glycoproteins*, in *The Extracellular Matrix: an Overview*, R.P. Mecham, Editor. 2011, Springer Berlin Heidelberg: Berlin, Heidelberg. p. 41-75.
130. Maurer, L.M., W. Ma, and D.F. Mosher, *Dynamic structure of plasma fibronectin*. Crit Rev Biochem Mol Biol, 2015. **51(4)**: p. 213-27.
131. Patel, R.S., et al., *Organization of the fibronectin gene provides evidence for exon shuffling during evolution*. EMBO J, 1987. **6(9)**: p. 2565-72.
132. Stine, J.M., et al., *Structure and unfolding of the third type III domain from human fibronectin*. Biochemistry, 2015. **54(44)**: p. 6724-33.
133. Schwarzbauer, J.E., *Identification of the fibronectin sequences required for assembly of a fibrillar matrix*. J Cell Biol, 1991. **113(6)**: p. 1463-73.
134. Hynes, J.P. and T.R. Klaenhammer, *Stuck in the Middle: Fibronectin-Binding Proteins in Gram-Positive Bacteria*. Front Microbiol, 2016. **7**: p. 1504.
135. Xu J., M.D., *Fibronectin and Other Adhesive Glycoproteins.*, in *Extracellular Matrix: an Overview.*, M.R. (eds), Editor. 2011, Springer: Berlin, Heidelberg.
136. Mecham, R.P., *Overview of extracellular matrix*. Curr Protoc Cell Biol, 2001. **Chapter 10**: p. Unit 10 1.
137. Potts, J.R. and I.D. Campbell, *Fibronectin structure and assembly*. Curr Opin Cell Biol, 1994. **6(5)**: p. 648-55.

138. Cho, J. and D.F. Mosher, *Enhancement of thrombogenesis by plasma fibronectin cross-linked to fibrin and assembled in platelet thrombi*. Blood, 2006. **107**(9): p. 3555-63.
139. Henderson, B., et al., *Fibronectin: a multidomain host adhesin targeted by bacterial fibronectin-binding proteins*. FEMS Microbiol Rev, 2011. **35**(1): p. 147-200.
140. Rostagno, A.A., J.E. Schwarzbauer, and L.I. Gold, *Comparison of the fibrin-binding activities in the N- and C-termini of fibronectin*. Biochem J, 1999. **338** (Pt 2): p. 375-86.
141. Sottile, J., et al., *Five type I modules of fibronectin form a functional unit that binds to fibroblasts and Staphylococcus aureus*. J Biol Chem, 1991. **266**(20): p. 12840-3.
142. Nikolajsen, C.L., et al., *Coagulation factor XIIIa substrates in human plasma: identification and incorporation into the clot*. J Biol Chem, 2014. **289**(10): p. 6526-34.
143. Chhum, P., et al., *Consequences of Glycine Mutations in the Fibronectin-binding Sequence of Collagen*. J Biol Chem, 2016. **291**(53): p. 27073-27086.
144. Erat, M.C., et al., *Structural analysis of collagen type I interactions with human fibronectin reveals a cooperative binding mode*. J Biol Chem, 2013. **288**(24): p. 17441-50.
145. Dessau, W., B.C. Adelman, and R. Timpl, *Identification of the sites in collagen alpha-chains that bind serum anti-gelatin factor (cold-insoluble globulin)*. Biochem J, 1978. **169**(1): p. 55-9.
146. Speziale, P., et al., *Purification of human plasma fibronectin using immobilized gelatin and Arg affinity chromatography*. Nat Protoc, 2008. **3**(3): p. 525-33.
147. Mao, Y. and J.E. Schwarzbauer, *Fibronectin fibrillogenesis, a cell-mediated matrix assembly process*. Matrix Biol, 2005. **24**(6): p. 389-99.
148. Baneyx, G., L. Baugh, and V. Vogel, *Fibronectin extension and unfolding within cell matrix fibrils controlled by cytoskeletal tension*. Proc Natl Acad Sci U S A, 2002. **99**(8): p. 5139-43.
149. Leahy, D.J., I. Aukhil, and H.P. Erickson, *2.0 A crystal structure of a four-domain segment of human fibronectin encompassing the RGD loop and synergy region*. Cell, 1996. **84**(1): p. 155-64.
150. Takada, Y., X. Ye, and S. Simon, *The integrins*. Genome Biol, 2007. **8**(5): p. 215.
151. Sechler, J.L., Y. Takada, and J.E. Schwarzbauer, *Altered rate of fibronectin matrix assembly by deletion of the first type III repeats*. J Cell Biol, 1996. **134**(2): p. 573-83.
152. Takahashi, S., et al., *The RGD motif in fibronectin is essential for development but dispensable for fibril assembly*. J Cell Biol, 2007. **178**(1): p. 167-78.
153. Leiss, M., et al., *The role of integrin binding sites in fibronectin matrix assembly in vivo*. Curr Opin Cell Biol, 2008. **20**(5): p. 502-7.
154. Sechler, J.L., et al., *A novel RGD-independent fibronectin assembly pathway initiated by alpha4beta1 integrin binding to the alternatively spliced V region*. J Cell Sci, 2000. **113** (Pt 8): p. 1491-8.
155. Moyano, J.V., et al., *Fibronectin type III5 repeat contains a novel cell adhesion sequence, KLDAPT, which binds activated alpha4beta1 and alpha4beta7 integrins*. J Biol Chem, 1997. **272**(40): p. 24832-6.
156. Sarrazin, S., W.C. Lamanna, and J.D. Esko, *Heparan sulfate proteoglycans*. Cold Spring Harb Perspect Biol, 2011. **3**(7).

157. Tang, N.H., et al., *N-terminal and C-terminal heparin-binding domain polypeptides derived from fibronectin reduce adhesion and invasion of liver cancer cells*. BMC Cancer, 2010. **10**: p. 552.
158. Mostafavi-Pour, Z., et al., *Identification of a novel heparin-binding site in the alternatively spliced IIIICS region of fibronectin: roles of integrins and proteoglycans in cell adhesion to fibronectin splice variants*. Matrix Biol, 2001. **20**(1): p. 63-73.
159. Castelletti, F., et al., *Mutations in FNI cause glomerulopathy with fibronectin deposits*. Proc Natl Acad Sci U S A, 2008. **105**(7): p. 2538-43.
160. Ohtsubo, H., et al., *Identification of mutations in FNI leading to glomerulopathy with fibronectin deposits*. Pediatr Nephrol, 2016. **31**(9): p. 1459-67.
161. Morla, A. and E. Ruoslahti, *A fibronectin self-assembly site involved in fibronectin matrix assembly: reconstruction in a synthetic peptide*. J Cell Biol, 1992. **118**(2): p. 421-9.
162. Brennan, J.R. and D.C. Hocking, *Cooperative effects of fibronectin matrix assembly and initial cell-substrate adhesion strength in cellular self-assembly*. Acta Biomater, 2016. **32**: p. 198-209.
163. White, E.S., F.E. Baralle, and A.F. Muro, *New insights into form and function of fibronectin splice variants*. J Pathol, 2008. **216**(1): p. 1-14.
164. Kumazaki, T., et al., *Detection of alternative splicing of fibronectin mRNA in a single cell*. J Cell Sci, 1999. **112 (Pt 10)**: p. 1449-53.
165. Schwarzbauer, J.E., et al., *Three different fibronectin mRNAs arise by alternative splicing within the coding region*. Cell, 1983. **35**(2 Pt 1): p. 421-31.
166. Schwarzbauer, J.E., *Alternative splicing of fibronectin: three variants, three functions*. Bioessays, 1991. **13**(10): p. 527-33.
167. Mao, Y. and J.E. Schwarzbauer, *Stimulatory effects of a three-dimensional microenvironment on cell-mediated fibronectin fibrillogenesis*. J Cell Sci, 2005. **118**(Pt 19): p. 4427-36.
168. Chauhan, A.K., et al., *Alternative splicing of fibronectin: a mouse model demonstrates the identity of in vitro and in vivo systems and the processing autonomy of regulated exons in adult mice*. Gene, 2004. **324**: p. 55-63.
169. Ffrench-Constant, C., et al., *Reappearance of an embryonic pattern of fibronectin splicing during wound healing in the adult rat*. J Cell Biol, 1989. **109**(2): p. 903-14.
170. Muro, A.F., et al., *Regulated splicing of the fibronectin EDA exon is essential for proper skin wound healing and normal lifespan*. J Cell Biol, 2003. **162**(1): p. 149-60.
171. Fukuda, T., et al., *Mice lacking the EDB segment of fibronectin develop normally but exhibit reduced cell growth and fibronectin matrix assembly in vitro*. Cancer Res, 2002. **62**(19): p. 5603-10.
172. Gehris, A.L., et al., *The region encoded by the alternatively spliced exon IIIA in mesenchymal fibronectin appears essential for chondrogenesis at the level of cellular condensation*. Dev Biol, 1997. **190**(2): p. 191-205.
173. Han, F., et al., *Transforming growth factor-beta1 regulates fibronectin isoform expression and splicing factor SRp40 expression during ATDC5 chondrogenic maturation*. Exp Cell Res, 2007. **313**(8): p. 1518-32.
174. Bentmann, A., et al., *Circulating fibronectin affects bone matrix, whereas osteoblast fibronectin modulates osteoblast function*. J Bone Miner Res, 2010. **25**(4): p. 706-15.

175. Sens, C., et al., *Fibronectins containing extradomain A or B enhance osteoblast differentiation via distinct integrins*. J Biol Chem, 2017. **292**(19): p. 7745-7760.
176. Bumol, T.F. and R.A. Reisfeld, *Biosynthesis and secretion of fibronectin in human melanoma cells*. J Cell Biochem, 1983. **21**(2): p. 129-40.
177. Lavietes, B.B., et al., *Synthesis, secretion, and deposition of fibronectin in cultured human synovium*. Arthritis Rheum, 1985. **28**(9): p. 1016-26.
178. Ali, I.U., *Analysis of phosphorylation sites on fibronectin*. FEBS Lett, 1984. **176**(1): p. 169-75.
179. Ali, I.U., *Phosphorylation of fibronectin in quiescent and growing cell cultures*. FEBS Lett, 1983. **151**(1): p. 45-8.
180. Mosher, D.F., *Plasma fibronectin concentration: a risk factor for arterial thrombosis?* Arterioscler Thromb Vasc Biol, 2006. **26**(6): p. 1193-5.
181. Kanters, S.D., et al., *Plasma levels of cellular fibronectin in diabetes*. Diabetes Care, 2001. **24**(2): p. 323-7.
182. Alberts B, J.A., Lewis J, et al., *Molecular Biology of the Cell.*, in *The Extracellular Matrix of Animals*. 2002, Garland Science: New York.
183. Frantz, C., K.M. Stewart, and V.M. Weaver, *The extracellular matrix at a glance*. J Cell Sci, 2010. **123**(Pt 24): p. 4195-200.
184. Ruoslahti, E., *Brain extracellular matrix*. Glycobiology, 1996. **6**(5): p. 489-92.
185. Gentili, C. and R. Cancedda, *Cartilage and bone extracellular matrix*. Curr Pharm Des, 2009. **15**(12): p. 1334-48.
186. Tom Strachan, A.R., *Human Molecular Genetics (Cell Adhesion and Tissue Formation)*. 2010: Garland Science. 782.
187. Schwarzbauer, J.E. and D.W. DeSimone, *Fibronectins, their fibrillogenesis, and in vivo functions*. Cold Spring Harb Perspect Biol, 2011. **3**(7).
188. Sottile, J. and D.C. Hocking, *Fibronectin polymerization regulates the composition and stability of extracellular matrix fibrils and cell-matrix adhesions*. Mol Biol Cell, 2002. **13**(10): p. 3546-59.
189. Pankov, R., et al., *Integrin dynamics and matrix assembly: tensin-dependent translocation of alpha(5)beta(1) integrins promotes early fibronectin fibrillogenesis*. J Cell Biol, 2000. **148**(5): p. 1075-90.
190. Wu, C., et al., *Integrin activation and cytoskeletal interaction are essential for the assembly of a fibronectin matrix*. Cell, 1995. **83**(5): p. 715-24.
191. Dzamba, B.J. and D.M. Peters, *Arrangement of cellular fibronectin in noncollagenous fibrils in human fibroblast cultures*. J Cell Sci, 1991. **100** (Pt 3): p. 605-12.
192. McKeown-Longo, P.J. and D.F. Mosher, *Binding of plasma fibronectin to cell layers of human skin fibroblasts*. J Cell Biol, 1983. **97**(2): p. 466-72.
193. Valenick, L.V., H.C. Hsia, and J.E. Schwarzbauer, *Fibronectin fragmentation promotes alpha4beta1 integrin-mediated contraction of a fibrin-fibronectin provisional matrix*. Exp Cell Res, 2005. **309**(1): p. 48-55.
194. Saoncella, S., et al., *Syndecan-4 signals cooperatively with integrins in a Rho-dependent manner in the assembly of focal adhesions and actin stress fibers*. Proc Natl Acad Sci U S A, 1999. **96**(6): p. 2805-10.
195. Galante, L.L. and J.E. Schwarzbauer, *Requirements for sulfate transport and the diastrophic dysplasia sulfate transporter in fibronectin matrix assembly*. J Cell Biol, 2007. **179**(5): p. 999-1009.

196. Frenz, D.A., N.S. Jaikaria, and S.A. Newman, *The mechanism of precartilaginous mesenchymal condensation: a major role for interaction of the cell surface with the amino-terminal heparin-binding domain of fibronectin*. Dev Biol, 1989. **136**(1): p. 97-103.
197. Hocevar, B.A., T.L. Brown, and P.H. Howe, *TGF-beta induces fibronectin synthesis through a c-Jun N-terminal kinase-dependent, Smad4-independent pathway*. EMBO J, 1999. **18**(5): p. 1345-56.
198. Munger, J.S. and D. Sheppard, *Cross talk among TGF-beta signaling pathways, integrins, and the extracellular matrix*. Cold Spring Harb Perspect Biol, 2011. **3**(11): p. a005017.
199. Klingberg, F., et al., *The fibronectin ED-A domain enhances recruitment of latent TGF-beta-binding protein-1 to the fibroblast matrix*. J Cell Sci, 2018. **131**(5).
200. Dallas, S.L., et al., *Fibronectin regulates latent transforming growth factor-beta (TGF beta) by controlling matrix assembly of latent TGF beta-binding protein-1*. J Biol Chem, 2005. **280**(19): p. 18871-80.
201. Cai, T., et al., *Dysplastic spondylosis is caused by mutations in the diastrophic dysplasia sulfate transporter gene*. Proc Natl Acad Sci U S A, 2015. **112**(26): p. 8064-9.
202. Rossi, A. and A. Superti-Furga, *Mutations in the diastrophic dysplasia sulfate transporter (DTDST) gene (SLC26A2): 22 novel mutations, mutation review, associated skeletal phenotypes, and diagnostic relevance*. Hum Mutat, 2001. **17**(3): p. 159-71.
203. Forlino, A., et al., *A diastrophic dysplasia sulfate transporter (SLC26A2) mutant mouse: morphological and biochemical characterization of the resulting chondrodysplasia phenotype*. Hum Mol Genet, 2005. **14**(6): p. 859-71.
204. Hocking, D.C., et al., *Inhibition of fibronectin matrix assembly by the heparin-binding domain of vitronectin*. J Biol Chem, 1999. **274**(38): p. 27257-64.
205. Danen, E.H., et al., *The fibronectin-binding integrins alpha5beta1 and alphavbeta3 differentially modulate RhoA-GTP loading, organization of cell matrix adhesions, and fibronectin fibrillogenesis*. J Cell Biol, 2002. **159**(6): p. 1071-86.
206. Ohashi, T., D.P. Kiehart, and H.P. Erickson, *Dual labeling of the fibronectin matrix and actin cytoskeleton with green fluorescent protein variants*. J Cell Sci, 2002. **115**(Pt 6): p. 1221-9.
207. Zhong, C., et al., *Rho-mediated contractility exposes a cryptic site in fibronectin and induces fibronectin matrix assembly*. J Cell Biol, 1998. **141**(2): p. 539-51.
208. Guan, J.L., *Role of focal adhesion kinase in integrin signaling*. Int J Biochem Cell Biol, 1997. **29**(8-9): p. 1085-96.
209. Woods, A., *Syndecans: transmembrane modulators of adhesion and matrix assembly*. J Clin Invest, 2001. **107**(8): p. 935-41.
210. Woods, A., et al., *Syndecan-4 binding to the high affinity heparin-binding domain of fibronectin drives focal adhesion formation in fibroblasts*. Arch Biochem Biophys, 2000. **374**(1): p. 66-72.
211. Zhang, X., et al., *A Comparative Study of Fibronectin Cleavage by MMP-1, -3, -13, and -14*. Cartilage, 2012. **3**(3): p. 267-77.
212. Trengove, N.J., et al., *Analysis of the acute and chronic wound environments: the role of proteases and their inhibitors*. Wound Repair Regen, 1999. **7**(6): p. 442-52.

213. Kulawig, R., et al., *Identification of fibronectin as a major factor in human serum to recruit subchondral mesenchymal progenitor cells*. Int J Biochem Cell Biol, 2013. **45**(7): p. 1410-8.
214. Kalkreuth, R.H., et al., *Fibronectin stimulates migration and proliferation, but not chondrogenic differentiation of human subchondral progenitor cells*. Regen Med, 2014. **9**(6): p. 759-73.
215. Gao, L., R. McBeath, and C.S. Chen, *Stem cell shape regulates a chondrogenic versus myogenic fate through Rac1 and N-cadherin*. Stem Cells, 2010. **28**(3): p. 564-72.
216. Chevalier, X., *Fibronectin, cartilage, and osteoarthritis*. Semin Arthritis Rheum, 1993. **22**(5): p. 307-18.
217. Roberts, C.J., et al., *Transforming growth factor beta stimulates the expression of fibronectin and of both subunits of the human fibronectin receptor by cultured human lung fibroblasts*. J Biol Chem, 1988. **263**(10): p. 4586-92.
218. Huang, C.H., et al., *Interactive effects of mechanical stretching and extracellular matrix proteins on initiating osteogenic differentiation of human mesenchymal stem cells*. J Cell Biochem, 2009. **108**(6): p. 1263-73.
219. Al-Jallad, H.F., et al., *Plasma membrane factor XIIIa transglutaminase activity regulates osteoblast matrix secretion and deposition by affecting microtubule dynamics*. PLoS One, 2011. **6**(1): p. e15893.
220. Miller, C.G., et al., *Minireview: Fibronectin in retinal disease*. Exp Biol Med (Maywood), 2017. **242**(1): p. 1-7.
221. Ruoslahti, E., *Fibronectin and its integrin receptors in cancer*. Adv Cancer Res, 1999. **76**: p. 1-20.
222. Wang, J.P. and A. Hielscher, *Fibronectin: How Its Aberrant Expression in Tumors May Improve Therapeutic Targeting*. J Cancer, 2017. **8**(4): p. 674-682.
223. Jones, R.J., et al., *Elevated c-Src is linked to altered cell-matrix adhesion rather than proliferation in KM12C human colorectal cancer cells*. Br J Cancer, 2002. **87**(10): p. 1128-35.
224. Maldonado, M. and J. Nam, *The role of changes in extracellular matrix of cartilage in the presence of inflammation on the pathology of osteoarthritis*. Biomed Res Int, 2013. **2013**: p. 284873.
225. Lust, G., N. Burton-Wurster, and H. Leipold, *Fibronectin as a marker for osteoarthritis*. J Rheumatol, 1987. **14 Spec No**: p. 28-9.
226. Neogi, T., *Clinical significance of bone changes in osteoarthritis*. Ther Adv Musculoskelet Dis, 2012. **4**(4): p. 259-67.
227. Zaira Y. García-Carvajal, D.G.-C., Carmen Parra- Cid, Rocío Aguilar-Gaytán, Cristina Velasquillo , Clemente Ibarra and Javier S. Castro Carmona, *Cartilage Tissue Engineering: The Role of Extracellular Matrix (ECM) and Novel Strategies, Regenerative Medicine and Tissue Engineering*, ed. P.J.A. Andrades. 2013: InTech.
228. Han, F., et al., *Transforming growth factor-beta1 (TGF-beta1) regulates ATDC5 chondrogenic differentiation and fibronectin isoform expression*. J Cell Biochem, 2005. **95**(4): p. 750-62.
229. Fitter, S., et al., *mTORC1 Plays an Important Role in Skeletal Development by Controlling Preosteoblast Differentiation*. Mol Cell Biol, 2017. **37**(7).
230. Imaizumi, M., et al., *Evaluation of the use of induced pluripotent stem cells (iPSCs) for the regeneration of tracheal cartilage*. Cell Transplant, 2013. **22**(2): p. 341-53.

231. Tsukamoto, I., et al., *Activating types 1 and 2 angiotensin II receptors modulate the hypertrophic differentiation of chondrocytes*. FEBS Open Bio, 2013. **3**: p. 279-84.
232. Yao, Y. and Y. Wang, *ATDC5: an excellent in vitro model cell line for skeletal development*. J Cell Biochem, 2013. **114**(6): p. 1223-9.
233. Estes, B.T. and F. Guilak, *Three-dimensional culture systems to induce chondrogenesis of adipose-derived stem cells*. Methods Mol Biol, 2011. **702**: p. 201-17.
234. Yu, D.A., J. Han, and B.S. Kim, *Stimulation of chondrogenic differentiation of mesenchymal stem cells*. Int J Stem Cells, 2012. **5**(1): p. 16-22.
235. Lewis, M.C., et al., *Extracellular Matrix Deposition in Engineered Micromass Cartilage Pellet Cultures: Measurements and Modelling*. PLoS One, 2016. **11**(2): p. e0147302.
236. Bosnakovski, D., et al., *Chondrogenic differentiation of bovine bone marrow mesenchymal stem cells in pellet cultural system*. Exp Hematol, 2004. **32**(5): p. 502-9.
237. Newton, P.T., et al., *Chondrogenic ATDC5 cells: an optimised model for rapid and physiological matrix mineralisation*. Int J Mol Med, 2012. **30**(5): p. 1187-93.
238. Harumi Kagiwada, T.F., Hiroko Machida, Hajime Ohgushi, *Effect of Gentamicin on Growth and Differentiation of Human Mesenchymal Stem Cells*. Journal of Toxicologic Pathology, 2008(21): p. 61-67.
239. Goldring, M.B., K. Tsuchimochi, and K. Ijiri, *The control of chondrogenesis*. J Cell Biochem, 2006. **97**(1): p. 33-44.
240. Zhong, L., et al., *The Regulatory Role of Signaling Crosstalk in Hypertrophy of MSCs and Human Articular Chondrocytes*. Int J Mol Sci, 2015. **16**(8): p. 19225-47.
241. Kozhemyakina, E., A.B. Lassar, and E. Zelzer, *A pathway to bone: signaling molecules and transcription factors involved in chondrocyte development and maturation*. Development, 2015. **142**(5): p. 817-31.
242. Li, H., et al., *Comparative analysis with collagen type II distinguishes cartilage oligomeric matrix protein as a primary TGFbeta-responsive gene*. Osteoarthritis Cartilage, 2011. **19**(10): p. 1246-53.
243. Zhao, Q., et al., *Parallel expression of Sox9 and Col2a1 in cells undergoing chondrogenesis*. Dev Dyn, 1997. **209**(4): p. 377-86.
244. Wigner, N.A., et al., *Functional role of Runx3 in the regulation of aggrecan expression during cartilage development*. J Cell Physiol, 2013. **228**(11): p. 2232-42.
245. Knudson, C.B. and W. Knudson, *Cartilage proteoglycans*. Semin Cell Dev Biol, 2001. **12**(2): p. 69-78.
246. Kosher, R.A., et al., *Cartilage proteoglycan core protein gene expression during limb cartilage differentiation*. Dev Biol, 1986. **118**(1): p. 112-7.
247. Ko, J.Y., et al., *In vitro chondrogenesis and in vivo repair of osteochondral defect with human induced pluripotent stem cells*. Biomaterials, 2014. **35**(11): p. 3571-81.
248. Kawelke, N., et al., *Fibronectin protects from excessive liver fibrosis by modulating the availability of and responsiveness of stellate cells to active TGF-beta*. PLoS One, 2011. **6**(11): p. e28181.
249. Yasuda, H., et al., *A Novel Regulatory Mechanism of Type II Collagen Expression via a SOX9-dependent Enhancer in Intron 6*. J Biol Chem, 2017. **292**(2): p. 528-538.

250. Sakai, T., et al., *Plasma fibronectin supports neuronal survival and reduces brain injury following transient focal cerebral ischemia but is not essential for skin-wound healing and hemostasis*. Nat Med, 2001. **7**(3): p. 324-30.
251. Moretti, F.A., et al., *A major fraction of fibronectin present in the extracellular matrix of tissues is plasma-derived*. J Biol Chem, 2007. **282**(38): p. 28057-62.
252. Nieves, J.W., et al., *Males have larger skeletal size and bone mass than females, despite comparable body size*. J Bone Miner Res, 2005. **20**(3): p. 529-35.
253. Dutta, S. and P. Sengupta, *Men and mice: Relating their ages*. Life Sci, 2016. **152**: p. 244-8.
254. Richardson, C.D., et al., *Enhancing homology-directed genome editing by catalytically active and inactive CRISPR-Cas9 using asymmetric donor DNA*. Nat Biotechnol, 2016. **34**(3): p. 339-44.
255. Prior, H., et al., *Highly Efficient, Rapid and Co-CRISPR-Independent Genome Editing in Caenorhabditis elegans*. G3 (Bethesda), 2017. **7**(11): p. 3693-3698.
256. Weiss, H.E., et al., *A semi-autonomous model of endochondral ossification for developmental tissue engineering*. Tissue Eng Part A, 2012. **18**(13-14): p. 1334-43.
257. Enochson, L., M. Brittberg, and A. Lindahl, *Optimization of a chondrogenic medium through the use of factorial design of experiments*. Biores Open Access, 2012. **1**(6): p. 306-13.
258. Temu, T.M., et al., *The mechanism of ascorbic acid-induced differentiation of ATDC5 chondrogenic cells*. Am J Physiol Endocrinol Metab, 2010. **299**(2): p. E325-34.
259. Kirimoto, A., et al., *Effects of retinoic acid on the differentiation of chondrogenic progenitor cells, ATDC5*. J Med Dent Sci, 2005. **52**(3): p. 153-62.
260. Shukunami, C., et al., *Cellular hypertrophy and calcification of embryonal carcinoma-derived chondrogenic cell line ATDC5 in vitro*. J Bone Miner Res, 1997. **12**(8): p. 1174-88.
261. Fujita, T., et al., *Dexamethasone inhibits insulin-induced chondrogenesis of ATDC5 cells by preventing PI3K-Akt signaling and DNA binding of Runx2*. J Cell Biochem, 2004. **93**(2): p. 374-83.
262. Mushtaq, T., et al., *Glucocorticoid effects on chondrogenesis, differentiation and apoptosis in the murine ATDC5 chondrocyte cell line*. J Endocrinol, 2002. **175**(3): p. 705-13.
263. Annefeld, M., *Changes in rat epiphyseal cartilage after treatment with dexamethasone and glycosaminoglycan-peptide complex*. Pathol Res Pract, 1992. **188**(4-5): p. 649-52.
264. Naito, M., A. Ohashi, and T. Takahashi, *Dexamethasone inhibits chondrocyte differentiation by suppression of Wnt/beta-catenin signaling in the chondrogenic cell line ATDC5*. Histochem Cell Biol, 2015. **144**(3): p. 261-72.
265. Shioi, A., et al., *Beta-glycerophosphate accelerates calcification in cultured bovine vascular smooth muscle cells*. Arterioscler Thromb Vasc Biol, 1995. **15**(11): p. 2003-9.
266. Altaf, F.M., et al., *Ascorbate-enhanced chondrogenesis of ATDC5 cells*. Eur Cell Mater, 2006. **12**: p. 64-9; discussion 69-70.
267. Guzzo, R.M. and H. Drissi, *Differentiation of Human Induced Pluripotent Stem Cells to Chondrocytes*. Methods Mol Biol, 2015. **1340**: p. 79-95.
268. Medvedev, S.P., A.I. Shevchenko, and S.M. Zakian, *Induced Pluripotent Stem Cells: Problems and Advantages when Applying them in Regenerative Medicine*. Acta Naturae, 2010. **2**(2): p. 18-28.

269. Nature Toxic Alert. 2007. DOI: <https://doi.org/10.1038/449378a>.
270. Watt, F.M. and K.J. Hodivala, *Cell adhesion. Fibronectin and integrin knockouts come unstuck*. Curr Biol, 1994. **4**(3): p. 270-2.
271. Matuskova, J., et al., *Decreased plasma fibronectin leads to delayed thrombus growth in injured arterioles*. Arterioscler Thromb Vasc Biol, 2006. **26**(6): p. 1391-6.
272. Aszodi, A., et al., *Beta1 integrins regulate chondrocyte rotation, G1 progression, and cytokinesis*. Genes Dev, 2003. **17**(19): p. 2465-79.
273. Barbaric, I., G. Miller, and T.N. Dear, *Appearances can be deceiving: phenotypes of knockout mice*. Brief Funct Genomic Proteomic, 2007. **6**(2): p. 91-103.
274. Luo, Y., I. Kostetskii, and G.L. Radice, *N-cadherin is not essential for limb mesenchymal chondrogenesis*. Dev Dyn, 2005. **232**(2): p. 336-44.
275. Mouse Genome Sequencing, C., et al., *Initial sequencing and comparative analysis of the mouse genome*. Nature, 2002. **420**(6915): p. 520-62.
276. Janne, P.A., et al., *Functional overlap between murine Inpp5b and Ocr1l may explain why deficiency of the murine ortholog for OCRL1 does not cause Lowe syndrome in mice*. J Clin Invest, 1998. **101**(10): p. 2042-53.
277. Schwarzbauer, J.E., C.S. Spencer, and C.L. Wilson, *Selective secretion of alternatively spliced fibronectin variants*. J Cell Biol, 1989. **109**(6 Pt 2): p. 3445-53.
278. Yoshihiro Ishikawa, S.I., Kazuhiro Nagata, Lynn Y. Sakai, and Hans Peter Bächinger, *Intracellular mechanisms of molecular recognition and sorting for transport of large extracellular matrix molecules*. PNAS, 2016. **113**.
279. Kii, I., T. Nishiyama, and A. Kudo, *Periostin promotes secretion of fibronectin from the endoplasmic reticulum*. Biochem Biophys Res Commun, 2016. **470**(4): p. 888-93.
280. Hashimoto, Y., et al., *Mutation (D472Y) in the type 3 repeat domain of cartilage oligomeric matrix protein affects its early vesicle trafficking in endoplasmic reticulum and induces apoptosis*. Am J Pathol, 2003. **163**(1): p. 101-10.
281. Walter, P. and D. Ron, *The unfolded protein response: from stress pathway to homeostatic regulation*. Science, 2011. **334**(6059): p. 1081-6.
282. Brewer, J.W. and J.A. Diehl, *PERK mediates cell-cycle exit during the mammalian unfolded protein response*. Proc Natl Acad Sci U S A, 2000. **97**(23): p. 12625-30.
283. Svensson, L., et al., *Cartilage oligomeric matrix protein-deficient mice have normal skeletal development*. Mol Cell Biol, 2002. **22**(12): p. 4366-71.
284. Hecht, J.T., et al., *Retention of cartilage oligomeric matrix protein (COMP) and cell death in redifferentiated pseudoachondroplasia chondrocytes*. Matrix Biol, 1998. **17**(8-9): p. 625-33.
285. Wang, H.Y., et al., *Identification of a mutated fibronectin as a tumor antigen recognized by CD4+ T cells: its role in extracellular matrix formation and tumor metastasis*. J Exp Med, 2002. **195**(11): p. 1397-406.
286. Trobisch, P., O. Suess, and F. Schwab, *Idiopathic scoliosis*. Dtsch Arztebl Int, 2010. **107**(49): p. 875-83; quiz 884.
287. Asher, M.A. and D.C. Burton, *Adolescent idiopathic scoliosis: natural history and long term treatment effects*. Scoliosis, 2006. **1**(1): p. 2.
288. Wise, C.A., et al., *Understanding genetic factors in idiopathic scoliosis, a complex disease of childhood*. Curr Genomics, 2008. **9**(1): p. 51-9.

Annexe I

*Mutations in Fibronectin Cause a Subtype of
Spondylometaphyseal Dysplasia with “Corner Fractures”
by Lee et al.*

Paper published in the American Journal of Human Genetics
November 2017

Mutations in Fibronectin Cause a Subtype of Spondylometaphyseal Dysplasia with “Corner Fractures”

Chae Syng Lee,¹ He Fu,² Nissan Baratang,² Justine Rousseau,² Heena Kumra,¹ V. Reid Sutton,³ Marcello Niceta,⁴ Andrea Ciolfi,⁴ Guilherme Yamamoto,⁵ Débora Bertola,⁵ Carlo L. Marcelis,⁶ Dorien Lugtenberg,⁶ Andrea Bartuli,⁴ Choel Kim,⁷ Julie Hoover-Fong,⁸ Nara Sobreira,⁸ Richard Pauli,⁹ Carlos Bacino,³ Deborah Krakow,¹⁰ Jillian Parboosingh,¹¹ Patrick Yap,¹² Ariana Kariminejad,¹³ Marie T. McDonald,¹⁴ Mariana I. Aracena,¹⁵ Ekkehart Lausch,¹⁶ Sheila Unger,¹⁷ Andrea Superti-Furga,¹⁷ James T. Lu,¹⁸ Baylor-Hopkins Center for Mendelian Genomics,¹⁹ Dan H. Cohn,²⁰ Marco Tartaglia,⁴ Brendan H. Lee,³ Dieter P. Reinhardt,^{1,21,*} and Philippe M. Campeau^{2,21,*}

Fibronectin is a master organizer of extracellular matrices (ECMs) and promotes the assembly of collagens, fibrillin-1, and other proteins. It is also known to play roles in skeletal tissues through its secretion by osteoblasts, chondrocytes, and mesenchymal cells. Spondylometaphyseal dysplasias (SMDs) comprise a diverse group of skeletal dysplasias and often manifest as short stature, growth-plate irregularities, and vertebral anomalies, such as scoliosis. By comparing the exomes of individuals with SMD with the radiographic appearance of “corner fractures” at metaphyses, we identified three individuals with fibronectin (*FN1*) variants affecting highly conserved residues. Furthermore, using matching tools and the SkelDys emailing list, we identified other individuals with *de novo FN1* variants and a similar phenotype. The severe scoliosis in most individuals and rare developmental coxa vara distinguish individuals with *FN1* mutations from those with classical Sutcliffe-type SMD. To study functional consequences of these *FN1* mutations on the protein level, we introduced three disease-associated missense variants (p.Cys87Phe [c.260G>T], p.Tyr240Asp [c.718T>G], and p.Cys260Gly [c.778T>G]) into a recombinant secreted N-terminal 70 kDa fragment (rF70K) and the full-length fibronectin (rFN). The wild-type rF70K and rFN were secreted into the culture medium, whereas all mutant proteins were either not secreted or secreted at significantly lower amounts. Immunofluorescence analysis demonstrated increased intracellular retention of the mutant proteins. In summary, *FN1* mutations that cause defective fibronectin secretion are found in SMD, and we thus provide additional evidence for a critical function of fibronectin in cartilage and bone.

Spondylometaphyseal dysplasias (SMDs), or bone dysplasias affecting the spine and growth plates, comprise a heterogeneous group of conditions from both a clinical and genetic perspective. Genetic mutations have been identified for several SMDs (in *COL2A1* [MIM: 120140], *TRPV4* [MIM: 605427], *SBDS* [MIM: 607444], *GPX4* [MIM: 138322], *PCYT1A* [MIM: 123695], and *ACP5* [MIM: 171640]), but rarer forms still escape molecular diagnosis.¹ One such condition is SMD with “corner fractures” (MIM: 184255). First recognized by Sutcliffe in 1966, fewer than 25 individuals or families have been reported.² These individuals generally show developmental coxa vara but no scoliosis (as was the case for several individuals in our cohort without *FN1* [MIM: 135600] mutations; see

Table S1).^{3,4} At the edges of the irregular metaphyses, flake-like, triangular, or curvilinear ossification centers simulate fractures. This specifically affects the distal tibia, the distal radius (ulnar aspect), the proximal humerus, and the proximal femur. The so-called “corner fractures” are unlikely to be true fractures but instead represent irregular ossification at the growth plates and secondary ossification centers.³ These fractures tend to become larger in older children and disappear after growth has stopped. Corner fractures on radiographs can also be seen in Duetting-type SMD (or SMD type A4 [MIM: 609052]),⁵ Schmid (MIM: 156500) and Jansen (MIM: 156400) types of metaphyseal chondrodysplasia, Strudwick-type spondyloepimetaphyseal dysplasia (MIM: 184250),⁶ Blount disease

¹Department of Anatomy and Cell Biology and Faculty of Dentistry, McGill University, Montreal, QC H3A 0C7, Canada; ²Centre Hospitalier Universitaire Sainte Justine Research Centre, University of Montreal, Montreal, QC H3T 1C5, Canada; ³Department of Molecular and Human Genetics, Baylor College of Medicine, Houston, TX 77030, USA; ⁴Genetics and Rare Diseases Research Division, Bambino Gesù Children’s Hospital, Istituto di Ricovero e Cura a Carattere Scientifico, Rome 00146, Italy; ⁵Clinical Genetics Unit, Instituto da Criança, Hospital das Clínicas da Faculdade de Medicina da Universidade de São Paulo, São Paulo SP 05403-000, Brazil; ⁶Department of Human Genetics, Radboud University Medical Center, 6500 HB Nijmegen, the Netherlands; ⁷Department of Pharmacology, Baylor College of Medicine, Houston, TX 77030, USA; ⁸McKusick-Nathans Institute of Genetic Medicine, Johns Hopkins University School of Medicine, Baltimore, MD 21287, USA; ⁹Midwest Regional Bone Dysplasia Clinic, University of Wisconsin, Madison, WI 53705, USA; ¹⁰Department of Human Genetics, David Geffen School of Medicine, University of California, Los Angeles, Los Angeles, CA 90095, USA; ¹¹Department of Medical Genetics and Alberta Children’s Hospital Research Institute, University of Calgary, Calgary, AB T2N 4N1, Canada; ¹²Genetic Health Service New Zealand (Northern Hub), Auckland 1023, New Zealand; ¹³Kariminejad-Najmabadi Pathology & Genetics Center, Tehran 14665, Iran; ¹⁴Department of Pediatrics, Division of Medical Genetics, Duke University Medical Center, Durham, NC 27710, USA; ¹⁵División de Pediatría, Pontificia Universidad Católica de Chile, Pediatra-Genetista, Unidad de Genética, Hospital Dr. Luis Calvo Mackenna, Santiago, Chile; ¹⁶Department of Pediatrics, Medical Center, Faculty of Medicine, University of Freiburg, Freiburg 79106, Germany; ¹⁷Service of Medical Genetics, Lausanne University Hospital (CHUV), Lausanne 1011, Switzerland; ¹⁸Helix, San Carlos, CA 94070, USA; ¹⁹Baylor-Hopkins Center for Mendelian Genomics, Houston, TX 77030, USA; ²⁰Department of Molecular, Cell, and Developmental Biology, University of California, Los Angeles, Los Angeles, CA 90095, USA

²¹These authors contributed equally to this work

*Correspondence: dieter.reinhardt@mcgill.ca (D.P.R.), p.campeau@umontreal.ca (P.M.C.)

<https://doi.org/10.1016/j.ajhg.2017.09.019>

© 2017 American Society of Human Genetics.

Table 1. Clinical Features

	Family 1	Family 2	Family 3	Family 4	Family 5	Family 6	Family 7	SMD Corner-Fracture Type or Sutcliffe Type (from Currarino et al.;³ n = 18)	
Individual in pedigree	II-2 (mother)	III-1 (first child)	III-2 (second child)	II-1	III-2 (child)	II-1	II-1	NA	
Gender	female	male	male	female	female	female	female	NA	
Age at last assessment	29 years	13 years	9 years	14 years	2 years, 1 month	5 years, 9 months	16 years, 11 months	4 years	
Height (cm)	147 (-3 SD)	113 (-5.7 SD)	107 (-4.6 SD)	136 (-3.38 SD)	83.7 (-0.9 SD)	97 (-3.3 SD)	137 (-4.66 SD)	89 (<3.0 SD)	
Ovoid vertebral bodies	NA	+	-	-	-	+	+	16/18	
Scoliosis	+	(operated)	+	(operated)	+	+	+	1/18	
Developmental coxa vara	-	-	-	+	-	+	+	18/18	
Irregular metaphyses	NA	+	+	+	+	+	+	16/18	
"Corner fractures"	-	+	+	+	+	+	+	15/18	
Knee anomalies	-	-	genu varum (operated)	-	genu varum (operated)	-	genu varum	one genu varum, one genu valgum	
Chest or rib anomaly (e.g., pectus)	pectus carinatum	pectus carinatum	pectus carinatum	-	pectus carinatum	-	-	NA	
Other	hip surgery at 18 years, pregnancy-induced hypertension	born at term, weight 1,673 g (-4.3 SD), length 38 cm (-2.7 SD), hyponatremia at 1 month (unknown cause), hypoplasia of T12 vertebra and triangular S1, back and leg pain	born at term, weight 1,729 g (-3.9 SD), length 39 cm (-2.6 SD), leg pain	facial asymmetry and dysmorphisms (dysplastic left ear), missing teeth 34 and 44 (island of compact bone instead), intradural lipoma and megacisterna magna on MRI	born at 36 weeks, weight 2,060 g (3 rd -10 th percentile), length 43.5 cm (3 rd -10 th percentile), OFC 29.5 cm (3 rd percentile), normal renal sonography and kidney function, no signs of proteinuria or microalbuminuria, leg pain	born at 39 weeks, weight 2,280 g (<3 rd percentile), length 45 cm (<3 rd percentile), OFC 32 (3 rd percentile), hip surgery at 2 years (both sides), multiple corrections to right hip and femur, shortening of right leg by 5 cm, bicuspid aortic valve	born at 39 weeks, weight 2,280 g (<3 rd percentile), length 45 cm (<3 rd percentile), OFC 32 (3 rd percentile), hip surgery at 2 years (both sides), multiple corrections to right hip and femur, shortening of right leg by 5 cm, bicuspid aortic valve	normal renal function, no proteinuria, no facial asymmetry or dysmorphisms	NA

The following abbreviations are used: OFC, occipitofrontal circumference; and NA, not available.

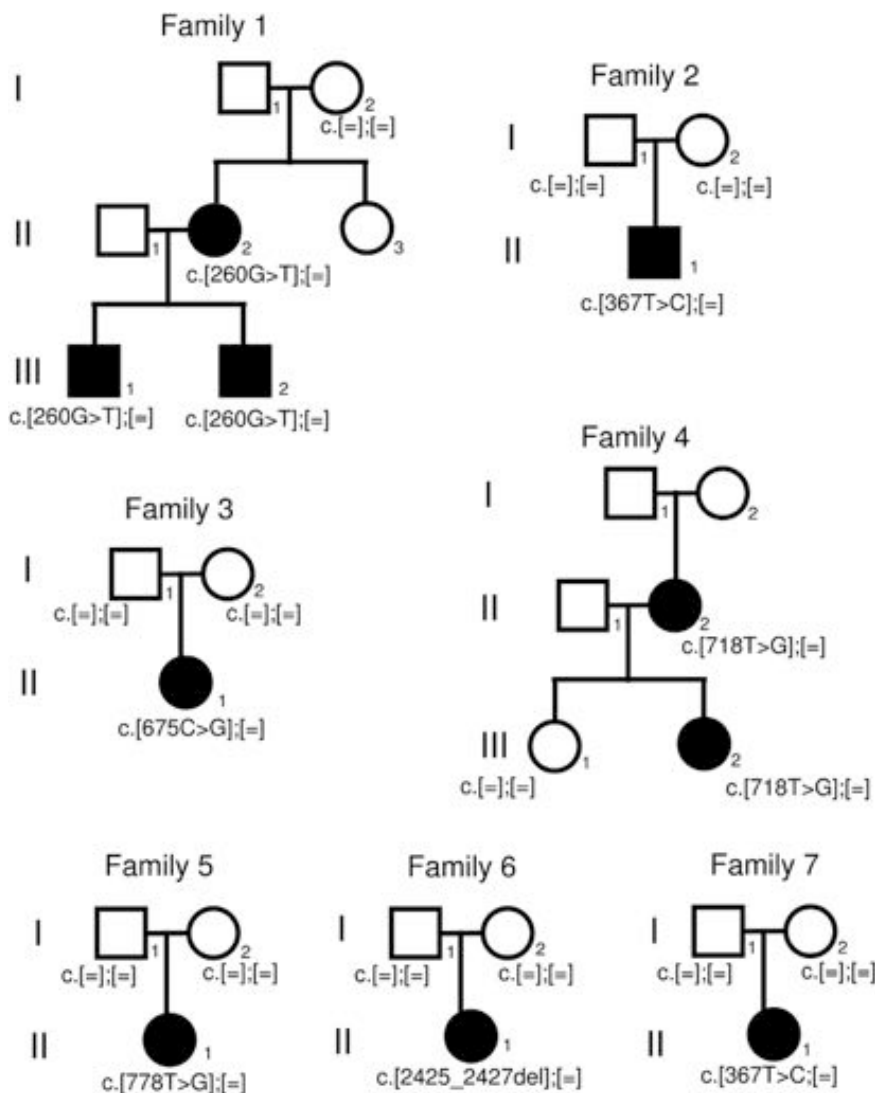
Table 2. Genetic Description of the FN1 Variants

Family	Genomic Change (hg19)	Coding Change (GenBank: NM_212482.2) ^a	Protein Change (GenBank: NP_997647.1)	Inheritance
1	chr2: g.216299436C>A	c.260G>T	p.Cys87Phe	dominant
2	chr2: g.216298095A>G	c.367T>C	p.Cys123Arg	<i>de novo</i>
3	chr2: g.216295448G>C	c.675C>G	p.Cys225Trp	<i>de novo</i>
4	chr2: g.216293029A>C	c.718T>G	p.Tyr240Asp	dominant
5	chr2: g.216292969A>C	c.778T>G	p.Cys260Gly	<i>de novo</i>
6	chr2: g.216273022_216273024del	c.2425_2427del	p.Thr809del	<i>de novo</i>
7	chr2: g.216298095A>G	c.367T>C	p.Cys123Arg	<i>de novo</i>

^aAll variants are absent from the ExAC Browser.

(MIM: 188700), Menkes disease (MIM: 309400), nonaccidental injury, congenital contractures, rickets, and scurvy.⁷ Some individuals initially thought to have SMD with corner fractures were later identified to have type 2 collagenopathy.⁶

Fibronectin is found in the human body in both a soluble form (~300 µg/mL in plasma) and an insoluble form as a principal component of the fibrillar extracellular matrix (ECM) of virtually all tissues.^{8,9} Fibronectin contains binding sites for integrins, collagens,

**Figure 1. Pedigrees of the Families with FN1 Mutations**

Co-segregation of the variants with the trait in families 1 and 4 suggests dominant inheritance. Consistently, *de novo* FN1 mutations in the affected individuals of simplex families 2, 3, 5, 6, and 7 were observed.

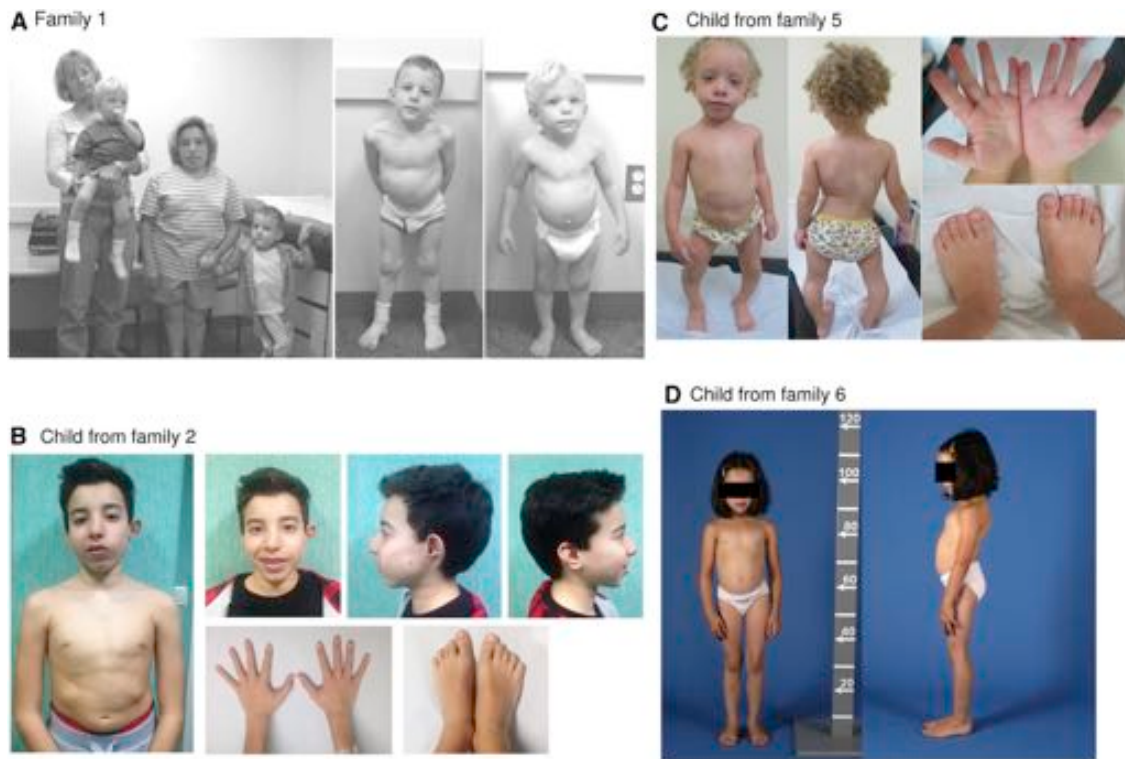


Figure 2. Photographs of Some of the Individuals with *FN1* Mutations

(A) Photographs in a figure reproduced with permission from Sutton et al.³⁰ (copyright © 2005 Wiley-Liss, Inc.). On the left are the three affected individuals who have an *FN1* mutation and the maternal grandmother. In the middle is the older child at age 5 years, and on the right is the younger child at age 3 years.

(B) Affected child from family 2 at age 13 years. Note the short trunk, facial asymmetry, dysplastic left ear, and normal hands and feet.

(C) Affected child from family 5 at age 2 years and 11 months. Note the scoliosis, genu varum, and normal hands and feet.

(D) Affected child from family 6 at age 8 years. Note the short trunk and scoliotic posture.

glycoproteins, and glycosaminoglycans, as well as self-association sites.¹⁰ It self-assembles in a cell-dependent manner upon binding to integrins and other cell-surface components⁹ and initiates the assembly of the ECM.^{11–13}

We performed exome sequencing in individuals with SMD with corner fractures, who had been identified through the Texas Children's Skeletal Dysplasia Program, International Skeletal Dysplasia Registry, Baylor-Hopkins Center for Mendelian Genetics, Skeldys emailing list of the International Skeletal Dysplasia Society (ISDS), Shriners Canada Skeletal Dysplasia Clinic, and existing collaborations. Families provided written informed consent for protocols approved by the institutional review board at Baylor College of Medicine or local institutions. The procedures followed were in accordance with the ethical standards of the relevant committees on human experimentation. Details on the exome sequencing libraries and alignment are presented in Table S2.

In two of the first few individuals sequenced, who have been previously reported, *COL2A1* mutations were identified.¹ In total, 13 individuals were exome sequenced, and a comparison of the rare or undescribed variants shared between these individuals revealed variants in

FN1 in three of these affected individuals (two variants segregating with the disease, c.260G>T [p.Cys87Phe] [GenBank: NM_212482.2 and NP_997647.1, respectively] in family 1 and c.718T>G [p.Tyr240Asp] in family 4, and a *de novo* variant, c.2425_2427del [p.Thr809del] in family 6). The genetic cause of SMD is still undetermined for the other individuals. Subsequently, through the ISDS emailing list, the GeneMatcher tool, and the Shriners Canada Skeletal Dysplasia Clinic,¹⁴ four other individuals with *de novo FN1* variants (c.367T>C [p.Cys123Arg] in families 2 and 7, c.675C>G [p.Cys225Trp] in family 3, and c.778T>G [p.Cys260Gly] in family 5) and SMD with corner fractures were identified. In one of them (individual 3, identified with the ISDS emailing list), only *FN1* was sequenced on the basis of the initial findings. Thus, in this cohort, previously unreported *FN1* variants were found in 7 of 16 families affected by SMD with corner fractures. The clinical phenotypes of the individuals with *FN1* variants are detailed in Table 1, and the variants are presented in Table 2. Figure 1 shows pedigrees, Figure 2 shows photographs, Figure 3 shows selected radiographs, and Figure S1 shows additional radiographs.

All *FN1* variants discovered in this study are absent from the ExAC Browser and affect highly conserved residues

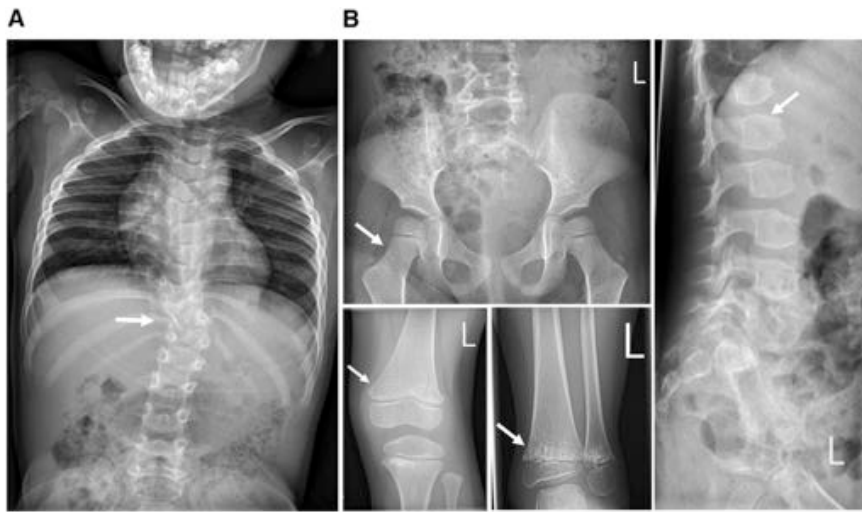


Figure 3. Radiographs Showing the "Corner Fractures" and Other Radiological Changes

(A) Individual from family 7; note the significant scoliosis.

(B) Individual from family 3; note the absence of coxa vara, the presence of irregular metaphyses with corner fractures, and the presence of ovoid vertebral bodies.

Additional radiographs from all families are available in [Figure S1](#).

(Figure 4). The majority (4/6) affect cysteine residues, all of which form disulfide bonds that are critical for the three-dimensional structure of the type I fibronectin domains.¹⁵ Five of the mutations (c.260G>T [p.Cys87Phe], c.367T>C [p.Cys123Arg], c.675C>G [p.Cys225Trp], c.718T>G [p.Tyr240Asp], and c.778T>G [p.Cys260Gly])

are located in the N-terminal assembly domain (spanning fibronectin domains I-1 through I-5), which is important to initiating assembly on the cell surface.⁹ The remaining mutation (c.2425_2427del [p.Thr809del]) was found in the III-2 domain, which contains a fibronectin binding site and is involved in conformational changes promoting fibronectin assembly.⁹ The Tyr240 residue has previously been mutated into a Ser residue *in vitro* and shown to be critical for fibronectin binding to fibroblasts.¹⁶

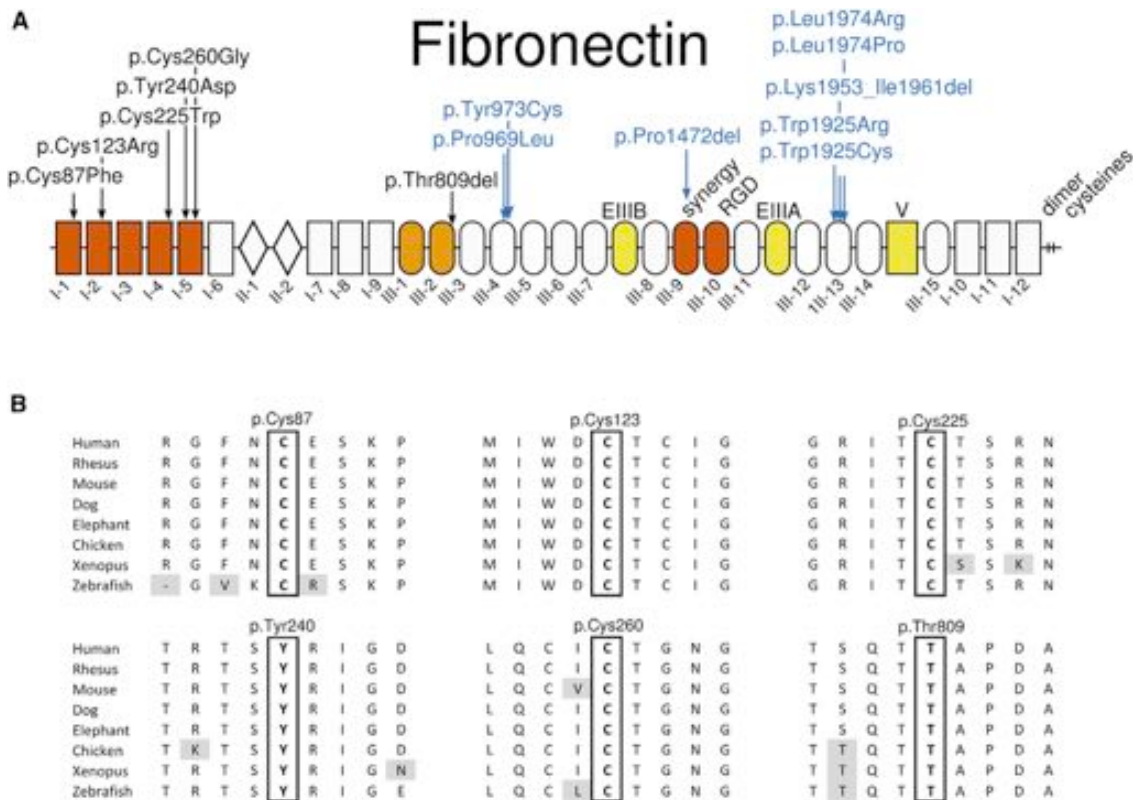


Figure 4. Position and Conservation of Amino Acids Affected by Substitutions

(A) Location of the SMD-associated fibronectin amino acid substitutions (in black) and those underlying glomerulopathy (in blue). The fibronectin domains I, II, and III are numbered, V stands for variable domain, and EIIIA and EIIB indicate the extra type III repeat A and B segments. These three domains in yellow are subject to alternative splicing. Domains I-1 to I-5 in red represent the N-terminal assembly domain. Domains III-9 and III-10, also in red, contain the synergy site and the RGD site. Domains III-1 and III-2, in orange, contain self-interaction sites and are involved in conformational changes promoting fibronectin assembly.

(B) Amino acid conservation of the mutated residues across vertebrates. Gray shading indicates non-conserved amino acid residues.

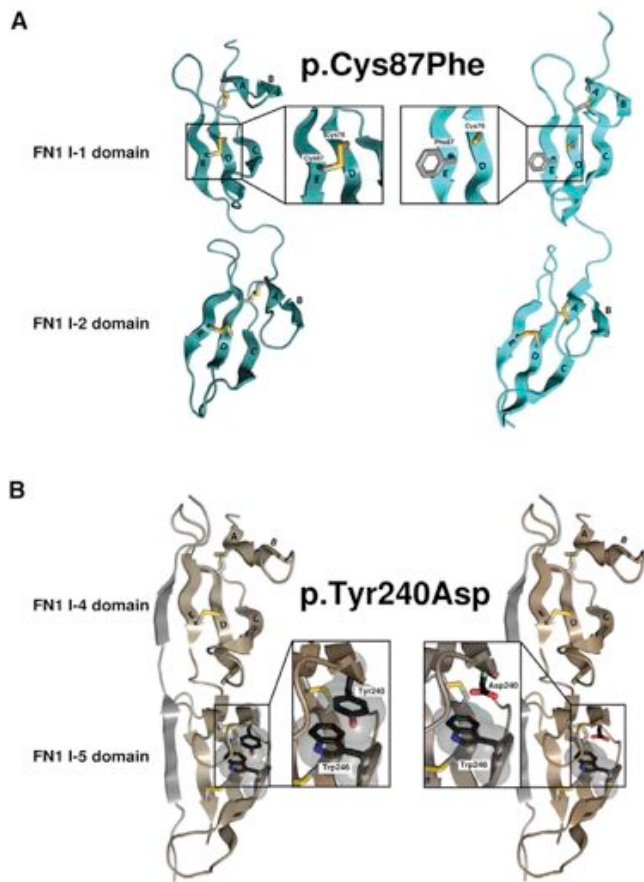


Figure 5. Structural Impact of SMD-Causing Mutations

(A) Structural models of fibronectin domains I-1 and I-2 (PDB: 1O9A,³¹ without the *S. dysgalactiae* FnBP B3 peptide). On the left is the wild-type protein, and on the right is the model with the variant. The model for the p.Cys87Phe substitution was generated by the ModWeb Server.³² The disulfide bond formed between Cys76 and Cys87 stabilizes domain I-1. The p.Cys87Phe substitution is predicted to destabilize the structure by breaking the disulfide bond and by displaying a hydrophobic residue at the surface.

(B) Structural models of fibronectin domains I-4 and I-5 (PDB: 2RKY,³³ without the *S. aureus* FnBPA peptide). To generate the model for the p.Tyr240Asp change, we replaced tyrosine with aspartic acid and manually adjusted the rotamer position to minimize the steric clash with the rest of the protein by using Coot.³⁴ For the wild-type protein, the side chains of Tyr240 and Trp246 interact through π stacking and stabilize the fibronectin domain. This interaction is predicted to be lost in the mutant protein.

Heterozygous *FN1* mutations have previously been reported in type 2 autosomal-dominant glomerulopathy with fibronectin deposits (MIM: 601894).¹⁷ Remarkably, all *FN1* mutations previously implicated in this glomerulopathy cluster in more C-terminally-located regions important for heparin binding and integrin binding (Figure 4).^{17–19} *In vitro*, the mutations cause decreased heparin and integrin binding, reduced endothelial cell spreading, and cytoskeletal reorganization, which has been hypothesized to affect glomerular size selectivity and protein trafficking. Importantly, none of the SMD individuals in our cohort had any evidence of renal disease.

As stated above, all cysteine residues affected by mutations in our cohort are involved in disulfide bonds in fibronectin type I domains (bridges form between Cys87 and Cys76, between Cys123 and Cys135, between Cys225 and Cys213, and between Cys260 and Cys231). We selected one of these (p.Cys87Phe) to model the consequence of the mutation on the three-dimensional structure of fibronectin domains (Figure 5A). The p.Cys87Phe substitution was predicted to destabilize the structure of the I-1 domain by breaking the disulfide bond with residue Cys76 and by displaying a hydrophobic residue at the surface. A similar disruptive impact was predicted for the other missense changes involving Cys123, Cys225, and Cys260. For the two other amino acid residues affected by mutations (Tyr240 and Thr809), 3D structures adequate for modeling the mutations were available only for p.Tyr240Asp (Thr809 was found only at the C-terminal end of a solution structure of III-2,²⁰ which limits the interpretation of its interactions). Modeling predicted that the p.Tyr240Asp variant would disrupt the π -stacking (or π - π stacking) of the side chains of Tyr240 and Trp246 and thus destabilize the I-5 domain (Figure 5B).

We next aimed to analyze the functional consequences of selected *FN1* mutations on the fibronectin protein. Because cells from affected individuals were not available for this study, we generated a recombinant 70 kDa N-terminal fragment of fibronectin (rF70K), spanning the region where five of the six missense variants identified in this study are located, and a full-length recombinant fibronectin (rFN) (Figure 6A). Expression vectors for the human wild-type rF70K and rFN, as well as selected mutants, were generated by standard cloning procedures in the pCDNA3.1+ plasmid (Thermo Fisher Scientific, V79020) with the sequence for a C-terminal V5 epitope tag to facilitate detection and a hexahistidine tag intended for chromatographic purification. At the 5' ends, the vectors contained the coding sequence for either the BM40 signal peptide (rF70K) or the native fibronectin signal peptide (rFN) to ensure secretion of the recombinant protein through the secretory pathway. The rFN expression plasmid was constructed with the sequence for the alternatively spliced EDA and EDB domains. For this analysis, we selected two cysteine missense variants (p.Cys87Phe and p.Cys260Gly) because they represent the major group of the identified mutations, as well as a non-cysteine missense variant (p.Tyr240Asp). These point mutants were generated from the wild-type plasmids via the QuikChange Site-Directed Mutagenesis Kit (Agilent Technologies, 200519).

The plasmids were transfected into human HEK293 cells, which synthesize and secrete endogenous fibronectin and represent an efficient system for producing a range of correctly folded and posttranslationally modified ECM proteins (subfragments as well as mutants).^{21–23} After the plasmids were stably transfected into human HEK293 cells as described previously,²⁴ the secreted wild-type recombinant proteins were readily identified in the

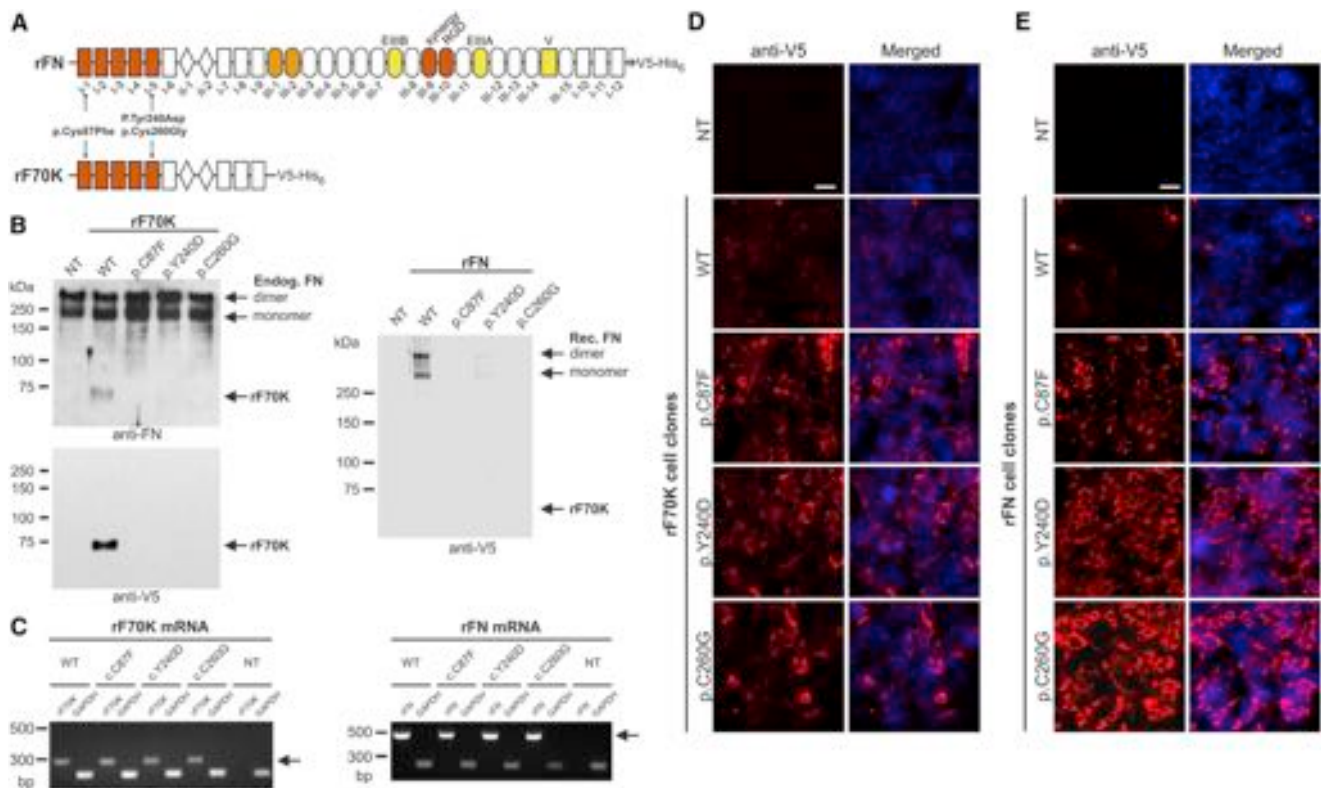


Figure 6. Analysis of Protein Secretion of Recombinant Wild-Type and SMD-Causing Mutants of rF70K and rFN

(A) Schematic overview of full-length fibronectin (rFN) and the 70 kDa N-terminal fragment of fibronectin (rF70K). To ensure secretion through the secretory pathway, the expression plasmids contain either the sequence coding for the endogenous fibronectin signal peptide (rFN) or a heterologous BM40 signal peptide (rF70K). The indicated SMD variants were engineered into the expression constructs. (B–E) NT refers to the non-transfected HEK293 controls, WT refers to the wild-type rF70K or rFN cell clones, and the mutant cell clones are indicated in the one-letter amino acid code. (B) Western blot analysis of conditioned cell-culture medium (for 2 days) harvested from HEK293 cells transfected with rF70K (left) and rFN (right). Analysis of rF70K was performed with a rabbit anti-fibronectin antibody (top; primary antibody, Sigma, F3648; secondary goat anti-rabbit horseradish-conjugated antibody, Agilent Technologies, K4008) and a horseradish-conjugated anti-V5 monoclonal antibody (bottom, Thermo Fisher Scientific, MA5-15253-HRP), whereas the rFN analysis was performed with only an anti-V5 antibody, given that the anti-fibronectin antibody also reacts with endogenous fibronectin. All samples were analyzed under reducing conditions, the blots for rF70K were developed with the SuperSignal West Pico Chemiluminescent Substrate (Thermo Fisher Scientific, 34080), and the blots for rFN were developed with 0.5 mg/mL 4-chloro-1-naphthol (Sigma, C8890) in Tris-buffered saline including 0.02% H₂O₂. (C) Specific RT-PCR analysis of mRNA coding for rF70K (left; 285 bp) or rFN (right; 440 bp) (excluding the endogenous *FN1* mRNA). *GAPDH* analysis (226 bp) was included as a control. RNA was extracted with the RNeasy Plus Mini Kit (QIAGEN, 74134) according to the manufacturer's protocol. Reverse transcription was performed with the ProtoScript II First Strand cDNA Synthesis Kit (New England Biolabs, E6560S), and PCR was performed for 40 cycles. (D and E) Immunofluorescence analysis of transfected HEK293 cells 3 days after seeding with anti-V5 antibodies (red; primary antibody, Thermo Fisher Scientific, R960-25; secondary antibody, Cy3-conjugated antibody, Thermo Fisher Scientific, A10521) for rF70K and rFN was performed according to a previously established protocol.³⁵ Cells were fixed with 4% paraformaldehyde and permeabilized with 0.5% Triton X-100; nuclei were counter-stained with DAPI (blue). The experiments were confirmed with three to four individual recombinant cell clones. The scale bar indicates 50 μm. Images were taken at 400× magnification with Zen software and an AxioImager M2 microscope (Zeiss) equipped with an ORCA-flash 4.0 camera (Hamamatsu, C11440). Note that all analyzed rF70K and rFN mutant proteins were retained intracellularly, but the wild-type proteins were not.

cell-culture medium (conditioned for 2 days) with fibronectin-specific or anti-V5-specific antibodies (Figure 6B). Surprisingly, all three rF70K and rFN mutants were either undetectable in the culture medium or detectable at much lower levels than the wild-type protein. Analysis of recombinant mRNA with primers excluding the endogenous fibronectin mRNA revealed that the amount of mutant mRNA was similar to that of wild-type mRNA (Figure 6C). Immunofluorescence analysis demonstrated very low amounts of the wild-type proteins within the stably transfected cells because the proteins secreted into

the culture medium (Figures 6D and 6E). In contrast to this finding, all three rF70K and rFN mutants consistently showed strong accumulation within the cells. These data clearly demonstrate that p.Cys87Phe, p.Tyr240Asp, and p.Cys260Gly exert a common molecular defect in fibronectin secretion. To assess whether the intracellular retention induced the unfolded protein response in HEK293 cells, we analyzed *XBPI* splicing (IRE1 pathway) and the mRNA expression levels of *CHOP* and *ATF4* (PERK pathway). However, no indication of increased *XBPI* splicing or changes in the *CHOP* or *ATF4* mRNA expression

levels was detected (Figure S2). In addition, the mutant rFN cell clones did not undergo caspase-3-mediated apoptosis (Figure S3).

Fibronectin is present throughout cartilage differentiation and persists in mature cartilaginous tissue.²⁵ However, little is known about the functional role of fibronectin in the development and homeostasis of cartilage. Given that fibronectin has been established as a key ECM protein that guides fibrillogenesis of several other ECM proteins, including proteins present in cartilage, such as fibrillin-1,²⁶ it is conceivable that a reduced amount of secreted fibronectin from chondrocytes could result in a deficient matrix network in cartilage. It is well known that mutations affecting another cartilage protein, cartilage oligomeric matrix protein (*COMP* [MIM: 600310]), lead to pseudoachondroplasia (MIM: 177170) and multiple epiphyseal dysplasia (MIM: 132400) through accumulation of mutant *COMP* in the endoplasmic reticulum of chondrocytes.²⁷ It is thought that this protein accumulation impairs secretion of other matrix proteins and leads to abnormal ECM and chondrocyte death.^{28,29} It is possible that a similar mechanism exists for retained mutant fibronectin and leads to the SMD phenotype observed in our cohort. Conditional double-knockout experiments of fibronectin in mouse cartilage and liver or knockin of some of the mutations are currently underway to further elucidate the molecular basis of fibronectin in the development and maintenance of cartilage.

Accession Numbers

The accession numbers for the variants identified in this study are ClinVar: SCV000574553–SCV000574558.

Supplemental Data

Supplemental Data include three figures and two tables and can be found with this article online at <https://doi.org/10.1016/j.ajhg.2017.09.019>.

Acknowledgments

This project was supported in part by operating grants from the Canadian Institutes for Health Research (clinician-scientist award RN315908 to P.M.C.; MOP-137091 to D.P.R.), the Fonds de Recherche du Québec - Santé clinical research scholar award 30647 to P.M.C., the Quebec Network for Oral and Bone Health Research (RSBO Emerging Collaborating Project 2014-2015 to P.M.C. and D.P.R.), the NIH (UM1 HG006542 to the Baylor Hopkins Center for Mendelian Genomics), the Heart and Stroke Foundation of Canada (G-16-00014634 to D.P.R.), the Italian Ministry of Health (Ricerca Corrente 2016 to M.T. and M.N.), and Fondazione Bambino Gesù (Vite Coraggiose grant to M.T.). This work was also supported by NIH P01 HD070394, by HD024064 from the Eunice Kennedy Shriver National Institute of Child Health & Human Development granted to the Baylor College of Medicine (BCM) Intellectual and Developmental Disabilities Research Center (for processing samples obtained and managing clinical protocols), by the BCM Advanced Technology Cores through funding from

the NIH (AI036211, CA125123, and RR024574), by the Rolanette and Berdon Lawrence Bone Disease Program of Texas, and by the BCM Center for Skeletal Medicine and Biology (to B.H.L.). Analysis of individual 5 was supported by the São Paulo Research Foundation (FAPESP 2015/21783-9; Centros de Pesquisa, Inovação, e Difusão [CEPID] 2013/08028-1) and National Council for Scientific and Technological Development (CNPq 302605/2013-4 and 304130/2016-8 to D. B.). E.L. is supported by grants from the German Research Foundation (CRC 1140), the German Ministry for Education and Research (MaTrOC), and the European Union (SYBIL grant agreement no. 602300; RARENET). We thank Dr. Deane Mosher and Dr. Douglas Annis for providing the FN1 pAcGP67A plasmid. We thank Dr. Reggie Hamdy for referring individual 7 to Dr. Campeau and Dr. Amélie Dampousse for the interpretation of the radiographs.

Received: April 24, 2017

Accepted: September 12, 2017

Published: November 2, 2017

Web Resources

Baylor-Hopkins Center for Mendelian Genetics (BH-CMG), <http://bhcmg.org/>

ExAC Browser, <http://exac.broadinstitute.org/>

GenBank, <http://www.ncbi.nlm.nih.gov/genbank/>

GeneMatcher, <https://www.genematcher.org>

International Skeletal Dysplasia Society (ISDS), <http://www.isds.ch/>

International Skeletal Dysplasia Registry (ISDR), <http://ortho.ucla.edu/isdr>

OMIM, <http://www.omim.org/>

RCSB Protein Data Bank, <https://www.rcsb.org/pdb/home/home.do>

UniProt, <http://www.uniprot.org/uniprot/>

References

1. Machol, K., Jain, M., Almannai, M., Orand, T., Lu, J.T., Tran, A., Chen, Y., Schlesinger, A., Gibbs, R., Bonafe, L., et al. (2017). Corner fracture type spondylometaphyseal dysplasia: Overlap with type II collagenopathies. *Am. J. Med. Genet. A*, *173*, 733–739.
2. Sutcliffe, J. (1966). Metaphyseal dysostosis. *Ann. Radiol. (Paris)* *9*, R215–R223.
3. Currarino, G., Birch, J.G., and Herring, J.A. (2000). Developmental coxa vara associated with spondylometaphyseal dysplasia (DCV/SMD): “SMD-corner fracture type” (DCV/SMD-CF) demonstrated in most reported cases. *Pediatr. Radiol.* *30*, 14–24.
4. Langer, L.O., Jr., Brill, P.W., Ozonoff, M.B., Pauli, R.M., Wilson, W.G., Alford, B.A., Pavlov, H., and Drake, D.G. (1990). Spondylometaphyseal dysplasia, corner fracture type: a heritable condition associated with coxa vara. *Radiology* *175*, 761–766.
5. Duetting, T., Schulze, A., Troeger, J., and Spranger, J. (1998). A rare form of spondylometaphyseal dysplasia-type A4. *Am. J. Med. Genet.* *78*, 61–66.
6. Walter, K., Tasek, M., Tobias, E.S., Ikegawa, S., Coucke, P., Hyland, J., Mortier, G., Iwaya, T., Nishimura, G., Superti-Furga, A., and Unger, S. (2007). *COL2A1*-related skeletal dysplasias with predominant metaphyseal involvement. *Am. J. Med. Genet. A*, *143A*, 161–167.
7. Kozlowski, K., and Beighton, P. (1984). *Gamut index of skeletal dysplasias: an aid to radiodiagnosis* (Springer-Verlag).

8. Mosher, D.F. (2006). Plasma fibronectin concentration: a risk factor for arterial thrombosis? *Arterioscler. Thromb. Vasc. Biol.* *26*, 1193–1195.
9. Singh, P., Carraher, C., and Schwarzbauer, J.E. (2010). Assembly of fibronectin extracellular matrix. *Annu. Rev. Cell Dev. Biol.* *26*, 397–419.
10. Pankov, R., and Yamada, K.M. (2002). Fibronectin at a glance. *J. Cell Sci.* *115*, 3861–3863.
11. Sabatier, L., Chen, D., Fagotto-Kaufmann, C., Hubmacher, D., McKee, M.D., Annis, D.S., Mosher, D.F., and Reinhardt, D.P. (2009). Fibrillin assembly requires fibronectin. *Mol. Biol. Cell* *20*, 846–858.
12. Sottile, J., and Hocking, D.C. (2002). Fibronectin polymerization regulates the composition and stability of extracellular matrix fibrils and cell-matrix adhesions. *Mol. Biol. Cell* *13*, 3546–3559.
13. Dallas, S.L., Sivakumar, P., Jones, C.J., Chen, Q., Peters, D.M., Mosher, D.F., Humphries, M.J., and Kielty, C.M. (2005). Fibronectin regulates latent transforming growth factor-beta (TGF beta) by controlling matrix assembly of latent TGF beta-binding protein-1. *J. Biol. Chem.* *280*, 18871–18880.
14. Sobreira, N., Schiettecatte, F., Valle, D., and Hamosh, A. (2015). GeneMatcher: a matching tool for connecting investigators with an interest in the same gene. *Hum. Mutat.* *36*, 928–930.
15. Baron, M., Norman, D., Willis, A., and Campbell, I.D. (1990). Structure of the fibronectin type I module. *Nature* *345*, 642–646.
16. Sottile, J., Schwarzbauer, J., Selegue, J., and Mosher, D.F. (1991). Five type I modules of fibronectin form a functional unit that binds to fibroblasts and *Staphylococcus aureus*. *J. Biol. Chem.* *266*, 12840–12843.
17. Ohtsubo, H., Okada, T., Nozu, K., Takaoka, Y., Shono, A., Asanuma, K., Zhang, L., Nakanishi, K., Taniguchi-Ikeda, M., Kaito, H., et al. (2016). Identification of mutations in FN1 leading to glomerulopathy with fibronectin deposits. *Pediatr. Nephrol.* *31*, 1459–1467.
18. Castelletti, F., Donadelli, R., Banterla, F., Hildebrandt, E., Zipfel, P.F., Bresin, E., Otto, E., Skerka, C., Renieri, A., Todeschini, M., et al. (2008). Mutations in FN1 cause glomerulopathy with fibronectin deposits. *Proc. Natl. Acad. Sci. USA* *105*, 2538–2543.
19. Ertoy Baydar, D., Kutlugun, A.A., Bresin, E., and Piras, R. (2013). A case of familial glomerulopathy with fibronectin deposits caused by the Y973C mutation in fibronectin. *Am. J. Kidney Dis.* *61*, 514–518.
20. Vakonakis, I., Staunton, D., Rooney, L.M., and Campbell, I.D. (2007). Interdomain association in fibronectin: insight into cryptic sites and fibrillogenesis. *EMBO J.* *26*, 2575–2583.
21. Kirschner, R., Hubmacher, D., Iyengar, G., Kaur, J., Fagotto-Kaufmann, C., Brömme, D., Bartels, R., and Reinhardt, D.P. (2011). Classical and neonatal Marfan syndrome mutations in fibrillin-1 cause differential protease susceptibilities and protein function. *J. Biol. Chem.* *286*, 32810–32823.
22. McKee, K.K., Harrison, D., Capizzi, S., and Yurchenco, P.D. (2007). Role of laminin terminal globular domains in basement membrane assembly. *J. Biol. Chem.* *282*, 21437–21447.
23. Fox, J.W., Mayer, U., Nischt, R., Aumailley, M., Reinhardt, D., Wiedemann, H., Mann, K., Timpl, R., Krieg, T., Engel, J., et al. (1991). Recombinant nidogen consists of three globular domains and mediates binding of laminin to collagen type IV. *EMBO J.* *10*, 3137–3146.
24. Lin, G., Tiedemann, K., Vollbrandt, T., Peters, H., Batge, B., Brinckmann, J., and Reinhardt, D.P. (2002). Homo- and heterotypic fibrillin-1 and -2 interactions constitute the basis for the assembly of microfibrils. *J. Biol. Chem.* *277*, 50795–50804.
25. Singh, P., and Schwarzbauer, J.E. (2012). Fibronectin and stem cell differentiation - lessons from chondrogenesis. *J. Cell Sci.* *125*, 3703–3712.
26. Keene, D.R., Jordan, C.D., Reinhardt, D.P., Ridgway, C.C., Ono, R.N., Corson, G.M., Fairhurst, M., Sussman, M.D., Memoli, V.A., and Sakai, L.Y. (1997). Fibrillin-1 in human cartilage: developmental expression and formation of special banded fibers. *J. Histochem. Cytochem.* *45*, 1069–1082.
27. Maddox, B.K., Keene, D.R., Sakai, L.Y., Charbonneau, N.L., Morris, N.P., Ridgway, C.C., Boswell, B.A., Sussman, M.D., Horton, W.A., Bächinger, H.P., and Hecht, J.T. (1997). The fate of cartilage oligomeric matrix protein is determined by the cell type in the case of a novel mutation in pseudoachondroplasia. *J. Biol. Chem.* *272*, 30993–30997.
28. Hecht, J.T., Montufar-Solis, D., Decker, G., Lawler, J., Daniels, K., and Duke, P.J. (1998). Retention of cartilage oligomeric matrix protein (COMP) and cell death in redifferentiated pseudoachondroplasia chondrocytes. *Matrix Biol.* *17*, 625–633.
29. Hashimoto, Y., Tomiyama, T., Yamano, Y., and Mori, H. (2003). Mutation (D472Y) in the type 3 repeat domain of cartilage oligomeric matrix protein affects its early vesicle trafficking in endoplasmic reticulum and induces apoptosis. *Am. J. Pathol.* *163*, 101–110.
30. Sutton, V.R., Hyland, J.C., Phillips, W.A., Schlesinger, A.E., and Brill, P.W. (2005). A dominantly inherited spondylometaphyseal dysplasia with “corner fractures” and congenital scoliosis. *Am. J. Med. Genet. A.* *133A*, 209–212.
31. Schwarz-Linek, U., Werner, J.M., Pickford, A.R., Gurusiddappa, S., Kim, J.H., Pilka, E.S., Briggs, J.A., Gough, T.S., Höök, M., Campbell, I.D., and Potts, J.R. (2003). Pathogenic bacteria attach to human fibronectin through a tandem beta-zipper. *Nature* *423*, 177–181.
32. Pieper, U., Webb, B.M., Barkan, D.T., Schneidman-Duhovny, D., Schlessinger, A., Braberg, H., Yang, Z., Meng, E.C., Petersen, E.F., Huang, C.C., et al. (2011). ModBase, a database of annotated comparative protein structure models, and associated resources. *Nucleic Acids Res.* *39*, D465–D474.
33. Bingham, R.J., Rudiño-Piñera, E., Meenan, N.A., Schwarz-Linek, U., Turkenburg, J.P., Höök, M., Garman, E.F., and Potts, J.R. (2008). Crystal structures of fibronectin-binding sites from *Staphylococcus aureus* FnBPA in complex with fibronectin domains. *Proc. Natl. Acad. Sci. USA* *105*, 12254–12258.
34. Emsley, P., and Cowtan, K. (2004). Coot: model-building tools for molecular graphics. *Acta Crystallogr. D Biol. Crystallogr.* *60*, 2126–2132.
35. Hubmacher, D., Sabatier, L., Annis, D.S., Mosher, D.F., and Reinhardt, D.P. (2011). Homocysteine modifies structural and functional properties of fibronectin and interferes with the fibronectin-fibrillin-1 interaction. *Biochemistry* *50*, 5322–5332.

Annexe II

Project II:
**Characterization of genes involved in the
biosynthesis of GPI-anchored proteins**

This annexe includes:

- 1) Presentation of the project and work that has been done by the author.
- 2) *Clinical variability in inherited glycosylphosphatidylinositol deficiency disorders* by Bellai-Dussault *et al.* Review published in Wiley Clinical Genetics (July 2018).
- 3) *Mutations in PIGS, Encoding a GPI Transamidase, Cause a Neurological Syndrome Ranging from Fetal Akinesia to Epileptic Encephalopathy* by Nguyen *et al.* Paper published in The American Journal of Human Genetics (October 2018).

In parallel with my project on fibronectin, I have also been working on a topic involving GPI-anchored proteins. While the main goal is also the characterization of mutations found in genes, the clinical features manifested by the patients in this project are more neurological as opposed to skeletal.

1. INTRODUCTION

Glycosylphosphatidylinositol (GPI) is a glycolipid that can anchor proteins at the cell surface. These proteins, collectively called GPI-anchored proteins (GPI-APs), play important roles, particularly in development and neurogenesis. The biosynthesis of GPI anchors is a highly regulated sequential process wherein more than 30 phosphatidylinositol glycan anchor biosynthesis (PIG) proteins and GPI-attachment to proteins (PGAP) proteins are involved [1]. The disruption in any of the steps in the biosynthesis can potentially cause a phenotype in the individual. Mutations in genes encoding the proteins involved in GPI biosynthesis have been identified, and can result in a group of developmental disorders termed “inherited GPI deficiencies” (IGDs). The most common characteristics reported in IGDs are intellectual deficiency, developmental delay, brain anomalies, seizures, and dysmorphic features [2]. A review was written and published by me and my colleagues that describes the clinical features that were reported as a consequence of mutations in GPI biosynthesis genes (see attached review by Bellai-Dussault et al., 2018).

So far, 17 of the genes encoding proteins involved in GPI biosynthesis have been associated to IGDs [3, 4]. We hypothesize that other genes are involved in proper GPI biosynthesis, and that mutations in any of these genes can disrupt the pathway and result in the phenotypes seen in the patients. In collaboration with other research teams, novel mutations in these genes have been identified in affected patients. The mutations, which were found by whole exome sequencing and confirmed by Sanger sequencing, are rare or have never been reported previously. In this work, the main objective is to study the effect of these identified mutations. Functional studies on blood cells and skin fibroblasts of affected individuals will be done to assess the effect of the mutations.

This project was done in close collaboration with Dr. Thi Tuyet Mai Nguyen, a post-doctoral researcher in the lab. Unless otherwise specified, experiments presented in this work were performed by the author. Clinical examination, mutation identification, and isolation of skin fibroblasts were done by other research members.

2. METHODS

2.1 Flow Cytometry

Flow cytometry on live granulocytes was performed as described by Johnstone et al. [5]. Briefly, fresh blood samples from patient and healthy control were stained with fluorescent-conjugated antibodies FLAER-Alexa 448 Proaerolysin (Cedarlane), PE Anti-Human CD16 (BioLegend), FITC Mouse Anti-Human CD55 (BD Pharmingen) and FITC Mouse Anti-Human CD59 (BD Pharmingen) for 1 hour on ice in the dark. Cells were collected and washed with cold incubation buffer (1% BSA in PBS), then red blood cells were lysed in BD FACS Lysing Solution (BD Biosciences) for 10min. White blood cells were collected by centrifugation and resuspended in PBS before analysis with BD FACScanto II system (BD Biosciences). Data obtained from the granulocytes were analyzed using the Cytobank online platform.

To perform flow cytometry on fibroblasts, transduced patient cells, untransduced patient cells, and fibroblasts from a healthy individual were harvested from cell culture plates with Accutase (Sigma) and stained with FLAER (Cedarlane), FITC Anti-Human CD73 (BioLegend) and/or PE Anti-Human CD87 (BioLegend) for 1 hour at room temperature. Unstained cells were also prepared. The cells were washed twice with cold incubation buffer (1% BSA in PBS), and were resuspended in PBS before analysis with the BD FACScanto II system.

2.2 Lentivirus production

Vector DNA used in this work are empty pLX304 (Addgene), PIGF-pLX304 (DNASU plasmid repository), PIGX-Lv105 (Genecopoeia), and empty Lv105 (gift from Devon Johnstone, University of Ottawa, Ontario). HEK293T cells were plated on 12-well plates, and at confluency, medium was changed to DMEM (Gibco) without antibiotics. Solutions containing 0.8 µg vector DNA, 0.3 µg envelope plasmid pMD2.G, and 0.5 µg packaging plasmid psPAX2

was mixed in 100 μ l media without antibiotics or serum, and was incubated with Lipofectamine 2000 transfection reagent (Thermo Fisher Scientific) for 20min before applying to the cells. The next day, the media was changed to DMEM with antibiotics and serum, and the supernatant was collected three times within 24 hours. In the last collection, all supernatants are pooled, centrifuged and filtered with a 0.45 μ m sterile filter.

2.3 Lentivirus transduction

Patient fibroblasts were plated in 24-well plates and at confluency, the media was changed to complete media (DMEM with 5% fetal bovine serum and 1% antibiotic-antimycotic solution) with 8 μ g/ml polybrene. The virus supernatant was then added to the media incubated overnight. The media was changed to fresh media the next day and two days later, cells transduced with Lv105 vector were selected with puromycin (1 μ g/ml) for 3 days, and those with pLX304 vector were selected with blasticidin (5 μ g/ml) for 10 days. Cells were then collected for FACS analysis.

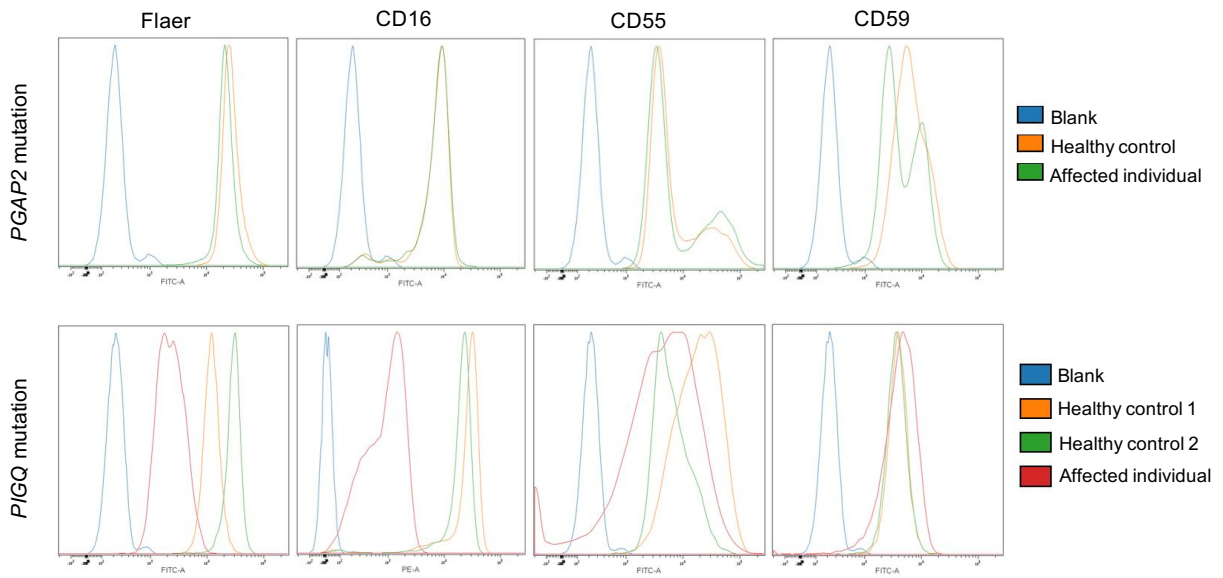
3. RESULTS

Analysis of cell surface expression of GPI-APs

A compound heterozygous mutation in the *PGAP2* gene was recently identified in an individual presenting with neurological anomalies and phenotypes comparable to previously reported IGDs. This gene encodes for the post-GPI attachment to proteins 2 (PGAP2) protein which participates in the attachment of a saturated fatty acid to the GPI anchor in the Golgi apparatus [2]. To determine if the affected patient had reduced levels of GPI-APs at the cell surface, blood samples from the patient and from a healthy control were collected for analysis. The blood samples were stained with fluorescent antibodies against GPI-APs (CD16, CD55 and CD59) as well as against the GPI anchor itself with fluorescein-labeled proaerolysin (FLAER). Fluorescence-activated cell sorting (FACS) analysis was then performed (Annexe Figure 1A) on the samples. Analysis in live granulocytes showed that compared to a healthy control, patient cells had an overall 37% decrease in FLAER and a 25% decrease in CD59, with no significant difference in CD55. Compound heterozygous mutations in the *PIGQ* gene were also identified using whole exome sequencing, and the same flow cytometry method on whole blood samples

was performed (Annexe Figure 1B). The *PIGQ* gene encodes a subunit of the first enzymatic step of GPI anchor formation [2]. Results show that, compared to the average expression of both controls, FLAER and CD16 decreased by at least 90% and CD55 decreased by 69%. No change was observed for CD59.

These results suggest that the identified compound heterozygous mutations in the *PGAP2* and *PIGQ* genes can result in a reduction of GPI-APs at the cell surface.

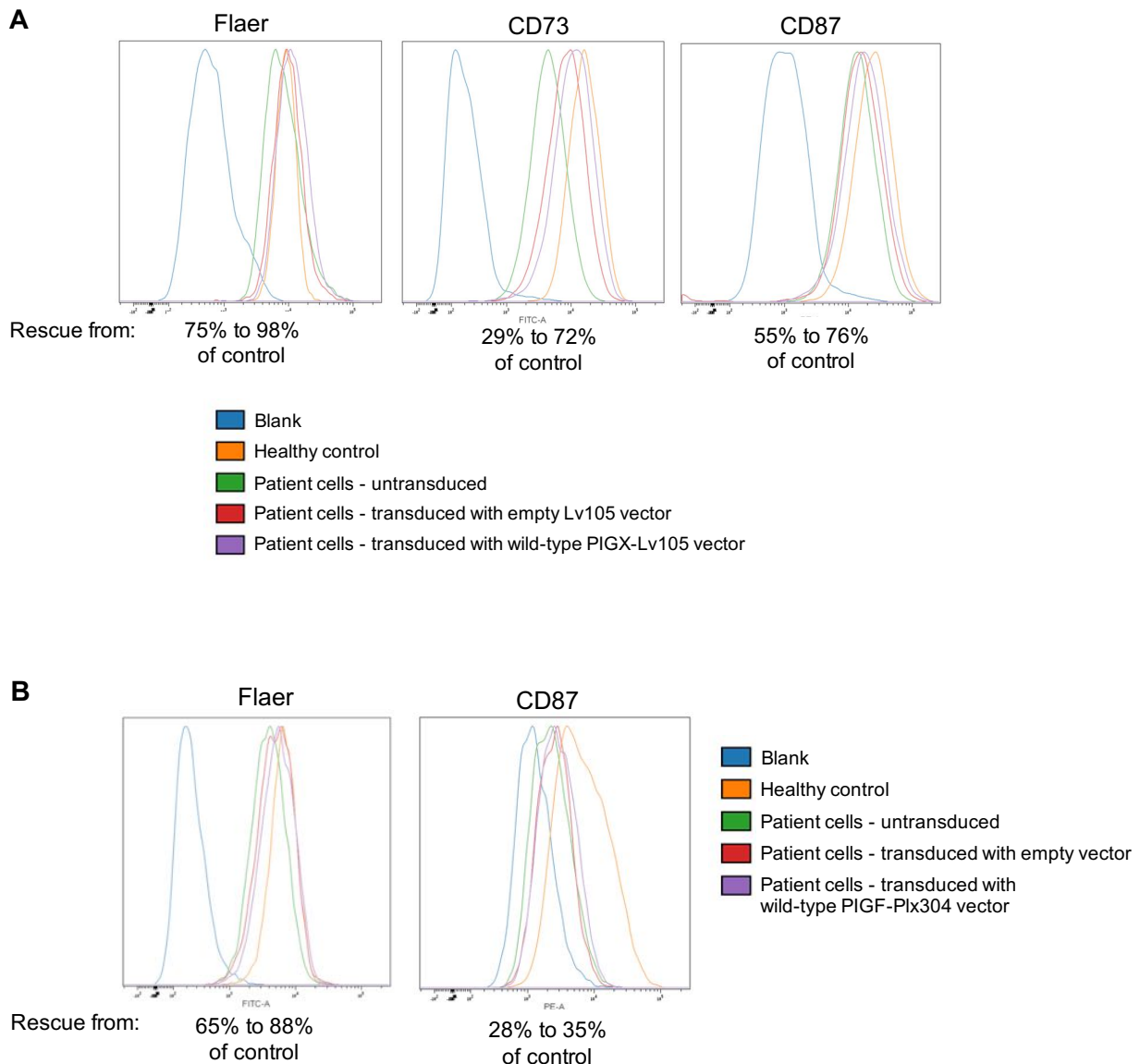


Annexe Figure 1: Cell surface expression of GPI-APs on granulocytes. Red blood cells from fresh blood samples of patients with a mutation in either the (A) *PGAP2* gene or (B) the *PIGQ* gene, along with blood cells of healthy controls were stained with GPI-AP markers (FLAER, CD16, CD55 and CD59) before analyzing by BD FACScanto II system. Representative figures show the cell surface expression of GPI-APs on granulocytes, relative to blank samples (blue), done in triplicates.

Lentiviral rescue assays

The abundance of GPI-AP on the cell surface of skin fibroblasts can also be assessed using various GPI-AP markers for fibroblasts such as FLAER, CD73, and CD87 antibodies. FACS analysis was done by Dr. Nguyen on patient fibroblasts harboring a mutation in the *PIGX* and *PIGF* genes, and both these patients showed decreased FLAER and CD73 and/or CD87 levels, indicating GPI-AP deficiency (results not shown). Because these individuals demonstrate a decreased expression, rescue assays were performed to examine how the mutation affects cell surface GPI-AP expression in comparison with non-rescued patient cells and cells from healthy controls.

Lentivirus was first produced in HEK293T cells, then transduced in patient fibroblasts. For each *PIGX* and *PIGF* patient, the cells were either untransduced, transduced with an empty lentiviral vector, or transduced with the vector encoding the wild-type gene (*PIGX*-Lv105 and *PIGF*-pLX304, respectively). The patient cells, along with fibroblasts from healthy individuals were then stained with FLAER, CD87, and/or CD73, and GPI-AP expression was analyzed by FACS. In the individual with a *PIGX* mutation, FLAER was completely rescued, and CD73 and CD87 expression increased significantly (Annexe Figure 2A). In the patient with a *PIGF* mutation, FLAER amounts increased, while CD87 only showed a very slight upregulation. These findings suggest that the mutations found in these patients which causes a reduction in cell-surface GPI-APs most likely cause their clinical phenotypes, and that the levels can be restored by infecting the cells with a lentivirus expressing the appropriate wild-type gene.



Annexe Figure 2: Lentiviral Rescue Assays in fibroblasts from affected individuals. (A) Dermal fibroblasts derived from a patient with a mutation in the *PIGX* gene were transduced with either an empty Lv105 vector lentivirus (red) or a lentivirus expressing the wild-type *PIGX* (purple). The transduced cells, along with untransduced patient cells (green), and cells from a healthy individual (orange) were stained with Flaer, CD73 and CD87 for one hour at room temperature, then washed to remove non-specific bindings. Unstained cells are shown in blue. **(B)** The same experiment was done with the fibroblasts of a patient with a *PIGF* mutation, but in this case, a PLX304 vector was used, and only Flaer and CD87 showed a rescue. Cell surface expression of GPI-APs were analyzed by the BD FACScanto II system. Graphs represent experiments done in triplicate.

4. DISCUSSION AND CONCLUSION

By functional analysis using flow cytometry on patient blood samples, a reduction in the GPI-AP cell surface expression was revealed in individuals with mutations in the *PGAP2* and *PIGQ* genes. Further, rescue assays on patient fibroblasts with *PIGF* and *PIGX* mutations showed a restoration of GPI-AP levels when infected with a lentivirus expressing the wild-type gene. These findings suggest that the mutation causes the GPI deficiency, demonstrating the role of these GPI-AP biosynthesis genes in the manifestation of IGDs.

Some mutations in GPI biosynthesis genes were found to be treatable such as vitamin B6 for *PIGO* and *PIGV* proteins [6, 7], or butyrate for mutated *PIGM* proteins [8]. This highlights the importance of performing functional analysis to determine the effect of the identified mutations. Understanding the cellular basis of the conditions will allow clinicians and scientists to identify the root cause of the neuronal anomalies reported in patients which, in turn, can help to optimize ways to treat the disease, or to limit the symptoms at the least. Recently, FACS analysis was done on amniocytes to examine GPI-AP levels in a fetus affected with mutations in the *PIGS* gene [3] (see attached paper by Nguyen et al., 2018). The development of such functional assay can eventually be used as a diagnostic tool during pregnancy, which can result in an earlier therapeutic intervention.



The ongoing identification of patients with IGDs and the continuous sequencing of the genome can only increase the understanding of this group of neurological disorders. For example, when analyzing all published variants in GPI biosynthesis genes, it was found that most reported pathogenic variants were in the *PGAP3* gene (Baratang et al., manuscript under review). This gene may therefore be more prone to mutations and would require closer monitoring. The discovery of disease-causing genes can contribute to a more accurate disease detection as the large heterogeneity of IGDs often makes for a challenging clinical diagnosis. The clinical spectrum for certain genetic mutations can consequently expand as more patients are identified. An interesting area of future work would be to investigate genes involved in the transport of GPI-APs. Proteins that participate in this process are currently not well known, but mutations in transport genes would be expected to interfere with the normal pathway and result in pathologies.

Bibliography

1. Kinoshita, T., *Glycosylphosphatidylinositol (GPI) Anchors: Biochemistry and Cell Biology: Introduction to a Thematic Review Series*. J Lipid Res, 2016. **57**(1): p. 4-5.
2. Bellai-Dussault, K., et al., *Clinical variability in inherited glycosylphosphatidylinositol deficiency disorders*. Clin Genet, 2018.
3. Nguyen, T.T.M., et al., *Mutations in PIGS, Encoding a GPI Transamidase, Cause a Neurological Syndrome Ranging from Fetal Akinesia to Epileptic Encephalopathy*. Am J Hum Genet, 2018. **103**(4): p. 602-611.
4. Cole, D.E. and M.D. Thompson, *Neurogenetic Aspects of Hyperphosphatasia in Mabry Syndrome*. Subcell Biochem, 2015. **76**: p. 343-61.
5. Johnstone, D.L., et al., *Compound heterozygous mutations in the gene PIGP are associated with early infantile epileptic encephalopathy*. Hum Mol Genet, 2017. **26**(9): p. 1706-1715.
6. Thompson, M.D., et al., *Hyperphosphatasia with neurologic deficit: a pyridoxine-responsive seizure disorder?* Pediatr Neurol, 2006. **34**(4): p. 303-7.
7. Kuki, I., et al., *Vitamin B6-responsive epilepsy due to inherited GPI deficiency*. Neurology, 2013. **81**(16): p. 1467-9.
8. Almeida, A.M., et al., *Targeted therapy for inherited GPI deficiency*. N Engl J Med, 2007. **356**(16): p. 1641-7.

REVIEW

Clinical variability in inherited glycosylphosphatidylinositol deficiency disorders

Kara Bellai-Dussault¹ | Thi Tuyet Mai Nguyen²  | Nissan V. Baratang² | Daniel A. Jimenez-Cruz² | Philippe M. Campeau³ 

¹Medical Genetics Division, Children's Hospital of Eastern Ontario, Ottawa, ON, Canada

²CHU Sainte-Justine Research Center, University of Montreal, Montreal, QC, Canada

³Department of Pediatrics, University of Montreal, Montreal QC, Canada

Correspondence

Philippe M. Campeau, Department of Pediatrics, University of Montreal, Montreal, QC, Canada.

Email: p.campeau@umontreal.ca

It is estimated that 0.5% of all mammalian proteins have a glycosylphosphatidylinositol (GPI)-anchor. GPI-anchored proteins (GPI-APs) play key roles, particularly in embryogenesis, neurogenesis, immune response and signal transduction. Due to their involvement in many pathways and developmental events, defects in the genes involved in their synthesis and processing can result in a variety of genetic disorders for which affected individuals display a wide spectrum of features. We compiled the clinical characteristics of 202 individuals with mutations in the GPI biosynthesis and processing pathway through a review of the literature. This review has allowed us to compare the characteristics and the severity of the phenotypes associated with different genes as well as highlight features that are prominent for each. Certain combinations, such as seizures with aplastic/hypoplastic nails or abnormal alkaline phosphatase levels suggest an inherited GPI deficiency, and our review of all clinical findings may orient the management of inherited GPI deficiencies.

KEYWORDS

genetic disorders, glycosylphosphatidylinositol, GPI, GPI-anchored proteins, PIG

1 | INTRODUCTION

Glycosylphosphatidylinositol (GPI) is a glycolipid anchoring proteins to the cell membrane. Its biosynthesis, attachment to proteins and processing requires proteins encoded by over 30 genes.¹ Mutations in some of those genes can result in decreased cell surface presentation of GPI-anchored proteins (GPI-APs), and lead to inherited GPI deficiency disorders (IGDs). As more than 150 proteins are anchored to the cell surface by GPI proteins, the disruption of GPI biosynthesis can potentially cause a large variety of consequences. These proteins play a crucial role in embryogenesis, neurogenesis, and transmission of cell signals. Therefore, germline mutations in GPI biosynthesis genes result in a wide spectrum of symptoms.

IGDs are transmitted in an autosomal recessive manner, with the exception of *PIGA* mutations, which are X-linked recessive. Studies have showed that mutations in GPI biosynthesis and processing genes result in a wide spectrum of phenotypes including cognitive impairment, epilepsy and various congenital malformations. Our goal is to analyze the clinical spectrum of patients with mutations in the GPI biosynthesis pathway by doing an extensive review of the literature.

2 | MATERIALS AND METHODS

A review of the literature was made using the PubMed database and OMIM with the words GPI and glycosylphosphatidylinositol.

3 | RESULTS AND DISCUSSION

Data from 202 patients with mutations in genes involved in this pathway were collected, including patients affected with mutations in the *PIGC*, *PIGP*, *PIGH*, and *GPAA1* genes that were studied by our own research group. Note that out of the 202 patients reported, there was limited data for some patients; in six cases the pregnancy was terminated, there were two stillbirths, and six patients deceased at a young age.

The GPI biosynthesis pathway is a multi-step process. Briefly, GPI-APs are synthesized in the endoplasmic reticulum (ER), move to the Golgi, then are transported to the cell surface. IGD genes can be involved in the biosynthesis of GPI-APs in the ER (*PIGA*, *PIGQ*, *PIGY*, *PIGC*, *PIGP*, *PIGH*, *PIGL*, *PIGW*, *PIGM*, *PIGV*, *PIGN*, *PIGO*, *PIGG*, *PIGT*,

GPA1). PGAP genes then play a role in the sorting and remodeling of the GPI-anchor in later steps in the ER (PGAP1) and the Golgi (PGAP3 and PGAP2) (Figure 1). We are only focusing in these genes, but it is important to note that there are other genes involved in the generation of GPI-APs which have not yet associated with disease in humans.

The most common features observed across these GPI genes are developmental delay and intellectual deficiency, seizures, other

neurological anomalies and dysmorphic features (Table 1). Hypotonia was reported for the majority, as well as spasticity, rigidity, dystonia, ataxia, reflex anomalies, tremors and choreiform movements. These characteristics can range from mild to severe for each patient. The phenotype severity appears to correlate with the genotype and the residual functional activity of the protein it encodes. Depending on the mutation, the resulting protein may have partial or abolished

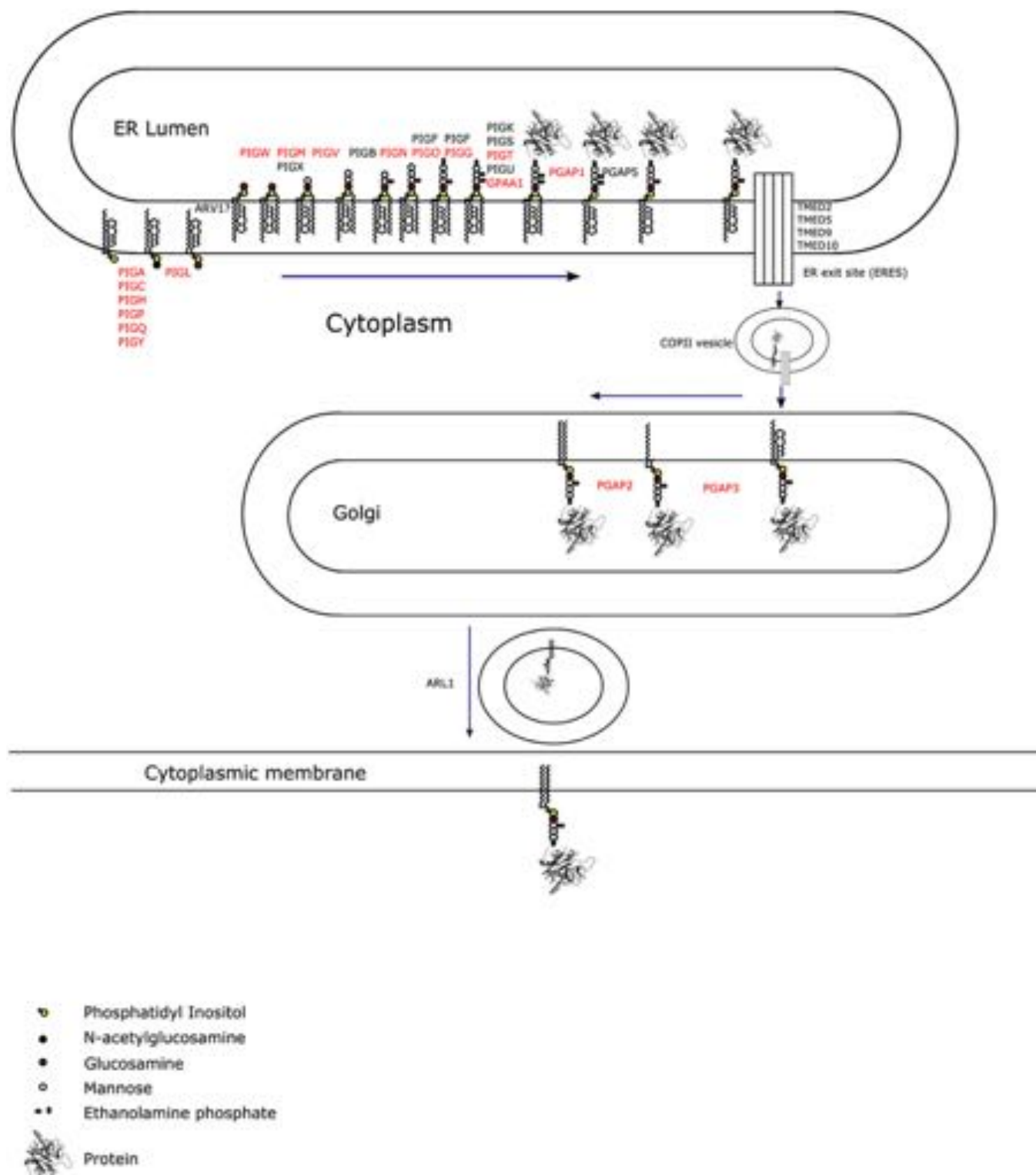


FIGURE 1 Summary of the metabolic processes and proteins involved in glycosylphosphatidylinositol (GPI) biosynthesis, protein attachment, and remodeling. Protein names in red letters are encoded by genes discussed here [Colour figure can be viewed at wileyonlinelibrary.com]

activity. Thus, as we discuss the patients' phenotypes, we will refer to the function of the proteins encoded by the affected gene and examine how its activity becomes altered by mutations.

3.1 | Phosphatidylinositol glycan class A

PIGA encodes the phosphatidylinositol glycan class A (*PIGA*) protein which is part of the GPI-N-acetylglucosaminyltransferase (GPI-GnT) complex, a collection of proteins that initiates GPI biosynthesis from phosphatidylinositol (PI) and N-acetylglucosamine (GlcNAc) to form an intermediate molecule called N-acetylglucosaminyl phosphatidylinositol (GlcNAc-PI) on the cytoplasmic side of the ER.²

Paroxysmal nocturnal hemoglobinuria (PNH) was the first disease to be associated with a GPI biosynthesis defect (*PIGA*).³ In this disorder, there is complement-mediated destruction of red blood cells due to a loss of GPI-APs CD55 and CD59 on red blood cells.² Since this disease is not inherited, but the result of an acquired somatic mutation, it will not be further discussed in this review. The most prominent clinical features of patients with inherited *PIGA* mutations are intellectual deficiency and developmental delay, as well as early onset epileptic encephalopathies in which all reported patients presented with seizures within their first year of life. The majority also showed brain anomalies such as white matter atrophy and delayed myelination, dysmorphic features and neurological anomalies (references in Supporting Information). Other phenotypes such as polyhydramnios, elevated alkaline phosphatase (ALP), cardiac anomalies, dental problems, visual impairment and deafness were also seen in these patients although less frequently, and some phenotypes were reported only once such as nephrocalcinosis, short fingers or hands, and skeletal anomalies. These widespread clinical features are consistent with the findings that the *PIGA* protein is expressed in a wide variety of tissues including brain, liver, heart and blood cells.⁴ In the 21 patients reported, about half of them died in which the cause of death was mainly due to liver failure and respiration pneumonia. Some patients also have evidence of mitochondrial dysfunction, although the mechanism for this phenomenon is not known.⁴ Studies in induced pluripotent stem cells showed decreased proliferation, abnormal synapse formation, membrane depolarization and an increased susceptibility to complement-mediated cytotoxicity.⁵

3.2 | PIGQ

PIGQ encodes another key component of the GPI-GnT complex. Very little information was available for the patient with a *PIGQ* mutation. The only description of this patient was the diagnosis of Ohtahara syndrome, with developmental delay and early onset epilepsy.⁶

3.3 | PIGY

PIGY is the smallest subunit of the GPI-GnT complex where it directly associates with the catalytic subunit *PIGA*.⁷ In the majority of the four patients with *PIGY* mutations, ophthalmologic, gastrointestinal and skeletal anomalies have been reported. The four patients reported were from two different families.⁸ The children from the first family (with a homozygous coding mutation) suffered from a more severe

disease where many organs were affected such as the bone and the GI tract resulting in early death, whereas the phenotype of the pair from the second family (with a homozygous promoter mutation) was limited to global developmental delay and microcephaly. In the first family, the children had elevated ALP, thus *PIGY* mutations are a cause of hyperphosphatasia with mental retardation syndrome (type 6, HPMRS6). The mutation in the first family caused a defect in the secondary structure of the protein which affected its association with the *PIGA* subunit, thus explaining the more severe phenotype than in the siblings with a decreased expression of a normal protein.

3.4 | PIGC

PIGC also encodes a subunit of the GPI-GnT complex and we recently reported three individuals with *PIGC* mutations from two unrelated families. These individuals have a seizure disorder responding to anti-epileptic drugs and severe global developmental delay or intellectual disability. ALP levels were normal.⁹

3.5 | PIGP

PIGP compound heterozygous mutations were found in two siblings of a non-consanguineous family. Both patients manifested seizures, dysmorphic features, gastroesophageal reflux disease (GERD), hypotonia and global developmental delay. These patients did not display elevated serum ALP levels, similar to many individuals with mutations in earlier steps of the GPI-AP synthesis pathway including *PIGC*.¹⁰

3.6 | PIGH

In addition to *PIGA*, C, P, Q and Y, the GPI-GnT complex is also composed of *PIGH*. Recently, a rare *PIGH* homozygous variant were reported in two siblings with epilepsy, microcephaly, and behavioral difficulties¹¹ while another *PIGH* homozygous mutation was found in an individual with moderate global developmental delay and autism but with only two episodes of febrile seizures occurred at the age of 17 months which did not recur.¹² Like *PIGC* and *PIGP* patients, all these patients with *PIGH* mutations have normal ALP.

3.7 | PIGL

The *PIGL* gene encodes a de-N-acetylase, an ER protein that is involved in the second step of GPI biosynthesis. It de-N-acetylates GlcNAc-PI which then allows GlcN-PI to flip (or be flipped) to the luminal side of the ER where it can undergo further modifications (Figure 1).

Of the 10 patients described with *PIGL* mutations, the main features include developmental delay, seizures, dysmorphic features and cranial shape anomalies. Deafness and ophthalmologic involvement were also described, in particular colobomas, which were not reported in patients with mutations in other GPI genes. Anomalies in the neuro, heart, as well as dental, hands and feet anomalies were also reported in the majority of these patients (references in Supporting Information). Mutations in *PIGL* have been identified in patients with CHIME syndrome which is a disease characterized by colobomas, heart defects, ichthyosiform dermatosis, mental retardation and ear

TABLE 1 Clinical features of collected patients with mutations in genes involved in GPI-AP synthesis pathway [Colour table can be viewed at wileyonlinelibrary.com]

Total	PIGA	PIGQ	PIGY	PIGC	PIGP	PIGH	PIGL	PIGW	PIGM	PIGV	PIGN	PIGO	PIGG	PIGT	GPAA1	PGAP1	PGAP3	PGAP2	Total
21 ^{a,b}	1	4	3	2	3	3	10	3	4 ^c	23 ^b	30 ^{a,d}	17	7	13	10	11	28	12	202
DD/ID	15/15	1/1	4/4	3/3	2/2	3/3	10/10	3/3	2/4	22/22	21/21	17/17	7/7	13/13	10/10	11/11	28/28	12/12	184/186 (99%)
Seizures	20/20	1/1	2/4	3/3	2/2	3/3	10/10	3/3	4/4	20/22	20/21	11/17	6/7	13/13	7/10	3/11	19/28	6/12	153/191 (80%)
Dysmorphic features	13/21	0/1	4/4	0/3	2/2	0/3	10/10	2/3	0/4	23/23	26/30	14/17	4/7	10/13	8/10	5/11	28/28	2/12	151/202 (75%)
Cranial shape anomalies	6/21	0/1	2/4	0/3	1/2	0/3	5/10	0/3	0/4	4/23	2/30	1/17	0/7	4/13	0/10	5/11	8/28	4/12	42/202 (21%)
Deafness	3/20	0/1	0/4	0/3	0/2	0/3	8/10	0/3	0/4	2/22	0/24	5/17	0/7	2/13	0/10	0/11	5/28	3/12	28/194 (14%)
Ophthalmological anomalies	4/21	0/1	3/4	0/3	2/2	0/3	9/10	0/3	0/4	3/23	17/30	3/17	2/7	11/13	9/10	4/11	8/28	3/12	78/202 (39%)
Cardiac anomalies	7/21	0/1	0/4	0/3	0/2	0/3	6/10	1/3	0/4	6/23	11/30	2/17	1/7	6/13	1/10	0/11	4/28	1/12	46/202 (23%)
GU malformation	8/21	0/1	1/4	0/3	0/2	0/3	5/10	0/3	0/4	9/23	9/30	3/17	0/7	6/13	0/10	0/11	3/28	0/12	43/202 (21%)
GI anomalies inc GERD	2/21	0/1	2/4	0/3	2/2	0/3	0/10	0/3	0/4	14/23	13/30	10/17	0/7	3/13	4/10	1/11	3/28	1/12	55/202 (27%)
Nephrocalcinosis	1/21	0/1	0/4	0/3	0/2	0/3	0/10	0/3	0/4	0/23	0/30	0/17	0/7	4/13	0/10	0/11	0/28	0/12	5/202 (2%)
Teeth anomalies	5/20	0/1	0/4	0/3	0/2	0/3	6/10	0/3	0/4	2/22	0/24	1/17	0/7	4/13	0/10	0/11	3/28	0/12	21/194 (11%)
Nail anomalies	2/21	0/1	0/4	0/3	0/2	0/3	2/10	0/3	0/4	17/23	8/30	7/17	0/7	0/13	0/10	0/11	5/28	1/12	42/202 (21%)
Short fingers or hands	1/21	0/1	2/4	0/3	0/2	0/3	6/10	0/3	0/4	19/23	12/30	12/17	1/7	1/13	2/10	1/11	0/28	0/12	57/202 (28%)
Hand/feet anomalies	4/21	0/1	0/4	0/3	0/2	2/3	7/10	0/3	0/4	13/23	12/30	0/17	0/7	0/13	2/10	0/11	1/28	0/12	41/202 (20%)
Skeletal findings	1/21	0/1	2/4	0/3	0/2	0/3	3/10	0/3	0/4	5/23	4/30	1/17	0/7	8/13	1/10	0/11	1/28	2/12	28/202 (14%)
Brain MRI/ CT anomalies	14/21	0/1	1/4	1/3	1/2	2/3	3/10	0/3	0/4	6/23	12/30	13/17	6/7	12/13	7/10	5/11	16/28	3/12	102/202 (50%)
Prenatal finding	7/21	0/1	1/4	0/3	0/2	0/3	2/10	0/3	0/4	4/23	11/30	0/17	0/7	2/13	0/10	0/11	0/28	0/12	27/202 (13%)
Elevated serum alkaline phosphatase	7/20	0/1	2/4	0/3	0/2	0/3	3/10	1/3	0/4	21/22	2/30	13/17	0/7	Low 7/13	0/10	0/11	27/28	5/12	High: 81/200 (41%) Low: 7/200 (4%)

Abbreviations: DD, developmental delay; ID, intellectual disability; GU, genitourinary; GI, gastrointestinal; inc, including; GERD, gastroesophageal reflux disease; MRI, magnetic resonance imaging; CT, computed tomography. Cells in bold represent features present in the majority of individuals, and in italics represent features present in the minority.

^a Three pts early death.

^b One stillbirth.

^c Very little information.

^d Six patients reported: interrupted pregnancy.

anomalies.¹³ This is consistent with the prominent characteristics in all 10 patients reported in the literature. *PIGL* mutations, however, do not only cause CHIME syndrome. A paper by Fujiwara et al presented a patient who did not have colobomas or heart defects. Instead, the patient had only strabismus as an ophthalmological anomaly.¹⁴ The clinical phenotype for *PIGL* deficiency is therefore expanding, but with the current clinical data that is available, ear anomalies and colobomas still appear to be hallmarks of this disease.

3.8 | PIGW

One of the components of the GPI structure is a glycan core that contains three mannose residues. These residues can be modified with various side chains such as ethanolamine phosphate (EtNP). *PIGW* encodes an inositol acyltransferase which introduces an acyl group to the inositol ring of the PI. It was also found to be required for the successful attachment of an EtNP to the third mannose of the GPI.¹⁵

Three patients with a *PIGW* mutation were described in the literature. Apart from the common phenotypes seen in other IGDs, namely intellectual disability, neurological anomalies and dysmorphic features, patients reported with a *PIGW* mutation did not present many additional clinical features. In fact, only one patient presented with an elevated serum ALP (thus *PIGW* mutations cause HPMRS5), another had cardiac anomalies, and the third patient did not have any other symptoms.^{16,17} When cells have a mutated *PIGW* gene, there is an accumulation of GPI intermediates with an abnormal structure. Chiyonobu et al found that these GPI intermediates activate GPI transamidase and cause hyperphosphatasia.¹⁷ However, in 2016, Hogrebe et al reported cases in which two patients with *PIGW* mutations had normal serum ALP levels.¹⁶ With a sample size of three, it is difficult to associate clinical features that are distinct to these patients. A larger group is necessary to highlight phenotypes specific to the *PIGW* gene.

3.9 | PIGM

The *PIGM* gene encodes a mannosyltransferase enzyme which transfers the first mannose to the GPI on the luminal side of the ER (Figure 1). Very little data was available for the four patients with *PIGM* mutations. A common characteristic that is evident is that all patients suffered from seizures, particularly absence seizures.^{18,19} Similar to mutations in *PIGA*, *PIGM* mutations were found to be hypomorphic and lead to a partial loss of GPI anchor biosynthesis.¹⁹ Further, it seems *PIGM*-deficient patients presented less frequently with neurologic impairment and facial dysmorphism compared to other IGD individuals.

3.10 | PIGV

The *PIGV* gene encodes the GPI mannosyltransferase 2 enzyme which adds the second mannose residue to the GPI anchor (Figure 1). The third mannose is added by the protein encoded by the *PIGB* gene, not discussed in this review. It has been found in earlier studies that mutations in the *PIGV* gene are the major cause of Hyperphosphatasia with mental retardation syndrome 1 (HPMRS1), also known as Mabry

syndrome.²⁰ Indeed, all the patients reported with severe intellectual disability and the majority (21/22) patients had an elevated ALP level (references in Supporting Information).

ALP is a GPI-AP found throughout the body. Studies have found that an elevated serum ALP level is a useful marker to diagnose defects in GPI genes involved in the later steps of the GPI-biosynthesis pathway.²¹ The process of how this occurs involves the GPI transamidase complex, an enzyme that mediates the attachment of the GPI anchor to proteins carrying a C-terminal GPI-attachment signal. In normal conditions, the GPI transamidase cleaves the GPI-attachment signal peptide on the protein and simultaneously adds the GPI moiety. In the case of *PIGV* mutations in which there is a lack of mature GPI synthesis, the GPI transamidase recognizes the incomplete GPI-bearing mannose and cleaves the GPI-attachment signal. However, the signal peptide cannot be replaced with a GPI anchor, resulting in the release of non-GPI anchored soluble proteins into the serum.²¹ This generation and secretion of soluble ALP from the ER leads to hyperphosphatasia. In contrast, in IGD genes involved in the earlier part of the pathway such as the *PIGA* gene, precursors of GPI-APs are mostly degraded in *PIGA*-defective cells and are therefore not released from the cells.²² As such, only a minority of the patients with mutations in the earlier IGD genes (or no patient depending on the gene) show an elevated ALP level.

Additional clinical features manifested by these patients indicate that mutations in this gene are not limited to these two clinical features. The majority of patients were also reported to have seizures, intellectual disability, dysmorphic features, anomalies of the gastrointestinal and urinary tracts with constipation and an anteriorly placed anus. They also suffer from hypoplastic or absent fingernails which seems to be a hallmark of patients with *PIGV* mutations as nail anomalies appear more frequently in this group than in patients with mutations in the other IGD genes.

3.11 | PIGN

The *PIGN* gene encodes one of the three EtNP transferases which adds an EtNP to the mannose residues on GPI. The other two enzymes with this function are *PIGG* and *PIGO*.²³ *PIGN* adds the EtNP to the first mannose residue.²⁴ The clinical phenotypes observed in 30 patients with *PIGN* mutations were diverse and affect multiple organs (references in Supporting Information). The most commonly reported clinical findings were ophthalmologic anomalies, along with hypotonia and seizures. Patients were also reported with diaphragmatic hernia suggesting Fryns syndrome. On the contrary, none of the patients were described to have any deafness, nephrocalcinosis or teeth anomalies, and only 2 of 30 patients showed an elevated level of ALP.

The phenotype manifests with different severity depending on the mutation, with the more severe ones often leading to early death. In fact, many deaths have been reported in patients with *PIGN* mutations compared to those with other GPI mutations: 10 patients died before the age of four, and 1 patient died at 14 years old. For six patients, the pregnancy was terminated so some clinical phenotypes could not be assessed in these individuals.

3.12 | PIGO

As mentioned, PIGO is part of the EtNP transferase enzymes. It is involved in attaching an EtNP on the third mannose of GPI in the later steps of the GPI biosynthesis pathway. This EtNP links the GPI anchor to the protein.²³

Seventeen patients with PIGO mutations were described in the literature (references in Supporting Information). In addition to intellectual deficiency and other neurological anomalies which all patients displayed, the majority presented with seizures, dysmorphic facial features, brachytelephalangy, hypoplastic nails, and anomalies in their brain structure such as cerebellar atrophy and thin corpus callosum. Gastrointestinal anomalies were seen, with anal atresia being the predominant GI malformation. Additionally, hyperphosphatasia was reported in the majority of these patients (13/17). This elevated ALP is caused by a similar mechanism as for patients with a PIGV mutation.

PIGO is one of the GPI genes associated with hyperphosphatasia mental retardation syndrome (HPMRS2). This disease is characterized by increased ALP, intellectual deficiency, seizures, hypotonia, and facial dysmorphic features.²⁵ These symptoms were present in the patients reported with PIGO mutations, but they are also present in patients with mutations in PIGV, PGAP2 and PGAP3 genes.^{20,26,27}

3.13 | PIGG

PIGG gene encodes the enzyme that attaches EtNP to the second mannose on the GPI. Later in the pathway, this EtNP is removed by the PGAP5 protein. It has therefore been reported that PIGG may not be essential for GPI-AP biosynthesis. This was confirmed with studies that showed that in PIGG-deficient cells, GPI-APs are present at normal levels and have normal structures,²³ in contrast with PIGO and PIGN-defective cells where the surface level of GPI-APs is decreased. Consistent with this, serum ALP levels in PIGG-deficient patients did not show an altered level of ALP.

The seven patients reported to have mutations in the PIGG gene all showed intellectual deficiency. The majority manifested seizures, other neurological anomalies such as severe hypotonia, and six of seven patients presented with brain anomalies including cerebral atrophy and hypoplasia of the cerebellum.^{23,28} Additionally, two patients had ophthalmological anomalies, and one of seven had cardiac anomalies and short fingers.

3.14 | PIGT

PIGT encodes for the protein phosphatidylinositol glycan biosynthesis class T, a crucial component of the GPI transamidase complex. A study found that PNH can also occur in patients with mutations in this gene. However, in contrast to PNH caused by the PIGA gene which requires only one somatic mutation event, a germline as well as a somatic mutation in PIGT are both needed to acquire the disease.²⁹ The 13 patients with PIGT mutations reported in this review does not include those with PNH. The majority of these reported individuals are severely affected; ophthalmologic, brain anomalies, and skeletal findings were noted for the majority of these patients. A few also had anomalies in other organs, including nephrocalcinosis which appeared more frequently in this cohort compared to those with mutations in other IGD genes.³⁰⁻³⁵

Interestingly, patients with PIGT mutations had a decreased level of serum ALP. This is striking as one of the diagnostic markers for inherited GPI-anchor deficiencies is usually an elevated ALP level.

Thus, low serum ALP can be caused not only by mutations in the ALP liver/bone/kidney (ALPL) gene which encodes ALP, but also by deficient linkage of GPI anchor to ALP. When PIGT is mutated, ALP precursors are not targeted by the GPI transamidase. They are consequently subjected to ER-associated degradation instead of being secreted.³⁶ This leads to hypophosphatasia which could be causally related to bone defects and epilepsy, consistent with the clinical features seen in this cohort. Hypophosphatasia, skeletal defects and nephrocalcinosis could therefore represent clinical characteristics of patients with PIGT mutations.

3.15 | GPAA1

GPAA1 encodes a protein belonging to the transamidase complex which is involved in the attachment of the GPI anchor to the C-terminus of precursor proteins in the ER (Figure 1). Among the components of this complex, only PIGT was earlier found to be mutated in many patients as mentioned above. We reported 10 individuals from five families with bi-allelic mutations in GPAA1. Most patients with GPAA1 mutations presented with early-onset seizures, hypotonia and global developmental delay which overlapped with those identified in individuals with PIGT mutations. In addition, these patients also suffered from osteopenia and cerebellar atrophy.³⁷

3.16 | PGAP1

PGAP1 stands for "post-GPI attachment to proteins 1" and is located in the ER. After the GPI anchors have been successfully attached to the proteins by the GPI transamidase enzyme, their acyl chain is cleaved from the inositol ring.³⁸ PGAP1 therefore catalyzes the first remodeling step of GPI anchors which is important for the efficient transport of GPI-APs to the Golgi for further remodeling. Mutations in PGAP1 were shown to lead to normal surface expression level of GPI-APs, but with a defect in their GPI-anchor structure.³⁶

A total of 11 patients with PGAP1 mutations are described in the literature. Most of them have intellectual disability and other neurological anomalies, and a minority has cranial shape and structural brain anomalies. Only three patients had epilepsy, which was surprising considering almost all patients with mutations in other genes of the GPI biosynthesis pathway suffered from seizures, with the exception of patients with PGAP2 mutations where less than half of the patients were affected. Furthermore, only a minority of patients had facial dysmorphism which was also unexpected as dysmorphic features were known as a common phenotype in patients with GPI disorders.^{36,39-44}

The abnormal structure of the GPI-APs' membrane anchors does not seem to translate into life-threatening phenotypes or obvious malformations in patients with mutations in the PGAP1 gene. However, affected patients still suffer severe intellectual deficiency with other neurological anomalies. Further, the patients showed normal serum levels of ALP suggesting that an elevated ALP level is not a characteristic of patients with PGAP1 mutations. This is supported by PGAP1 mouse models which showed normal ALP levels despite PGAP1 anomalies.³⁶

3.17 | PGAP3

PGAP3 is expressed in the Golgi and encodes an enzyme that plays a role in fatty acid remodeling of the GPI-anchor. This modification is important for the proper association between GPI-APs and lipid rafts.⁴⁵ In the Golgi, PGAP3 proteins first remove unsaturated fatty acids from the lipid moiety of the GPI-AP. Saturated fatty acids are then attached by PGAP2 proteins.⁴⁶

Of the 28 patients with *PGAP3* mutations described in the literature, few major anomalies were reported except for abnormal brain structures notably an atrophy of the temporal lobes and the corpus callosum, dysmorphic facial features and an elevated serum ALP seen in almost all patients (references in Supporting Information). This can be a characteristic feature for patients with *PGAP3* mutations, and thus mutations in this gene are responsible for HPMRS4.

In patients with a *PGAP3* mutation, surface levels of GPI-APs are normal. However, because their lipid structure is not remodeled, they cannot localize on lipid rafts and therefore cannot be properly sorted to the plasma membrane.⁴⁶ Additionally, the GPI-APs that manage to reach the plasma membrane are more prone to cleavage.⁴⁵

3.18 | PGAP2

PGAP2 is involved in the maturation of the GPI anchor on GPI-APs. It is located in the Golgi and is involved in the re-acylation of the GPI-anchor, the final step in the fatty-acid remodeling. This fatty acid modification is necessary for the stable association between GPI-APs and the lipid rafts that transport them to the cell surface.⁴⁷

The clinical description of patients with *PGAP2* mutations is similar to patients with *PGAP1* mutations in that only the minority presented with facial dysmorphism. For the 12 patients reported in this cohort, intellectual disability, severe motor developmental delay and seizures were the most predominant features. Only a minority of patients manifested additional features.^{26,48-50}

Deficiency of *PGAP2* affects the re-acylation step in GPI-anchor remodeling, leading to the formation of GPI-APs that lack the lipid moiety. These proteins are more prone to cleavage by phospholipase D where, after their transport to the plasma membrane, they get cleaved and released from the cell surface.²⁶ A consequence of this is hyperphosphatasia as GPI-APs are released from the plasma membrane. This is supported by the literature where five of the reported patients have shown an elevated ALP level (thus, mutations in this gene are responsible for HPMRS3). However, it is not a key diagnosing feature as it does not represent the majority of the cohort. Intellectual deficiency seems to be the main feature of *PGAP2*-deficient patients because it was present in all individuals and mutations in this gene expand the clinical spectrum of IGDs to isolated intellectual disability.⁴⁸

3.19 | Overall analysis

The great majority of patients reported presented with developmental delay or intellectual disability. Most frequently, the patients also presented with epilepsy, although this was observed to a lesser extent in patients with mutations in genes *PGAP1*. Several patients also presented with additional neurologic findings, this was predominantly the

case for patients with mutations in genes *PIGA*, *PIGL*, *PIGG*, *PIGN*, *PIGO*, *PIGT*, *PIGV*, *PIGW*, *PIGY*, *PGAP1*, *PGAP3*, *PIGP* and *GPAA1*. Hypotonia was reported for the majority. Spasticity, rigidity, dystonia, ataxia, reflex anomalies, tremors and choreiform movements were also commonly reported.

Craniofacial dysmorphism varying from mildly dysmorphic facies to coarse features were noted, in particular for patients with mutations in *PIGA*, *PIGG*, *PIGL*, *PIGN*, *PIGO*, *PIGP*, *PIGT*, *PIGV*, *PIGW*, *PIGY*, *GPAA1* and *PGAP3* genes.

Hearing impairment was reported for 8 of 10 patients with *PIGL* mutations and in a minority of patients with *PIGA*, *PIGO*, *PIGT*, *PIGV*, *PGAP2* and *PGAP3* mutations, while it was not reported for other genes.

Ophthalmological anomalies were seen in a majority of individuals with *PIGL*, *PIGP*, *PIGT*, *PIGN*, *PIGY* and *GPAA1* mutations. Colobomas were described in 8 out of 10 patients with *PIGL* mutations but not in patients with mutations in other genes. For the other patients, cortical visual impairment, strabismus and nystagmus were the most common findings.

As for cardiac anomalies, they were observed in the majority of patients with *PIGL* mutations (6/10). Patients with mutations in genes *PIGA*, *PIGW*, *PIGV*, *PIGN*, *PIGO*, *PIGG*, *PIGT*, *GPAA1*, *PGAP3*, *PGAP2* also suffer from cardiac anomalies, although less frequently. Patients with *PIGL* mutations presented with ventricular septum defects, transposition of great vessels and subaortic stenosis. Patients with mutations in the other genes, on the other hand, had a variety of cardiac anomalies such as patent ductus arteriosus, increased atrial load, restrictive cardiomyopathy, borderline long QT (the time between the start of the Q wave and the end of the T wave in the heart electrical cycle) and atrial septal defect. Cardiac anomalies therefore appear non-specific to the mutated gene, but are more frequent with *PIGL* mutations.

Urologic or renal malformations were present in half of the reported patients with *PIGL* mutations, and in a small proportion of patients with *PIGT*, *PIGA*, *PIGN*, *PIGO*, *PIGV*, *PIGY*, and *PGAP3* mutations. Malformations include ureteral dilation, hydronephrosis and dysplastic kidney.

Gastrointestinal anomalies were present in the majority of patients with *PIGY*, *PIGP*, *PIGV*, and *PIGO* mutations (2/4, 2/2, 14/23, and 10/17, respectively), and in a minority of patients with *PIGA*, *PIGN*, *PIGT*, *GPAA1*, *PGAP1*, *PGAP3*, and *PGAP2* mutations. Recurrent gastrointestinal features included GERD, Hirschsprung disease, anal atresia, anal stenosis and anteriorly placed anus.

Nephrocalcinosis was present in a small group of patients with *PIGA* (1/21), and *PIGT* (4/13).

As for teeth anomalies, they were present in a majority of individuals with *PIGL* mutations but a minority of those with *PIGT*, *PIGV*, *PIGA*, *PIGO* and *PGAP3* mutations. The common teeth anomalies were widely spaced teeth, microdontia, shape anomalies and delayed eruption/absence of teeth. Other patients showed gingival hypertrophy.

Many of the patients were reported with short fingers or hands, but some were also described as having other hand and feet anomalies. Anomalies of the digits were reported for at least half of the patients with *PIGV*, *PIGO*, *PIGL*, *PIGH* and *PIGY* mutations, and a minority of patients with *PIGA*, *PIGG*, *PIGN*, and *GPAA1* mutations.

The hand and feet anomalies described included deepened plantar creases, camptodactyly, clinodactyly, oligodactyly, brachytelephalangy and others. Nail anomalies (hypoplasia) was a finding for 17 of 23 patients with *PIGV* mutations. Nail anomalies were present in a minority of individuals with *PIGA*, *PIGL*, *PIGN*, *PIGO*, *PGAP3* and *PGAP2* mutations. The most common findings were hypoplastic or absent nails. Short fingers and nails in an individual with intellectual disability should therefore increase the index of suspicion of IGDs in addition to Coffin-Siris syndrome (MIM: PS135900),^{51,52} DOORS syndrome (MIM: 220500),⁵³ Zimmermann-Laband syndrome (MIM: PS135500),⁵⁴ and Kaufman oculocerebrofacial syndrome (MIM: 244450).^{55,56}

Skeletal findings were identified in all 8 of 13 patients with *PIGT* mutations, 2 of the 4 patients with *PIGY* mutations and some patients with mutations in genes *PIGA*, *PIGL*, *PIGV*, *PIGN*, *PIGO*, *PGAP2*, *PGAP3*, and *GPAA1*. Examples of skeletal findings include scoliosis, osteoporosis, reduced mineralization, delayed bone age, and hip dysplasia.

The majority of patients with *PIGA*, *PIGP*, *PIGH*, *PIGO*, *PIGG*, *PIGT*, *GPAA1* and *PGAP3*, and some patients with *PIGY*, *PIGC*, *PIGL*, *PIGV*, *PIGN*, *PGAP1* and *PGAP2* presented findings on magnetic resonance imaging (MRI) or head computed tomography (CT). The most common anomalies reported by brain imaging are thin corpus callosum, cerebellar and cerebral atrophy and white matter loss. However, neuroimaging was not reported for a great number of patients; and can therefore not be fully compared here. Also, for some patients with neuroimaging findings, their first imaging was normal and in subsequent imaging, anomalies were noted, such as cerebellar atrophy. Thus, it is important to note that the central nervous system anomalies can progress, both on imaging and clinically.

Prenatal findings were noted for a minority of patients, but were mostly unspecific: polyhydramnios, increased nuchal fold and pyelectasis. Some patients also presented with various neonatal complications such as a low APGAR score, neonatal hypotonia with feeding difficulties, breathing difficulties, hyperbilirubinemia, and hypoglycemia.

Unfortunately, serum ALP was not measured for several patients. However, it was reported to be increased in a number of patients with mutations in *PIGO*, *PIGV*, *PIGY* and *PGAP3* genes, and in some patients with mutations in *PIGA*, *PIGL*, *PIGN*, *PIGW* and *PGAP2* genes, while patients with *PIGT* mutations had low levels of serum ALP. As described above, previous data suggested that the elevated serum ALP observed in some GPI-biosynthesis defects could be explained by cleavage of the signal peptide and secretion of soluble ALP because of abnormal GPI structure,²¹ but this was dependent on the mannose composition of the abnormal GPI.

3.20 | Treatment

Limited therapies are available for GPI-AP deficiency. Treatment with the histone deacetylase inhibitor butyrate resolved intractable epilepsy in an individual who presented with mutations in the *PIGM* promoter. Lymphoblast studies showed the drug also rescued levels of the GPI-AP as it increased the expression of *PIGM* gene affected by the promoter mutation.¹⁸

Since ALP is essential to allow pyridoxal-phosphate to pass through the blood-brain barrier and pyridoxine passes through the

blood-brain barrier and is converted to pyridoxal-phosphate, important for GABA synthesis, pyridoxine (B6) supplementation can help control seizures in individuals with GPI-biosynthesis defects. Indeed, in a patient with Mabry syndrome (*PIGV* gene), Thompson et al. noticed a resolution of seizures with a dose increase in pyridoxine.⁵⁷ In a patient with *PIGO* mutations, Kuki et al also noted a complete resolution of seizures.⁵⁸

4 | SUMMARY

Despite minor limitations (lack of detailed clinical descriptions for some individuals), this review of literature has enabled us to better characterize the phenotypes associated with mutations in genes involved in the biosynthesis of GPI. In addition, a comparison could be made between the different mutated genes, which helped define the clinical findings associated with the different genes that were studied. A thorough workup following an initial diagnosis should be done to look for the clinical features mentioned in this review. Moreover, exploring the extent of the anomalies for this group of disorder might influence management, by highlighting the systems more affected by mutations in one gene rather than another. This compilation of data might help reaching a diagnosis based either on clinical signs alone, or clinical and genetic testing alone without performing GPI studies. For example, seizures combined with either aplastic/hypoplastic nails or abnormal ALP levels are highly suggestive of GPI biosynthesis disorders, so if bi-allelic mutations in one of the above genes are also found, flow cytometry studies would not be necessary to confirm the diagnosis.

Conflict of interest

Nothing to declare.

ORCID

Thi Tuyet Mai Nguyen  <http://orcid.org/0000-0002-9572-118X>

Philippe M. Campeau  <http://orcid.org/0000-0001-9713-7107>

REFERENCES

- Kinoshita T. Glycosylphosphatidylinositol (GPI) anchors: biochemistry and cell biology: introduction to a thematic review series. *J Lipid Res.* 2016;57(1):4-5.
- Brodsky RA. Advances in the diagnosis and therapy of paroxysmal nocturnal hemoglobinuria. *Blood Rev.* 2008;22(2):65-74.
- Takeda J, Miyata T, Kawagoe K, et al. Deficiency of the GPI anchor caused by a somatic mutation of the *PIG-A* gene in paroxysmal nocturnal hemoglobinuria. *Cell.* 1993;73(4):703-711.
- Tarailo-Graovac M, Sinclair G, Stockler-Ipsiroglu S, et al. The genotypic and phenotypic spectrum of *PIGA* deficiency. *Orphanet J Rare Dis.* 2015;10:23.
- Yuan X, Li Z, Baines AC, et al. A hypomorphic *PIGA* gene mutation causes severe defects in neuron development and susceptibility to complement-mediated toxicity in a human iPSC model. *PLoS One.* 2017;12(4):e0174074.
- Martin HC, Kim GE, Pagnamenta AT, et al. Clinical whole-genome sequencing in severe early-onset epilepsy reveals new genes and improves molecular diagnosis. *Hum Mol Genet.* 2014;23(12):3200-3211.
- Murakami Y, Siripanyaphinyo U, Hong Y, Tashima Y, Maeda Y, Kinoshita T. The initial enzyme for glycosylphosphatidylinositol

- biosynthesis requires PIG-Y, a seventh component. *Mol Biol Cell*. 2005;16(11):5236-5246.
8. Ilkovski B, Pagnamenta AT, O'Grady GL, et al. Mutations in PIGY: expanding the phenotype of inherited glycosylphosphatidylinositol deficiencies. *Hum Mol Genet*. 2015;24(21):6146-6159.
 9. Edvardson S, Murakami Y, Nguyen TT, et al. Mutations in the phosphatidylinositol glycan C (PIGC) gene are associated with epilepsy and intellectual disability. *J Med Genet*. 2017;54(3):196-201.
 10. Johnstone DL, Nguyen TT, Murakami Y, et al. Compound heterozygous mutations in the gene PIGP are associated with early infantile epileptic encephalopathy. *Hum Mol Genet*. 2017;26(9):1706-1715.
 11. Pagnamenta AT, Murakami Y, Anzilotti C, et al. A homozygous variant disrupting the PIGH start-codon is associated with developmental delay, epilepsy, and microcephaly. *Hum Mutat*. 2018;39:822-826.
 12. Nguyen TTM, Mahida SD, Smith-Hicks C, Campeau PM. A PIGH mutation leading to GPI deficiency is associated with developmental delay and autism. *Hum Mutat*. 2018;39:827-829.
 13. Knight Johnson A, Schaefer GB, Lee J, Hu Y, Del Gaudio D. Alu-mediated deletion of PIGL in a patient with CHIME syndrome. *Am J Med Genet A*. 2017;173(5):1378-1382.
 14. Fujiwara I, Murakami Y, Niihori T, et al. Mutations in PIGL in a patient with Mabry syndrome. *Am J Med Genet A*. 2015;167A(4):777-785.
 15. Murakami Y, Siripanyapinyo U, Hong Y, et al. PIG-W is critical for inositol acylation but not for flipping of glycosylphosphatidylinositol-anchor. *Mol Biol Cell*. 2003;14(10):4285-4295.
 16. Hoglebe M, Murakami Y, Wild M, et al. A novel mutation in PIGW causes glycosylphosphatidylinositol deficiency without hyperphosphatase. *Am J Med Genet A*. 2016;170(12):3319-3322.
 17. Chiyonobu T, Inoue N, Morimoto M, Kinoshita T, Murakami Y. Glycosylphosphatidylinositol (GPI) anchor deficiency caused by mutations in PIGW is associated with West syndrome and hyperphosphatase with mental retardation syndrome. *J Med Genet*. 2014;51(3):203-207.
 18. Almeida AM, Murakami Y, Baker A, et al. Targeted therapy for inherited GPI deficiency. *N Engl J Med*. 2007;356(16):1641-1647.
 19. Almeida AM, Murakami Y, Layton DM, et al. Hypomorphic promoter mutation in PIGM causes inherited glycosylphosphatidylinositol deficiency. *Nat Med*. 2006;12(7):846-851.
 20. Horn D, Wieczorek D, Metcalfe K, et al. Delineation of PIGV mutation spectrum and associated phenotypes in hyperphosphatase with mental retardation syndrome. *Eur J Hum Genet*. 2014;22(6):762-767.
 21. Murakami Y, Kanzawa N, Saito K, et al. Mechanism for release of alkaline phosphatase caused by glycosylphosphatidylinositol deficiency in patients with hyperphosphatase mental retardation syndrome. *J Biol Chem*. 2012;287(9):6318-6325.
 22. Johnston JJ, Gropman AL, Sapp JC, et al. The phenotype of a germline mutation in PIGA: the gene somatically mutated in paroxysmal nocturnal hemoglobinuria. *Am J Hum Genet*. 2012;90(2):295-300.
 23. Makrythanasis P, Kato M, Zaki MS, et al. Pathogenic variants in PIGG cause intellectual disability with seizures and hypotonia. *Am J Hum Genet*. 2016;98(4):615-626.
 24. Maeda Y, Watanabe R, Harris CL, et al. PIG-M transfers the first manose to glycosylphosphatidylinositol on the luminal side of the ER. *EMBO J*. 2001;20(1-2):250-261.
 25. Krawitz PM, Murakami Y, Hecht J, et al. Mutations in PIGO, a member of the GPI-anchor-synthesis pathway, cause hyperphosphatase with mental retardation. *Am J Hum Genet*. 2012;91(1):146-151.
 26. Krawitz PM, Murakami Y, Riess A, et al. PGAP2 mutations, affecting the GPI-anchor-synthesis pathway, cause hyperphosphatase with mental retardation syndrome. *Am J Hum Genet*. 2013;92(4):584-589.
 27. Knaus A, Awaya T, Helbig I, et al. Rare noncoding mutations extend the mutational spectrum in the PGAP3 subtype of hyperphosphatase with mental retardation syndrome. *Hum Mutat*. 2016;37(8):737-744.
 28. Zhao JJ, Halvardson J, Knaus A, et al. Reduced cell surface levels of GPI-linked markers in a new case with PIGG loss of function. *Hum Mutat*. 2017;38(10):1394-1401.
 29. Krawitz PM, Hochsmann B, Murakami Y, et al. A case of paroxysmal nocturnal hemoglobinuria caused by a germline mutation and a somatic mutation in PIGT. *Blood*. 2013;122(7):1312-1315.
 30. Nakashima M, Kashii H, Murakami Y, et al. Novel compound heterozygous PIGT mutations caused multiple congenital anomalies-hypotonia-seizures syndrome 3. *Neurogenetics*. 2014;15(3):193-200.
 31. Lam C, Golas GA, Davids M, et al. Expanding the clinical and molecular characteristics of PIGT-CDG, a disorder of glycosylphosphatidylinositol anchors. *Mol Genet Metab*. 2015;115(2-3):128-140.
 32. Skauli N, Wallace S, Chiang SC, et al. Novel PIGT variant in two brothers: expansion of the multiple congenital anomalies-hypotonia seizures syndrome 3 phenotype. *Genes (Basel)*. 2016;7(12):108.
 33. Kohashi K, Ishiyama A, Yuasa S, et al. Epileptic apnea in a patient with inherited glycosylphosphatidylinositol anchor deficiency and PIGT mutations. *Brain and Development*. 2017;40(1):53-57.
 34. Kvarnung M, Nilsson D, Lindstrand A, et al. A novel intellectual disability syndrome caused by GPI anchor deficiency due to homozygous mutations in PIGT. *J Med Genet*. 2013;50(8):521-528.
 35. Pagnamenta AT, Murakami Y, Taylor JM, et al. Analysis of exome data for 4293 trios suggests GPI-anchor biogenesis defects are a rare cause of developmental disorders. *Eur J Hum Genet*. 2017;25(6):669-679.
 36. Murakami Y, Tawamie H, Maeda Y, et al. Null mutation in PGAP1 impairing Gpi-anchor maturation in patients with intellectual disability and encephalopathy. *PLoS Genet*. 2014;10(5):e1004320.
 37. Nguyen TTM, Murakami Y, Sheridan E, et al. Mutations in GPAA1, encoding a GPI transamidase complex protein, cause developmental delay, epilepsy, cerebellar atrophy, and osteopenia. *Am J Hum Genet*. 2017;101(5):856-865.
 38. Ng BG, Freeze HH. Human genetic disorders involving glycosylphosphatidylinositol (GPI) anchors and glycosphingolipids (GSL). *J Inher Metab Dis*. 2015;38(1):171-178.
 39. Novarino G, Fenstermaker AG, Zaki MS, et al. Exome sequencing links corticospinal motor neuron disease to common neurodegenerative disorders. *Science*. 2014;343(6170):506-511.
 40. Kettwig M, Elpeleg O, Wegener E, et al. Compound heterozygous variants in PGAP1 causing severe psychomotor retardation, brain atrophy, recurrent apneas and delayed myelination: a case report and literature review. *BMC Neurol*. 2016;16:74.
 41. Bosch DG, Boonstra FN, Kinoshita T, et al. Cerebral visual impairment and intellectual disability caused by PGAP1 variants. *Eur J Hum Genet*. 2015;23(12):1689-1693.
 42. Granzow M, Paramasivam N, Hinderhofer K, et al. Loss of function of PGAP1 as a cause of severe encephalopathy identified by whole exome sequencing: lessons of the bioinformatics pipeline. *Mol Cell Probes*. 2015;29(5):323-329.
 43. Williams C, Jiang YH, Shashi V, et al. Additional evidence that PGAP1 loss of function causes autosomal recessive global developmental delay and encephalopathy. *Clin Genet*. 2015;88(6):597-599.
 44. Trujillano D, Bertoli-Avella AM, Kumar Kandaswamy K, et al. Clinical exome sequencing: results from 2819 samples reflecting 1000 families. *Eur J Hum Genet*. 2017;25(2):176-182.
 45. Howard MF, Murakami Y, Pagnamenta AT, et al. Mutations in PGAP3 impair GPI-anchor maturation, causing a subtype of hyperphosphatase with mental retardation. *Am J Hum Genet*. 2014;94(2):278-287.
 46. Maeda Y, Tashima Y, Houjou T, et al. Fatty acid remodeling of GPI-anchored proteins is required for their raft association. *Mol Biol Cell*. 2007;18(4):1497-1506.
 47. Tashima Y, Taguchi R, Murata C, Ashida H, Kinoshita T, Maeda Y. PGAP2 is essential for correct processing and stable expression of GPI-anchored proteins. *Mol Biol Cell*. 2006;17(3):1410-1420.
 48. Hansen L, Tawamie H, Murakami Y, et al. Hypomorphic mutations in PGAP2, encoding a GPI-anchor-remodeling protein, cause autosomal-recessive intellectual disability. *Am J Hum Genet*. 2013;92(4):575-583.
 49. Jezela-Stanek A, Ciara E, Piekutowska-Abramczuk D, et al. Congenital disorder of glycosylphosphatidylinositol (GPI)-anchor biosynthesis--the phenotype of two patients with novel mutations in the PIGN and PGAP2 genes. *Eur J Paediatr Neurol*. 2016;20(3):462-473.
 50. Naseer MI, Rasool M, Jan MM, et al. A novel mutation in PGAP2 gene causes developmental delay, intellectual disability, epilepsy and microcephaly in consanguineous Saudi family. *J Neurol Sci*. 2016;371:121-125.
 51. Bramswig NC, Ludecke HJ, Alanay Y, et al. Exome sequencing unravels unexpected differential diagnoses in individuals with the tentative diagnosis of coffin-Siris and Nicolaidis-Baraitser syndromes. *Hum Genet*. 2015;134(6):553-568.
 52. Campeau PM, Hennekam RC, DOORS Syndrome Collaborative Group. DOORS syndrome: phenotype, genotype and comparison with

- coffin-Siris syndrome. *Am J Med Genet C Semin Med Genet.* 2014; 166C(3):327-332.
53. Campeau PM, Kasperaviciute D, Lu JT, et al. The genetic basis of DOORS syndrome: an exome-sequencing study. *Lancet Neurol.* 2014; 13(1):44-58.
54. Kortum F, Caputo V, Bauer CK, et al. Mutations in *KCNH1* and *ATP6V1B2* cause Zimmermann-Laband syndrome. *Nat Genet.* 2015; 47(6):661-667.
55. Mucha BE, Hennekam RCM, Sisodiya S, Campeau PM. TBC1D24--related disorders. In: Pagon RA, Adam MP, Ardinger HH, et al., eds. *GeneReviews(R)*. Seattle, WA; 1993.
56. Kariminejad A, Ajeawung NF, Bozorgmehr B, et al. Kaufman oculo-cerebro-facial syndrome in a child with small and absent terminal phalanges and absent nails. *J Hum Genet.* 2017;62(4):465-471.
57. Thompson MD, Killoran A, Percy ME, Nezarati M, Cole DE, Hwang PA. Hyperphosphatasia with neurologic deficit: a pyridoxine-responsive seizure disorder? *Pediatr Neurol.* 2006;34(4):303-307.
58. Kuki I, Takahashi Y, Okazaki S, et al. Vitamin B6-responsive epilepsy due to inherited GPI deficiency. *Neurology.* 2013;81(16):1467-1469.

SUPPORTING INFORMATION

Additional supporting information may be found online in the Supporting Information section at the end of the article.

How to cite this article: Bellai-Dussault K, Nguyen TTM, Baratang NV, Jimenez-Cruz DA, Campeau PM. Clinical variability in inherited glycosylphosphatidylinositol deficiency disorders. *Clin Genet.* 2018;1-10. <https://doi.org/10.1111/cge.13425>

Mutations in *PIGS*, Encoding a GPI Transamidase, Cause a Neurological Syndrome Ranging from Fetal Akinesia to Epileptic Encephalopathy

Thi Tuyet Mai Nguyen,¹ Yoshiko Murakami,² Kristen M. Wigby,³ Nissan V. Baratang,¹ Justine Rousseau,¹ Anik St-Denis,¹ Jill A. Rosenfeld,⁴ Stephanie C. Laniewski,⁵ Julie Jones,⁶ Alejandro D. Iglesias,⁷ Marilyn C. Jones,³ Diane Masser-Frye,⁸ Angela E. Scheuerle,⁹ Denise L. Perry,¹⁰ Ryan J. Taft,¹⁰ Françoise Le Deist,¹ Miles Thompson,³ Taroh Kinoshita,² and Philippe M. Campeau^{1,*}

Inherited GPI deficiencies (IGDs) are a subset of congenital disorders of glycosylation that are increasingly recognized as a result of advances in whole-exome sequencing (WES) and whole-genome sequencing (WGS). IGDs cause a series of overlapping phenotypes consisting of seizures, dysmorphic features, multiple congenital malformations, and severe intellectual disability. We present a study of six individuals from three unrelated families in which WES or WGS identified bi-allelic phosphatidylinositol glycan class S (*PIGS*) biosynthesis mutations. Phenotypes included severe global developmental delay, seizures (partly responding to pyridoxine), hypotonia, weakness, ataxia, and dysmorphic facial features. Two of them had compound-heterozygous variants c.108G>A (p.Trp36*) and c.101T>C (p.Leu34Pro), and two siblings of another family were homozygous for a deletion and insertion leading to p.Thr439_Lys451delinsArgLeuLeu. The third family had two fetuses with multiple joint contractures consistent with fetal akinesia. They were compound heterozygous for c.923A>G (p.Glu308Gly) and c.468+1G>C, a splicing mutation. Flow-cytometry analyses demonstrated that the individuals with *PIGS* mutations show a GPI-AP deficiency profile. Expression of the p.Trp36* variant in *PIGS*-deficient HEK293 cells revealed only partial restoration of cell-surface GPI-APs. In terms of both biochemistry and phenotype, loss of function of *PIGS* shares features with *PIGT* deficiency and other IGDs. This study contributes to the understanding of the GPI-AP biosynthesis pathway by describing the consequences of *PIGS* disruption in humans and extending the family of IGDs.

Recent advances in next-generation sequencing and the widespread application of whole-exome sequencing (WES) and whole-genome sequencing (WGS) have led to the discovery of the molecular basis of a growing number of congenital disorders of glycosylation (CDGs). The inherited glycosylphosphatidylinositol-anchored protein (GPI-AP) deficiencies (IGDs) are a growing group of disorders that are a subset of CDGs. To date, there are 17 IGDs that share overlapping features, including developmental delay, seizures, hypotonia, weakness, ataxia, and dysmorphic features.¹ A recent study of 4,293 parent-child triads reported that IGDs alone might account for 0.15% of all developmental disorders,² suggesting that IGDs could be more common than previously recognized.

In many cases, IGDs result from the failure of the GPI anchor to regulate APs, which has global consequences for development. The GPI anchor serves as a tether for APs at the external cell surface. The majority of over 150 mammalian GPI-APs act as ectoenzymes critical to many cell functions, such as the actions of hydrolytic enzymes, adhesion molecules, receptors, protease inhibitors, and complement regulatory proteins.³ The essential role of

GPI-APs in many human tissues became evident as the effects of genetic disruptions of GPI anchor biosynthesis and remodeling were identified.

Approximately 31 enzymes are integral to the post-translational modification that results in the biosynthesis of GPI-APs, and a multitude of genetic disruptions that could produce related phenotypes are possible. IGD-associated phenotypes that result from complete or partial inactivation of these GPI biosynthesis enzymes often include seizures, intellectual disability, coarse facial features, and hypotonia. Microcephaly, hearing impairment, joint contractures, skin anomalies, congenital heart defects, urinary-tract defects, and skeletal anomalies are less common features.^{4–42} 17 genes in the GPI-AP biosynthesis pathway have been linked to human disease.^{6–44} All of these disorders are autosomal recessive, except that *PIGA*-associated disease (MIM: 300868) is X-linked recessive.

In this report, we describe an IGD disorder resulting from recessive inheritance of variants affecting phosphatidylinositol glycan, class S (*PIGS*). *PIGS* (MIM: 610271) mutations were found in six individuals from three unrelated families by WES or WGS after informed consent was

¹Centre Hospitalier Universitaire Sainte Justine Research Center, University of Montreal, Montreal, QC H3T1C5, Canada; ²Research Institute for Microbial Diseases, Osaka University, Osaka 565-0871, Japan; ³Department of Pediatrics, University of California, San Diego, San Diego, CA 92093, USA; ⁴Department of Molecular & Human Genetics, Baylor College of Medicine, Houston, TX 77030, USA; ⁵University of Rochester Medical Center, New York, NY 14642, USA; ⁶Greenwood Genetic Center, Greenwood, SC 29646, USA; ⁷NewYork-Presbyterian Morgan Stanley Children's Hospital, New York, NY 10032, USA; ⁸Rady Children's Hospital-San Diego, San Diego, CA 92123, USA; ⁹University of Texas, Southwestern Medical Center, Dallas, TX, USA; ¹⁰Illumina Inc., San Diego, CA 92121, USA

*Correspondence: p.campeau@umontreal.ca

<https://doi.org/10.1016/j.ajhg.2018.08.014>

© 2018 American Society of Human Genetics.



Table 1. Phenotypes Identified in Individuals with Bi-allelic P/GS Mutations

System	Features	Individual 1a	Individual 1b	Individual 2a	Individual 2b	Individual 3a	Individual 3b	
CNS	microcephaly	-	-	+	+	-	-	
	global developmental delay	+	+	+	+	NA	NA	
	hypotonia	+	+	+	+	NA	NA	
	ataxia and balance problems	+	+	+	+	NA	NA	
	seizures	+	+	+	+	NA	NA	
	CNS atrophy	cerebellar	cerebellar	diffuse cortical	diffuse cortical	NA	NA	
	nystagmus	+	+	+	-	NA	NA	
	cortical blindness	+	+	+	-	NA	NA	
	coarse facial features	+	+	+	+	-	-	
	arched eyebrows	+	+	+	+	-	-	
Craniofacial	thickened helices	+	+	+	+	-	-	
	broad tongue	+	+	+	+	-	-	
	gingival hypertrophy	+	+	+	-	-	-	
	other	preauricular tag, deep philtrum	deep philtrum	widely spaced teeth wrinkled forehead	wrinkled forehead	small chin	-	
	feeding problems	oral feeding	oral feeding	gastrostomy tube for aspiration	oral feeding	NA	NA	
	hepatomegaly	-	-	+	+	-	-	
	constipation	-	-	-	+	NA	NA	
	cryptorchidism	-	-	+	-	NA	NA (because the individual is female)	
	Musculoskeletal	hand anomalies	brachydactyly fifth-finger clinodactyly	brachydactyly, fifth-finger clinodactyly	short, stubby digits fifth-finger clinodactyly	brachydactyly, fifth-finger clinodactyly	-	-
		other	short fourth metacarpals and metatarsals	short fourth metacarpals and metatarsals	pectus carinatum, joint laxity, scoliosis	pectus carinatum, joint laxity	multiple joint contractures, consistent with fetal akinesia	multiple joint contractures, consistent with fetal akinesia
Alkaline phosphatase		145 IU/L at 1 year (reference: 25–500), 122 IU/L at 8.5 years (reference: 150–300)	116 IU/L at 8.5 years (reference: 150–300 IU/L)	98 IU/L at 7.5 years (reference: 38–126 IU/L)	130 IU/L at 9 months (reference: 38–126 IU/L)	NA	NA	
Other	-	-	inguinal hernias	cardiomegaly	thickened nuchal fold	glomerular cysts, cystic hygroma		

The following abbreviation is used: NA, not available.

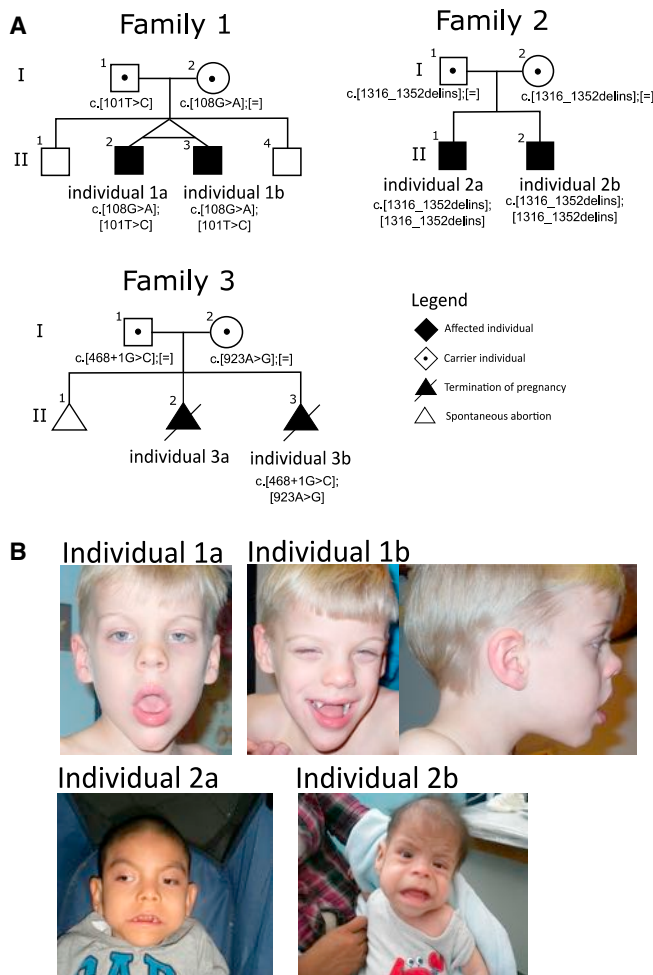


Figure 1. Pedigrees of Three Families Carrying *PIGS* Mutations in This Study and Composite Showing the Characteristics of Individuals in Families 1 and 2

(A) Pedigrees of three families.

(B) Photos of individuals from families 1 and 2: individuals 1a and 1b at 5.5 years of age, individual 2a at 7.5 years, and individual 2b at 9 months.

approved by the ethics committees of the institutions where the families were seen. We hypothesize that *PIGS* mutations cause a deficiency of GPI-AP biosynthesis in these individuals and that this results in severe global developmental delay, hypotonia, seizures, weakness, balance problems, ataxia, and dysmorphic facial features. The biochemistry and phenotype of this putative IGD are discussed in the context of the other known GPI-deficiency disorders.¹

An overview of the affected individuals' symptoms is presented in Table 1. Additional detailed clinical descriptions are provided in the Supplemental Data. In family 1, individuals 1a and 1b are monozygotic twin brothers born to unrelated parents of European descent (Figure 1A). In family 2, individuals 2a and 2b are the only children born to Mexican parents with an otherwise unremarkable family history (Figure 1A). These individuals share a phenotype of hypotonia,

severe global developmental delay, seizures, visual impairment, CNS atrophy on radiological studies, and hand anomalies (including brachydactyly and clinodactyly). Characteristic facial features, as seen in Figure 1B, include coarse facies with arched eyebrows, thickened helices, gingival hypertrophy, broad tongue, and nystagmus. Two fetuses, 3a and 3b, from family 3 had multiple joint contractures, consistent with fetal akinesia. In addition, individual 3a had a thickened nuchal fold, and individual 3b had glomerular cysts and a cystic hygroma. The pregnancies were terminated after 19 weeks for fetus 3a and after 13 weeks for fetus 3b.

By WES, we found heterozygous *PIGS* mutations, including c.108G>A (p.Trp36*) and c.101T>C (p.Leu34Pro) (GenBank: NM_033198.3), in individuals 1a and 1b in family 1. WGS was performed for individuals 2a and 2b in family 2, and they were found to have the homozygous mutation c.1316_1352delCCACCA CCCTTACCTCCCTGGCGCAGCTTCTGGGCAAinsGGTTGCT (p.Thr439_Lys451delinsArgLeuLeu) within a region of homozygosity (ROH). Although the parents were not known to be consanguineous, both were from the same small rural community, which most likely explains the homozygosity. This in-frame deletion-and-insertion event was not observed in the ExAC Browser or NHBLI Exome Sequencing Project Exome Variant Server. It results in the insertion of 7 bases and the deletion of 37 bases within a highly conserved region of *PIGS*. *In silico* analyses predicted this variant to be damaging. Finally, two individuals (3a and 3b) were compound heterozygous for the missense mutation c.923A>G (p.Glu308Gly) and the splicing mutation c.468+1G>C (Figure 2).

To study the expression of *PIGS* in individuals 1a and 1b, we used B lymphoblastoid cell lines (LCLs) established by Epstein-Barr virus immortalization of peripheral-blood mononuclear cells (PMBCs) of these individuals, as well as healthy control individuals, for real-time PCR and western blotting. The results indicated a decrease in *PIGS* expression of up to 50% in qPCR and a significant decrease in protein levels in western blotting (Figure 3). This indicates that the stop codon introduced by c.108G>A results in the low *PIGS* mRNA and protein levels in these individuals.

We next assessed whether the GPI-anchoring process was deficient in individual cells. To determine whether individual cells had reduced cell-surface expression of GPI-APs, we stained whole-blood samples from four affected individuals and control individuals with fluorescent antibodies for GPI-APs (CD16, CD55, and CD59), as well as with fluorescein-labeled proaerolysin (FLAER), which binds to the GPI anchor itself, and performed fluorescence-activated cell sorting (FACS) analysis to assess relative fluorescence.²⁸ Analysis on granulocytes indicated that individual cells had less signal of CD16 (all individuals) and CD55 and CD59 (individuals 1a and 1b) than age-matched control cells (Figure 4).

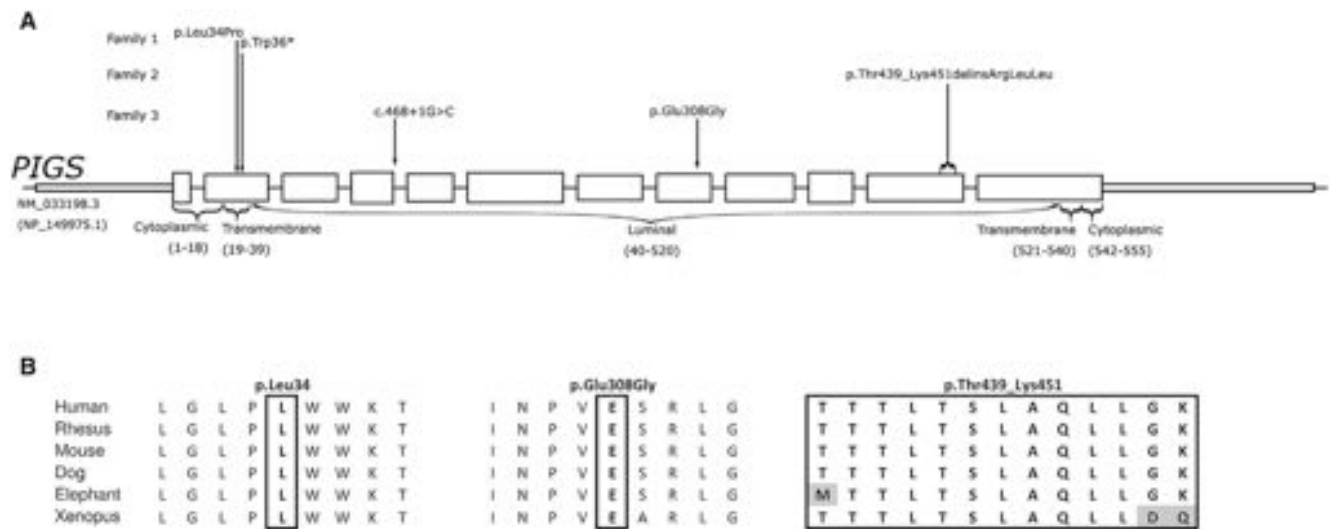


Figure 2. Mutations in *PIGS*

(A) Location of the mutations in *PIGS* and the corresponding protein. Introns are not drawn to scale.
 (B) Conservation in vertebrates of the amino acids affected by missense mutations and indels.

In all of these individuals, the level of FLAER in lymphocytes was also significantly downregulated (Figure 5). Thus, the compound-heterozygous mutations c.108G>A (p.Trp36*) and c.101T>C (p.Leu34Pro) in family 1 and the homozygous mutation c.1316_1352del CCACCACCCTTACCTCCCTGGCGCAGCTTCTGGGCAA insGGTTGCT (p.Thr439_Lys451delinsArgLeuLeu) in family 2 in *PIGS* result in low amounts of GPI-AP in peripheral white blood cells. We conclude that insufficient amounts of *PIGS* and/or defective *PIGS* function in individual cells leads to reduced amounts of GPI-AP at the cell surface.

To study the role of each mutation found in individuals 1a and 1b, we established *PIGS*-knockout HEK293 cells with the CRISPR-Cas9 system and transfected them with wild-type or mutant pME-FLAG h*PIGS* (a strong SR α promoter), pTK-FLAG h*PIGS* (a weaker, thymidine kinase promoter), or pTA-FLAG h*PIGS* (a weak TATA-box-only promoter). FACS analysis was performed 3 days after transfection with FLAER, CD55 (DAF), and CD59.

The results showed that, compared with the wild-type, the Trp36* mutant only partially restored the surface expression of GPI-APs on HEK293 cells even when driven by a strong promoter, whereas Leu34Pro mutants showed slight but significant reduction in restoration even when driven by a weak promoter (Figures 6 and 7). It is interesting to note that the p.Leu34Pro variant is in a helical transmembrane domain and affects a residue with a low missense tolerance ratio (MTR).⁴³ Western blots from cell lysates of N-terminal FLAG-tagged Trp36* mutants with a FLAG-tagged antibody showed almost no FLAG-*PIGS* expression, whereas similar expression was observed between the wild-type and the Leu34Pro mutant (Figure 8). Western blots from cell lysates of C-terminal HA-tagged Trp36* mutants with an HA-tagged antibody showed two truncated isoforms of *PIGS*-HA (Figure 8). This indicates that the *PIGS* proteins that start from the downstream methionines have some residual activities.

We next analyzed the amount of GPI-AP in amniocytes from individual 3b by using FLAER, as well as GPI markers

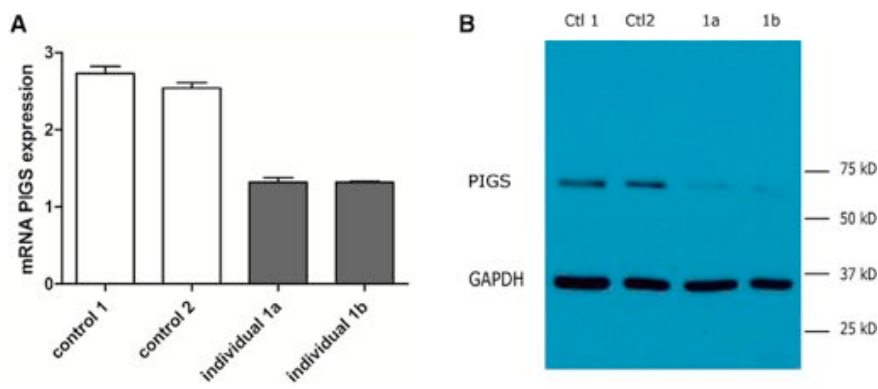


Figure 3. *PIGS* Expression in Individuals with *PIGS* Mutations

(A) Real-time PCR on subject LCL extracts shows that the affected males have reduced transcript levels of *PIGS*. RNA extractions from LCLs of individuals 1a and 1b were subjected to qRT-PCR according to the Δ Ct method. The results were normalized to TBP expression from quadruplicate experiments. Error bars represent standard errors (n = 3).

(B) Western blot using a specific antibody against human *PIGS* and anti-GAPDH as a reference protein on LCLs from individuals 1a and 1b.

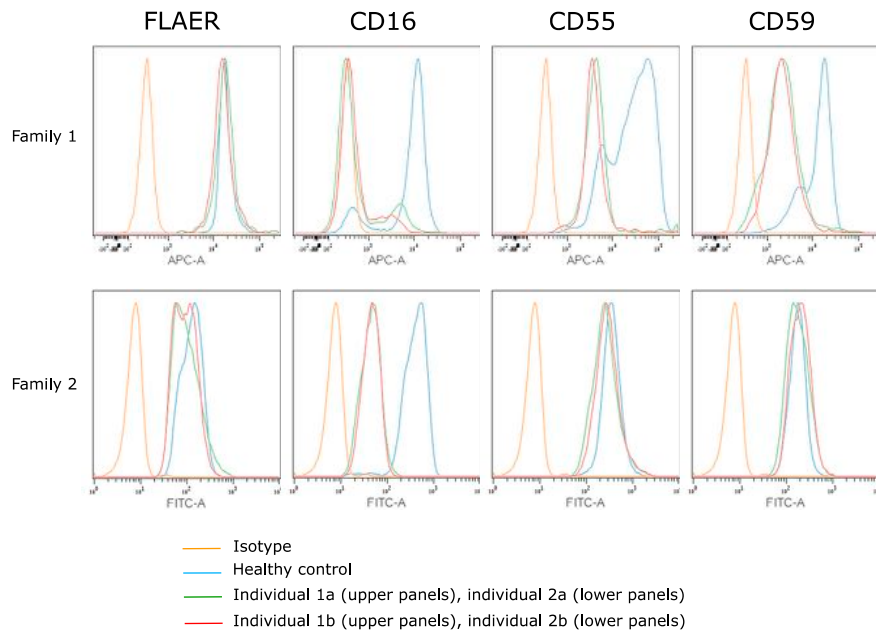


Figure 4. Impact of the *PIGS* Mutations on Individual Granulocyte Cell-Surface GPI-APs

Red blood cells were lysed in BD FACS lysing solution (BD Biosciences) from fresh blood of the individuals in families 1 and 2 and control cells, and then the samples were stained with GPI-AP markers (FLAER, CD16-FITC, CD55-FITC, and CD59-FITC) for 20 min on ice. The nonspecific binding was washed before analysis by the BD FACSCanto II system. Shown is a representative analysis of the amount of cell-surface GPI-AP on granulocytes from triplicate experiments.

CD24, CD55, CD59, and CD73 (Figure 9). CD3, a non-GPI-AP marker, was used as a negative control. FACS analyses indicated decreases in all used markers in the individual cells, and the highest reduction was found for CD24, which was 85% lower than in similar gestation-age control cells.

Here, we describe a recessive genetic GPI biosynthesis disorder caused by bi-allelic *PIGS* mutations that result in loss of function and decreased GPI-AP expression on flow cytometry. The index subjects share a core phenotype of coarse facial features, seizures, hypotonia, and developmental delay, which overlap the phenotype of other IGDs that result from failure to synthesize functional

GPI-APs. Contractures as seen in family 3 are also seen with *PIGA*, *PIGY* (MIM: 616809), and *PIGG* (MIM: 616917) mutations.^{9,29,44}

This disorder results from the failure of the GPI transamidase complex, which includes *PIGS*,⁴⁵ to transfer the GPI anchor to the precursor protein bearing a GPI-attachment signal sequence. *PIGS* and *PIGT* are members of the GPI transamidase complex and have been demonstrated to be essential for the formation of carbonyl intermediates during the transfer of the GPI group to the protein.^{45,46} The *PIGS* pattern of reduced GPI-AP resembles the *PIGT* (MIM: 610272)-associated reduction in CD16 and FLAER on granulocytes.³²

The biochemical analysis of the consequences of the *PIGS* variants supports this observation. We have shown that individuals 1a and 1b in family 1 have low amounts of *PIGS* mRNA and protein. *PIGS* is

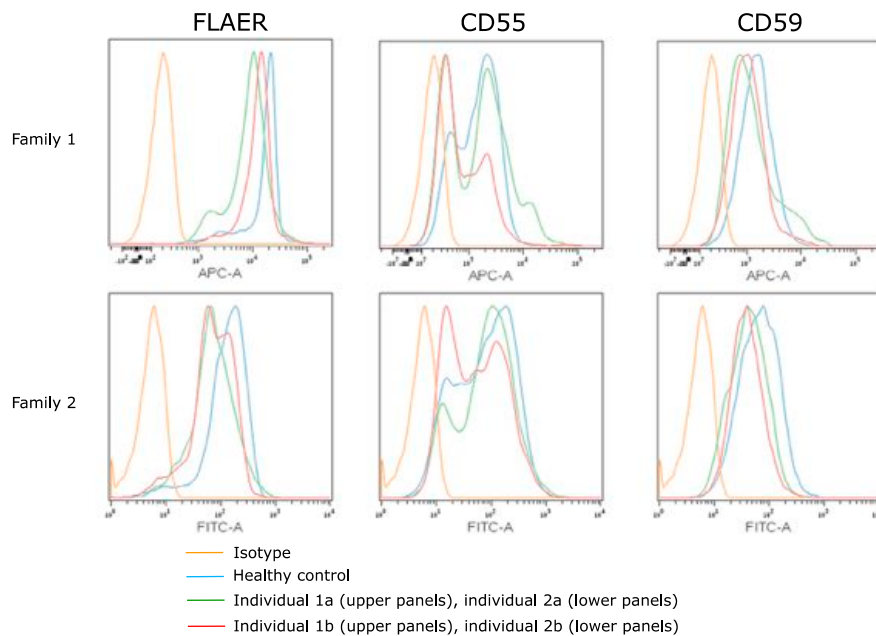


Figure 5. Impact of the *PIGS* Mutations on Individual Lymphocyte Cell-Surface GPI-APs

Flow-cytometry analysis of lymphocytes from the same experiments described in Figure 4. Shown is a representative analysis of the amount of cell-surface GPI-AP on lymphocytes from triplicate experiments.

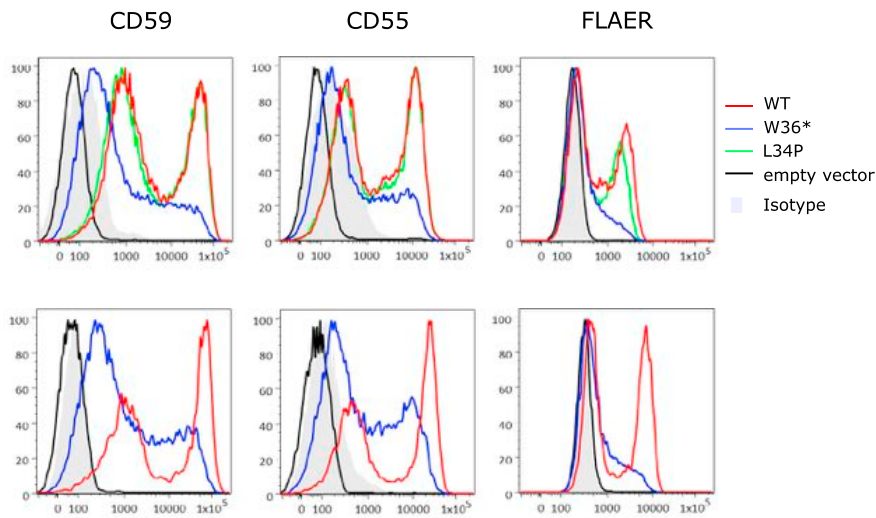


Figure 6. PIGS Functional Assay for Mutations Found in Individuals 1a and 1b

PIGS-deficient HEK293 cells were transfected with wild-type or mutant pME-FLAG hPIGS (top) or pME-HA hPIGS (bottom). FACS analysis was performed 3 days later.

are essential for the formation of the carbonyl intermediates necessary when the transamidase complex transfers the GPI group to the protein.^{45,46}

The phenotypic features resulting from disruption of *PIGS*, including coarse facies, developmental delay, hypotonia, and seizures, overlap

downregulated or expressed as a truncated isoform in *PIGS*-deficient HEK293 cells transfected with mutant *PIGS* (c.108G>A [Trp36*]), which leads to a decrease in *PIGS* function, as demonstrated by rescue assays of GPI-AP expression at the cell surface. In addition, all available blood samples from affected individuals showed reduced cell-surface expression of GPI-APs, including CD16 in granulocytes and FLAER in lymphocytes. It is worth noting, however, that whereas individuals 1a and 1b showed reduced CD55 and CD59, we found these to be normal for individuals 2a and 2b. The low signals seen for all GPI-AP markers in individual 3b amniocytes correlates with the severe phenotypes caused by the mutations found in individuals 3a and 3b.

In addition to having biochemical similarities, disruptions of *PIGS* and *PIGT* result in phenotypic similarities. This is consistent with the fact that both *PIGS* and *PIGT* are components of the GPI transamidase complex and

not just those of other IGDs but also those of other types of CDGs (MIM: PS212065) and numerous other Mendelian disorders. Many of these disorders can be distinguished on the basis of physical exam findings or biochemical findings (e.g., peroxisomal disorders and mucopolysaccharidoses). The findings of brachytelephalangy in conjunction with seizures and intellectual disability could be considered for DOORS syndrome (MIM: 220500),⁴⁷ which is caused by mutations in *TBC1D24* (MIM: 613577). Laboratory findings that can help distinguish *PIGS*-associated disorders from other Mendelian disorders include flow-cytometry analysis with reduced CD16 expression (with or without reduced CD55 expression), a lack of elevated serum tissue-nonspecific alkaline phosphatase (observed to be elevated in a number of other IGDs but normal in others), a lack of 2-oxoglutaric aciduria (occasionally seen with *TBC1D24* mutations), and normal serum transferrin isoelectric focusing (abnormal with several

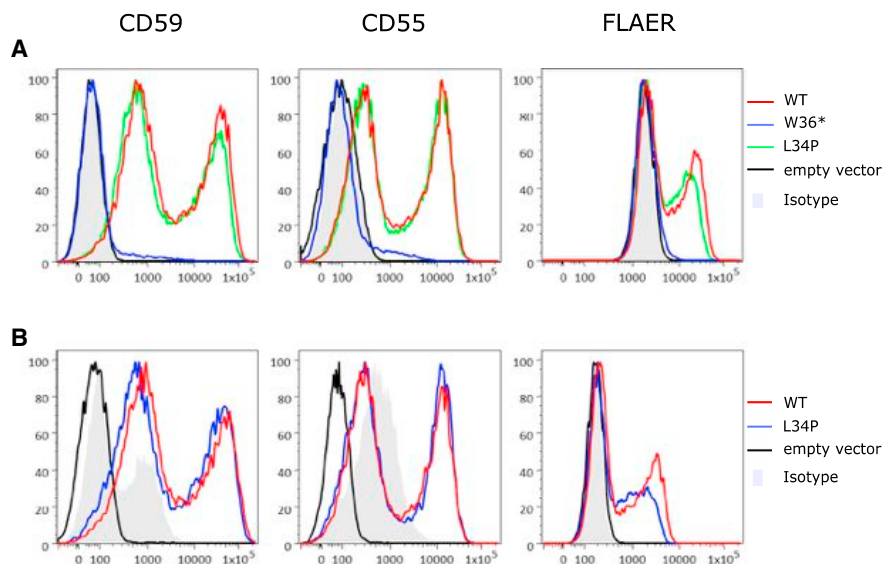


Figure 7. PIGS Functional Assay with pTK and pTATA Promoters for Mutations Found in Individuals 1a and 1b

(A) *PIGS*-knockout HEK293 cells were transfected with wild-type or mutant pTK-FLAG hPIGS (*PIGS* driven by a weaker, thymidine kinase promoter). FACS analysis was performed 3 days later. The geometric means decreased by 97% and 24% for CD59 by 65% and 19% for FLAER with the c.108G>A (p.Trp36*) and c.101T>C (p.Leu34Pro) mutations, respectively.

(B) *PIGS* driven by a weak TATA-box-only promoter. The geometric means decreased by 18% for CD59 and by 25% for FLAER with the c.101T>C (p.Leu34Pro) mutation.

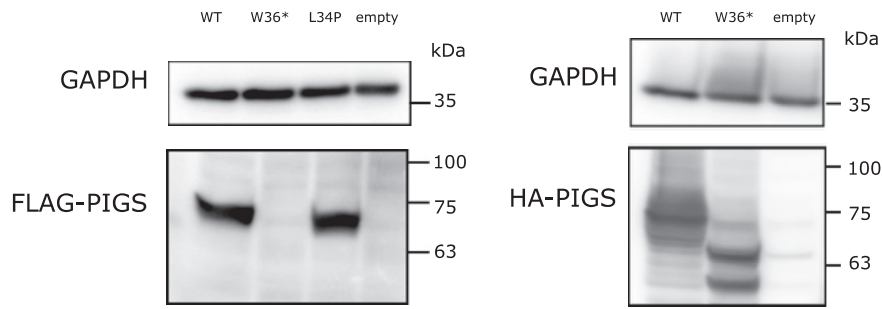


Figure 8. Expression of FLAG- and HA-Tagged PIGS in PIGS-Deficient HEK293 Cells Transfected with PIGS Mutants
Cell lysates from PIGS-deficient HEK293 cells transfected with N-terminal FLAG-tagged and C-terminal HA-tagged wild-type or mutants were used for western blot analysis using FLAG tag and HA tag antibodies, respectively.

CDGs). These can help support the diagnosis for those whose access to sequencing is limited or in the interpretation of variants of unknown significance identified on genetic testing.

It is noteworthy that pyridoxine hydrochloride improved the seizures in one of the affected probands. This success has been observed in other IGDs.^{28,48} Given that many of the IGDs can manifest with early-onset seizures, a trial of pyridoxine hydrochloride would be warranted as part of the epilepsy treatment. Similarly, the diagnosis of an IGD should be considered among the causes of pyridoxine-responsive epilepsies. The ketogenic diet could be another effective treatment for epilepsy given that Joshi et al. reported two *PIGA*-deficiency-affected siblings who became seizure-free on a ketogenic diet.⁴⁹

Collectively, these data provide evidence of the existence of a *PIGS*-disease relationship that shares some of the characteristics of IGDs. Studies using an animal model could

represent a good strategy for investigating the pathophysiology of *PIGS* mutations. Because GPI-APs are widely expressed during mammalian development and their absence frequently results in lethal global deficits in knockout mouse models, a preferred strategy might involve using CRISPR-Cas9 to knock human *PIGS* mutations into mice. As more IGDs are identified, it might become possible to discover genotype-phenotype correlations that could be useful in predicting the severity of a condition on the basis of the disrupted step in the pathway.¹

Accession Numbers

The mutations reported in this paper have been deposited in LOVD at <https://databases.lovd.nl/shared/genes/PIGS>.

Supplemental Data

Supplemental Data include more clinical details on the affected individuals and can be found with this article online at <https://doi.org/10.1016/j.ajhg.2018.08.014>.

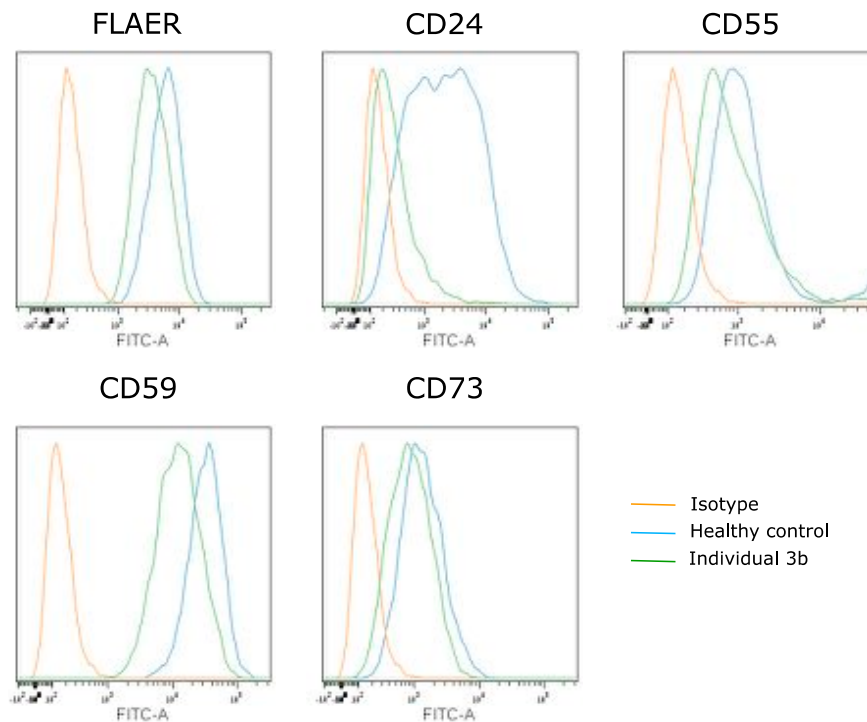


Figure 9. Impact of the PIGS Mutations on Individual 3b Amniocyte Cell-Surface GPI-APs

15-week-old amniocytes derived from individual 3b and similarly aged amniocytes from healthy control individuals were stained with FLAER, CD24, CD55, CD59, and CD73 for 1 hr on ice, nonspecific bindings were washed, and cells were then fixed in paraformaldehyde before analysis by the BD FACSCanto II system. Shown is a representative analysis of the amount of cell-surface GPI-AP on amniocytes of individual 3b and a control individual from triplicate experiments.

Acknowledgments

We acknowledge funding by the Canadian Institutes of Health Research (grant RN 324373), the Fonds de Recherche en Santé Québec (award 30647), and the Fondation du Grand Défi Pierre Lavoie. Whole-genome sequencing of family 2 was supported by the Illumina iHope program.

Declaration of interests

D.L.P. and R.J.T. are employees of Illumina Inc., which sells technologies that can be used to diagnose this condition.

Received: March 6, 2018

Accepted: August 23, 2018

Published: September 27, 2018

Web Resources

ExAC Browser, <http://exac.broadinstitute.org/>

GenBank, <http://www.ncbi.nlm.nih.gov/genbank/>

Leiden Open Variation Database (LOVD), <https://databases.lovd.nl/shared/genes/PIGS>

OMIM, <http://www.omim.org/>

UniProt, <http://www.uniprot.org/uniprot/>

References

1. Cole, D.E., and Thompson, M.D. (2015). Neurogenetic aspects of hyperphosphatasia in Mabry syndrome. *Subcell. Biochem.* *76*, 343–361.
2. Pagnamenta, A.T., Murakami, Y., Taylor, J.M., Anzilotti, C., Howard, M.F., Miller, V., Johnson, D.S., Tadros, S., Mansour, S., Temple, I.K., et al.; DDD Study (2017). Analysis of exome data for 4293 trios suggests GPI-anchor biogenesis defects are a rare cause of developmental disorders. *Eur. J. Hum. Genet.* *25*, 669–679.
3. Kinoshita, T., Fujita, M., and Maeda, Y. (2008). Biosynthesis, remodelling and functions of mammalian GPI-anchored proteins: Recent progress. *J. Biochem.* *144*, 287–294.
4. Fauth, C., Steindl, K., Toutain, A., Farrell, S., Witsch-Baumgartner, M., Karall, D., Joset, P., Böhm, S., Baumer, A., Maier, O., et al. (2016). A recurrent germline mutation in the PIGA gene causes Simpson-Golabi-Behmel syndrome type 2. *Am. J. Med. Genet. A.* *170A*, 392–402.
5. Johnston, J.J., Gropman, A.L., Sapp, J.C., Teer, J.K., Martin, J.M., Liu, C.F., Yuan, X., Ye, Z., Cheng, L., Brodsky, R.A., and Biesecker, L.G. (2012). The phenotype of a germline mutation in PIGA: The gene somatically mutated in paroxysmal nocturnal hemoglobinuria. *Am. J. Hum. Genet.* *90*, 295–300.
6. Kato, M., Saito, H., Murakami, Y., Kikuchi, K., Watanabe, S., Iai, M., Miya, K., Matsuura, R., Takayama, R., Ohba, C., et al. (2014). PIGA mutations cause early-onset epileptic encephalopathies and distinctive features. *Neurology* *82*, 1587–1596.
7. Martin, H.C., Kim, G.E., Pagnamenta, A.T., Murakami, Y., Carvill, G.L., Meyer, E., Copley, R.R., Rimmer, A., Barcia, G., Fleming, M.R., et al.; WGS500 Consortium (2014). Clinical whole-genome sequencing in severe early-onset epilepsy reveals new genes and improves molecular diagnosis. *Hum. Mol. Genet.* *23*, 3200–3211.
8. Edvardson, S., Murakami, Y., Nguyen, T.T., Shahrour, M., St-Denis, A., Shaag, A., Damsch, N., Le Deist, F., Bryceson, Y., Abu-Libdeh, B., et al. (2017). Mutations in the phosphatidylinositol glycan C (*PIGC*) gene are associated with epilepsy and intellectual disability. *J. Med. Genet.* *54*, 196–201.
9. Ilkovski, B., Pagnamenta, A.T., O'Grady, G.L., Kinoshita, T., Howard, M.F., Lek, M., Thomas, B., Turner, A., Christodoulou, J., Sillence, D., et al. (2015). Mutations in PIGY: Expanding the phenotype of inherited glycosylphosphatidylinositol deficiencies. *Hum. Mol. Genet.* *24*, 6146–6159.
10. Barone, R., Aiello, C., Race, V., Morava, E., Foulquier, F., Riemersma, M., Passarelli, C., Concolino, D., Carella, M., Santorelli, F., et al. (2012). DPM2-CDG: A muscular dystrophy-dystroglycanopathy syndrome with severe epilepsy. *Ann. Neurol.* *72*, 550–558.
11. Fujiwara, I., Murakami, Y., Niihori, T., Kanno, J., Hakoda, A., Sakamoto, O., Okamoto, N., Funayama, R., Nagashima, T., Nakayama, K., et al. (2015). Mutations in PIGL in a patient with Mabry syndrome. *Am. J. Med. Genet. A.* *167A*, 777–785.
12. Ng, B.G., Hackmann, K., Jones, M.A., Eroshkin, A.M., He, P., Williams, R., Bhide, S., Cantagrel, V., Gleeson, J.G., Paller, A.S., et al. (2012). Mutations in the glycosylphosphatidylinositol gene PIGL cause CHIME syndrome. *Am. J. Hum. Genet.* *90*, 685–688.
13. Nicklas, J.A., Carter, E.W., and Albertini, R.J. (2015). Both PIGA and PIGL mutations cause GPI-a deficient isolates in the Tk6 cell line. *Environ. Mol. Mutagen.* *56*, 663–673.
14. Chiyonobu, T., Inoue, N., Morimoto, M., Kinoshita, T., and Murakami, Y. (2014). Glycosylphosphatidylinositol (GPI) anchor deficiency caused by mutations in PIGW is associated with West syndrome and hyperphosphatasia with mental retardation syndrome. *J. Med. Genet.* *51*, 203–207.
15. Almeida, A.M., Murakami, Y., Layton, D.M., Hillmen, P., Sellick, G.S., Maeda, Y., Richards, S., Patterson, S., Kotsianidis, I., Mollica, L., et al. (2006). Hypomorphic promoter mutation in PIGM causes inherited glycosylphosphatidylinositol deficiency. *Nat. Med.* *12*, 846–851.
16. Horn, D., Krawitz, P., Mannhardt, A., Korenke, G.C., and Meinel, P. (2011). Hyperphosphatasia-mental retardation syndrome due to PIGV mutations: Expanded clinical spectrum. *Am. J. Med. Genet. A.* *155A*, 1917–1922.
17. Krawitz, P.M., Schweiger, M.R., Rödelsperger, C., Marcelis, C., Kölsch, U., Meisel, C., Stephani, F., Kinoshita, T., Murakami, Y., Bauer, S., et al. (2010). Identity-by-descent filtering of exome sequence data identifies PIGV mutations in hyperphosphatasia mental retardation syndrome. *Nat. Genet.* *42*, 827–829.
18. Thompson, M.D., Roscioli, T., Marcelis, C., Nezarati, M.M., Stolte-Dijkstra, I., Sharom, F.J., Lu, P., Phillips, J.A., Sweeney, E., Robinson, P.N., et al. (2012). Phenotypic variability in hyperphosphatasia with seizures and neurologic deficit (Mabry syndrome). *Am. J. Med. Genet. A.* *158A*, 553–558.
19. Xue, J., Li, H., Zhang, Y., and Yang, Z. (2016). Clinical and genetic analysis of two Chinese infants with Mabry syndrome. *Brain Dev.* *38*, 807–818.
20. Brady, P.D., Moerman, P., De Catte, L., Deprest, J., Devriendt, K., and Vermeesch, J.R. (2014). Exome sequencing identifies a recessive PIGN splice site mutation as a cause of syndromic congenital diaphragmatic hernia. *Eur. J. Med. Genet.* *57*, 487–493.
21. Maydan, G., Noyman, I., Har-Zahav, A., Neriah, Z.B., Pasmannik-Chor, M., Yeheskel, A., Albin-Kaplanski, A., Maya, I.,

- Magal, N., Birk, E., et al. (2011). Multiple congenital anomalies-hypotonia-seizures syndrome is caused by a mutation in PIGN. *J. Med. Genet.* *48*, 383–389.
22. McInerney-Leo, A.M., Harris, J.E., Gattas, M., Peach, E.E., Sinnott, S., Dudding-Byth, T., Rajagopalan, S., Barnett, C.P., Anderson, L.K., Wheeler, L., et al. (2016). Fryns syndrome associated with recessive mutations in PIGN in two separate families. *Hum. Mutat.* *37*, 695–702.
23. Ohba, C., Okamoto, N., Murakami, Y., Suzuki, Y., Tsurusaki, Y., Nakashima, M., Miyake, N., Tanaka, F., Kinoshita, T., Matsumoto, N., and Saitsu, H. (2014). PIGN mutations cause congenital anomalies, developmental delay, hypotonia, epilepsy, and progressive cerebellar atrophy. *Neurogenetics* *15*, 85–92.
24. Couser, N.L., Masood, M.M., Strande, N.T., Foreman, A.K., Crooks, K., Weck, K.E., Lu, M., Wilhelmsen, K.C., Roche, M., Evans, J.P., et al. (2015). The phenotype of multiple congenital anomalies-hypotonia-seizures syndrome 1: Report and review. *Am. J. Med. Genet. A*. *167A*, 2176–2181.
25. Fleming, L., Lemmon, M., Beck, N., Johnson, M., Mu, W., Murdock, D., Bodurtha, J., Hoover-Fong, J., Cohn, R., Bosemani, T., et al. (2016). Genotype-phenotype correlation of congenital anomalies in multiple congenital anomalies hypotonia seizures syndrome (MCAHS1)/PIGN-related epilepsy. *Am. J. Med. Genet. A*. *170A*, 77–86.
26. Krawitz, P.M., Murakami, Y., Hecht, J., Krüger, U., Holder, S.E., Mortier, G.R., Delle Chiaie, B., De Baere, E., Thompson, M.D., Roscioli, T., et al. (2012). Mutations in PIGO, a member of the GPI-anchor-synthesis pathway, cause hyperphosphatasia with mental retardation. *Am. J. Hum. Genet.* *91*, 146–151.
27. Nakamura, K., Osaka, H., Murakami, Y., Anzai, R., Nishiyama, K., Koder, H., Nakashima, M., Tsurusaki, Y., Miyake, N., Kinoshita, T., et al. (2014). PIGO mutations in intractable epilepsy and severe developmental delay with mild elevation of alkaline phosphatase levels. *Epilepsia* *55*, e13–e17.
28. Kuki, I., Takahashi, Y., Okazaki, S., Kawawaki, H., Ehara, E., Inoue, N., Kinoshita, T., and Murakami, Y. (2013). Vitamin B6-responsive epilepsy due to inherited GPI deficiency. *Neurology* *81*, 1467–1469.
29. Makrythanasis, P., Kato, M., Zaki, M.S., Saitsu, H., Nakamura, K., Santoni, F.A., Miyatake, S., Nakashima, M., Issa, M.Y., Guipponi, M., et al. (2016). Pathogenic variants in PIGG cause intellectual disability with seizures and hypotonia. *Am. J. Hum. Genet.* *98*, 615–626.
30. Kvarnang, M., Nilsson, D., Lindstrand, A., Korenke, G.C., Chiang, S.C., Blennow, E., Bergmann, M., Stöberg, T., Mäkitie, O., Anderlid, B.M., et al. (2013). A novel intellectual disability syndrome caused by GPI anchor deficiency due to homozygous mutations in PIGT. *J. Med. Genet.* *50*, 521–528.
31. Nakashima, M., Kashii, H., Murakami, Y., Kato, M., Tsurusaki, Y., Miyake, N., Kubota, M., Kinoshita, T., Saitsu, H., and Matsumoto, N. (2014). Novel compound heterozygous PIGT mutations caused multiple congenital anomalies-hypotonia-seizures syndrome 3. *Neurogenetics* *15*, 193–200.
32. Lam, C., Golas, G.A., Davids, M., Huizing, M., Kane, M.S., Krasnewich, D.M., Malicdan, M.C.V., Adams, D.R., Markello, T.C., Zein, W.M., et al. (2015). Expanding the clinical and molecular characteristics of PIGT-CDG, a disorder of glycosylphosphatidylinositol anchors. *Mol. Genet. Metab.* *115*, 128–140.
33. Murakami, Y., Tawamie, H., Maeda, Y., Büttner, C., Buchert, R., Radwan, F., Schaffer, S., Sticht, H., Aigner, M., Reis, A., et al. (2014). Null mutation in PGAP1 impairing Gpi-anchor maturation in patients with intellectual disability and encephalopathy. *PLoS Genet.* *10*, e1004320.
34. Granzow, M., Paramasivam, N., Hinderhofer, K., Fischer, C., Chotewutmontri, S., Kaufmann, L., Evers, C., Kotzaeridou, U., Rohrschneider, K., Schlesner, M., et al. (2015). Loss of function of PGAP1 as a cause of severe encephalopathy identified by whole exome sequencing: Lessons of the bioinformatics pipeline. *Mol. Cell. Probes* *29*, 323–329.
35. Williams, C., Jiang, Y.H., Shashi, V., Crimian, R., Schoch, K., Harper, A., McHale, D., Goldstein, D., and Petrovski, S. (2015). Additional evidence that PGAP1 loss of function causes autosomal recessive global developmental delay and encephalopathy. *Clin. Genet.* *88*, 597–599.
36. Howard, M.F., Murakami, Y., Pagnamenta, A.T., Daumer-Haas, C., Fischer, B., Hecht, J., Keays, D.A., Knight, S.J., Kölsch, U., Krüger, U., et al. (2014). Mutations in PGAP3 impair GPI-anchor maturation, causing a subtype of hyperphosphatasia with mental retardation. *Am. J. Hum. Genet.* *94*, 278–287.
37. Knaus, A., Awaya, T., Helbig, I., Afawi, Z., Pendziwiat, M., Aburachma, J., Thompson, M.D., Cole, D.E., Skinner, S., Anese, F., et al. (2016). Rare noncoding mutations extend the mutational spectrum in the PGAP3 subtype of hyperphosphatasia with mental retardation syndrome. *Hum. Mutat.* *37*, 737–744.
38. Hansen, L., Tawamie, H., Murakami, Y., Mang, Y., ur Rehman, S., Buchert, R., Schaffer, S., Muhammad, S., Bak, M., Nöthen, M.M., et al. (2013). Hypomorphic mutations in PGAP2, encoding a GPI-anchor-remodeling protein, cause autosomal-recessive intellectual disability. *Am. J. Hum. Genet.* *92*, 575–583.
39. Krawitz, P.M., Murakami, Y., Rieß, A., Hietala, M., Krüger, U., Zhu, N., Kinoshita, T., Mundlos, S., Hecht, J., Robinson, P.N., and Horn, D. (2013). PGAP2 mutations, affecting the GPI-anchor-synthesis pathway, cause hyperphosphatasia with mental retardation syndrome. *Am. J. Hum. Genet.* *92*, 584–589.
40. Jezela-Stanek, A., Ciara, E., Piekutowska-Abramczuk, D., Trubicka, J., Jurkiewicz, E., Rokicki, D., Mierzewska, H., Spychalska, J., Uhrynowska, M., Szwarc-Bronikowska, M., et al. (2016). Congenital disorder of glycosylphosphatidylinositol (GPI)-anchor biosynthesis—The phenotype of two patients with novel mutations in the PIGN and PGAP2 genes. *Eur. J. Paediatr. Neurol.* *20*, 462–473.
41. Johnstone, D.L., Nguyen, T.T., Murakami, Y., Kernohan, K.D., Tétreault, M., Goldsmith, C., Doja, A., Wagner, J.D., Huang, L., Hartley, T., et al.; Care4Rare Canada Consortium (2017). Compound heterozygous mutations in the gene PIGP are associated with early infantile epileptic encephalopathy. *Hum. Mol. Genet.* *26*, 1706–1715.
42. Khayat, M., Tilghman, J.M., Chervinsky, I., Zalman, L., Chakravarti, A., and Shalev, S.A. (2016). A PIGN mutation responsible for multiple congenital anomalies-hypotonia-seizures syndrome 1 (MCAHS1) in an Israeli-Arab family. *Am. J. Med. Genet. A*. *170A*, 176–182.
43. Traynelis, J., Silk, M., Wang, Q., Berkovic, S.F., Liu, L., Ascher, D.B., Balding, D.J., and Petrovski, S. (2017). Optimizing genomic medicine in epilepsy through a gene-customized approach to missense variant interpretation. *Genome Res.* *27*, 1715–1729.
44. Tarailo-Graovac, M., Sinclair, G., Stockler-Ipsiroglu, S., Van Allen, M., Rozmus, J., Shyr, C., Biancheri, R., Oh, T., Sayson, B.,

- Lafek, M., et al. (2015). The genotypic and phenotypic spectrum of PIGA deficiency. *Orphanet J. Rare Dis.* *10*, 23.
45. Ohishi, K., Inoue, N., and Kinoshita, T. (2001). PIG-S and PIG-T, essential for GPI anchor attachment to proteins, form a complex with GAA1 and GPI8. *EMBO J.* *20*, 4088–4098.
46. Kinoshita, T. (2014). Biosynthesis and deficiencies of glycosylphosphatidylinositol. *Proc. Jpn. Acad., Ser. B, Phys. Biol. Sci.* *90*, 130–143.
47. Qazi, Q.H., and Nangia, B.S. (1984). Abnormal distal phalanges and nails, deafness, mental retardation, and seizure disorder: a new familial syndrome. *J. Pediatr.* *104*, 391–394.
48. Thompson, M.D., Killoran, A., Percy, M.E., Nezarati, M., Cole, D.E., and Hwang, P.A. (2006). Hyperphosphatasia with neurologic deficit: A pyridoxine-responsive seizure disorder? *Pediatr. Neurol.* *34*, 303–307.
49. Joshi, C., Kolbe, D.L., Mansilla, M.A., Mason, S., Smith, R.J., and Campbell, C.A. (2016). Ketogenic diet - A novel treatment for early epileptic encephalopathy due to PIGA deficiency. *Brain Dev.* *38*, 848–851.